SCUOLA DI DOTTORATO
UNIVERSITÀ DEGLI STUDI DI MILANO-BICOCCA

Department of

Biotechnology and Bioscience

PhD program: **Biology and Biotechnology**

Cycle: **XXXII**

Curriculum in Biomolecolare - funzionale

Role of glucose and peroxiredoxin 6 in human chondrocytes and novel biomaterial for in vitro three-dimensional chondrocytes culture

Surname: **Stucchi** Name: **Simone**

Registration number: **752363**

Tutor: **Dr.ssa Michela Ceriani**

Coordinator: **Prof. Paola Branduardi**

ACADEMIC YEAR 2018-2019

INDEX

Abstract

Osteoarthritis (OA) is the most common rheumatic disease in the world and represents the first cause of disability in the world after 40 years old (Vos et al., 2012). It is frequently associated with aging, trauma, genetic predisposition, obesity and diabetes. OA results from the loss of balance between degradation and repair inside cartilage, in favor of degradation, with increased activity of catabolic enzymes such as matrix metalloproteinases (MMP-1, -3 and -13) and decreased production of type II collagen and aggrecans. Chondrocytes, the only cell type found in cartilage, are responsible for the repair and biosynthesis of elements of the extracellular matrix (Le Clanche et al. 2016; Goldring and Marcu 2009). Experimental findings support the hypothesis that diabetes is an independent risk factors for OA development (Le Clanche et al. 2016). In diabetes the chronic hyperglycemic state may induce glycation of various structural and functional proteins and collagen (Snedeker & Gautieri, 2014). Moreover chronic hyperglycemia as well as aging increase the oxidative stress in chondrocytes promoting the activation of pro-inflammatory MAPKs pathways leading to increase cytokine and MMPs release which are responsible for cartilage matrix degradation and OA progression (Le Clanche et al. 2016; Firestein et al. 2017). Furthermore, ROS levels increase apoptosis and cell death and chondrocytes loss by cell death could be an important events in OA (Del Carlo & Loeser, 2008). Despite a lot of studies, correct molecular mechanisms underlying the diabetes-associated OA phenotypes is still largely unknown.

In the second chapter of this PhD thesis we decide to analyze the effect of glucose on human C28/I2 chondrocyte cells. Firstly chondrocytes cell growth were analyzed using 6 different glucose concentration media to define which glucose concentration is preferred by chondrocytes. Results shown that chondrocytes prefer 2.5 mM of glucose which was used as normal glucose concentration and

25 mM of glucose was used as high glucose concentration. ROS levels and cell death increase in chondrocytes growth in high glucose environment for 72 h. Also cytoskeletal network become more disorganized in C28/I2 cells growth at high glucose concentration, this correlates with a different RalA-GTP levels in C28/I2 growth in high glucose media. RalA is a small G protein which is involved in the regulation of both tubulin and actin cytoskeleton organization towards Cdc42 and Rac1. However, to better simulate the chondrocyte behavior, experiments were performed even in cells cultured in medium supplemented ITS (Insulin-transferrin-selenium) which promote the chondrocyte differentiation. Chondrocytes cultured in ITS supplemented media were then stimulated with or without IL-1β to stimulate the osteoarthritic cartilage environment. Chondrocyte cultured at 2,5 mM of glucose concentration in ITS supplemented media seems to have an higher amount of Ral-A GTP even in cells stimulated with IL1β the pattern is the same. Ral A-GTP levels are lower in cells grown in 25 mM of glucose and stimulated with IL1β. We decide to analyze if the glucose concentration can influence the levels of MAPK pathways. Precisely we evaluate the expression of ERK1/2 which is a pathway involved in the production of MMP13. Levels of p-ERK1/2 decrease in cells grown at high glucose concentration and in cells stimulated with IL1β. Furthermore, NF-κB and iNOS levels were evaluated to understand if the increase of glucose concentration could be related to an increase of inflammatory state. NF-κB levels are higher in C28/I2 cells growth at high glucose concentration, both in cells grown in FBS and ITS supplemented media. Also iNOS seems to be higher in C28/I2 cells growth at high glucose concentration. NF-κB activation could lead cells into autophagic or apoptosis process and autophagy is key fundamental process activated in chondrocytes cells to maintain cartilage homeostasis (Lotz & Caramés, 2011); for this reason levels of LC3I/II were analyzed into cells growth at different glucose concentration. Results demonstrate that high glucose media block

autophagic process in chondrocytes and this reduction is higher than the effect generated by IL-1β stimulation. At the end effect of glucose concentration on human primary chondrocytes cells was evaluated after only 24 h to understand which signaling pathways can be activated by high glucose environment. In particular phosphorylation of ERK1/2, p38, Akt and p65 is altered in chondrocytes growth at high glucose concentration and this correlates with an increase secretion of MMP-13 which is the major MMP involved in cartilage matrix degradation and OA.

ROS levels seems to have a central role in chondrocytes alteration induced by high glucose. To analyze better the role of ROS levels in the chondrocytes I had the possibility to work for 6 months in the Dr.Loeser Lab at the School of Medicine in the University of North Carolina at Chapel Hill, which is one of the best lab in the cartilage biology field. So, the third chapter of this thesis is about my work on PRX6 which is a peroxiredoxin involved in the recovery from the H_2O_2 generated in cells. In human there are 6 PRX proteins, but PRX6 is the only one having only one cysteine residue responsible for the reducing of H_2O_2 generated inside the cells (Cox, Winterbourn, & Hampton, 2010; Aron B. Fisher, 2017). Analyses of the mass spectrometry data, obtained from cell lysates of primary chondrocytes treated with 30 min with H_2O_2 or 30 min with Fn-f, revealed that PRX6 was the second protein with oxidation on cysteine residue by the treatment with H_2O_2 and Fn-f. For this reason, PRX6 could play a central role in the answer against ROS generated in chondrocytes. Normal primary chondrocytes cells were used to produce the cell lysates and analyzed with western blots to see if the oxidation state of PRX6 can change in response to different stimuli, like H_2O_2, Fn-f, menadione (men), DMNQ. All these molecules are used to increase the production of ROS inside the cells. Chondrocytes cell are treated with these molecules from 0 to 60 min, and the cell lysates were analyzed using reducing and non-reducing SDS page. Chondrocytes treatment with H_2O_2

and menadione induce a PRX6 band shift in the non-reducing gels, so an oxidation occur after this treatment. The shift is not detectable when cells are stimulated with Fn-f or DMNQ. PRX6 require GSH to resolve the cysteine oxidation, for this reason experiment of immunoprecipitation were done to observe if the shift is due to the binding of PRX6 with GSH. PRX6 were immunoprecipitated (IP) in cell lysates from chondrocytes treated for 30 min with H_2O_2, menadione, Fn-f. A strong band of GSH were found in the IP sample treated with H_2O_2 for 30 min. PRX6 is involved in the resolving of the lipid peroxidation of membrane phospholipids. For this reason 4-HNE protein adducts were evaluated after treatment with H_2O_2 or menadione. However, no lipid peroxidation was induced by H_2O_2 or menadione treatment. After this experiment, we wanted to see if PRX6 could impact the MAPK signaling pathways in cells. So chondrocytes cell overexpressing PRX6 were treated with IGF-1, menadione and combination with menadione and IGF-1. Overexpression of PRX6 change the basal levels of phosphor Akt in chondrocytes and altered the phosphorylation of p38 in chondrocytes cells pretreated with menadione and then treated with IGF-1. The effect of PRX6 overexpression on MAPK pathways was also evaluated in chondrocytes treated with Fn-f. Pathways of JNK, c-Jun, p38, ERK1/2 and NF-κB were evaluated. Overexpression of PRX6 decrease the Fn-f-induced phosphorylation of p38 and c-Jun. Surprisingly, the overexpression of Prdx6 increase the levels of MMP-13 released by chondrocytes. At the end the localization of PRX6 was analyzed using nuclear and cytoplasm extraction. PRX6 is not only a cytoplasmatic protein and is present in the nuclear extract of all cells. So PRX6 could interact with some nuclear protein and influence the transcription of some genes. In conclusion in this chapter oxidation state of PRX6 and the effect of PRX6 on ROS-induced cell signaling was evaluated in human primary chondrocytes given a brief description on the roles of PRX6 in chondrocytes cells.

In the fourth chapter of this thesis, made in collaboration with the Prof. Laura Cipolla and Prof. Maddalena Collini laboratories, we developed and characterized a new gelatin-based hydrogel. Recent therapy, used to increase self-repair of cartilaginous tissue, which is composed mainly of intricated ECM, is to inject and to use biomaterials scaffold. Scaffold design for tissue engineering has to face several challenges, such as suitable mechanical properties, cell adhesive cues, as well as excellent biocompatibility and biodegradability (H. Long, Ma, Xiao, Ren, & Yang, 2017). Three-dimensional cell culture platforms offer in vitro better chances to mimic the native microenvironment (extra-cellular matrix, ECM) and cell behavior over 2D cell culture techniques (Edmondson, Broglie, Adcock, & Yang, 2014). Among natural polymers, gelatin (obtained from collagen hydrolysis) is an attractive candidate for hydrogel preparation, since it is biocompatible, possess cell-adhesive properties, has limited costs and it is easily accessible. Gelatin is water-soluble at 37 °C and is featured by poor mechanical properties (Jaipan, Nguyen, & Narayan, 2017) however, the mechanical and chemical properties of gelatin can be modified with different crosslinking agents (Caliari & Burdick, 2016; Tam, Smith, & Shoichet, 2017). In this work we investigate the properties of gelatin-based hydrogels obtained using 3,4-diethoxy-3-cyclobutene-1,2-dione or diethyl squarate (DES) as homobifunctional cross-linker. Two different gelatin based hydrogels were produced changing the initial weight of gelatin used for the cross-link reaction. Cross-linked gelatin hydrogels (5% and 10% Gel-DES) were lyophilized, and then characterized for their chemical, physical and biological properties. Infrared (IR) peaks confirms the gelatin cross-linking by DES and SEM images demonstrate that average pores dimension of 5% Gel-DES is higher than average pores dimension of 10% Gel-DES. Water retaining ability is also highter in 5% Gel-DES in comperison to 10% Gel-DES and it's degradation time is faster then 10% Gel-DES. For biocompatibility analyses C28/I2 chondorcytes and HEK293

cells were plated on the hydrogels and mantained for 2 weeks. Both cell lines attach the material and colonize the hydrogels, however C28/I2 cells seems to prefer more the 5% Gel-DES instead of 10% Gel-DES. Cells morphology was different and HEK293 cells appera more rounded and seems to prefer cell-cell contact instead to cell-hydrogel contact, forming aggregates of rounded cells. Also we analyse the drug release ability of the 5% Gel-DES, using rhodamine. However the behaviour suggest that hydrogel is more efficent in drug diffusion among its pores than in drug release. Diffusion properties were analyzed as well and also the ability of glod nanoparticles to move inside the hydrogel after laser exitation. Diethyl squarate (DES) resulted an effective cross-linking agent for the production of novel gelatin-based hydrogels which can be used for multiple applications.

Riassunto

L'osteoartrite (OA) è una delle malattie reumatiche con più alta incidenza nel mondo moderno e rappresenta la pricipale cause di disabilità dopo i 40 anni (Vos et al., 2012). L'invecchiamento, traumi articolari e ossei, predisposizione genetica, obesità e diabete sono spesso associati all'insorgenza di tale malattia. L'OA è caratterizzata da un'alterata omeostasi del tessuto cartilagineo che porta ad un aumento delle attività degli enzimi catabolici quali metalloproteinasi della matricie (MMP-1, -3 e -13) e alla bassa produzione di collagene di tipo II e aggrecani, aumentando quindi la degradazione della matrice cartilaginea. I condrociti sono le uniche cellule presenti nella cartilagine e sono responsabili della biosintesi e del riparo della matrice cartilaginea (Le Clanche et al. 2016; Goldring and Marcu 2009). Diversi studi hanno dimostrato che vi è un'associazione tra diabete di tipo 2 e OA (Le Clanche et al. 2016). In particolare, l'iperglicemia, presente in pazienti diabetici, può alterare proteine strutturali e funzinali presenti nella matrice cartilaginea come il collagene, favorendo processi di glicazione non enzimatica che ne alterano le proprietà (Snedeker & Gautieri, 2014). Inoltre l'iperglicemia e l'invecchiamento favoriscono la generazione di specie reattive dell'ossigeno (ROS) nei condrociti promuovendo l'attivazione di pathways pro-infiammatori. Questo aumenta il rilascio di citochine e MMPs da parte dei condrociti, favorendo la degradazione della matrice e processi infiammatori a livello articolare (Le Clanche et al. 2016; Firestein et al. 2017). L'aumento dei ROS intracellulari porta anche ad un incremento della morte cellulare che può essere alla base di una decellularizzazione del tessuto cartilagineo. Questo processo è frequentemente associato alla patogenesi dell'OA (Del Carlo & Loeser, 2008). Nonostante i numerosi sforzi il corretto meccanismo molecolare che sta alla base dell'associazione tra diabete e OA è ancora da scoprire.

Il secondo capitolo di questa tesi ha come scopo quello di analizzare gli effetti dell'alto glucosio sui condrociti umani C28/I2. Prima di tutto 6 differenti concentrazioni di glucosio sono state utilizzate per valutare la concentrazione migliore in cui crescere i condrociti. I risultati hanno dimostrato che i condrociti C28/I2 crescono meglio se mantenuti in terreno con 2.5 mM di glucosio che è stata utilizzata come concentrazione normale di glucosio mentre la concentrazione di 25 mM di glucosio è stata usata per simulare un ambienta ad alto glucosio. I condrociti cresciuti in alto glucosio presentano livelli alti di ROS e un abbassamento della vitalità cellulare. Inoltre il citoscheletro di tali cellule è profondamente disorganizzato e correla con un'abbassamento dei livelli di RalA-GTP. RalA è una piccola proteina G che è in grado di regolare l'organizzazione del citoscheletro grazie a Cdc42 e Rac1 che sono suoi effettori. Lo stesso esperimento è stato ripetuto crescendo le cellule C28/I2 in un terreno conenente ITS che viene utilizzata per bloccare il dedifferenziamento i condrociti in piastra. Inoltre l'IL-1β è stata utilizzata per simulare un'ambiente di tipo osteoartritico. I livelli di RalA-GTP sono più alti in cellule C28/I2 cresciute in terreni con livelli normali di glucosio e il trattamento con IL-1β riduce i livelli di RalA-GTP. L'alto glucosio inoltre diminuisce drasticamente i livelli di RalA-GTP. Successivamente i livelli di ERK1/2 sono stati analizzati ed è stato riscontrato che l'alto glucosio e l'IL-1β diminuiscono la fosforilazione di ERK1/2 in condrociti C28/I2. I livelli di NF-κB e iNOS sono stati analizzati per capire se l'alto glucosio può alterane i livelli simulando uno stato infiammatorio nei condrociti. I livelli di entrambe le proteine sembrano aumentare nei condrociti manteuti per 72 h in alto glucosio. L'attivazione del fattore NF-κB può promuovere processi autofagici o apoptotici nelle cellule. Inoltre l'autofagia è un processo chiave per il mantenimento dell'omeostasi della matrice cartilaginea da parte dei condrociti (Lotz & Caramés, 2011); per questo il livelli della proteina LC3I/II sono stati valutati in condrociti cresciuti a differenti concentrazioni di

glucosio. I risultati dimostrano che l'alto glucosio è in grado di bloccare l'autofagia nei condrociti e che l'effetto inibitorio del glucosio è maggire rispetto all'inibizione dell'autofagia che si ottiene dall'aggiunta dell'IL-1β. In conclusione gli effetti del alto glucosio sono stati valutati anche usando condrociti primari per capire gli effetti di una breve esposizione (24h) analizzando pathway chive dei condrociti. In particolare l'alto glucosio è in grado di alterare i pathway di ERK1/2, p38, Akt e p65 portando ad un aumento dei livelli di secrezione della MMP-13 associata allo sviluppo di osteoartrite.

L'alto glucosio favorisce la produzione di ROS nei condrociti e proprio la genesi di ROS intracellulari sembra avere un ruolo preponderante nella risposta dei condrociti ad alti livelli di glucosio. Con lo scopo di analizzare meglio il ruolo dei ROS nei condrociti, ho avuto la possibilità di lavorare per 6 mesi nel laboratorio del Dott. Richard Loeser presso la School of Medicine dell'Università della North Carolina a Chapel Hill, il quale è uno dei massimi esperti nel campo dei ROS e della biologia dei condrociti. Il terzo capitolo di questa tesi di dottorato è focalizzato sul ruolo di PRX6; una perossiredossina coinvolta necessaria per la detossificazione del perossido di idrogeno generata nelle cellule. Nell'uomo vi sono 6 differenti proteine appartenenti alla famiglia della perossiredossine, tuttavia, PRX6 è unica nel suo genere, in quanto la sua attività catalitica si basa su un solo residuo di cisteina che viene utilizzato per ridurre l'H_2O_2. Dati ottenuti tramite spettrometria di massa da condrociti primari trattati con H_2O_2 o con Fn-f per 30 min, dimostrano che la PRX6 è la seconda proteina a livello di abbondanza relativa che presenta ossidazione a livello delle cisteine nei campioni trattati con H_2O_2 o con Fn-f. PRX6 potrebbe quindi essere fondamentale per la risposta allo stress ossidativo nei condrociti. Lo stato di ossidazione della PRX6 è stato valutato tramite western blot usando lisati cellulari di condrociti primari trattati con H_2O_2, Fn-f, menadione (men) e DMNQ. La risposta dei condrociti a tali trattamenti porta all'aumento dei ROS intracellulari. I condrociti sono stati

stimolati con queste molecole per differenti tempi da 0 a 60 min e successivamente i lisati cellulari sono stati analizzati tramite SDS-gel page in condizioni riducenti e non riducenti. Uno shift di banda relativo a PRX6 è stato osservato nei lisati dei cellule trattate con H_2O_2 o con menadione in condizioni di SDS-page non riducenti. Tale spostamento non è osservabile nei campioni delle cellule trattate con DMNQ e Fn-f. Inoltre, la PRX6 per poter completare il ciclo catalitico necessita del legame di una molecola di GSH tramite ponte disolfuro sulla cisteina ossidata da H_2O_2. Tramite un'esperimento di immunoprecipitazione si è voluto verificare se lo spostamento di banda fosse dovuto al legame con GSH. I lisati proteici di condrociti trattati per 30 min con H_2O_2, Fn-f e menadione, sono stati utilizzati per immunoprecipitare PRX6 ed un grade segnale relativo a GSH è stato osservato nel campione trattato con H_2O_2 per 30 min. Siccome la PRX6 è in grado di risolvere i prodotti dovuti all'ossidazione dei lipidi di membrana, i livelli di 4-HNE sono stati analizzati per valutare se il trattamento dei condrociti con l'H_2O_2 e il menadione può favorire tale processo. Tuttavia, i trattamenti con H_2O_2 o con menadione non inducono un aumento dei livelli di 4-HNE nei condrociti. Dopo questi esperimenti abbiamo valutato se PRX6 è in grado di influenzare l'attivazione di pathway MAP chinasici. Quindi, condrociti primari che overesprimono PRX6 sono stati stimolati con IGF-1, menadione e una combinazione tra menadione e IGF-1. I livelli basali di fosfo-Akt sono sensibilmente più alti in condrociti che overesprimono PRX6. Inoltre l'overespressione di PRX6 modifica i livelli di fosfo-p38 in condrociti pretrattati con menadione e in seguito trattati con IGF-1. Successivamente l'effetto dell'overespressione di PRX6 è stata valutata sui pathway attivati dalla Fn-f. l'aumento dei livelli intracellulari di PRX6 mantiene bassi i livelli di fosfo-p38 e fosfo-c-Jun in cellule trattate con Fn-f. Sorprendentemente, nonostante l'abbassamento dei livelli di fosfo-p38 e fosfo-c-Jun, i livelli di secrezione della MMP-13 sono sensibilmente più alti in

condrociti che overespriono PRX6. Infine la localizzazione della PRX6 è stata valutata tramite l'uso di lisati proteici ottenuti dal nucleo e lisati citosolitici. Il rispultato dimostra che la PRX6 non è soltanto una proteina citoplasmatica ma è presente anche nel nucleo dove potrebbe interagire con fattori di trascrizione e altre proteine influenzando l'espressione di alcuni geni. In colclusione in questo capitolo è stata valutato lo stato di ossidazione di PRX6, gli effetti di PRX6 sui pathways attivati dai ROS nei condrociti primari umani, dando una breve descrizione del ruolo che la PRX6 può avere in queste cellule.

Il quarto ed ultimo capitolo di questa tesi è dedicato al lavoro relativo allo sviluppo e caratterizzazione delle proprietà chimico-fisico di un nuovo hydrogel a base di gelatina. Numerose terapie volte ad incrementare l'autoriparazione dei tessuti cartilaginei, utilizzano hydrogel iniettabili o biomaterialli innovativi sviluppati per mimare le proprietà della matrice extracellulare. Tuttavia tali approcci innovativi di ingegneria tissutale devono far fronte a numerose problematiche come il mimare correttamente le proprietà meccaniche del tessuto, favorire l'adesione cellulare al nuovo biomateriale che deve necessariamente essere altamente biocompatibile e biodegradabile (H. Long et al., 2017). Inoltre l'uso di hydrogel permette di crescere cellule in un ambiente 3D che risulta più simile al microambiente fisiologico cellulare e il comportamento cellulare è più simile a quello fisiologico ripetto a cellule cresciute in una superficie bidimensionale (Edmondson et al., 2014). La gelatina è altamente biocompatibile, è in grado di favorire l'adesione cellulare, ha basso costo e si ottiene per idrolisi acida del collagene, queste proprietà la rendono uno dei polimeri naturali più adatto per lo sviluppo di nuovi hydrogels. Tuttavia hydrogel a base di sola gelatina si sfaldano a 37°C (Jaipan et al., 2017); per tale motivo agenti crosslinkanti sono necessari per cambiarne le proprietà chimiche e meccaniche (Caliari & Burdick, 2016; Tam et al., 2017). In collaborazione con i laboratorio della professoressa Laura Cipolla e il laboratorio della professoressa

Elisabetta Collini, è stato sviluppato un nuovo hydrogel a base di gelatina crosslinkata tramite dietilsquarato (DES). Sono stati prodotti due differenti hydrogels che si differenziano per la quantità iniziale di gelatina utilizzata per la reazione di crosslink. Gli hydrogels creati (5% e 10% Gel-DES) sono stati liofilizzati e sono stati caratterizzati per le loro proprietà chimico-fisiche e biologiche. I picchi ottenuti tramite analisi di spettroscopia IR a trasformata di Fourier dimostrano che la reazione di crosslink è avvenuta perfettamente in entrambi gli hydrogels e le immagini al SEM dimostrano che i pori del 5% Gel-DES sono di dimensioni maggiori rispetto ai pori dell'hydrogel 10% Gel-DES. Inoltre l'hydrogel 5% Gel-DES presenta un ritenzione idrica maggiore rispetto a quella del 10% Gel-DES. Le cellule di condrociti umani C28/I2 e la linea cellulare HEK293 sono state utilizzate per verificare la biocompatibilità del nuovo biomateriale. Le cellule sono state coltivate all'interno dell'hydrogel per due settimane e le cellule C28/I2 preferiscono di gran lunga l'hydrogel 5% Gel-DES rispetto al 10% Gel-DES. La morfologia delle due linee cellulari cresiute all'interno dell'hydrogel risulta molto differente; in particolare le cellule HEK293 appaiono più rotondeggianti e preferiscono il contatto cellula-cellula rispetto al contatto cellula-hydrogel, infatti formano aggregati che colonnizzano anche la parte centrale delle maglie dell'hydrogel. Inoltre, grazie all'uso di rodamina si è analizzata la propensione dell'hydrogel per il rilascio graduale di molecole farmacologicamente attive. Tuttavia, l'hydrogel sembra molto più efficiente nel diffondere il farmaco tra le sue magle rispetto al rilasio del farmaco. Sono quindi state analizzate le proprietà diffusive del nuovo biomateriale e anche il movimento di nanoparticelle d'oro inglobate all'interno dell'hydrogel attraverso l'eccitazione di un laser simulando una terapia fototermica. In conclusione il dietilsquarato è risultato essere una molecola promettente per il crosslink chimico della gelatina atto alla produzione di nuovi hydrogels utilizzabili per differenti applicazioni e studi.

Chapter 1 - Introduction

1.1 ARTICULAR CARTILAGE

Cartilage is a flexible, avascular, aneural and alymphatic connective tissue. Cartilage is found in the synovial joint, spine, ribs, external ears, nose and airways and is fundamental for the correct bone growth in the children and adolescence (Athanasiou, Darling, DuRaine, Hu, & Hari Reddi, 2013; Wachsmuth, Söder, Fan, Finger, & Aigner, 2006). Cartilage exert different functions in different part of the body. In the joint, articular cartilage is responsible for resist to the mechanical loading. However, cartilage present in the nose and ear has the aim to maintain the form. While, the tracheal cartilage is responsible for preventing the organ from collapse during the inspiration (Wachsmuth et al., 2006). For this reasons, there are three major types of cartilage found in humans which differs one from the other one for their biomechanical properties given by their extracellular matrix: hyaline, fibrous and elastic cartilage (Armiento, Alini, & Stoddart, 2019; Wachsmuth et al., 2006). Cartilage is composed for more than 95% by water dissolved solutes and structural proteins like collagens and proteoglycans (Athanasiou et al., 2013; Wachsmuth et al., 2006). All three types of cartilage have low density of cells, called chondrocytes which are the unique terminally differentiated cell unit, present into the tissue (Stockwell, 1967). Chondrocytes synthesize and secrete the major components of the extracellular matrix (ECM) which is different between the three cartilage tissues.

Fibrous cartilage, found in the intervertebral discs and in other locations such as the menisci, bone-tendon interface and ligament tendon interface (Apostolakos et al., 2014; Benjamin & Ralphs, 1998), has high density of type I collagen that guarantee an high tensile strength (Benjamin & Ralphs, 2004). Fibrocartilage has type VI collagen in the pericellular matrix and low amount of type II collagen

and proteoglycans into the ECM (Wachsmuth et al., 2006). Chondrocytes are very low in number and are aligned with the thick collagen fibers (Armiento et al., 2019).

Elastic cartilage, is flexible and elastic cartilage is able to resist to a repeated bending. The ECM of elastic cartilage is composed by type II collagen, proteoglycans and elastin fibers (Armiento et al., 2019; Krishnan & Grodzinsky, 2018). Chondrocyte are larger and are lying between the elastin fibers; there are fewer isogenous groups compared to the hyaline cartilage. The function of this cartilage is to give elasticity to the organs within which it is present such as: epiglottis, auricle and eustachian tube (Armiento et al., 2019; Krishnan & Grodzinsky, 2018).

Hyaline cartilage is the most common type of cartilage encountered in the human body (Armiento et al., 2019; Sun & Beier, 2014). Hyaline cartilage has a central role in the development of the skeleton in fact during the embryotic phase the skeleton is composed by hyaline cartilage that is gradually replaced by the bone tissue during the development (Onyekwelu, Goldring, & Hidaka, 2009). Hyaline growth cartilage or growth plate serves as a template for the long bone formation in children (Charlier et al., 2019). It is present at the connection of the ribs and the sternum, nose, trachea, bronchi, larynx, growth plates and in the articular surfaces of the synovial joints (Krishnan & Grodzinsky, 2018). Articular hyaline cartilage enables joint movements by providing a lubrication surface with an extremely low coefficient of friction (Unsworth, Dowson, & Wright, 1975). Hyaline cartilage acts as a damper and has high resiliency and deformability; all these properties are needed to protect joint from compressive loads (Cohen, Foster, & Mow, 1998). Articular cartilage is 2 to 4 mm thick tissue composed of a dense ECM with a sparse distributions of chondrocytes cells (Sophia Fox, Bedi, & Rodeo, 2009). The ratio volume matrix/cell is high, and chondrocytes account

only for 10% of the wet weight of articular cartilage (Charlier et al., 2019; Cohen et al., 1998). The ECM is principally composed of water, collagen and proteoglycans with other non collagenous proteins and glycoproteins present in lesser amount (J. A. Buckwalter & Mankin, 1998; Sophia Fox et al., 2009). These components help to retain water within the ECM and are fundamental for the biomechanics of the tissue (S. R. Goldring & Goldring, 2016). Water account for 60 to 85% of the wet weight of the tissue (Mow, Ratcliffe, & Robin Poole, 1992). Different types of collagen molecules are expressed in the articular cartilage, but the backbone of type II collagen fibrillar network is an heteropolymeric structure with collagen IX molecules covalently linked to the surface of collagen II and collagen XI forming the inner filamentous template of the fibril as a whole (D. R. Eyre, Weis, & Wu, 2006). The physical properties of the articular cartilage are determined by this fibrillar collagen network, which provides tensile strength, and by the entrapped proteoglycan aggregates which provide compressive resilience (Andriacchi & Favre, 2014; S. R. Goldring & Goldring, 2016; H. Guo, Maher, & Torzilli, 2015). During compression, water molecules associated with the hydrophilic glycosaminoglycan chains and the charged solutes are extruded. When the compression forces ended, the proteoglycans have sufficient fixed charge to osmotically reabsorb the water and small solutes into the matrix, resulting in restoration of the original cartilage dimensions (S. R. Goldring & Goldring, 2016). Type VI collagen is found in the pericellular matrix and enables chondrocytes to feel changes in the surrounding matrix and respond to them (D. Eyre, 2002). However articular cartilage hasn't a simple structure at all, collagen is quite heterogeneous in terms of collagen fibrils orientations as well as in cell shape and distribution (Charlier et al., 2019). These different orientations of collagen fibrils define 4 zones in cartilage that are seen with the cross sectional view with electron microscopy: the superficial zone, the middle zone, the deep zone and the calcified zone (Ernst B. Hunziker, Michel, & Studer, 1997; Sophia

Fox et al., 2009). Within each zone, there are three regions: pericellular region, territorial region and interterritorial region (Sophia Fox et al., 2009).

The superficial zone or tangential zone represents 10 to 20% of the total cartilage thickness, and protects the deeper layers from the shear stresses. Chondrocytes in this zone are elongated and they secrete type II, IX and XI collagen fibrils, which are disposed in tangential array (D. Eyre, 2002; Firestein et al., 2017). There are high concentration of small proteoglycan like decorin, and a low concentration of aggrecan.

The middle zone or transitional, accounts for 40% to 60% of cartilage weight, is composed of rounded chondrocytes surrounded by radial bundles of collagen fibrils thicker than in other zones (Richardson et al., 2003). This is the first line of resistance to compressive forces.

In the deep (or radial) zone represent from 30% to 40% of the total cartilage and chondrocyte are grouped in columns or clusters (Akkiraju & Nohe, 2015). It provides the greatest resistance to compressive forces; collagen fibrils are arranged perpendicular to the articular surface. There are collagen fibrils with the largest diameter and in radial disposition and chondrocytes are arranged parallel to the collagen fibers and perpendicular to the joint line. The deep zone contains the highest proteoglycan content and the lowest water content (Firestein et al., 2017; Sophia Fox et al., 2009).

The profound layer is the thinnest one called calcified cartilage and is behind the tide mark which divide the deep zone from the calcified cartilage. These calcified layers plays an important role in securing the cartilage to bone and in anchoring the collagen fibrils of the deep zone to the subchondral bone. Chondrocytes resident in the calcified cartilage are scarce and with an hypertrophic phenotypes (Akkiraju & Nohe, 2015; Sophia Fox et al., 2009). This layer is the result of the

endochondral ossification and persists after growth plate closure (Firestein et al., 2017; Onyekwelu et al., 2009; Simkin, 2012). Undulation in the interfaces between the articular cartilage, calcified cartilage, ad underlying cortical plate help to transform shear stresses into compressive and tensile stress during joint loading and motion (Burr & Gallant, 2012).

Cell density decreases from the surface to the deep zone, but the chondrocytes volume increase in the middle zone and deep zone; here chondrocytes volume is twice respect to cell volume of superficial chondrocytes (Firestein et al., 2017).

Furthermore, other to differ 4 zones (Fig.1), the ECM of each zone can be divided into 3 regions based to the proximity to the chondrocytes, composition and collagen fibers. ECM regions are pericellular, territorial and interterritorial regions. The thin layer of ECM which surround the chondrocyte cells are called the pericellular matrix. Together the pericellular matrix and chondrocyte are termed chondron. It contains mainly proteoglycan, especially biglycan and perlecan, fibronectin 1, and type VI collagen, however, other collagen type are present like type II and type IX collagen (Guilak, Nims, Dicks, Wu, & Meulenbelt, 2018; C. A. Poole, Ayad, & Gilbert, 1992). Pericellular matrix has an important role in regulating the function of the chondrocytes, is the first line of matrix that connect the chondrocyte to the extracellular environment. Every type of chemical or physical signals that arrived to the chondrocytes pass through the pericellular matrix which can modulate these signals (Guilak et al., 2018; Wilusz, Sanchez-Adams, & Guilak, 2014). Data from experimental studies confirm that pericellular matrix has an important role in regulate chondrocyte physiology and cartilage ECM homeostasis. It can modulate the stress-strain, osmotic and fluid flow environments of chondrocyte, influencing the chondrocyte mechanotransduction process (Guilak et al., 2018; Vincent, 2013; L. Xu et al., 2011).

The territorial matrix surrounds the pericellular matrix and connect it to the interterritorial regions. The composition of territorial matrix is mostly by fine collagen fibrils forming a basketlike network around the cells (Muir, 1995; Sophia Fox et al., 2009). That region is thicker than the pericellular matrix, and it may protect cartilage cells against mechanical stresses and may contribute to the resiliency of the articular cartilage structure and its ability to withstand to substantial loads (Sophia Fox et al., 2009).

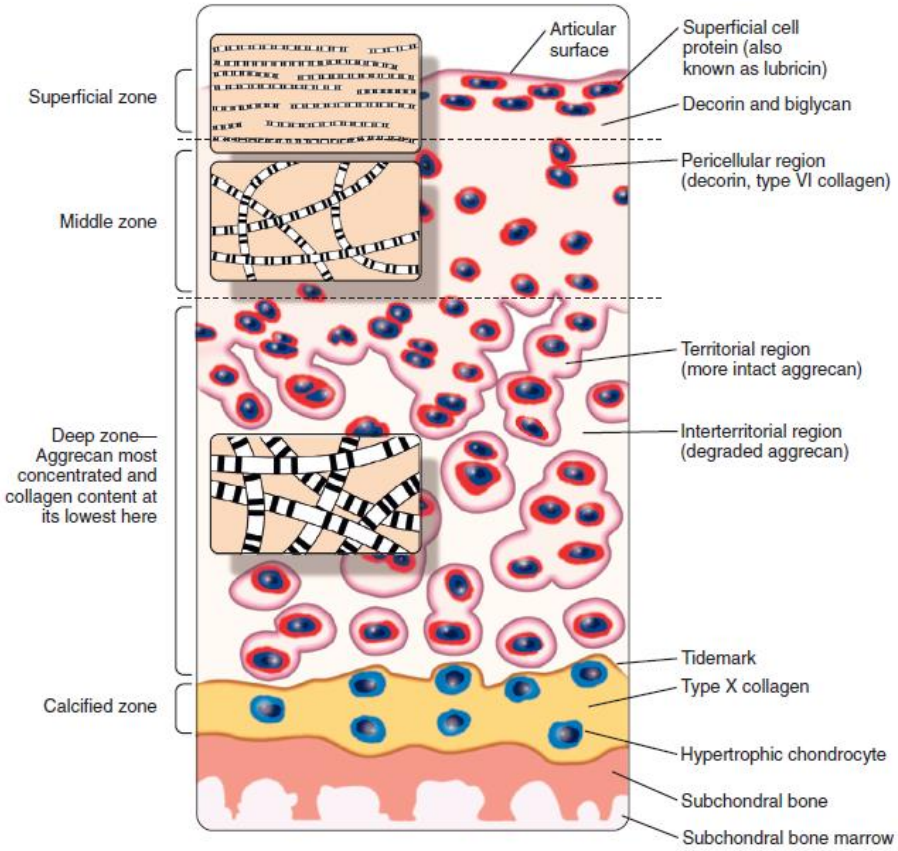

Figure 1. **Structure of human articular cartilage with the different zones: Superficial, middle, deep and calcified.** The image shows the chondrocyte cells in red and blue, with the ECM divided into pericellular, territorial and interterritorial regions. Collagen fibrils orientation are represented in the rectangle inserts on the left of the image. From (A. R. Poole et al., 2001).

The largest region is the interterritorial regions which is the most important region that regulate the biomechanical properties of articular cartilage (Mow & Guo, 2002; Sophia Fox et al., 2009). Collagen fibrils are large and oriented parallel to the surface in the superficial zone, obliquely in the middle zone and perpendicular to the joint surface in the deep zone (Sophia Fox et al., 2009).

1.2 CHONDROCYTES

Chondrocytes are the resident cell type present in articular cartilage. Chondrocytes play an active role in the development, maintenance and repair of the ECM. Chondrocytes of the articular cartilage are metabolically active cells that synthesize and turnover a large volume of ECM components such as collagen, glycoproteins, proteoglycans and hyaluronan (Archer & Francis-West, 2003). Mature chondrocytes cells are round or polygonal cells located into the ECM of articular cartilage with a mean diameter of 13 μm, chondrocytes represent only 1% to 5% of the total cartilage volume (Bhosale & Richardson, 2008; Z. Lin, Willers, Xu, & Zheng, 2006; Sophia Fox et al., 2009). Nucleus of chondrocytes are usually round or oval containing one or several nucleoli, based on the species. In the cytoplasm chondrocytes contain elongated mitochondria, occasionally lipid droplets and variable amount of glycogen. When new components of ECM is produced the cytoplasm becomes more basophilic and the Golgi region becomes unusually large (Z. Lin et al., 2006).

Because cartilage is not a vascularized tissue, chondrocytes must rely on diffusion form the articular surface or subchondral bone for exchange nutrients and metabolites. Chondrocytes maintain active membrane transport system for exchange cation like Na^+, K^+, Ca^{2+} and H^+. Their concentration change with load and different composition of ECM (Firestein et al., 2017). Mechanical loading is essential for chondrocyte and they can feel different pressure and change the composition of the ECM. On this way, cytoskeleton have a big role in the sensing

of mechanical stimuli and regulate the downstream signaling (Blain, 2009). Chondrocyte cytoskeleton comprises actin microfilaments, tubulin microtubules and vimentin intermediate filaments (Benjamin, Archer, & Ralphs, 1994). F-actin is cortical in localization and is mostly distributed at the periphery of the chondrocyte (Blain, 2009; Trickey, Vail, & Guilak, 2004). The tubulin microtubules form a loose basket-like mesh uniformly distributes throughout the chondrocyte cytoplasm (Trickey et al., 2004). Vimentin intermediate filament are distributed in the cytoplasm of the cells from the cell periphery to the nuclear membrane forming and highly organized network (Blain, 2009; Fioravanti, Nerucci, Annefeld, Collodel, & Marcolongo, 2003; Trickey et al., 2004). Actin filament is essential in the maintenance of chondrocyte phenotype by regulating the cells shape. Actin stress fibres are produced in de-differentiated chondrocyte, which has found to have flattened shape, increase expression of type I collagen and decrease expression of type II collagen and aggrecan (Archer, Rooney, & Wolpert, 1982; Glowacki, Trepman, & Folkman, 1983). However chondrocyte re-differentiation is possible growing the cell in a three dimensional environment or using cytochalasin B/D to restore the rounded shape (Blain, 2009; Loty, Forest, Boulekbache, & Sautier, 1995). In chondrocytes, the tubulin network is essential for the synthesis and secretion of both collagens and proteoglycans. Furthermore tubulin is present in the primary cilia of chondrocytes, in which there is a direct connection between the extracellular collagen fibres and the proteins which decorate the ciliary microtubules (Poole, Zhang, and Ross 2001). Disruption of microtubular network in chondrocyte using colchicine inhibited the synthesis and the secretion of proteoglycans and collagen (Blain, 2009; Takigawa, Takano, Shirai, & Suzuki, 1984).

According to the secretory and morphology profiles chondrocyte can be divided into different phenotypes. Pre-chondrocytic mesenchymal cells express type I, type III and type V collagens (Mary B. Goldring, 2012), whereas differentiated

chondroprogenitor cells express type IIA procollagen (McAlinden, Shim, Wirthlin, Ravindran, & Hering, 2012; Sandell, Nalin, & Reife, 1994). Differentiated chondrocytes produce type II, type IX and XI collagens, however the most prominent form in the type II collagen (D. Eyre, 2002; D. R. Eyre et al., 2006). Hypertrophic chondrocytes at the terminal differentiation stage secrete type X collagen (Charlier et al., 2019). Post-hypertrophic chondrocytes are characterized in vitro by the secretion of type I and type X collagen (Charlier et al., 2019; Kirsch, Swoboda, & von der Mark, 1992). Furthermore, fibroblastic-like cells, called dedifferentiated chondrocytes secreting type I and type III collagen has been identified in vitro (Z. Lin et al., 2006; Sokolove & Lepus, 2013).

1.3 CHONDROGENESIS

Chondrocytes cells arise from pluripotential MSCs and chondrogenesis is a very important passage for the skeleton development during the embryogenesis. MSCs of the blastema can differentiate into cartilage, muscle or bone cells. Differentiation process to produce chondrocytes from MSC is named chondrogenesis and required four general step: cells migration, aggregation by mesenchymal-epithelial cell interaction, condensation and chondrocytes differentiation. Craniofacial cartilage is formed from cranial neural crest cells; the cartilage of the axial skeleton is formed from paraxial mesoderm while the articular cartilage is derived from the lateral plate mesoderm (Firestein et al., 2017). Primary chondrocyte arise in the embryo from mesoderm or from the neural crest where the facial skeleton is generated (Archer & Francis-West, 2003; Z. Lin et al., 2006). Secondary chondrocytes arise from the periosteal layer surrounding membranous bone upon mechanical stimulation (Archer & Francis-West, 2003). Commitment of mesenchymal limb bud cells of mesodermal origins to this chondrogenic fate is evident when their aggregation forms cellular

condensation that prefigure the skeletal analgen (Thorogood & Hinchliffe, 1975), these chondroprogenitor cells express type IIA collagen and are embedded in a hyaluronan-rich ECM. The aggregation coincides with the depletion of hyaluronan from the ECM and the expression of cadherin-2 (neural cadherin), neural cell adhesion molecule 1, tenascin-C and the transcription factor SOX9 which is essential for chondrocyte differentiation (Onyekwelu et al., 2009). These condensation step is facilitated by the collective contribution of both cell-cell interaction and cell-matrix interactions. Recent studies shown that cell-cell adhesion proteins NCAM and N-cadherin, and ECM protein fibronectin are essential for this initial step (Singh & Schwarzbauer, 2014). Condensed cells differentiate into chondrocytes in a process tightly regulated by the transcription factors SOX9 (Lefebvre & Dvir-Ginzberg, 2017). These transcription factor is necessary for early chondrogenesis and for the subsequent differentiation program of growth plate chondrocytes including the transition to hypertrophy (Singh, Marcu, Goldring, & Otero, 2019). In mice, deletion of SOX9 in the mesenchyme disrupts condensation events and it's inactivation at later stage of development restricts proliferation and induces cartilage and joint formation defects (Akiyama, Chaboissier, Martin, Schedl, & De Crombrugghe, 2002; Akiyama et al., 2005). Recent studies shown that SOX9 in conjunction with SOX5, SOX6 and interaction with CEBP/p300, regulates the expression of the chondrocyte specific genes like *Col2a1* and *Acan*, leading to deposition of type II collagen and proteoglycans (Lefebvre & Dvir-Ginzberg, 2017; Singh et al., 2019; Tsuda, Takahashi, Takahashi, & Asahara, 2003). Some studies suggested that also Notch signaling coordinates these chondrogenic differentiation initiate by *Sox9*, and that SOX9 has role in pre-chondrocytic mesenchymal commitment and an intimate link with type IIA collagen expression (Mead & Yutzey, 2009; Pitsillides & Beier, 2011). So SOX9 is an early marker of the differentiating chondrocytes and is required for the expression of the main ECM components,

and the expression of SOX proteins depends on the signaling through mammalian homologs of *Drosophila* mothers against decapentaplegic (SMADs) which are functionally active in differentiation chondrocytes (Firestein et al., 2017; Song, Estrada, & Lyons, 2009). SOX9 may interact directly or indirectly with other transcription factors to regulate the expression of COL2A1, aggrecan (ACAN) and other cartilage specific genes at early stages of chondrogenesis (Elena Kozhemyakina, Lassar, & Zelzer, 2015).

During cell differentiation is essential the cell-matrix interactions, because these process is associated with a massive ECM synthesis. A switch from type IIA to type IIB collagen secretion and synthesis of hyaluronan-containing, aggrecan-rich ECM is also crucial (Pitsillides & Beier, 2011; Sandell et al., 1994). For example chondrocytes proliferation and differentiation require signaling via integrins and the collagen receptor DDR2 (Pitsillides & Beier, 2011; Woods, Wang, & Beier, 2007). Chondrocytes express a wide number of extracellular receptors used to feel and to interact with the ECM. Integrin subunits expressed by chondrocytes include Fibronectin receptors (α5β1, αnβ3, αnβ5), a Laminin receptor (α6β1), and collagen receptors (α1β1, α2β1, α10β1) (Richard F. Loeser, 2000, 2002; Woods et al., 2007). Inactivation of β1 integrin gene results in a severe cartilage phenotype. Mice without these subunits develop chondrodysplasia, with distorted growth plates due to a loss of adhesion to collagen II (Aszodi, Hunziker, Brakebusch, & Fässler, 2003). Knock out of the α10 integrin gene leads to dysfunctional growth plate and growth retardation (Bengtsson et al., 2005). Integrins are not the only receptor needed for a correct growth plate formation and correct chondrogenesis. The discoidin domain receptor (DDR) are members of a tyrosine kinase receptors whose ligands are collagens (Leitinger & Kwan, 2006; Vogel, Gish, Alves, & Pawson, 1997; Woods et al., 2007). Knock down of DDR2 in mice leads to dwarfism due to decreased proliferation of growth plate chondrocytes (Labrador et al., 2001).

However studies shown that in osteoarthritic mice chondrocytes increased expressions of DDR2 and re-express type IIA collagen, suggesting a crucial role of these cell-matrix interaction in controlling chondrocytes proliferation and differentiation in OA (Thomas Aigner et al., 1999; L. Xu et al., 2010). Another receptor involved in the chondrogenesis is CD44 which is a cell surface glycoprotein that acts as a receptor for collagens and Hyaluronan. During differentiation process to chondrocytes, CD44 expression increases as well as the expression of some hyaluronidases, suggesting an important role of Hyaluronan signaling and turnover in chondrogenesis (Nicoll, Barak, Csóka, Bhatnagar, & Stern, 2002).

Differentiated chondrocytes follow two distinct fates during limb development, they can become the cartilage elements in articular joints or they can proliferate and undergo the complex process of terminal differentiation to hypertrophy chondrocytes to facilitate the bone formation (Onyekwelu et al., 2009; Singh et al., 2019). Furthermore RUNX2 and ETS transcription factors acting downstream of GDF5 maintain chondrocyte in a differentiation state but inhibits the progression to hypertrophy (Iwamoto et al., 2007). Hypertrophy is the terminal differentiation state of growth plate chondrocytes, these cells decrease the proliferation rates, increase cells volume and produce different type of extracellular matrix components. More in detail, hypertrophic chondrocytes increased the production of COL10A1, MMP9, MMP13 and SSP1 (Charlier et al., 2019; Elena Kozhemyakina et al., 2015). Hypertrophic chondrocytes may undergo apoptosis or survive in the mineralized matrix and started the osteogenic differentiation and these process enables bone formation. During the chondrocyte differentiation form the stating point to the terminal differentiated hypertrophic chondrocytes the ECM has an important role and the composition switch on every passage, from the fibronectin and type I collagen rich matrix of precondensing mesenchymal cells, to the type II collagen and aggrecan-rich

matrix deposited by differentiated chondrocytes, this process ended in the degradation of the latter constituent and their replacement with collagen X-rich ECM, which then undergoes to mineralization at terminal differentiation in the growth plate (Johnson & Terkeltaub, 2005). Changes in the ECM composition are required for the normal endhocondral ossification and long bone formation and are mediated by the continuous remodeling operated by the multiple matrix metalloproteinases (MMPs) (Ortega, Behonick, & Werb, 2004). MMPs required for this process include collagenase 3 (MMP13), stromelysins (MMP3 and MMP10), gelatinases (MMP2 and MMP9) and MT1-MMP (Ortega et al., 2004; Singh et al., 2019). Hypertrophic chondrocytes express at high levels MMP13, and in mice it's expression during development colocalize with type X collagen (Tuckermann, Pittois, Partridge, Merregaert, & Angel, 2000). MMP13 seems to work in synergy with MMP9 and they are essential for a correct endochondral ossification. Indeed double knock out mice for MMP13 and MMP9 has problem in the endochondral ossification due to reduced ECM remodeling, prolonged hypertrophic chondrocytes survival and delayed in vascular recruitment that results in severely shortened bones (Stickens et al., 2004). New studies reveled that another metalloproteinases essential for the chondrocyte terminal differentiation is the membrane anchored metalloproteinase ADAMT17 (a disintegrin and metalloproteinase 17) (Hall et al., 2013; Horiuchi et al., 2009).

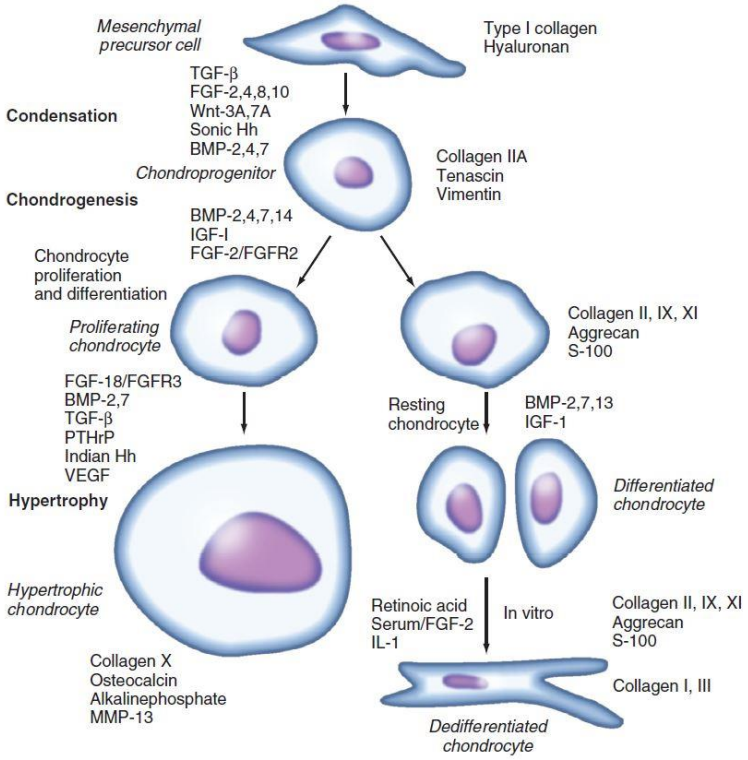

Figure **2 Schematic representation of chondrogenesis and chondrocyte phenotypes from mesenchymal precursor cells to hypertrophic and dedifferentiated chondrocytes.** Each cell phenotype produces different ECM protein which are listed near the cell differentiation stage. The principal growth factor, cytokine and signaling pathways involved in the transition from one phenotype to the other are listed near the arrows. From (Firestein et al., 2017).

Chondrogenesis and chondrocyte differentiation (figure 2) are controlled by interacting patterning system involving fibroblast growth factor (FGF), transforming growth factor β (TGF-β), Bone morphogenic proteins (BMP), Indian hedgehog, parathyroid hormone-related protein (PTHrP), NF-κB, insulin-like growth factor (IGF-1), and Wnt/β-catenin pathways.

Many studies have shown that FGFs play a fundamental role in the chondrocytes proliferation (Inoue et al., 1989; Kato & Gospodarowicz, 1985; KATO et al., 1983; Rosselot, Vasilatos-Younken, & Leach, 1994). In human growth plate chondrocyte culture system, FGF-1, -2 and -18 stimulate proliferation more than FGF-4 and FGF-9, whereas FGF-10 suppress chondrocytes proliferation (Olney,

Wang, Sylvester, & Mougey, 2004). Furthermore FGF-2 treatment of chondrocytes cultured in serum-containing medium and in serum-free medium, blocks the dedifferentiation process during the monolayer culture (I. Martin et al., 2001).

Wnt signaling modulates chondrogenesis and chondrocyte hypertrophy via canonical and non-canonical signaling pathways. Canonical Wnt/β-catenin signaling promotes chondrocyte hypertrophy by redirecting TGF-β signaling toward ALK1/SMAD1/5/8 pathway (Van den Bosch et al., 2014). Non-canonical Wnt pathways, which is independent by β-catenin, promote chondrogenic differentiation of bone marrow derived mesenchymal stem cells and increase chondrocytes differentiation while repressing chondrocyte hypertrophy (Bradley & Drissi, 2010; S. Liu, Zhang, Yang, & Lu, 2014).

PTHrP/IHH signaling pathways works together and has a significant role during the chondrogenesis and chondrocyte hypertrophy. Pre-hypertrophic and early hypertrophic chondrocytes express Indian hedgehog which regulates chondrocyte proliferation and the rate of hypertrophic differentiation (St-Jacques, Hammerschmidt, & McMahon, 1999). IHH modulates hypertrophy in a PTHrP-dependent manner, however, it controls proliferation via mechanism independent by PTHrP (Karp et al., 2000; Ohba, 2016). So IHH and PTHrP regulate the cell fate transiently inducing the proliferation and repressing the differentiation; this determine which cells enter to the hypertrophic maturation. PTHrP block hypertrophy differentiation by signaling to its receptor in pre-hypertrophic chondrocytes (Firestein et al., 2017; Vortkamp et al., 1996). PTHrP also regulates HDAC4 activity which leads to repress the MEF2 activity inhibiting the chondrocytes hypertrophy (E. Kozhemyakina, Cohen, Yao, & Lassar, 2009; Sasagawa et al., 2012; Singh et al., 2019).

TGF-β/BMP superfamily has a significant role in the chondrogenesis and in skeletal development, proteins of this superfamily regulates the early commitment of mesenchymal cells to chondrogenic and osteogenic lineages during cartilage development. Members of TGF-β family include TGF-β1, TGF-β2 and TGF-β3. TGF-β1 is expressed in the proliferative and upper hypertrophic zones of cartilage (Horner et al., 1998). TGF-β1 stimulation of mesenchymal stem cells result in increase expression of type II collagen, and is required for chondrocyte differentiation in mesenchymal cells (Z. Lin et al., 2006). So TGF-β1 and also TGF-β3 plays an essential role in the regulation of the chondrogenic maturation in MSCs inducing the expression of type II collagen, aggrecan and proteoglycan (Firestein et al., 2017; Johnstone, Hering, Caplan, Goldberg, & Yoo, 1998; Z. Lin et al., 2006; Mackay et al., 1998).

BMP is a large subclass of TGF-β superfamily; members of this subfamily are even the cartilage-derive morphogenic protein (CDMP-1,-2,-3) also known as growth/differentiation factor (GDF-5,-6,-7). It has been show that CDMP-1 contributes to the early stage of chondrogenesis and chondrocyte differentiation, and has been found to stimulate the aggrecan and glycosaminoglycan (GAG) production both in vitro and in vivo (Erlacher, Ng, Ullrich, Krieger, & Luyten, 1998; Firestein et al., 2017; Hötten et al., 1996). CDMP-2 has major role in the hypertrophic chondrocytes and is involved in the terminal differentiation of chondrocytes (Chang et al., 1994; Z. Lin et al., 2006). Differentiation of mesenchymal stem cells into chondrocytes and terminal differentiation to hypertrophic phenotype are regulate even by BMP-2 and BMP-7. In vitro BMP-2, -4, -6, -7, -9 and -13 enhance the expression of collagen II and aggrecan in chondrocyte, by the upregulation of Sox9 gene (Fernández-Lloris et al., 2003; Firestein et al., 2017; Pizette & Niswander, 2000; Zehentner, Dony, & Burtscher, 1999).

Another important growth factor involved in the preservation and stimulation of chondrogenic differentiation is IGF-1, which as been observed to stimulate the chondrocyte phenotype in vitro by promoting the expression on type II collagen and aggrecan. Studies on mesenchymal cell lines shown that IGF-1 induce both chondrocyte proliferation and differentiation. Its signaling is believed to be required for the correct ECM homeostasis, by promoting the secretion of proteoglycans and type II collagen both in vitro and in vivo (Firestein et al., 2017; Z. Lin et al., 2006; J. Martel-Pelletier, Di Battista, Lajeunesse, & Pelletier, 1998; Oh & Chun, 2003).

1.4 CHONDROCYTE CELLUAR MODEL SYSTEM

A variety of cellular model system have been used to study and understand better cartilage formation, proliferation, differentiation; gene expression, pathways associated to normal and pathological disease of cartilage. To reach this goal a variety of cellular model are commonly used in the research field. Primary chondrocytes culture are initiated directly from donor cartilage tissue (Harrison et al., 2000). However primary chondrocytes can proliferate in vitro with a limited number of cell divisions. Human articular chondrocytes can be grown from donor of a wide age range. Chondrocyte primary culture are an excellent model to study the normal cell physiology and mechanism of degenerative joint disease. However articular chondrocytes shown a lower proliferation rates and may de-differentiate after extended cultivation time. Indeed its difficult to have enough number of cells, and this is a limitation of this type of culture (Mary B. Goldring, 2004; Harrison et al., 2000).

Normal clonal cell lines are non-transformed cells with different life-span generated by a single ancestor. This cells remain genetically identical through serial passage in vitro, and are used because its easy to obtain enough cells for research purposes. Non-transformed clonal cells are usually initiated from tumor

tissue an example is HCS-2/8 cell line generated from an aggressive chondrosarcoma of a 72 years-old man (Takigawa et al., 1989). HCS-2/8 are widely characterized for the synthesis of proteoglycans and collagen which are in line with chondrocyte phenotype (Jung et al., 2004). However this tumor derivation may affect their biological characteristics. Another normal clonal cell lines generated from human chondrosarcoma is Ch-1 which is commonly used to define the difference in the gene expression profile between normal cartilage and tumorigenic cartilage (Chansky et al., 1998). ATDC-5 is a prechondrogenic stem cell line and are frequently used to study the chondrogenesis process because it can be used to produce each chondrocyte phenotype in monolayer culture. ATDC-5 display an entire spectrum of chondrocyte differentiation (Atkinson, Fantle, Benedict, Huffer, & Gutierrez-Hartmann, 1997).

Another widely used cell model are the immortalized clonal cell line, obtained by a genetic modification of human primary chondrocyte cells that induce the immortalization (Mary B. Goldring, 2004). T/C-28a2, T/C-28a4 and C-28/I2 were established by retroviral-mediated transfection of primary rib chondrocytes with the large T antigen of Simian virus 49 (SV40). Initially T/C-28a2 were produced and from them were derived C-28/I2 and T/C-28a4 cell lines. They can maintain the correct chondrocytes morphology for more than 80 passage in monolayer culture with the serum-conditioned medium and are commonly used in numerous studies to investigate chondrocytes specific response patterns to IL-1β and interferon-γ and to a physical loading. Of the three cell lines C-28/I2 is reported to be closest to primary chondrocytes with a similar anabolic and catabolic gene expressions (Finger et al., 2003; Mary B. Goldring, 2004). Temperature sensitive immortalized chondrocytes like tsT/AC62 were developed to study the chondrocytes biology, by using a retrovirus expressing a temperature sensitive mutant SV40-large T antigen which is expressed at permissive temperature (32°C) stimulating cell proliferation. Large T antigen expression was

lost when cells are growth at non permissive temperature (37-39°C) with decreased cell proliferation (Robbins et al., 2000).

1.5 OSTEOARTHRITS

Osteoarthritis is the most common degenerative joint disorder that affects small joints (such as those in the hands) and large joints (like the knee and hip joint) and is one of the leading causes of disabilities worldwide. Most mammalian population are affected including humans, cats, dogs, sheep and horses (Clarke et al., 2005; Clements, Fitzpatrick, Carter, & Day, 2009; Ireland, Wylie, Collins, Verheyen, & Newton, 2013; Vandeweerd et al., 2013). The principal OA characteristics are erosion of articular cartilage, hypertrophy of bone at the margins (osteophytes) subchondral sclerosis and different alteration in the synovium. Symptoms of OA most commonly include pain, swelling and stiffness in the affected joint resulting from the degradation of cartilage (Madry, Luyten, & Facchini, 2012). Structural OA of the hands is reported in c.a. 60%, of the knee in 33% and of the hip in 5% of adults ≥65 years old in North America and Europe (David T. Felson et al., 1987; Van Saase, Van Romunde, Cats, VanDenBroucke, & Valkenburg, 1989). OA is more frequent among women than man and this sex differences is most pronounced for hand and knee OA. However prevalence incidence rises steeply with the age in both sexes. Furthermore ageing is the factor that has the greatest influence in the pathogenesis of OA. The main risk factors for development of OA include joint injury, obesity, genetic predisposition and abnormal joint shape and alignment, metabolic dysfunction and sex. However with ageing, increases obesity and articular injuries in the global population, the OA disease is becoming more prevalent and a worldwide estimation suggest that are currently affected about 250 million of people (Hunter & Bierma-Zeinstra, 2019) becoming an important socioeconomic problem (Herndon, Davidson, & Apazidis, 2001). Typical clinical symptoms are pain and

stiffness, particularly after prolonged activity. Among man and woman, pain in hand OA is only present in 15% of cases, whereas 50% of patients with knee OA and even highest portion of hip OA has pain has primal symptom. Furthermore half of patients with knee pain and structural changes has disability associated with a loss of productivity. In USA has been estimated that the loss of productivity due by OA disease cost $27 billion (Richard F. Loeser, 2017).

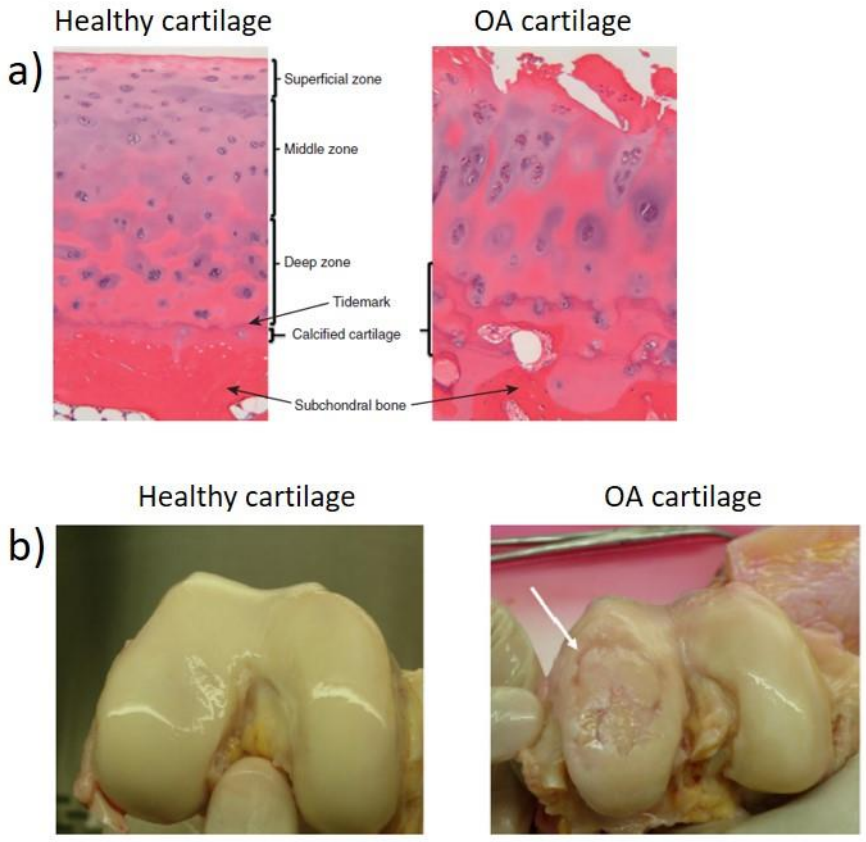

Figure 3 **Images of osteoarthritic and healthy cartilage.** a) histologic images of human healthy and OA cartilage stained with safranin O staining (Firestein et al., 2017) b) Macroscopic cartilage degradation in human femoral cartilage caused by OA (right) (Krishnan & Grodzinsky, 2018).

OA may be classified as primary (idiopathic) and secondary based on the generation cause or major predisposing factors (Firestein et al., 2017; Johanne Martel-Pelletier et al., 2016). Primary OA, the most common form of OA, has no

identifiable etiology or predisposing cause and can result for a combination of risk factors like ageing, obesity, knee malalignment, increased biomechanical loading of joints, genetics and low grade inflammation state (Johanne Martel-Pelletier et al., 2016; Sellam & Berenbaum, 2013). Secondary OA is based on the attribution to recognized causative factors which are responsible of the disease, however primary and secondary OA are pathologically indistinguishable. The most common causes for secondary OA are traumatic events, metabolic conditions, anatomic factors or others inflammatory disorders (Firestein et al., 2017).

It is accepted that age is the major risk factor for OA. Normal cartilage of older people appear slightly brown due to an accumulation of advanced glycation end products (AGEs) and is thinner than in young adults but is still smooth and intact (Nicole Verzijl, Bank, TeKoppele, & DeGroot, 2003). Accumulation of AGEs can alter the biomechanical properties of cartilage structure making it more brittle and susceptible to degeneration (Richard F. Loeser, Collins, & Diekman, 2016). Hallmarks of aging have been identified that represent the processes most likely to contribute to age related conditions and include stem cell exhaustion, altered intracellular communication, genomic instability, telomere attrition, epigenetic alteration, loss of proteostasis, deregulation of nutrient sensing, cellular senescence and mitochondrial dysfunction (López-Otín, Blasco, Partridge, Serrano, & Kroemer, 2013). Moreover, the age-related tissue changes are due to a decrease in chondrocyte ability to maintain and repair the tissue. During aging, chondrocytes decrease their mitotic and synthetic activity and among with decrease in responsiveness to anabolic stimuli and lower production of proteoglycans and functional proteins are responsible for the age related changes occurring in older cartilage (R. F. Loeser, 2009; J. A. Martin & Buckwalter, 2002). There is substantial evidence that links aging with cellular senescence in vivo. Cellular senescence developed with aging seems to play a fundamental role

in the development of age related diseases (S. He & Sharpless, 2017). Senescence is a cell response to different persistent stresses, and is characterized in a cell-cycle arrest, increase expression of $p16^{Ink4a}$, and increase secretion of inflammatory cytokines and others factors known as senescence-associated secretory phenotype (SASP) (Collins, Diekman, & Loeser, 2018; R. F. Loeser, 2009). Recent studies showed that OA severity correlates with the senescence-associated β-galactosidase activity which is a common marker of senescence (Gao et al., 2016). Another research found that increased SASP secretion can caused cartilage degradation and can drive OA (M. Xu et al., 2017). So an important new strategies could be to treat the OA patients with the new type of compound called "senolytics", with the aim to kill senescent cells that arise with aging (Collins et al., 2018). These compounds try to inhibit pathways which are upregulated in senescent cells, using an approach similar to the chemotherapeutic compounds with oncogenic cells. One example is the Navitoclax (ABT-263) which inhibit Bcl-2 and Bcl-xL that allows senescence cells to survive in the context of persistent stress activating an antiapoptotic machinery (Zhu et al., 2016). Direct application of one senolytic compound on anterior cruciate ligament transection (ACTL) mice showed reduction in the burden of senescence chondrocytes and production of SASP. This treatment also limited the development of OA and improved the function of the injured joint (Jeon et al., 2017). Moreover aged chondrocytes produce lower mechanical quality ECM and among with reduced cellularity and reduced synthetic activity of aged cells, all of these contribute to increase OA risk in aged cartilage. Age is an independent factor that predisposes articular chondrocytes to apoptosis, with higher expression of proapoptotic genes in aged cartilage (Allen et al., 2004; Robertson et al., 2006).

Obesity is a well known risk factors for development and progression of OA. Increased mechanical loading on the joint can not be the only factor involved in

the OA development in obese patient (Zhuo, Yang, Chen, & Wang, 2012). These patient have higher risk to develop OA than in lean patients even in joint not concerned by increase loading like hands. The risk ratio for obese patient to develop hand OA is 1.9 (D. T. Felson & Chaisson, 1997; Yusuf et al., 2010). In joint concerned by body weight, such as knee, body fat is a predictor of cartilage loss, independent of fat-free mass (C. Ding, Stannus, Cicuttini, Antony, & Jones, 2013). Indeed the risk of total knee or hip replacement for OA is three-fold or four-fold higher in individuals which are in the highest quartile of fat-mass (C. Ding et al., 2013). However, the association between obesity and OA are not due only by excessive mass loading and the adipose tissue itself could play a central role in this association by secreting hormones, growth factors and adipokines in abnormal concentrations (Abella et al., 2014). For example leptin is an adipokine secreted by adipose tissue and could play a role in the link between obesity and OA (Le Clanche et al., 2016b). Chondrocytes can synthesize leptin and its receptors are found in articular cartilage (Figenschau, Knutsen, Shahazeydi, Johansen, & Sveinbjörnsson, 2001; Simopoulou et al., 2007). Leptin and its receptors levels are higher in advanced OA cartilage. Furthermore, synovial fluid of obese patient exhibit and increased expression of leptin with a decreased sOB-R levels (receptor of leptin) (Simopoulou et al., 2007). Leptin was also found to be responsible for the increase MMP-3,-9 and -13, IL-1β, nitric oxide (NO), prostaglandin E_2, IL-6 and IL-8 production in human OA cartilage (Le Clanche et al., 2016b). Not only leptin was found to be involved in the link between OA and obesity but also adiponectin, which is not normally detected in the healty cartilage but high levels were found in OA cartilage increasing the PGE2 and MMP-13 production (Francin et al., 2014). However the correct role of adiponectin in the pathogenesis of OA is under debate. One study shown that adiponectin in OA has a protective role increasing TIMP-s expression and downregulating IL-1β-induced MMP-13 (T. H. Chen et al., 2006). On the

contrary there are some study which demonstrate that adiponectin is responsible for induction of nitric oxide synthase 2 (NOS2) in human chondrocytes increasing the production of •NO by chondrocytes, leading to chondrocytes apoptosis and ECM degradation (Lago et al., 2008). However, receptors for adiponectin are downregulated in chondrocytes from OA patients compared to healthy chondrocytes, this reduced sensitivity of adiponectin could lead to a faster development of OA (Q. Wang et al., 2014). Moreover, adiponectin was found to induce IL-6, MMP-3 and -9 and monocyte chemoattractant protein-1 (MCP-1) production which are all involved in the OA development and progression (Hao et al., 2011). Other adipokines found to have a role in the OA development are visfatin and resistin. Visfatin has a deleterious effect on articular cartilage, and stimulate chondrocyte production of MMP-3 and -13, ADAMT-S 4 and 5, and increasing the general tissue inflammation state (Gosset et al., 2008; McNulty, Miller, O'Connor, & Guilak, 2011). Resistin is able to induce pro-inflammatory cytokine production like IL-6, TNF-α and PGE2 leading to a proteoglycan degradation (Le Clanche et al., 2016b; J. H. Lee et al., 2009). This new discovery has driven the division of OA into different phenotypes and one of them is the metabolic OA which is characterized by its major causative features such adipokines, hyperglycemia, obesity and hormone imbalance. Metabolic OA is targeting by middle age people (45-65 years old) and is the second most frequent OA subtype after aging (Le Clanche et al., 2016b; Zhuo et al., 2012).

Another independent risk factor for the development of OA is type 2 diabetes mellitus (T2DM). An association between these two disease has been demonstrated and two-recent meta-analyses reported that T2DM is an OA risk factor whatever the localization (Louati, Vidal, Berenbaum, & Sellam, 2015; M. F. Williams, London, Husni, Navaneethan, & Kashyap, 2016). Data for an association between T2DM and site of OA gives different outcomes, for example

the association between hand OA and T2DM is strong and especially younger patients had two times higher rate of hand OA than non-diabetic. Furthermore there is a strong association between erosive hand OA, which is very painful form of hand OA, and T2DM (Dahaghin, Bierma-Zeinstra, Koes, Hazes, & Pols, 2007; Louati et al., 2015; Magnusson et al., 2015; Visser et al., 2015). Furthermore T2DM was found to be a risk factor even for OA progression in man with established knee OA (Schett et al., 2013). The risk of arthroplasty was correlated with T2DM duration and T2DM patients had more inflammation of synovium and more pain (Schett et al., 2013). T2DM has a pathogenic effect on OA through 2 major pathways. First, chronic hyperglycemia induces oxidative stress, overproduction of pro-inflammatory cytokines and AGEs in joint tissues and also reduced the stem cells potential of differentiation. Second the insulin resistance could play a role locally but also through the systemic low-grade inflammation state (Courties & Sellam, 2016).

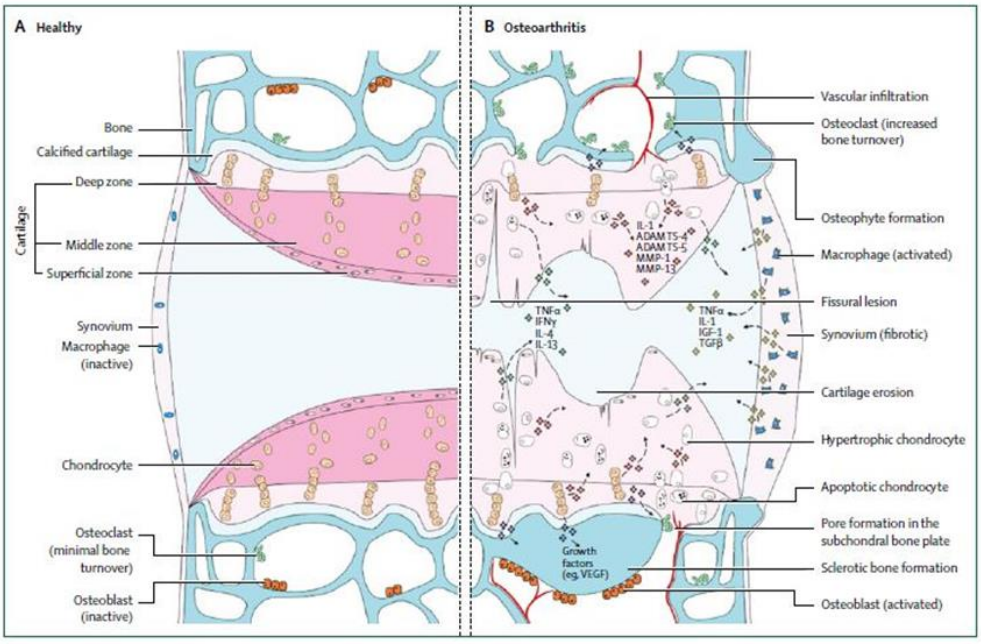

Figure 4 **Representation of principal signaling pathways and structural changes in the development of OA** (Hunter & Bierma-Zeinstra, 2019).

Glucose is an important metabolic compound and a structural precursor that plays a key role in the synthesis of molecules of extracellular matrix in articular cartilage (Ali Mobasheri, 2012). First of all, glucose is the major source of energy for development, growth and maintain the articular cartilage. It is an essential compound for osteogenesis and chondrogenesis used as a precursor of glycosaminoglycan and glycoproteins. Glucose concentration in the articular cartilage can vary depending on age, physical activity and endocrine state. However glucose can modify and regulate the expression of several genes, for example, in cartilage can modulate the expression of anabolic and catabolic genes such as type I and type II collagen and MMP-1 and MMP-13 in human healthy and OA chondrocytes (Grayson, 2010; Susana C. Rosa et al., 2011). Cartilage is a non-vascularized and non-innervated tissue and receives nutrients from its connection with subchondral bone and synovial fluid through joint cavity. However chondrocytes are glycolytic cells that express glucose transporter (GLUT), especially GLUT-1, GLUT-3 and GLUT-9 and are able to sense the glucose concentration in the media and to adapt GLUT expression under normal condition (A. Mobasheri, Neama, Bell, Richardson, & Carter, 2002). Under glucose deprivation, normal chondrocytes increased the expression of GLUT-1 which decreased under high glucose condition. This capacity to adapt the GLUT expression to the local glucose levels is lost during OA, which is responsible for a high glucose uptake and potential glucose toxicity (Susana C. Rosa et al., 2009). GLUT expression is under the control of several factors. Their expressions raised under pro-inflammatory stimuli as TNF-α and IL-1β through phosphokinase C, but also under metabolic and hypoxic factors which are involved and increased in OA (Shikhman, Brinson, Valbracht, & Lotz, 2001). Local high glucose concentration leads to a reduction in chondrogenic differentiation of mesenchymal, muscle, and adipose-derived stem cells which may further decrease the potential regeneration of cartilage that is already decreased in OA

patients (Aguiari et al., 2008; Cramer et al., 2010; Tsai, Manner, & Li, 2013). Furthermore, chronic high glucose environment has a deleterious effect on chondrocytes metabolism. Human cartilage of diabetics patients produce more IL-6 and PGE_2 under IL-1β stimulation than non-diabetic patients and showed reduce autophagy and heme oxygenase expression (Laiguillon et al., 2015; Ribeiro, López de Figueroa, Blanco, Mendes, & Caramés, 2016; Vaamonde-Garcia et al., 2017). High glucose exposure also increases MMP production especially in human OA chondrocytes and decreases the production of collagen type II (Y. J. Chen et al., 2015; Susana C. Rosa et al., 2011). High glucose concentration increases glycolysis enzymes like enolase, glycealdehyde-3-phosphate dehydrogenase and fructose-biphosphate aldolase, leading to accumulated intracellular glucose (Ruiz-Romero et al., 2008). The hyperglycemic environment favors the formation of advanced glycation end products (AGEs), created by a non-enzymatic condensation reaction between glucose and amino groups of proteins. AGEs are involved in a lots of diseases like Alzheimer's disease, diabetes or end-chronic renal failure (Le Clanche et al., 2016a). Accumulation of AGEs in OA cartilage modified its mechanical properties, including stiffness and resistance, making the tissues less able to deform under and increased load (Nicole Verzijl et al., 2002). Type II collagen is the preferential target for AGE formation because its half-live is more than 100 years (N Verzijl et al., 2000). This process is responsible for a stiff collagen network which make cartilage more susceptible to trauma and injury. Also AGEs can induce pro-inflammatory and pro-catabolic phenotype of chondrocytes via the receptor of AGE (RAGE) and Toll-like receptors (TLRs). The activation of RAGEs in chondrocytes induce a decrease in peroxisome proliferator-activated receptor gamma (PPAR-γ) and an activation of NF-kβ and MAPK pathways. Furthermore RAGEs activation leads to an increase production of reactive oxygen species (ROS), nitric oxide and cytokine release by chondrocytes (Y. J.

Chen, Sheu, Tsai, Yang, & Liu, 2013; Rasheed, Akhtar, & Haqqi, 2011; Rasheed & Haqqi, 2012; J. Wang, Wang, & Sun, 2016).

Human chondrocytes express functional insulin receptors that respond to physiologic insulin concentrations. The insulin receptors are more abundant in normal than OA chondrocytes and some responses are impaired while others are fully activated (S. C. Rosa et al., 2011). In immortalized human chondrocytes and cultures of primary human chondrocytes it is found that insulin downregulates autophagy by reducing LC3 II expression and increasing Akt and rpS6 phosphorylation. Autophagy is an essential homeostasis mechanism in articular cartilage which is defective in T2DM and OA. Especially in cartilage in which the oxygen concentration is lower chondrocytes lives in an hypoxic environment and autophagy protects from normal and pathological aging by converting organelles and protein to energy supply for cells. In chondrocytes after the differentiation autophagy become active and protect the differentiation of chondrocytes and normal chondrocytes to avoid premature apoptosis and replacement of the bone (Luo et al., 2019). Chondrocytes from diabetic patients with OA showed decreased LC3 and increased p-rpS6 expression compared to healthy subjects and non-diabetic OA patients (Ribeiro et al., 2016). Insulin resistance and T2DM are associated to a visceral obesity, which is an important source of cytokines causing low-grade inflammation state that can lead to structural damage in the joints (Gregor & Hotamisligil, 2011).

The destruction and loss of articular cartilage is central in the development of OA and most studies are focused on the cartilage changes during OA (Richard F. Loeser, 2017). One of the earliest osteoarthritic changes in the cartilage is the increased water content, which is associated with the loss of the negatively charged glycosaminoglycans and results in swelling of the matrix (Akizuki, Mow, Muller, Pita, & Howell, 1987; S. R. Goldring & Goldring, 2016). This

suggest there has been weakening of the collagen network, in fact type II collagen fibrils have smaller diameter than normal cartilage. Cartilage matrix degradation occurs initially in the superficial zone of the cartilage and later extends to deeper zones as OA progresses (W. Wu et al., 2002). Proteoglycan degradation is mediated by aggrecanases of the ADAMTS family that cleaves the aggrecan core. Decrease in proteoglycans density is one of the first steps in the cartilage degradation (M. B. Goldring, Otero, Tsuchimochi, Ijiri, & Li, 2008). This opens up the cartilage porosity to make it more permeable to collagenases and other proteases, exposing collagen fibrils. So the interactions between type II collagen network and other ECM proteins, like aggrecans an other non-collagenous proteins become more susceptible to disruption by physical forces or by the increased activity of MMPs (D. R. Eyre, 2004; M. Wang et al., 2013). Collagen epitopes become accessible to the DDR2 receptor on cell surface leading to an increase production of MMP-13 through activation of the Ras/Raf/MEK/ERK and p38 signal cascades (L. Xu et al., 2010). The partially digested matrix components have cytokine-like activity enhancing the inflammatory response and promoting matrix degradation. At this point, the destruction of cartilage become irreversible (Firestein et al., 2017). In the early stages of OA, chondrocytes, which are normally quiescent cells in healthy cartilage, become active and start to increase the synthetic activity producing proteoglycans around the cells trying to repair the loss of proteoglycans (Lorenzo, Bayliss, & Heinegård, 2004). However with the progression, the depletion of matrix is associated with the appearance of chondrocytes in cluster due by increase number of proliferating chondrocytes, which continue to express matrix proteins like aggrecan, type II collagen and proteoglycans, as well as stem cell markers and markers of hypertrophic differentiation (Joseph A. Buckwalter, Mankin, & Grodzinsky, 2005; Grogan, Miyaki, Asahara, D'Lima, & Lotz, 2009). These chondrocyte cluster are a hallmark of OA. Decreased chondrocytes density at late

stages of OA along with the presence of cell-membrane ghost, fragmentation of chondrocytes nuclei are signals of increased apoptosis due by an earlier death events (H. S. Hwang & Kim, 2015). In the later stages of OA type I collagen concentration in the ECM increases and proteoglycans falls to 50% or less than normal with shorter glycosaminoglycans side chains and less aggregation (Inerot, Heinegard, Audell, & Olsson, 1978). Keratan sulfate concentration decreases and the ratio of chondroitin-4-sulfate to chondroitin-6-sulfate increases, reflecting synthesis by chondrocytes of a proteoglycan profile more typical of immature cartilage (Bollet & Nance, 1966). Increased numbers of chondrocytes with features of SASP, which produce more cytokines, chemokines and MMPs, are characteristic of aging cartilage predispose to cartilage destruction and OA (Richard F. Loeser, 2013). The increased activity of degradative enzymes produced by chondrocytes not only disrupts the cartilage matrix but also leads to the generation of cartilage matrix breakdown products (like fibronectin fragment) and the secretion of damage-associated molecular patterns (DAMPs) and alarmins that deregulate chondrocytes function through Toll-like receptors, integrins and other cell-surface receptors (S. R. Goldring & Goldring, 2016; Liu-Bryan & Terkeltaub, 2015; Richard F. Loeser, Goldring, Scanzello, & Goldring, 2012). DAMPs and alarmins also acts and stimulates the adjacent synovial tissue to induce inflammation and the release of proinflammatory products like cytokines and ROS that feed back to the chondrocytes enhancing the catabolic state.

1.6 ROS SIGNALLING IN CHONDROCYTES

Articular cartilage homeostasis is a state in which degradation of ECM componence is balanced by synthesis. In normal cartilage, chondrocytes are quiescent cells with low metabolic activity and very low turn-over of matrix is present. The abnormal joint tissue metabolism in chondrocytes, synovium,

subchondral bone and ECM leads to cartilage degradation and contribute to OA pathogenesis. Recently alteration in ROS production and pathways have been implicated in OA progression (Lepetsos & Papavassiliou, 2016). Aging has been associated with an increase levels of ROS due to mitochondrial dysfunction. Under normal condition ROS are generated at low concentration in articular chondrocytes mainly by NADPH oxidase, and they actively participate in intercellular signaling mechanism and regulate cartilage metabolism modulating chondrocytes apoptosis, gene expression, ECM synthesis and degradation, and cytokine production (Collins et al., 2018; Hiran, Moulton, & Hancock, 1997; Lepetsos, Papavassiliou, & Papavassiliou, 2019). In OA chondrocytes was found an increase ROS production, decreased antioxidant enzymes production and activities suggest a key role of ROS in the OA pathogenesis (Altindag et al., 2007; Del Carlo & Loeser, 2003; Lepetsos et al., 2019). The types of ROS produced and associated to chondrocyte cells and cartilage homeostasis are superoxide (O_2•) and hydrogen peroxide (H_2O_2). Reactive nitrogen species, as •NO and peroxynitrite (ONOO•) are also able to regulate chondrocytes function. O_2• is generated mainly from two sources: incomplete oxidative phosphorylation in the mitochondria and non-mitochondrial membrane-bound nicotinamide adenine dinucleotide phosphate (NADPH) oxidase (Altenhöfer et al., 2012; Turrens, 2003). O_2• is a potent ROS and it can directly oxidase proteins regulating signal transduction, gene expression and cell cycling. Superoxide dismutase (SOD) is the enzyme involved in the conversion from O_2• to H_2O_2. SOD can also generate the hydroxyl radical (OH•), which is the most damaging ROS but its lifetime is shorter. H_2O_2 is less detrimental than O_2• and OH• but its lifetime is longer and persist more time in the cell before further reduction by enzymes like peroxiredoxin and catalase (Dickinson & Chang, 2011). Another source of H_2O_2 and O_2• are the NADPH oxidase (Nox) enzymes family. There are seven Nox enzymes: Nox1-5 and dual oxidase (Duox)1-2. All Nox can produce O_2• but

Nox4 and Duoxs can be a source of H_2O_2 (Bolduc, Collins, & Loeser, 2019; Panday, Sahoo, Osorio, & Batra, 2015). In OA cartilage Nox4 is the predominant isoform active in chondrocytes, and its activation after proinflammatory cytokines stimulation increases both H_2O_2 and O_2• inside the cells. Increase activation of Nox4 and ROS production influence signaling events responsible for the production of MMPs in chondrocytes increasing cartilage destruction (Rousset et al., 2015). Redox imbalance in OA chondrocytes is also due to a decreased levels of antioxidant enzymes like SOD and peroxiredoxins (PRXs) (Collins et al., 2016; Scott et al., 2010). Compared to normal cartilage SOD2 and SOD3, as well as glutathione peroxidase are downregulated in human OA cartilage (Thomas Aigner et al., 2006). During aging levels of SOD2 increase in cartilage isolated from old rats, however the activity of SOD2 is declined (Y. Fu et al., 2016). In these mice was found a decrese Sirt3 activity leading to and increase SOD2 acetylation responsible for a decrese enzymatic activity and contributing to the development of age-related OA. H_2O_2 can be produced by xanthine oxidase (XO) but its activity is higher in synovial membranes rather than in chondrocytes (Aibibula et al., 2016; Stabler, Zura, Hsueh, & Kraus, 2015). PRXs are a enzyme family primarily responsible for the reduction and detoxification of H_2O_2, but also can reduce organic hydroperoxides (ROOH) and peroxynitrite (Rhee & Kil, 2017). PRXs compete with catalase and glutathione peroxidase for the detoxification of H_2O_2, however PRXs are responsible for reducing the 90% cellular peroxides (Perkins, Nelson, Parsonage, Poole, & Karplus, 2015). PRXs are divided into three classes depending on the number of catalytic cysteine (Cys). In humans Prx1-4 are typical 2-Cys Prxs, the additional Cys are the resolving Cys allowing the formation of inter-subunit disulfide bond between two monomers to resolve the oxidation occurring on the peroxide Cys, sulfenic form (PRX-SOH) when it reduce the H_2O_2 producing H_2O (L. B. Poole & Nelson, 2016). Prx5 is an atypical 2-Cys Prx in which the resolving Cys and

the peroxide Cys are in a position allowing the intersubunit disulfide bond formation (Knoops, Goemaere, Van Der Eecken, & Declercq, 2011). Prx6 is the only 1-Cys Prx, and the oxidation to PRX6-SOH is resolved by the binding with a molecule of glutathione (GSH) mediated by glutathione S-transferase. Prx6 has another enzymatic activity and can function as a calcium-independent phospholipase (PLA_2) promoting the hydrolysis of acyl group of phospholipids. Prx6 was found to be implicated especially in the pathogenesis of diabetes. Prx6-null mice showed and increased insulin resistance but its role is not enough understood (Patel & Chatterjee, 2019). However under high levels of ROS and H_2O_2 hyperoxidation of PRXs to the sulfinylated ($PRX\text{-}SO_2H$) and sulfonylated ($PRX\text{-}SO_3H$) forms can occur leading to enzymatic inactivation and inhibition of peroxidase function (Collins et al., 2016; Z. A. Wood, Poole, & Karplus, 2003). Hyperoxidazed $PRX\text{-}SO_2H$ form can be reduced by ATP-dependent sulfiredoxin but this reaction is very slower, and if H_2O_2 and other ROS rise to levels that overwhelm the antioxidant capacity of the cell than the oxidative stress occurs with a disruption in normal physiologic signaling (Cross & Templeton, 2006; Lowther & Haynes, 2011). Increased levels of hyperoxidized PRXs are present in human cartilage from older adults with a further increase in OA cartilage (Collins et al., 2016). Chondrocytes from older patients are more susceptible to PRXs hyperoxidation when exposed to ROS and this with inhibition of IGF-1-mediated phosphoinositide 3 (PI-3) kinase-Akt signaling and promotion of p38 activation that results in chondrocytes cell death promoting OA development (Collins et al., 2016). High levels of ROS are implicated in reducing chondrocytes sensitivity to key growth factors like IGF-1 and OP-1. Low levels of ROS have benefic effect on IGF-1 signaling, however under excessive ROS levels IGF-1 mediated Akt-activation is inhibited, this leads to a decrease chondrocytes ECM matrix production and increase activation of catabolic MAPK pathways (R. F. Loeser, 2009; Richard F. Loeser, Gandhi, Long, Yin, &

Chubinskaya, 2014). Chondrocytes ROS-mediated signaling that regulates MMPs expression has been noted in response to cytokines like IL-1β and TNF-α and to stimulation with fibronectin fragment (FN-f) which accumulate in OA cartilage (Del Carlo, Schwartz, Erickson, & Loeser, 2007; Richard F. Loeser, 2017). Furthermore chondrocytes from older adults become more responsive to IL-1β and FN-f stimulation (Forsyth et al., 2005). Another mechanism contributing to the OA progression and pathogenesis is the cell death. Enhanced ROS levels play a key role in activation cell pathways to promote cell death. Mitochondrial H_2O_2 activate MKK3/6-p38 signaling inducing rapid cell death in human chondrocytes (Collins et al., 2016). Pharmacological inhibition of p38 helps to maintain cell viability in response to H_2O_2 because cell death in chondrocytes is, in part, dependent on p38 MAPK pathway. ERK, C-Jun NH_2-terminal kinase (JNK) and p38 are heavily implicated in OA development and progression and are activated by ROS. High levels of ROS induce the activation and the phosphorylation of ERK, p38 and JNK in chondrocytes initiating the catabolic signaling events through the release of cartilage matrix degrading enzymes (Forsyth et al., 2005; S. T. Wood et al., 2016). ROS also contributes to inhibition of pro-anabolic signaling including BMP7 and IGF-1, downregulation of cartilage matrix synthesis and chondrocyte cell death (Richard F. Loeser, 2017). OA chondrocytes display enhance protein sulfenylation, in response to ROS induce by FN-f treatment, if compared to non-OA chondrocytes. One sulfenylated protein is Src which enhance its activity leading to JNK activation and subsequently MMP-13 production and release (S. T. Wood et al., 2016). Moreover H_2O_2 participates in the activation of JNK by IL-1β and TNF-α and in the IL-1β upregulation of c-Fos in chondrocytes (Lo, Conquer, Grinstein, & Cruz, 1998). IL-1β induce inflammation and ROS production can be inhibited by the activation of Nrf2 (Xue et al., 2017). ROS can attack lipid producing the phenomenon called lipid peroxidation, which produce as toxic product HNE that

can activate caspase -3, -8 and -9, dowregulates Bcl-2, upregulate Bax and suppresses pro-survival Akt kinase activity promoting chondrocytes apoptosis (Abusarah et al., 2017; D. Fu, Lu, & Yang, 2016). Furthermore increased levels of ROS are responsible for increasing DNA-damage in chondrocytes, affecting gene transcription and protein synthesis inducing apoptosis (T. Aigner et al., 2001; H. A. Kim, Lee, Seong, Choe, & Song, 2000). Nrf2 is a transcription factors that regulates the expression of antioxidant enzymes and has a chondroprotective effect reducing OA chondrocytes apoptosis (N. M. Khan, Ahmad, & Haqqi, 2018). ROS in chondrocyte was found to be able to promote chondrocytes dedifferentiation through the activation of ERK, PI3K and p38 pathways (Yu & Kim, 2015). Mitochondrial ROS generation increase after IL-1β and TNF-α treatment. These mitochondrial ROS inhibits mitochondrial respiratory chain and cause mtDNA mutation and damage, this promote inflammatory process and enhance cartilage functional failure and promote cell death (J. Kim et al., 2010; López-Armada et al., 2006). Increased ROS levels in chondrocytes inhibit the proteoglycan synthesis by reducing the rate of glycolytic ATP synthesis and intracellular concentration ATP and interrupting the IGF-1 signaling pathway (Baker, Feigan, & Lowther, 1989).

In OA cartilage ROS regulate the activity of NF-κB, which is a transcription factors activated by IL-1β, TNF-α, FN-f and others pro-inflammatory cytokines. Activation of NF-κB pathways alone or in combination with the activation of Wnt or BMP pathways, suppresses chondrocytes anabolism and triggers the expression of several matrix proteinases like MMPs (MMP-1,-2,-3,-7,-8,-9 and -13), ADAMTS (ADAMTS4 and 5) resulting to cartilage erosion (Mary B Goldring & Marcu, 2009; Shakibaei, John, Schulze-Tanzil, Lehmann, & Mobasheri, 2007). Additionally, the OA chondrocytes generate a lot of number of NF-κB-mediated catabolic cytokine and chemokines like TNF-α, IL-1β, IL-6, IL-8 and RANKL, that support the production and secretion of MMPs, reduce

production of collagen and proteoglycan and act as a positive feedback loop to increase and power up NF-κB activation (Kapoor, Martel-Pelletier, Lajeunesse, Pelletier, & Fahmi, 2011). Also NF-κB promotes articular damage through induction of NO, COX2, NOS and PGE_2 which enhance production of catabolic factors leading to cartilage degradation, chondrocytes apoptosis and constitutive expression of NF-κB molecules (Marcu, Otero, Olivotto, Borzi, & Goldring, 2010). Sustained NF-κB activation stimulates other regulatory transcription factors like ELF3, HIF-2α and RUNX2 enhancing the production of MMP-13 and ADAMTS5 facilitating the differentiation from pre-hypertrophic chondrocyte to a terminal hypertrophic chondrocytes (Mary B. Goldring et al., 2011). NF-κB is a key transcription factors in chondrocytes; it can mediate the expression of TLR2 leading to suppression of chondrocytes proliferation and increasing cell apoptosis (Y. X. Liu, Wang, Wang, Zhang, & Zhang, 2017). Increase ROS levels can mediate the degradation of NF-κB inhibitor IκB leading to NF-κB activation (Glineur, Davioud-Charvet, & Vandenbunder, 2000; Janssen-Heininger, Poynter, & Baeuerle, 2000). ROS-mediated NF-κB upregulation contribute to proinflammatory phenotype alteration in OA tissue such as production of iNOS, IL-8 and COX-2. Osteopontin which is a marker associated to the progression of OA promotes the expression of MMP-2, -9 and -13 through activation of NF-κB (Y. Li et al., 2016). PRX-1, an enzyme linked to H_2O_2 detoxification, is able to regulate NF-κB activities. H_2O_2 promotes premature senescence in chondrocytes enhancing caveolin-1 mRNA and protein expression via regulation of p-38, MAPK, NF-κB, and COX-2 (S. M. Dai et al., 2006). Also HNE, toxic product generated after lipid peroxidation, affects type II collagens and MMP-13 production by downregulating iNOS via NF-κB inactivation. Moreover HNE can react with IKKα; this inactivate its kinase activity leading to NF-κB inactivation. So HNE abolishes the IL-1β-induced NF-κB activation (C. Ji, Kozak, & Marnett, 2001; Lepetsos et al., 2019). Together

NADPH oxidase-dependent ROS generation in combination with activation of RAGE, mediate advanced oxidation protein products (AOPPs)-induced chondrocytes apoptosis through the activation of NF-κB (Ye et al., 2016).

1.7 NOVEL THERAPEUTHIC APPROACHES FOR INCREASE CARTILAGE REPAIR

Articular cartilage is a highly specialized tissue in which lesions seldom heals or heal only partially under certain biologically conditions. Injuries can progress rapidly and lead to destruction of cartilage structure and its mechanical features. Due to difficulties in self-repair various interventions have been developed to facilitate regeneration of cells and cartilaginous matrix. Surgical treatments are needed because injuries at cartilage are associated with a lot of symptoms including, joint pain, joint-locking phenomena and reduced or disturbed joint function leading sometime to a permanent disabilities. Traditionally cartilage repair has been pursued by the application of two main treatments. If cartilage is severely damaged and the majority of articular cartilage is disabled, whole joint surgery can be performed where the living biological tissue is replaced with a prosthetic device. However the synthetic material cannot fully substitute the complexity of the biologically nature cartilage matrix. If cartilage injury is small and localized, an autograft or allograft can be trimmed to size and fit into the defects. However this solution offer limited-term benefits especially in older patients with low differentiation abilities (Madry, Grün, & Knutsen, 2011). Some techniques were developed to try to enhance the spontaneous repair response in cartilage such as abrasion chondroplasty, Pridie drilling and microfracturing (microdrilling). The aim of these treatments is to expose the lesioned cartilaginous tissue to the bone-marrow spaces, leading to a spontaneous repair response which is based upon surgically-induced bleeding from the subchondral bone spaces and subsequent blood-clot formation. However the healing response

is highly variable and non-reproducible, and the tissue that is formed is more fibrous than hyaline (Charalambous, 2014; Jackson, Lalor, Aberman, & Simon, 2001). The success of these techniques depends on some factors like patients age and physical activity level, the severity of the trauma and the follow-up period (Bert, 1993). The idea of drilling holes in the damage cartilage was made by Pridie in 1959, with the aim to stimulate the spontaneous repair reaction in cartilage (Insall, 1974). However the tissue that is formed is variable in composition, structure and durability. So the intervention is nowadays performed in young patients with OA condition with the aim to improve joint functionality and decrease the power of symptoms (Müller & Kohn, 1999). However this procedure confer short-term benefits only in younger patients (E. B. Hunziker, Lippuner, Keel, & Shintani, 2015). Microfracturing technique is a modification of Pridie drilling. After removal the calcified-cartilage layer, multiple holes are created in the bone plate and the bone trabeculae. This process is associated with bleeding and blood clot formation. The technique was updated and called midrodrilling which is better controllable, more reproducible and less traumatic (H. Chen et al., 2009; Sledge, 2001). Now microdriling is performed more widely than any other bone-marrow stimulation techniques. These techniques has been used for lots of younger patients, given good results, improved joint functionality and relief from pain in 60-80% of cases (Asik, Ciftci, Sen, Erdil, & Atalar, 2008). This is probably due to the large numbers and high activity-levels of the participating precursor-cell pools in younger patients, responsible for an increased repair capacity than in older people (Kreuz et al., 2006). Nowadays these technique has been combined with the introduction of thin-layered, blood-adsorbing matrix of collagen type I and II or chitosan glycerol phosphate (Gille et al., 2010; Marchand et al., 2012). However the highly bio-incompatibility of the implanted matrix material and the fibrin itself generated after bleeding increase the inflammatory response. Some good results are obtained using

collagenous matrix introduced into the defect void after a stimulation of bone-marrow by microdrilling. These technique is called autologous matrix-induced chondrogenesis. Advantages are that it doesn't need cell transplantation and it can be performed during a single surgical intervention (Dhollander et al., 2011; E. B. Hunziker et al., 2015).

Another widely known technique is the osteochondroal transplantation, in which the idea is to implant chondral and ostechondral tissue itself inside the articular cartilage damages. This transplantation technique can be both autografts or allografts (Brent, Tanzer, Rueckert, & Brown, 1992; Hangody et al., 2001; E. B. Hunziker et al., 2015). The autologous osteochondral treatmen strategies currently in use is called mosaicplasty and is used for full-thickness lesions. Into these defects surgeons introduce several or multiple pieces (plugs) of autologous graft material. One of the most serious problems is related to the area from which the autologous osteochondral plugs are removed, because surgeon is accidentally creating additional lesions generating new sites that can be responsible for the joint degeneration, exacerbating the pathological process. Than the plugs are press-fitted with hammering into the subchondral bone. This process can induce injuries in the transplanted cartilage leading to an immediate death of chondrocytic population (Quinn, Grodzinsky, Hunziker, & Sandy, 1998). Moreover, the plugs can be transplanted into a site with different mechanical loading leading degeneration due to unphysiological loading.

Allogenic osteochondral graft does not try to induce cartilage repair but the aim is to substitute the failed or lost tissue with healthy articular cartilage derived from cadavers. An important drawbacks of this technique is the inevitably immunological problems (Stevenson, 1987). However patients with large cartilage damage and large osteochondral defect due to tumor resection,

osteonecrosis, extensive trauma, severe OA benefit greatly from this technique (E. B. Hunziker et al., 2015; Zouzias & Bugbee, 2016).

Cell are the driving forces of cartilage formation and for the maintaining the homeostasis inside the cartilage. For this reason cell based therapies to promote cartilage repair were developed. The idea is to implant externally cultivated cells to replicate and stimulate native regeneration. Chondrocytes was the first cell used to attempt cartilage repair, and the technique was called autologous chondrocytes implantation (ACI) (Brittberg et al., 1994). Initially a biopsy of healthy cartilage is arthroscopically harvested from a low- or a non-load-bearing location of a damaged cartilage. The tissue is then enzymatically digested to release the chondrocytes which are expanded in culture to obtain enough cell for the treatment (Grande, Pitman, Peterson, Menche, & Klein, 1989). In this treatment a membrane is placed over the defect and filled out with a suspension of chondrocytes and sutured to the surrounding cartilage to ensure chondrocyte localization within the lesion. Initially a periosteal cut from the patient's bone was used as membrane. Nowadays synthetic membranes made of collagen type I and type III are also used. More recently a matrix associated variant of ACI-approach was introduced in which autologous chondrocytes are embedded within a matrix rather than suspended in a fluid and the membrane is not needed (Jones et al., 2008). However clinical trials reported no significant better result of ACI in comparison to microfracture surgeries (Knutsen et al., 2007). When chondrocytes are expanded in vitro on plastic they tend to dedifferentiate and start producing type I collagen. These can lead to hypertrophic chondrocytes differentiation when they are implanted into the lesion. Nevertheless it has been noted that the cartilage formed following ACI procedure seems to be fribrocartilage rather than hyaline cartilage, and lacks in compressive strength and frictionless properties of hyaline cartilage (Bernhardt et al., 2009; Madry et al., 2011).

Many research teams tend to focus on the elaboration of novel tissue-engineering based strategies. This approach combines cells and biomaterial scaffold trying to reconstruct the tissue both functionally and structurally. Reconstruction can be conducted entirely in vitro, initially in vitro and then in vivo, or entirely in vivo. Success in this process is to use another type of cells avoiding the autologous transplantation of cartilaginous tissue from the patients. For this reasons mesenchymal stem cell (MSCs) are frequently used for tissue engineering and for transplantation itself (Arthur, Zannettino, & Gronthos, 2009). Amongst the various tissue sources bone-marrow-derived MSCs are the most used both in vitro and in vivo (Johnstone et al., 1998; Yoo et al., 1998). These cells have a high capacity for chondrogenesis only in presence of appropriate stimulation factors. This technique was used to treat large lesion within the femoral condyle of an athlete. The bone-marrow MSC were aspirated 4 weeks before the treatment and expanded in culture. Then cells were embedded in a collagenous gel and transferred into the articular lesion (Kuroda et al., 2007). Knee outcome scores improved but biopsies revealed the presence of fibrocartilage instead of hyaline cartilage. Importantly, MSCs are heterogeneous cell population that can generate fibrocartilage and hypertrophic chondrocytes along with the desired articular-cartilage-producing chondrocytes (Huey, Hu, & Athanasiou, 2012). To guide the differentiation towards the correct cell type MSCs require the presence of appropriate stimulation factors. One of the limitation of the use of MSCs is that their chondrogenic potential declines with the age (Zheng, Martin, Duwayri, Falcon, & Buckwalter, 2007). To overcome this problem MSCs can be taken from different sources like synovium. MSCs from synovium have the higher chondrogenic potential which doesn't decline with age (De Bari, Dell'Accio, Tylzanowski, & Luyten, 2001).

Trying to derive articular chondrocytes that produce matrix and regenerate cartilage researches investigate the capacity of pluripotent stem cells, such as

embryonic stem cells (ESCs) and the induced pluripotent stem cells (iPSCs). ESCs use in highly debated due to the ethical problems around their derivation. However, iPSCs provide the same pluripotency without this drawback. iPSCs can be autologous, because they can be derived from small sample of various tissues including skin and blood. Moreover the differentiation process into chondrocytes can be achieved using two different ways; by deriving firstly a population of MSCs, or by differentiating the cells directly into chondrocytes (Craft et al., 2013; Diekman et al., 2012; Weil et al., 2012). In comparison to chondrocyte derived from MSCs, chondrocytes differentiate from pluripotent stem cells had higher gene expression of cartilage specific genes (SOX9, COL2A1, AGC) and reduced expression of hypertrophic and bone-producing genes (COL10A1, COL1A1, RUNX2) (Ko, Kim, Park, & Im, 2014). The challenge is to efficiently produce and safely controlling these cells, because iPSCs production has low yields for low mass production. Moreover occasionally the implantation of pluripotent stem cells has occasionally resulted in teratoma generation (Saito et al., 2015).

Another type of therapies is to inject and to use biomaterials scaffold to increase the self-repair of cartilaginous tissue, which is composed mainly of intricated ECM. Scientist are now trying to develop a biomaterial that can mimic cartilage. In particular, these biomaterials need to have the same mechanical properties of cartilage, the possibilities of integration with the adjacent cartilage and durability (Cucchiarini et al., 2014). Currently the biomaterial used in clinical are biodegradable, with the aim that the biomaterial is eliminated from the body after providing the functional properties for the regeneration. Up of 80% of articular cartilage is made of water so hydrogel polymer networks are ideal for regenerating cartilage in situ and in vitro. Hydrogels can be tailored for the desired application, modulating the type of polymer, the crosslinking method, the degradation rates and the incorporation of various molecules (Spiller, Maher, &

Lowman, 2011). Hydrogels can be classified based on the polymer composition into natural or synthetic materials, but some mixed hydrogels are now commonly used. Natural polymers can derive from both animals or plant source, and the most used are alginate, agarose, silk collagen and hyaluronan. Mechanical properties of these hydrogels can be modulates using right formulations and postprocessing methods (Bernhard & Vunjak-Novakovic, 2016; Elisseeff, Puleo, Yang, & Sharma, 2005). Collagen and hyaluronan are the two most popular natural polymers used for cartilage tissue engineering (Di Lullo, Sweeney, Körkkö, Ala-Kokko, & San Antonio, 2002). Collagen can support cell attachment and stimulate the synthesis and assembly of new ECM. However collagen hydrogels are mechanically weaker than the surrounding tissue and degrade too fast, to overcome this problem collagen can be crosslinked but this process can impact cells differentiation and viability (C. R. Lee, Grodzinsky, & Spector, 2001; C. H. Li et al., 2011). Hyaluronan based hydrogels was introduced because chondrocytes surrounded themselves with a pericellular matrix made by hyaluronan. These hydrogels permit the attachment of cells and they trigger the differentiation into chondrocytes stimulation the production of new ECM (Bernhard & Vunjak-Novakovic, 2016; Foss, Merzari, Migliaresi, & Motta, 2013; Tognana, Padera, Chen, Vunjak-Novakovic, & Freed, 2005). Some drawbacks of hyaluronan based hydrogels are the insufficient mechanical integrity and short lifetime for fast degradation by MMPs (Bernhard & Vunjak-Novakovic, 2016).

Synthetic polymers allow scientist to control all structural and mechanical properties. Polyglycolic acid (PGA) and polylactic acid (PLA) are most used synthetic polymer due to their capability to be degraded by simple hydrolysis with a controllable rate by adjusting the composition and monomers (Shen et al., 2014). However, the problem of these materials it that they doesn’t provide motive that permit cell attachment. So some biological motifs or bioactive

molecules can be functionalized into the hydrogel mashes to promote cell attachment (Shen et al., 2014; Vinatier, Mrugala, Jorgensen, Guicheux, & Noël, 2009). An important trend in joint surgery is to use the arthroscopic procedure or to minimize the severity of the intervention. For this reasons the use of injectable hydrogels is very interesting (Hou, De Bank, & Shakesheff, 2004). Nowadays there are some injectable hydrogels that are liquid during the injection and can change their physical properties becoming hydrogel in the body due to thermal activation mediated crosslinking at the body temperature or by light activation (Elisseeff et al., 1999; Munarin, Petrini, Bozzini, & Tanzi, 2012).

The incorporation of cells into biomaterials scaffold makes cartilage repair more complex but overcome some problems to use the two technique alone. Recently biphasic scaffold become more popular, these bilayers consist of two different materials, an upper one to conduct chondrogenesis and destinated for the cartilaginous compartment and a lower one of ceramic-like substance which can be pressed as a plug into the subchondral bone (I. M. Khan, Gilbert, Singhrao, Duance, & Archer, 2008). One challenge is to develop a construct with matrix cells and signaling molecule which can be used to trigger differentiation into chondrocytes and ECM production. In vitro some experiments have involved various combination of matrix cell types and growth factors. These include collagenous and gelatin matrices containing MSCs and TGF-β1, agarose matrices with chondrocytes and FGF-2, fibrinous matrices with chondrocytes and IGF-1 and PLA matrices with perichondral cells and TGF-β1 (Andrades et al., 1999; Angele et al., 1999; E. B. Hunziker et al., 2015). The incorporation of growth factors and biomolecules like dexamethasone and TGF-β1 facilitate cartilage regeneration (Bae, Choi, Han, & Park, 2010; Park, Temenoff, Holland, Tabata, & Mikos, 2005). Another approach is to use signaling molecule entrapped in an appropriate delivery system. This ensure that the differentiation process takes place in a controlled and timely manner and this differentiation process can occur

in vivo under physiological condition of mechanical loading (Višňa, Paša, Čižmář, Hart, & Hoch, 2004).

Articular cartilage is a complex environment in which a lot of factors are involved. For this reason mechanical stimulation, oxygen tension and 3D bioprinting are utilized to replicate this in-vivo environment supporting chondrocytes differentiation and matrix production. To replicate the mechanical forces present in articular cartilage, compressive forces are applied to the tissue-engineered constructs during in-vitro calculation. Special bioreactors were produced to control the rate and the amplitude of the applied stress (Schulz & Bader, 2007). This promotes chondrocytes differentiation, stimulate matrix production ad increase cell viability (Bhardwaj, Devi, & Mandal, 2015; Vinatier et al., 2009). Constructs made into this bioreactors are more closely to the compressive properties of natural cartilage and forces direct matrix alignment and deposition by chondrocytes (Arokoski, Jurvelin, Väätäinen, & Helminen, 2000). However some studies revealed that chondrocytes don't experience direct compressive stress but a hydrostatic pressure due to the movement of extracellular fluids. For this reason hydrostatic bioreactor are produced to try to replicate the in-vivo environment of articular cartilage loading (Pörtner et al., 2009; Schulz & Bader, 2007). Another factor is that cartilage is an hypoxic environment, so a lot of in vitro culture are performed in a low oxygen tension. This permits to enhance MSC chondrocyte differentiation and arrest hypertrophic maturation (Gawlitta, Van Rijen, Schrijver, Alblas, & Dhert, 2012; Zscharnack, Poesel, Galle, & Bader, 2009). Due to its ability to provide a precise control of the initial structure of the construct 3D bioprinting technique is gained a lot of attention. With this method specific structure of cartilage can be replicated depositing an appropriate pericellular environment for the cells located in each cell zone (Klein, Malda, Sah, & Hutmacher, 2009). Despite the increased ability of tissue engineering to mimic the native environment of cartilage current tissue

structure and still not mechanically and structural functional to be used in clinical. For these reasons research of new biomaterials is still the focus of research for cartilage degeneration to find a new matrix or to combine the already used matrix to better mimic the cartilage tissue (Bernhard & Vunjak-Novakovic, 2016).

Chapter 2 - Role of high glucose environment on immortalized chondrocyte C28/I2 cell lines

2.1 Aim of the work

Osteoarthritis (OA) is the most common type of joint arthritis disease and also one of the leading causes of pain and disability worldwide (S. R. Goldring & Goldring, 2016; Johanne Martel-Pelletier et al., 2016). OA is characterized by progressive degeneration of articular cartilage and signs and symptoms of inflammation, leading to structural and functional impairments of the joint (Mary B. Goldring et al., 2011; Marcu et al., 2010). The heritability, ageing, female gender and previous knee trauma have long been recognized as the major risk factors of OA (Johanne Martel-Pelletier et al., 2016). Several recent studies have pointed out that the metabolic factors are also be involved in the pathophysiology of OA and these include obesity, diabetes, hypertension and dyslipidemia (Courties & Sellam, 2016; Le Clanche et al., 2016b). The type 2 diabetes mellitus (T2DM) is a chronic metabolic disease associated with many complications, and accumulating epidemiological and experimental observations support that T2DM is an independent risk factor for OA progression (Louati et al., 2015; Schett et al., 2013). However the correct molecular mechanism underlying the connection between OA and T2DM are still less known. T2DM has a pathogenic effect on OA through 2 major pathways. First, chronic hyperglycemia induces oxidative stress, overproduction of pro-inflammatory cytokines and AGEs in joint tissues and also reduced the stem cells potential of differentiation. Second the insulin resistance could play a role locally but also through the systemic low-grade inflammation state (Courties & Sellam, 2016). It has been proposed that local inflammation may be an important mechanism link between the two disease. Glucose concentration has an important role in the link of the two pathologies. In particular local hyperglycemia can increase the AGEs activating the production of catabolic and proinflammatory mediators leading to cartilage remodeling and

degradation (Berenbaum, 2011). Moreover hyperglycemia cause a low-grade systemic inflammation that may contribute to OA progression (Courties & Sellam, 2016; Robinson et al., 2016). Nevertheless high glucose concentration in the media can reduce the cell viability of chondrocytes (Hosseinzadeh, Bahrampour Juybari, Kamarul, & Sharifi, 2019). However the cartilage environment is scarce in glucose and estimates predict that glucose concentration in cartilage may reach 1 mM and chondrocytes are well adapted to take glucose from this environment. However a lot of studies used 5.5 mM or more as a normal glucose concentration for chondrocytes and cartilage (Y. J. Chen et al., 2015; M. Lin et al., 2012).

Here in this studies we used the immortalized chondrocytes C28/I2 which are a good model to reproduce the chondrocytes behaviors and to study the signaling pathways activated by different stimuli. We tried to study the effect of an high glucose environment in chondrocytes cells, focusing our attention on the cytoskeleton proteins and RalA pathway which can regulate cytoskeleton network. We further investigate the effect of high extracellular glucose on some key protein like MAPK and NF-κB. Then we used different media containing FBS or ITS using the IL-1β to stimulate the OA chondrocytes phenotype. To make the study more reliable we changed every day the media to see the real effect of glucose concentration and all the analyses were made after 72h, to stimulate a long exposure to an high glucose environment.

2.2 Materials and Methods

2.2.1 Antibodies and Reagents

For experiments with C28/I2 antibodies purchased from Cell Signaling Technology were to iNOS, vinculin, actin and LC3I/II. Antibodies purchased from Santa Cruz Biotechnology were to GAPDH, NF-κB and phospho-ERK, total-ERK and SOX9. Mouse monoclonal anti-β-tubulin was purchased from Sigma Aldrich. Anti-RalA mouse antibodies were obtained from Transduction Laboratories. Recombinant human IL-1β was purchased from Immunotools. TRTC-labelled phalloidin was purchased from Sigma Aldrich. Alexa Fluor 488 goat anti-mouse IgG were obtained from Life Technologies. For western blot analysis, the following antibodies were used: peroxidase-conjugated donkey anti-rabbit or anti-mouse secondary antibodies were from Amersham BioSciences

For experiments with human primary chondrocytes, antibodies purchased from Cell Signaling Technology were to phospho-Akt (Ser473), total-Akt, phospho-p38 (Thr180/Tyr182), total-p38, phospho-ERK (Thr202/Tyr204), total-ERK, phospho-p65 (Ser536), total-p65, and GAPDH. Antibodies purchased from Abcam were to MMP-13 and MMP-2.

2.2.2 Cell Culture

The immortalized chondrocyte cell line, C28/I2, was a kindly gift from Prof. Francesco Dell'Accio (Queen Mary University of London, London, UK). C28/I2 cell line was originally obtained from cells isolated from cartilage and transduced with simian virus 40 containing T-antigen and was employed in this study (Mary B. Goldring, 2004). Frozen C28/I2 cells were revived by thawing in a 37°C water bath and then cultured in Dulbecco's modified Eagle's medium (DMEM)/ F-12 medium (1:1) medium (DMEM/F12; L0091-500, Biowest®) containing 10% heat inactivated fetal bovine serum (FBS) (EuroClone®), 1% penicillin/streptomycin

and 17 mM of D-Glucose monohydrate (Biowest®) at 37°C and 5% CO_2 till 90% confluence with the medium changed every three days in a Galaxy 170 S Incubator (Eppendorf®). Cells were washed with 1 X phosphate buffered saline (PBS) and were harvested using Trypsin-EDTA 1X in PBS (Euroclone®) digestion at 37°C for 5 min. The cells were claimed by centrifugation and resuspended in DMEM/F12 medium supplemented with 10% FBS and 1% penicillin/streptomycin followed by incubation for cell propagation and right glucose concentration was added.

Normal articular cartilage was obtained from the talus of human tissue donors provided by the Gift of Hope Organ and Tissue Donor Network (Itasca, IL) through collaboration with Rush University Medical Center (Chicago, IL). Prior to dissection, cartilage was macroscopically inspected for gross evidence of damage and only normal appearing cartilage was used. Chondrocytes were isolated and cultured in monolayer culture. Cartilage was dissected from the joint, with care taken to avoid underlying bone or tissue from osteophytes. Cartilage slices were digested in DMEM/F-12 medium (1:1) containing 0.2% Pronase (Calbiochem, San Diego, CA) in an incubator with continuous agitation for 1 hour, and then overnight with 0.025% collagenase P (Roche, Indianapolis, IN) in DMEM/F-12 supplemented with 5% fetal bovine serum. After isolation, the cells were counted. Prior to culture viability was assessed using trypan blue dye exclusion and was determined to be 90% (Richard F. Loeser, Pacione, & Chubinskaya, 2003).

2.2.3 Trypan blue exclusion assay (cell growth)

C28/I2 cells were plated at a density of 20000 cell/ml in a 24 well plate and for each different glucose concentrations (0.25 mM, 2.5 mM, 25 mM, 50 mM, 100 mM and 150 mM) were used 4 wells. Each media was changed gently every day to maintain the exact glucose concentration for all time required for the

experiment. At desired time point (48 h, 72 h and 96 h) cells were harvested with trypsin-EDTA and collected in conic tubes which contain completed medium (ratio 1:1, v/v, trypsin/medium). Live cells were recognized by trypan blue exclusion assay and counted using a Bürker chamber. Cell number were collected and % of cell growth were obtained dividing the N° of cells at that time point/N° of cell plated X 100. For cells growth experiment using preconditioned cells, C28/I2 cells were maintained in 6 different 10 cm dishes, each one for a different glucose concentration used (0.25 mM, 2.5 mM, 25 mM, 50 mM, 100 mM and 150 mM), for 7 days before harvesting and plating cells in 24 wells as previously described.

2.2.4 ROS analyses by DCFDA

The level of intracellular ROS was quantified by fluorescence using dichlorofluorescein diacetate (DCFDA, Invitrogen). C28/I2 confluent monolayer culture were harvested and 10^4 cells were plates in each well of 96 wells plate using DMEM/F-12 medium without glucose. Immediately after plating in media supplemented with 10% of FBS or 1% of ITS (Insulin-Transferrin-Selenium, Invitrogen®); 10 ng/µL of IL-1β was added when required. Glucose was added to reach the final concentration of 0.25, 2.5 or 25 mM. Media was replaced every 24 h to maintain the correct glucose concentration. After 72 h cells were washed with PBS and stained with 17 µM DCFDA in PBS for 1 h at 37°C in the dark. Fluorescence was recorded with an excitation wavelength of 490 nm and an emission wavelength of 525 nm using VICTOR multilabel plate reader (PerkinElmer). Then cells were washed twice with PBS and extracted with 0.5 mM NaOH in PBS for 10 min at 37°C. Protein were quantified by Bradford technique using VICTOR multilabel plate reader. Then fluorescent intensity for each well were normalized on the total protein amount for each wells (Mendis,

Kim, Rajapakse, & Kim, 2008). Each experiments were made 3 times in triplicate.

2.2.5 ROS quantification using DHR-123

C28/I2 cells were plated at a density of $5x10^4$ cell/mL on gelatin pre-treated coverslips. Cells were growth for 72 h with DMEM/F12 + 10% FBS using 3 different D-glucose concentration: 0.25 mM, 2.5 mM and 25 mM. Media was replaced every 24 h. Then cells were washed gently with PBS and 10 µM of DHR-123 (Sigma-Aldrich) was added to the cells in HBSS solution for 1 h at 37°C in the dark. Then slides are mounted using Mowiol mounting media (Sigma Aldrich) and fluorescent images were captured using a Leica DMIRE2 inverted microscope equipped with 63x/1.4 NA Plan-Aphocromat oil immersion objective. Using ImageJ, an outline was drawn around each cell and circularity, area, mean fluorescence measured along with several adjacent background readings. The total correct cellular fluorescent (CTCF) = integrated density – (area of selected cell × mean fluorescence of background readings), was calculated. Bar graphs and statistical analyses (Two ways-ANOVA and Tukey HSD post-hoc tests) were performed using GraphPad Prism 6.

2.2.6 Apoptosis with Annexin V/propidium iodide staining

Apoptosis was evaluated by Annexin V-binding assay (MArca) in C28/I2 cells treated for 72 h with different glucose concentration media supplemented with FBS (0.25 mM, 2.5 mM, 25 mM). Cells were harvested by pipetting with PBS and were washed with cold PBS. Cell suspensions were resuspended in binding buffer (10 mM HEPES-NaOH, pH 7.4, 2.5 mM $CaCl_2$, and 140 mM NaCl). A fraction of 10^6 cells were incubated in binding buffer at room temperature in the dark for 15 min with 5 µL of FITC-conjugated Annexin V and 10 µL of 2.5 µg/mL propidium iodide (Sigma-Aldrich). Annexin V binding was detected

by flow cytometry using CytoFLEX (Beckman Coulter) cytofluorimeter. At least 5×10^4 events/sample were acquired and analyzed using a specific software (CytExpert, Beckman Coulter).

2.2.7 Immunofluorescence

C28/I2 chondrocytes were plated at a density of $5x10^4$ cell/mL on gelatin pre-treated coverslips. Cells were maintained for 72 h in DMEM/F12 + 10% FBS using 3 different D-glucose concentration (0.25 mM, 2.5 mM and 25 mM). Media was replaced gently every 24 h. Cells were then fixed for 10 min with 3.7% paraformaldehyde in phosphate buffered saline (PBS), permeabilized for 4 min with 0.1% Triton X-100 in PBS and stained with different antibodies. In particular cells were treated with TRITC-phalloidin for actin staining as described previously (Ceriani et al., 2007). For tubulin staining, anti-mouse monoclonal anti-β-tubulin primary antibodies (1:150) were used; secondary antibodies were Alexa Fluor 488 goat anti-mouse IgG (1:200). Fluorescence images were captured with a Leica TCSSP2 confocal microscope equipped with a 63x/1.4 NA Plan-Apochromat oil immersion objective. Using ImageJ, an outline was drawn around each cell and circularity, area, mean fluorescence measured along with several adjacent background readings. The total correct cellular fluorescent (CTCF) = integrated density – (area of selected cell × mean fluorescence of background readings), was calculated. Bar graphs and statistical analyses (Two ways-ANOVA and Tukey HSD post-hoc tests) were performed using GraphPad Prism 6.

2.2.8 Western Blots

Cell proteins extract were made using RIPA buffer [20 mM Tris, pH 7.5, 150 mM NaCl, 1 mM EDTA, 1 mM EGTA, 1% Triton X-100, 0.25% sodium deoxycholate, 2.5 mM sodium pyrophosphate, 1 mM glycerol phosphate, and 1

mM Na3VO4, with 2 mM phenylmethylsulphonyl fluoride(PMSF, Sigma)] to detect SOX9, phospho/total ERK1/2, NF-κB, phospho/total p65, phospho/total p38, phospho/total Akt, LC3I/II and iNOS. Then Ral Buffer [50 mM Tris–HCl, pH 7.4, 10% glycerol w/v, 200 mM NaCl, 2.5 mM MgCl2, 1% NP-40 (Sigma) w/v, 1 mM DTT, 25 mM NaF, 1 mM Na_3VO_4, 1 mM PMSF] was used to detect tubulin, vinculin, actin and RalA. For C28/I2, cells were plated in 10 cm dishes and after 72 h in the described conditions cell protein extract were prepared and 30 μg of total protein extract were loaded on polyacrylamide gels. Western blots were made according to standard procedures using nitrocellulose membranes (Protran). Immunoblots were probed with anti-tubulin, anti-vinculin, anti-actin, anti-SOX9, anti-LC3I/II, anti-phospho-ERK1/2, anti-total ERK1/2 and anti-iNOS primary antibodies. Signals were detected using peroxidase-conjugated donkey anti-rabbit and anti-mouse secondary antibodies and reveled by ECL detection system WESTAR NOVA 2.0 (Cyanagen). Experiments were repeated three times. Densitometry were made using imageJ software and GAPDH was used as loading control. Tot-ERK1/2 was used as loading control for p-ERK1/2. GraphPad Prism 6 was used for graphical representations and statistical analyses.

For human primary chondrocytes, cells were plated at a density of $5x10^5$ cell/ml in 6 wells plates and maintained in medium supplemented with 10% FBS for 48 h. Media was changed with serum-free media and cells were maintained overnight. Then glucose was added to reach 50 mM or 75 mM as final concentration in the media. Cells were maintained for 24 h with the chosen glucose concentration. At the end of the time cell extract were made using RIPA buffer (Cell Signaling) and approximately 15 μg of of total protein extract were loaded on polyacrylamide gels. Immunoblotting and analysis was performed as described before. Analysis of phosphoproteins was conducted using phospho specific antibodies, and blots were stripped and reprobed with antibodies to the total protein as a loading control. Experiments were repeated three times.

Densitometry were made using imageJ software. GraphPad Prism 6 was used for graphical representations and statistical analyses.

For MMP-13, primary chondrocytes were growth as said before then conditioned media were taken and concentrated (10:1) and 30 µl was analyzed by immunoblotting as described for signaling studies but using antibody to MMP-13. Densitometric analysis of MMP-13 bands was performed using ImageJ software. MMP-2 was used as loading control and data were normalized on cells maintained at 25 mM of glucose concentration (Forsyth, Pulai, & Loeser, 2002; S. T. Wood et al., 2016).

2.2.9 RalA pull down

C28/I2 chondrocytes were plated in 10 cm dishes and maintained for 72 h in media supplemented with 10% FBS or 1% ITS with different glucose concentration (2.5 mM and 25 mM). IL-1β (10 ng/ml) was added when described to simulate OA environment. Media was replaced every 24 h. After 72 h cells were lysed with Ral buffer supplemented with Complete ™ EDTA Free. The GTP-bound form of RalA was isolated using activation-specific probes and subsequently quantified as described (De Rooij & Bos, 1997; Rebhun, Chen, & Quilliam, 2000). Briefly, a recombinant RID-GST (Ral Interacting Domain) fusion protein, coupled to Glutathione–Sepharose beads, was used to isolate the active Ral-A from total cell lysates. Approximately 20 µg of GST-RID was bound to 60 µl of Glutathione-Sepharose beads (50% slurry) and 800 µg of total C28/I2 protein lysates were used for the assay. 60 µl of SDS-PAGE sample buffer was finally added to beads; 30 µg of total protein extract was loaded on 8% SDS-polyacrylamide gel while for Ral-GTP extracts the whole sample was loaded on 8% SDS polyacrylamide gels. The RalA protein was visualized using anti-RalA antibodies. C28/I2 growth in 2.5 mM glucose media supplemented with FBS or

ITS was used as control. Differences between groups were tested for significance by applying the ANOVA test and Dunnett post-hoc test.

2.2.10 Statistical analyses

Data were analyzed by Student's *t* test (for two-sample comparisons) or a one-way or two-way ANOVA (for comparison of more than two samples) with a Dunnett's or Tukey honestly significant difference post hoc correction, as appropriate, using GraphPad Prism version 6 (GraphPad Software, Inc.). Results are presented as mean values ±S.D. from a minimum of three independent biological replicates. A level of $p < 0.05$ was considered to be significant.

2.2.11 Study approval

Use of human tissue was in accordance with the Institutional Review Board at the Rush University Medical Center and the University of North Carolina at Chapel Hill.

2.3 Results

2.3.1. *C28/I2 chondrocytes prefer to growth in media supplemented with 2.5 mM of glucose.*

C28/I2 cell line is well characterized and as already use as a good cellular model to study chondrocytes behaviors in response to different stimuli and as already used for study the glucose effect in chondrocytes (Finger et al., 2003; Hosseinzadeh et al., 2019; Robbins et al., 2000). For this reasons in order to study the molecular effect of high glucose concentration in chondrocytes C28/I2 were chosen as a cellular model. Firstly we evaluated the best growth condition of C28/I2 in FBS supplemented media under different glucose concentration (0.25 mM, 2.5 mM, 25 mM, 50 mM, 100 mM, 150 mM of D-glucose in DMEM/F12 media). Briefly, C28/I2 cells were plated in 24 well plate at 20000 cell/ml using media with 6 different glucose concentration. Media was changed every 24h to maintain the correct glucose concentration. After 48 h, 72 h and 96 h C28/I2 chondrocytes were counted. Percent (%) of cell growth were calculated based on the cells number used for plating. As shown in Figure 5 A after 72h of cell growth using a specific glucose concentration C28/I2 growth faster using 2.5 mM and 25 mM of glucose concentration. However, after 96 h C28/I2 cells prefer 2.5 mM of glucose concentration into the media; the other glucose concentration exhibit a decrease in % of cell number in comparison to C28/I2 cells growth in media with 2.5 mM of glucose (Figure 5 A and B). To better understand the real role of glucose concentration on C28/I2 cell growth and to produce a more physiologic models to study the effect of glucose on cartilage, the same experiment were reproduced using C28/I2 cells which were maintained for 1 week in media with each different glucose concentration used. These preconditioned cells were used for the same cell growth experiment. However, no significant changing between the previous experiment were seen and the outcomes were quite the same (Figure

5 A and C). At 96 h C28/I2 growth more using media supplemented with 2.5 mM of glucose concentration respect to other conditions (Figure 5 C). After 96 h, significant decrease in % of cell growth respect to the initial cell number were detected in C28/I2 cells growth at 0.25 mM, 25 mM, 50 mM, 100 mM and 150 mM of glucose concentration in comparison to 2.5 mM which has used as control for the further experiment. From these experiment, 0.25 mM, 2.5 mM and 25 mM of glucose concentration were chosen to be evaluated for the further experiment (0.25 mM as low glucose concentration, 2.5 mM as normal glucose concentration and 25 mM as high glucose concentration). Furthermore, for the future experiments C28/I2 were cultivated with the selected glucose concentration for 72 h to determine the molecular events which leads to this different cell growth.

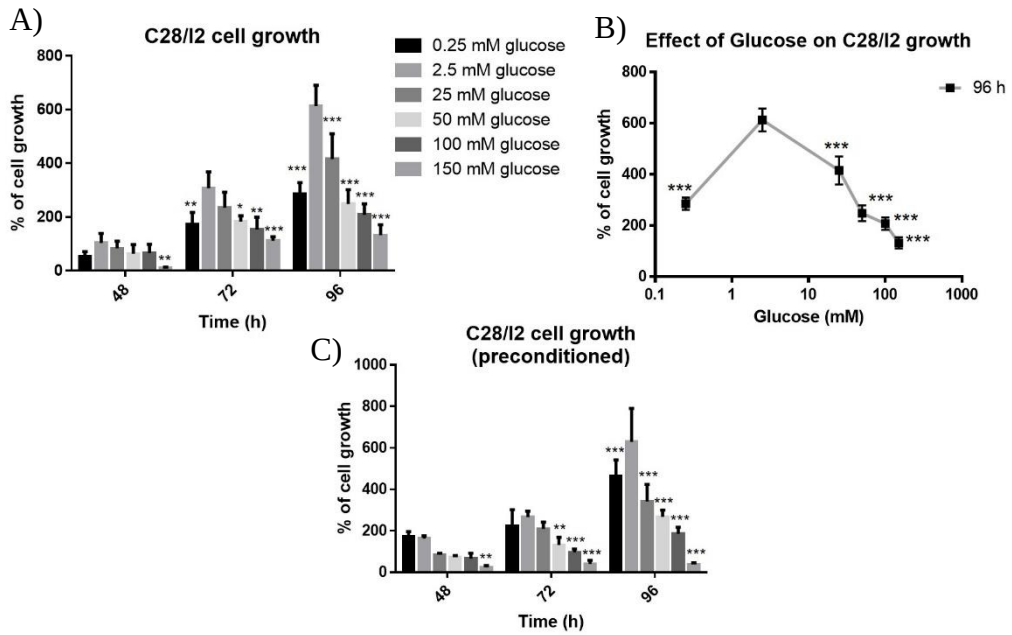

Figure 5 **Effect of glucose concentration on C28/I2 cell growth**. A) Graph showing at different time points the % of C28/I2 cell growth using different glucose concentration. B) Dose/response curve using % of cell growth of C28/I2 after 96 h. 10000 C28/I2 cells were plated into a 24 well plate with 6 different glucose concentrations: 0.25 mM, 2.5 mM, 25 mM, 50 mM, 100 mM and 150 mM (4 wells for each condenctration). Each media was changed gently every day to maintain the exact glucose concentration for all time required for the experiment. At desired time point (48 h, 72 h and 96 h) cells were harvested with trypsin-EDTA and

live cells were recognized by trypan blue exclusion and counted using a Bürker chamber. Cell number were collected and % of cell growth were obtained dividing (N° of cells at time point/ N° of cell plated) * 100. Data of three independent experiment were shown and bars represent standard deviation. Graph were made using Graphpad Prism and statistical analyses were made using the same program. C) Graph showing at different time points the %of C28/I2 cell growth using different glucose concentration. C28/I2 were maintained in six 10 cm dishes using different glucose concentration (0.25 mM, 2.5 mM, 25 mM, 50 mM, 100 mM and 150 mM) for 1 week. Then cells were harvested and used for the growth experiments following the same protocols previously described and used for the A and B image. Data are presented as means ± S.D. Asterisks represents significant differences between cells growth at 2.5 mM (* $p < 0.05$, ** $p < 0.01$, *** $p < 0.001$) (two-way ANOVA).

2.3.2 *High glucose concentration increase ROS levels in C28/I2*

To determine the possible molecular events underlying the lower % of cell growth seen in C28/I2 growth under high glucose and low glucose concentration (0.25 mM and 25 mM) after 96 h (Figure 5), ROS levels were analyzed after 72 h, using two different techniques. Firstly, chondrocytes C28/I2 cells were growth on coverslips with the three different glucose concentrations for 72 h and Dihydrorhodamine-123 (DHR-123) molecular probe were added. DHR-123 fluorescence were visualized using a Leica confocal microscopy and corrected total cell fluorescence (CTCF) were measured. CTCF is higher in C28/I2 growth using 25 mM of glucose concentration, indicating an higher amount of ROS levels (figure 6 A). To confirm this result, ROS levels were also analyzed using 2',7'-Dichlorofluorescein diacetate (DCFDA) fluorescent probe. Cell fluorescence was analyzed using a Victor plate reader. Subsequently fluorescent were corrected using the µg of protein present in each well. Even using this technique, fluorescence/µg were significantly higher in C28/I2 growth for 72 h with 25 mM of glucose concentration in FBS supplemented media (figure 6 B). So, high glucose concentration increase ROS levels in C28/I2 after 72 h.

2.3.3 *High glucose concentration leads to C28/I2 cell death*

To determine if high glucose concentration environment change C28/I2 cell viability, FACS analyses with Annexin V/propidium iodide staining were used. As shown in figure 6 C no significant changes are present into the groups of cells under early apoptotic events, late apoptotic events and necrosis. However, a significant decrease of % of live cells were shown in C28/I2 growth under high glucose concentration media, this is in accordance with a significant increase in the overall cell death occurring in C28/I2 growth in high glucose concentration media supplemented with FBS for 72 h.

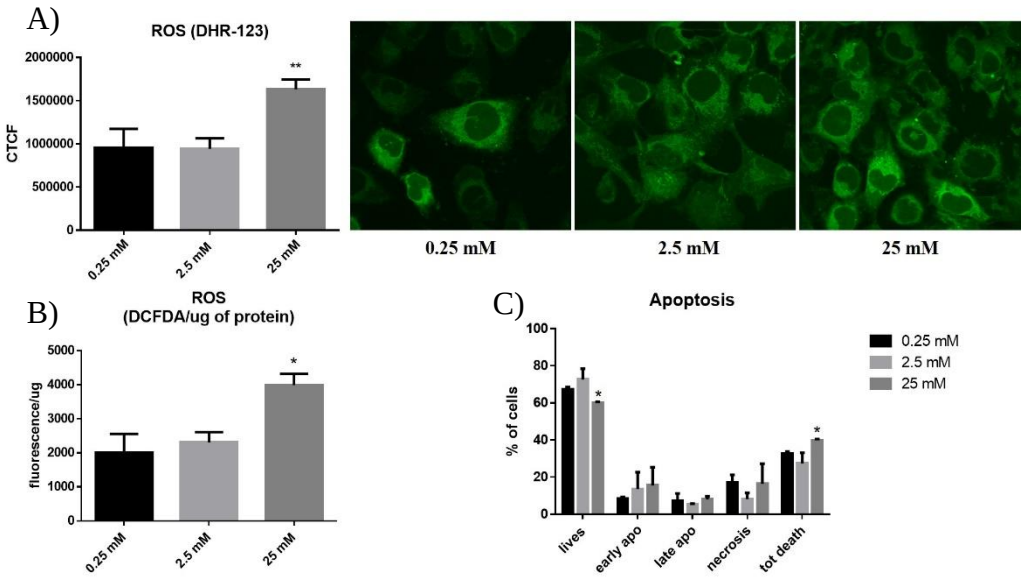

Figure 6 **High glucose concentration increase ROS levels and cell death in C28/I2.** A) C28/I2 were plated on coverslips in three different 35 mm plates, cells were grown for 72 h in DMEM/F12 + 10% FBS with different glucose concentration. Media were changed every 24 h. After 72 h cells were incubated for 1 h with DHR-123 at final concentration of 10 µM. After some washes with PBS, images were collected using Leica TCSSP2 confocal microscope. CTCF were calculated using imageJ software. Data represent the mean of three experiments and for each condition CTCF of 30 cells were measured. B) Cells were growth in 96 wells plate for 72 h with different glucose concentration and media was changed every 24 h. Media was changed with PBS and DCFDA (17 µM) were added for 1 h. Fluorescence intensity were measured using VICTOR multilabel plate reader (PerkinElmer). Then protein quantity were measured using Bradford methods. Fluorescence intensity were normalized on protein levels present in each well. C) Apoptosis were

measured using FACS. C28/I2 were growth in 10 cm dishes with three different glucose concentration for 72 h. Media was changed every 24 h. Then cells were harvested, and 10^6 cells were stained with Annexin V and propidium iodide. Fluorescence intensity was measured using CytoFLEX (Beckman Coulter) cytofluorimeter. Data represent mean of 3 independent experiments. Graph and statistical analyses were made using GraphPad Prism software. Data are presented as means ± S.D. Asterisks represents significant differences between cells growth at 2.5 mM (* $p < 0.05$, ** $p < 0.01$, *** $p < 0.001$) (ANOVA).

2.3.4 *High glucose concentration induce a tubulin cytoskeleton network disorganization without a changing in tubulin expressions.*

Previous studies on different kind of cells showed that glucose concentration can alter the expression levels, structure and functionality of tubulin and actin cytoskeletal proteins (T. Dai et al., 2006; Hien et al., 2016; Z. Lv et al., 2016; S. K. Williams, Howarth, Devenny, & Bitensky, 1982; You et al., 2016). To evaluate if different glucose concentrations could impact actin and tubulin network or the morphology of C28/I2 cells, actin and tubulin cytoskeleton protein were visualized using immunofluorescence technique. Actin and tubulin network disorganization were detected in C28/I2 growth for 72 h in high glucose environment (25 mM); as it is shown in figure 7-A tubulin network appear more disorganized and more near the nucleus in comparison to the C28/I2 cell growth at 2.5 mM which present a tubulin network well organized with microtubules that formed a nest from the nucleus to plasma membrane. C28/I2 growth at low glucose concentration has a well organized tubulin network similar to cells growth at 2.5 mM of glucose concentration (figure 7 A Tubulin). However in this cells tubulin network is highly present inside the nucleus of the cells. Actin network as the same pattern and appear more disorganized in cells growth at 25 mM of glucose, were single actin filaments are not well formed in comparison to the cell growth at 2.5 mM and 0.25 mM of glucose (figure 7 A TRITC). Cell shape appear to change as well, C28/I2 growth at 2.5 mM and 0.25 mM appear more polygonal which is the cell shape of the cell lines growth on plates. However, cells growth at 25 mM appear to be smaller and with more rounded shape respect of C28/I2 growth under the other glucose conditions. CTCF

analyses and western blots reveled no significant changing in the expression of tubulin, actin and vinculin proteins (figure 7 B-C). So, high glucose concentration in 10% FBS supplemented media, induces disorganization of tubulin and actin networks in C28/I2.

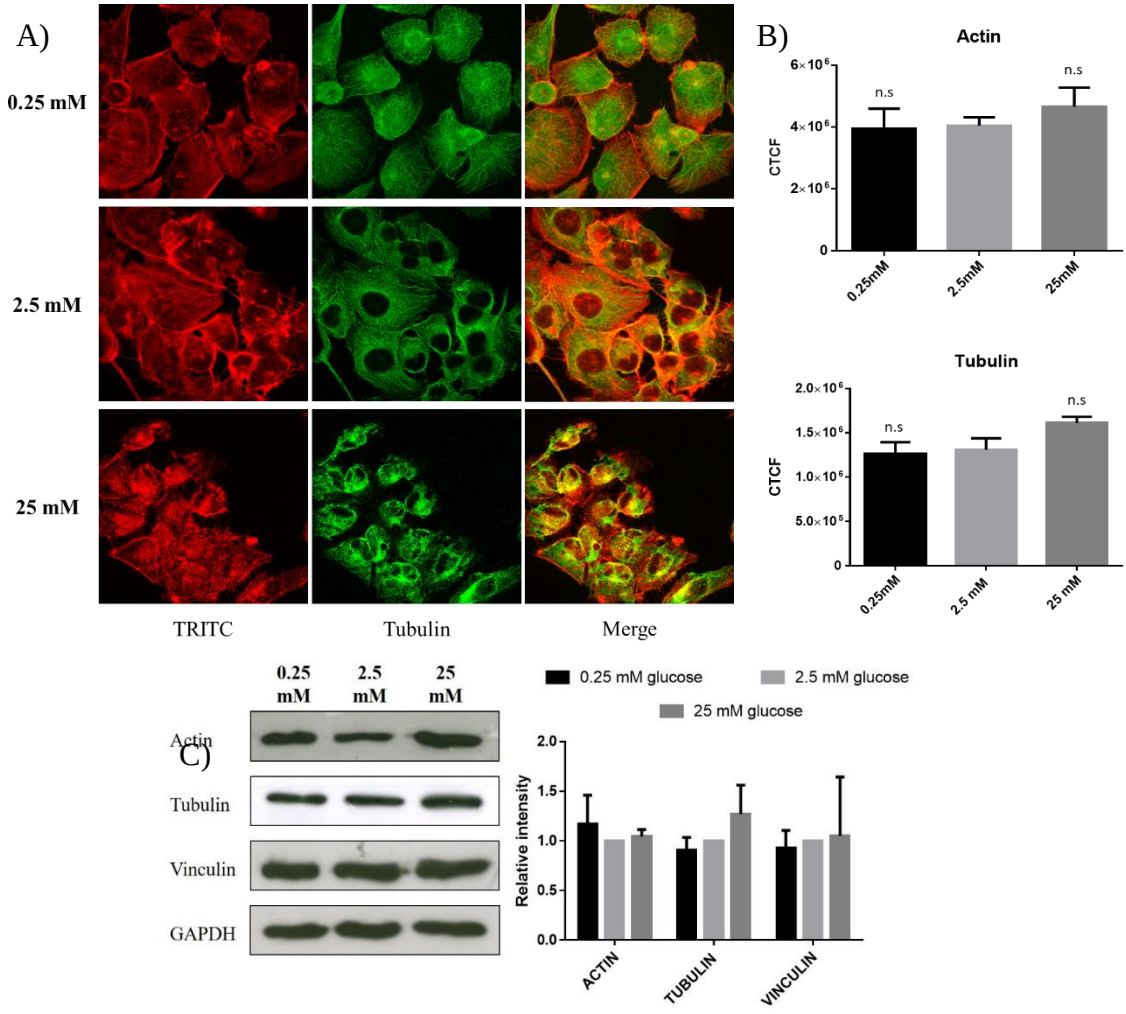

Figure 7 **Cytoskeletal changing in C28/I2 induced by high glucose environment.** A-B) C28/I2 cells were plated on coverslips and after 72 h, cells were fixed with PFA 4% and actin was stained using TRITC-phalloidin, tubulin was stained using anti-β-tubulin primary antibodies followed by a secondary antibody conjugated with Alexa Fluor 488. A) Fluorescence images are shown. B) CTCF were calculated using ImageJ software. Data represent the mean of three experiments and for each condition CTCF of 30 cells were measured. C) Representative immunoblots of tubulin, actin, vinculin and GAPDH expression in C28/I2 growth at different glucose concentration for 72 h, and graph showing the quantification of each protein band intensity normalized on GAPDH signal. Data represent mean of 3 independent experiments. Graph

and statistical analyses were made using GraphPad Prism software. Data are presented as means ± S.D and analyzed by one-way or two way ANOVA (n.s non significative).

2.3.5 *RalA-GTP levels decrease in C28/I2 growth in high glucose media.*

Morphological changing in chondrocytes were frequently associated with dedifferentiation leading to a fibroblast-like shape or to hypertrophy (Blain, 2009; Fioravanti et al., 2003; Woods et al., 2007). So, SOX9 expression was evaluated in C28/I2 cells growth using the three different glucose concentration previously cited. However, no changing was shown among cells growth at different glucose concentration (Figure 8 A).

Cytoskeletal protein organization are regulated by different pathways in cells but it's well known that RalA small GTPase are key regulator protein for cytoskeleton organization (D'Aloia et al., 2018). For this reason, RalA activation was evaluated using pull down technique in cells growth at 2.5 and 25 mM of glucose concentrations. As shown in figure 8 B, C28/I2 cells growth at high glucose concentration exhibits a significant decrease in RalA-GTP amount in comparison to C28/I2 growth at 2.5 mM.

2.3.6 *Autophagy mechanism is down-regulated by high glucose concentration*

Autophagy is an essential process for the maintenance of homeostasis in cartilage by chondrocytes cells (Luo et al., 2019; Ribeiro et al., 2016). Previously it was demonstrated that the enhancement of chondrocytes autophagy can delay the progression of OA (Luo et al., 2019). For this reason autophagy process was evaluated in C28/I2 growth at 2.5 mM and 25 mM of glucose concentration, and to simulate OA chondrocyte phenotype IL1-β was added in the media (Toegel et al., 2008). As you see in figure 8 C, LC3-II levels are higher in cell growth at 2.5 mM of glucose indicating an active autophagy process (Kabeya, 2000). When IL1-β was added to the media the basal level of LC3-II significantly decreases. However, higher decrease of LC3-II levels was detected in C28/I2 growth with

high glucose, and this decrease was detectable even in cells growth with 25 mM of glucose and IL1-β. So, high glucose concentration and IL1-β leads to a decrease autophagy process in immortalized C28/I2 chondrocytes. Furthermore, glucose is more powerful than IL1-β as autophagy inhibitor in C28/I2 cells.

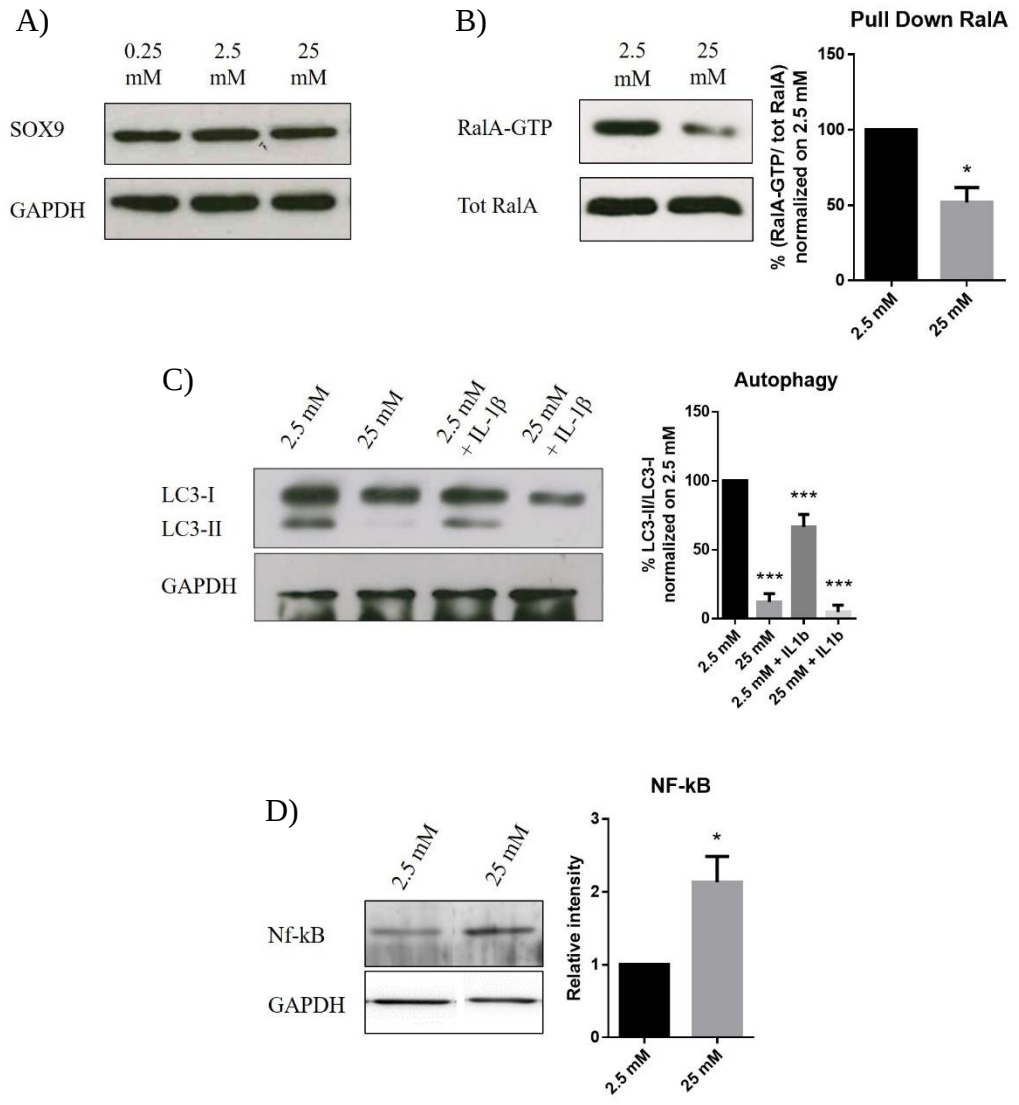

Figure 8 **RalA-GTP, LC3-II and NF-κB but not SOX9 levels changed in C28/I2 growth at high glucose concentration.** C28/I2 were growth using 10% FBS media with the relative glucose concentration for 72 h media was replaced every 24 h. Protein extracts were made using RIPA buffer to detect SOX9, LC3-I and -II and NF-κB, and RalA-buffer was used for the pull down experiment. A) SOX9 expression was evaluated

by immunoblots in C28/I2 cells growth at different glucose concentration. B) Recombinant GST-RID (Ral Interacting Domain) of RalBP1 fusion protein, coupled to Glutathione-Sepharose beads, was used to isolate RalA-GTP. RalA-GTP and RalA was visualized using a anti-RalA antibody. On the left graphical representation of the percentage of active RalA. C) Immunoblots and graphical representation of LC3B-I and LC3B-II proteins obtained from cells growth for 72 h with normal and high glucose concentration media (2.5 mM and 25 mM), IL-1β 10 ng/mL to mimic an osteoarthritic environment. On the left graphical representation of the % LC3B-II on LC3B-I indicating the activation of the autophagy by the formation of autophagosomes which leads to the conversion of LC3B-I into LC3B-II (Kabeya, 2000; Kegel et al., 2000; Luo et al., 2019). D) NF-κB expression in C28/I2 cells growth at 2.5 mM and 25 mM of glucose concentration for 72 h. On the left graphical representation of NF-κB expression normalized on 2.5 mM. Data represent mean of 3 independent experiments. Graph and statistical analyses were made using GraphPad Prism software. Data are presented as means ± S.D and analyzed by student t-test or one-way ANOVA. Asterisks represents significant differences between cells growth at 2.5 mM (* $p < 0.05$, ** $p < 0.01$, *** $p < 0.001$)

2.3.7 NF-κB levels are regulated by glucose concentration in C28/I2

Inflammation is one of the leading causes of OA disease, one of the main inflammatory pathways is the NF-κB pathway. Activation of NF-κB pathways leads to cartilage degradation and destruction and NF-κB is abundant in OA synovium (Roman-Blas & Jimenez, 2006). Furthermore NF-κB is a key regulator of apoptosis, MMPs production and response to cytokines in chondrocytes (Choi, Jo, Park, Kang, & Park, 2019; Olivotto, Otero, Marcu, & Goldring, 2015). So, NF-κB expression was evaluated in human immortalized C28/I2 chondrocytes growth at high or normal glucose concentration by immunoblots. High glucose concentration for 72 h in the media leads to an increase amount of NF-κB in C28/I2 chondorcytes in comparison to chondrocytes maintained using normal glucose concentration media (Figure 8 D). High levels of NF-κB could promote a strong activation of NF-κB pathway by cytokine and the power of NF-κB pathway could be stronger in cells growth using high glucose concentration.

Furthermore, iNOS expression levels were evaluated in C28/I2 chondrocytes maintained at different glucose concentration because previous study demonstrate that NF-κB activation and de-regulation in chondrocytes pathways could promote the expression of iNOS, which start to produce nitric oxide (NO) know to be implicated in the pathogenesis of OA (Schmidt et al., 2010; Vuolteenaho, Moilanen, Al-Saffar, Knowles, & Moilanen, 2001). iNOS

expression seems to increase when glucose concentration is higher into the media, however, more experiment are needed to obtain a statistical significant increase (Figure 9).

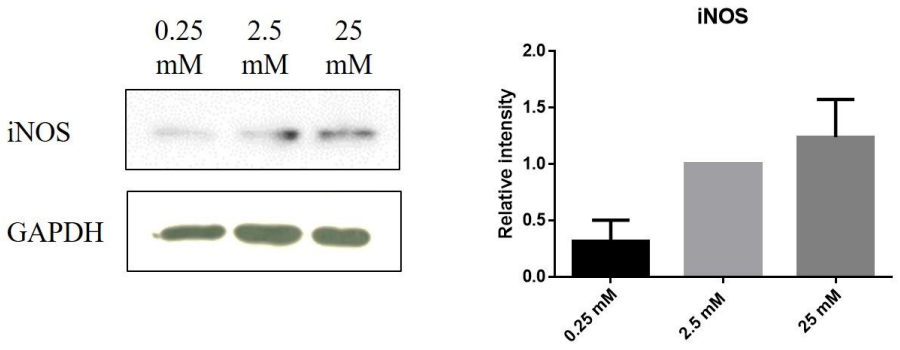

Figure 9 **iNOS expression seems to be regulated by glucose concentration in the media.** C28/I2 were growth using media supplemented with FBS and with the relative glucose concentration for 72 h. Media was replaced every 24 h. Protein extracts were made using RIPA buffer. Immunoblots were incubated with antibody against iNOS and GAPDH as loading control. On the left graphical representation of iNOS relative intensity normalized on 2.5 mM. Data represent mean of 3 independent experiments. Graph and statistical analyses were made using GraphPad Prism software. Data are presented as means ± S.D.

2.3.8 *Glucose-induced ROS don't significantly increase in C28/I2 chondrocytes growth in ITS media.*

ITS (insulin, transferrin, selenium) supplemented media was previously described as the best media for proteoglycan and collagen production in immortalized human chondrocytes and for maintenance of chondrocyte phenotype in monolayer culture (Chua, Aminuddin, Fuzina, & Ruszymah, 2005; Greco et al., 2011; Kokenyesi, Tan, Robbins, & Goldring, 2000). For this reason, we repeated some experiment with different glucose concentration in C28/I2 growth using DMEM/F12 media supplemented with 1% of ITS alone or in combination with IL-1β to mimic the OA environment (Figure 10 A-D). Firstly ROS levels were analyzed used the DCFDA fluorescent probe and fluorescence was normalized on the total amount of protein present into the well. As shown in

figure 10 A no significant increase in ROS levels were shown in C28/I2 cells growth using 0.25, 2.5 and 25 mM of glucose concentration in media supplemented with ITS alone and with IL-1β.

2.3.9 *RalA-GTP levels decrease in C28/I2 cells growth in high glucose environment and tubulin levels don't change significantly.*

RalA-GTP levels and tubulin expression were evaluated in C28/I2 maintained for 72 h in normal and high glucose concentration media supplemented with ITS alone or in combination with IL-1β (figure 10 B and C). Results are in accordance with the data obtained in C28/I2 growth using FBS supplemented media. Tubulin expression don't change significantly between the different groups of cells. However, RalA-GTP levels decrease in human C28/I2 chondrocytes growth in an high glucose environment. Furthermore, IL-1β stimulated C28/I2 cells exhibit low levels of RalA-GTP in comparison to C28/I2 growth without IL-1β. In conclusion RalA activation is inhibited by high glucose environment and by IL-1β. RalA activation is inhibited more by glucose concentration than IL-1β.

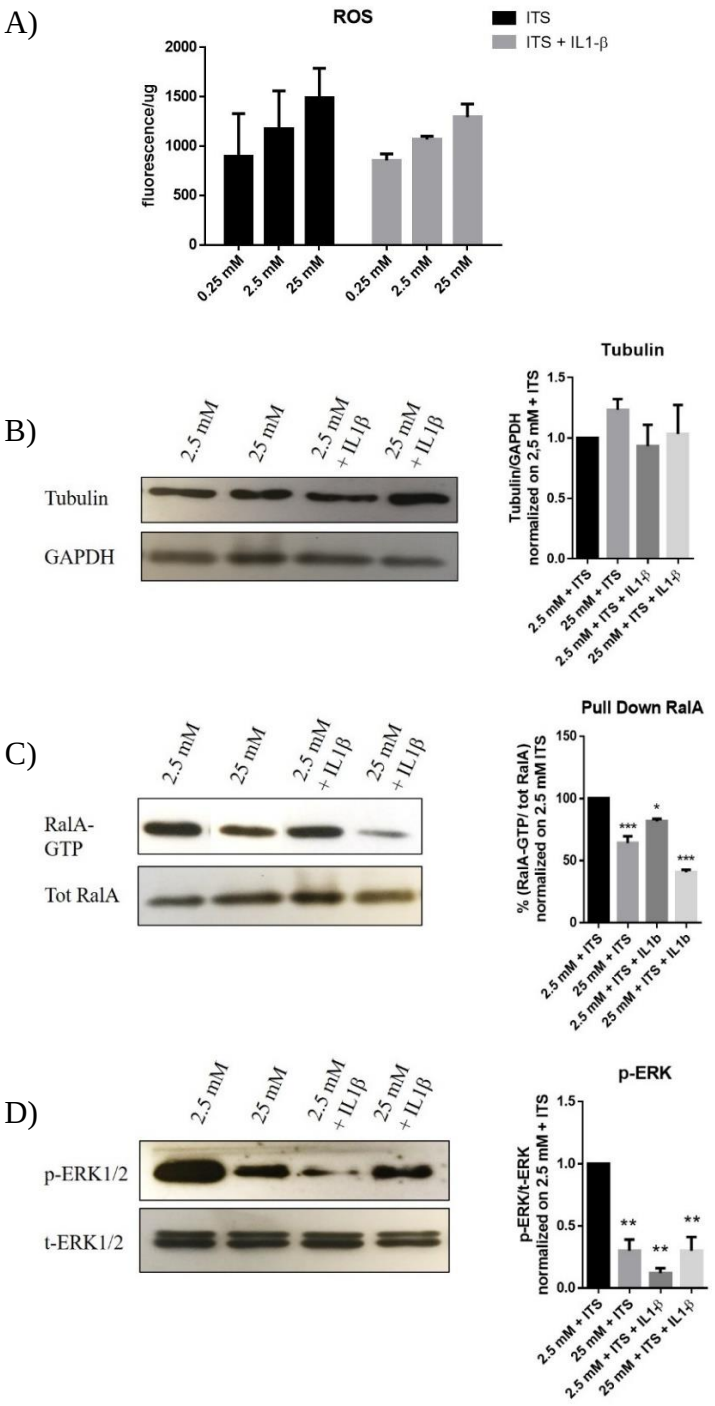

Figure 10 **High glucose effects on C28/I2 cells growth in media supplemented with ITS alone or with IL-1β** A) C28/I2 cells were growth in 96 wells plate for 72 h with different glucose concentration (2.5 and 25

mM) in media supplemented with 1% of ITS alone or with IL-1β. Media was replaced every 24 h. Media was changed with PBS before the experiment, and DCFDA (17 μM) were added for 1 h. Fluorescence intensity were measured using VICTOR multilabel plate reader (PerkinElmer). Then protein quantity was measured using Bradford methods. Fluorescence intensity were normalized on protein levels present in each well. B-C) C28/I2 cells were growth in 10 cm dishes for 72 h with different glucose concentration (2.5 and 25 mM) in media supplemented with 1% of ITS alone or with IL-1β. Media was replaced every 24 h. Protein extracts were made using Ral Buffer for Tubulin and RalA pull down, and RIPA buffer for ERK1/2. B) Immunoblots of tubulin expression and (on the left) graphical representation of densitometry analyses. C) Recombinant GST-RID (Ral Interacting Domain) of RalBP1 fusion protein, coupled to Glutathione-Sepharose beads, was used to isolate RalA-GTP. RalA was visualized using an anti-RalA antibody. On the left graphical representation of the percentage of active RalA. D) Immunoblots of total and phosphorylated ERK1/2 levels and (on the left) graphical representation of densitometry analyses. Data represent mean of 3 independent experiments. Graph and statistical analyses were made using GraphPad Prism software. Data are presented as means ± S.D an analyzed by one way or two way ANOVA. Asterisks represents significant differences between cells growth at 2.5 mM (* $p < 0.05$, ** $p < 0.01$, *** $p < 0.001$).

2.3.10 *ERK1/2 phosphorylation is attenuated by high glucose and IL-1β*

ERK1/2 are two kinases which activation is associated to OA and this is one of the major pathways activated in chondrocytes after stimulation with cytokines and other factors. For this reason, phosphorylation of ERK1/2 was detected by immunoblots in C28/I2 chondrocytes maintained for 72 h in normal and high glucose media supplemented with ITS and IL-1β (Figure 10 D). ERK1/2 phosphorylation decrease in C28/I2 chondrocytes growth in media with IL-1β and with high glucose concentration in comparison to C28/I2 maintained in normal glucose condition (Figure 10 D).

2.3.11 *Autophagic process is not activated by normal and high glucose concentration in ITS supplemented media.*

As previously described autophagy is a key process in the metabolic activity of chondrocytes (Luo et al., 2019). For this reason, autophagy activation was evaluated even in C28/I2 chondrocytes growth using normal and high glucose concentrations in media supplemented with ITS alone or in combination with IL-1β (Figure 11 A). However, autophagy is not activated in C28/I2 chondrocytes maintained in normal and high glucose media, even in presence of IL-1β (figure 11 A).

2.3.12 *NF-κB expression seems to increase in chondrocytes growth in high glucose media supplemented with ITS and IL-1β*

Inflammation is one of the leading causes of OA disease; one of the main inflammatory pathways is the NF-κB pathway. Activation of NF-κB pathways leads to cartilage degradation and destruction and NF-κB is abundant in OA synovium (Roman-Blas & Jimenez, 2006). Furthermore NF-κB is a key regulator of apoptosis, MMPs production and response to cytokines in chondrocytes (Choi et al., 2019; Olivotto et al., 2015). So, NF-κB expression was evaluated in human immortalized C28/I2 chondrocytes growth at high or normal glucose concentration in media supplemented with ITS alone or in combination with IL-1β by immunoblots. High glucose concentration for 72 h in the media leads to little increase amount of NF-κB in C28/I2 chondrocytes in comparison to chondrocytes maintained in normal glucose concentration media. However IL-1β seems to duplicate NF-κB levels in C28/I2 cells with another increase in cells maintained in high glucose (Figure 11 B). High levels of NF-κB could promote a strong activation of NF-κB pathway by cytokine and the powerfulness of NF-κB pathway could be stronger in cells growth using high glucose concentration.

Furthermore, iNOS expression levels were evaluated in C28/I2 chondrocytes maintained at different glucose concentration in 1% ITS supplemented media alone or with IL-1β (Figure 11 C). Higher iNOS levels were detected in chondrocytes maintained at 25 mM of glucose concentration without IL-1β, however more experiments are needed to statistically confirm the increase. Furthermore, IL-1β seems to increase iNOS expression which is higher respect to cell maintained at 2.5 mM of glucose concentration in ITS supplemented media without IL-1β. High glucose concentration in combination with IL-1β don’t change iNOS expression levels detected in cells growth in 1% ITS media with IL-1β and 2.5 mM of glucose (Figure 11 C).

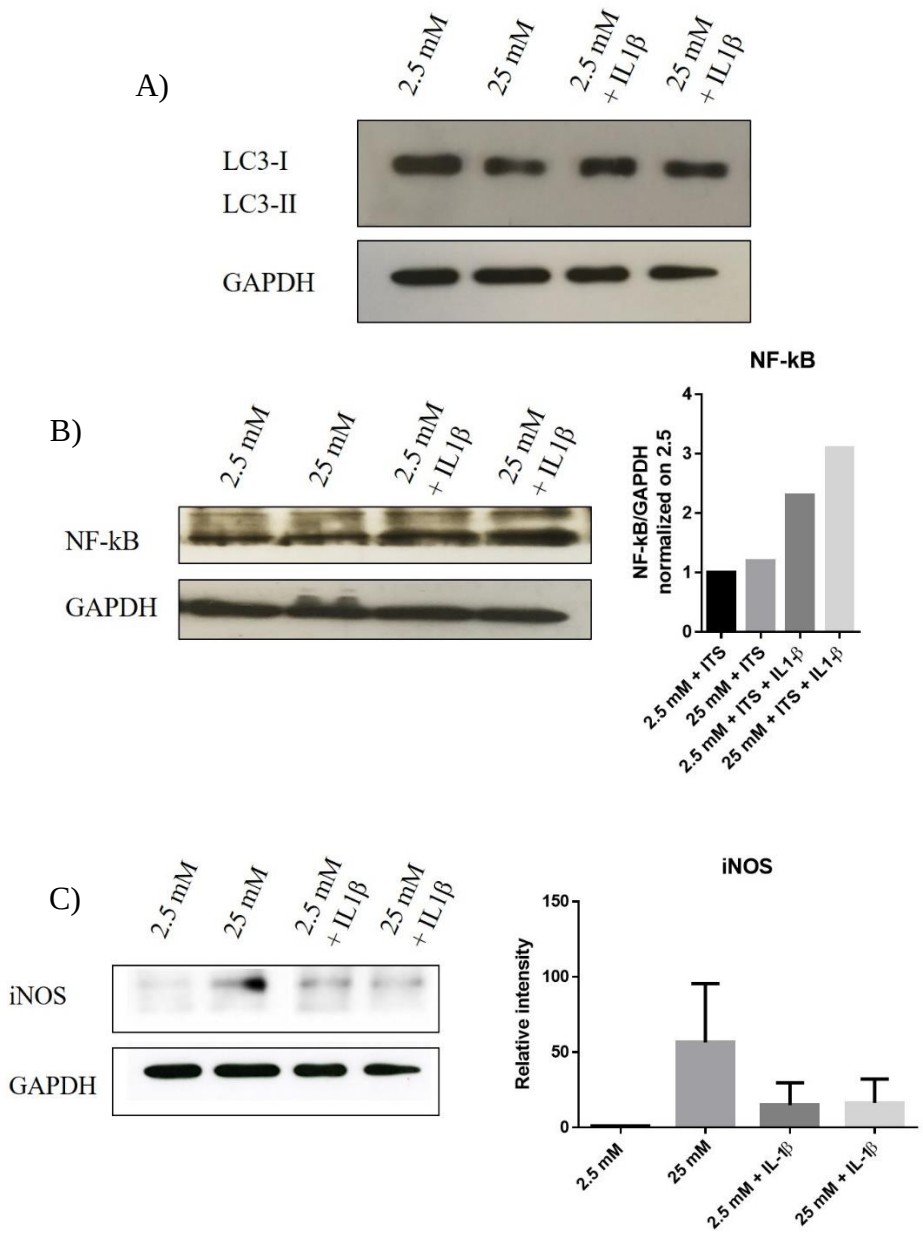

Figure 11 **Autophagy and NF-κB expression in cells growth in for 72 h with different glucose concentration (2.5 and 25 mM) media supplemented with 1% of ITS alone or with IL-1β**. A) Immunoblots and graphical representation of LC3B-I and LC3B-II proteins were obtained from cells growth for 72 h with normal and high glucose concentration media (2.5 mM and 25 mM) supplemented with 1% ITS; IL-1β 10 ng/mL were added to mimic an osteoarthritic environment. LC3-II and LC3-I indicate the activation of autophagy by the formation of autophagosomes which leads to the conversion of LC3-I into LC3-II (Kabeya, 2000; Kegel et al., 2000; Luo et al., 2019). B) NF-κB expression in C28/I2 cells growth at 2.5 mM and 25 mM of glucose concentration for 72 h. On the left graphical representation of NF-κB expression normalized on

2.5 mM (single experiment). C) C28/I2 were growth using media supplemented with 1% ITS alone or with IL-1β 10 ng/mL and with the relative glucose concentration (2.5 and 25 mM) for 72 h. Media was replaced every 24 h. Protein extracts were made using RIPA buffer. Immunoblots were incubated with antibody against iNOS and GAPDH as loading control. On the left graphical representation of iNOS relative intensity normalized on 2.5 mM glucose medium. For A and C, data represent mean of 3 independent experiments. Graph and statistical analyses were made using GraphPad Prism software. Data are presented as means ± S.D.

2.3.13 *High glucose concentration regulate key pathways in human primary chondrocytes and increase the secretion of MMP-13.*

High glucose effect on pathways important for chondrocytes were evaluated in human primary chondrocytes in collaboration with the laboratory of Dr. Richard F. Loeser at the University of North Carolina at Chapel Hill. High glucose effect on these pathways was evaluated after 24 h; for this reason and for the media usually used in Loser's Lab to isolate primary chondrocytes from cartilage of normal donor (media with 25 mM of glucose), glucose concentration used was elevated to 25 mM (normal glucose), 50 mM and 75 mM as high glucose condition. Glucose concentrations were elevated also because the time of exposure to the high glucose environment was decreased to 24 h. Chondrocytes cells were isolated and after 48 h media was changed with serum-free media for overnight stimulation, then glucose was added to reach the 50 mM or 75 mM as final concentrations. As shown in figure 12 A-B phosphorylation levels of ERK1/2, p38 and p65 significantly increase in primary chondrocytes maintained for 24 h in media with 75 mM of glucose concentration in respect of cells maintained at 25 mM of glucose concentration. Only the phosphorylation levels of p38 significantly increase in cells stimulated with 50 mM of glucose concentration respect cells maintained in media with 25 mM of glucose. High glucose concentration (75 mM) media also promote decrease in the basal Akt phosphorylation levels in respect of basal levels detected in chondrocytes maintained in normal glucose media (25 mM).

Due to the results obtained by the analyses of signaling pathways altered by high glucose in primary chondrocytes, 25 mM and 75 mM of glucose concentrations were chosen to observe MMP-13 released by chondrocytes cells in the media. As shown in figure 12 C, MMP-13 levels increased in chondrocytes cell maintained for 24 h in media with 75 mM of glucose.

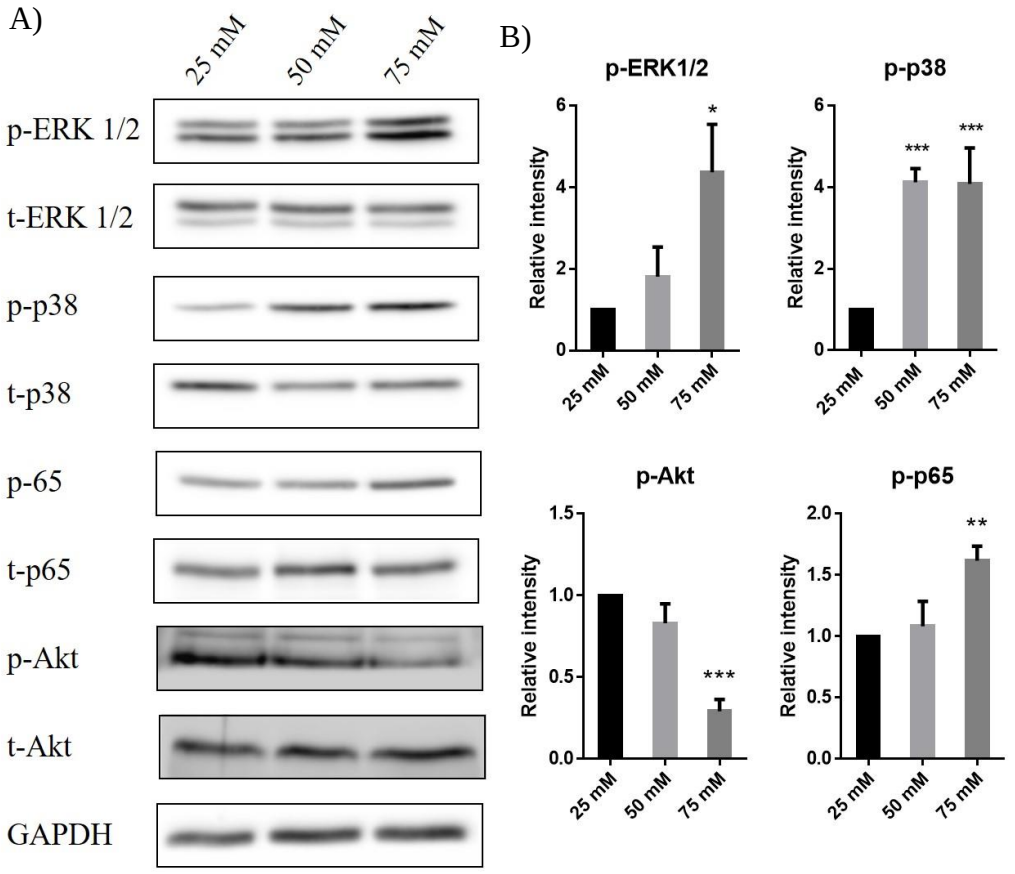

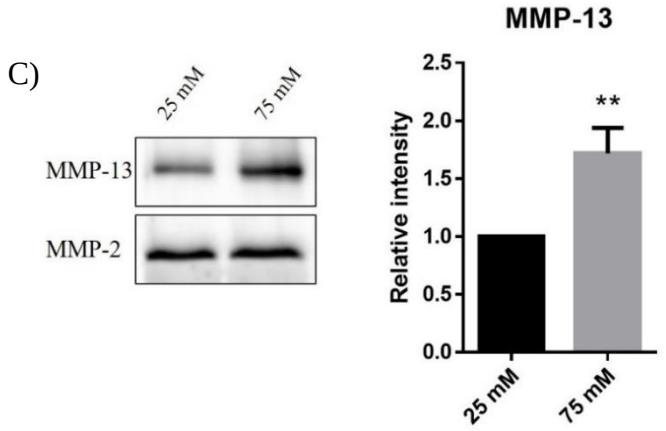

Figure 12 **High glucose media regulate phosphorylation of ERK1/2, p38, Akt and p65 in human primary chondrocytes and increase MMP-13 secretion.** Primary chondrocytes were isolated from normal cartilage and cells were plated in 6 wells plate. After 48 h, media was changed with serum-free media and cells were maintained overnight. Then glucose was added to reach 50 mM or 75 mM as final concentration in the media. Cells were stimulated for 24 h with the chosen glucose concentration. At the end of the time cell extract were made using RIPA buffer and 10 µg of protein were used for the immunoblots. A) Representative immunoblots of three independent experiment are shown. B) Graphical representation of p-ERK1/2, p-38, p-Akt and p-p65 normalized on 25 mM. C) Primary chondrocytes were isolated from normal cartilage, cells were plated in 6 wells plate. After 48 h, media was changed with serum-free media and cells were maintained overnight. Then glucose was added to reach 75 mM as final concentration in the media. Cells were stimulated for 24 h with the chosen glucose concentration. At the end of the time media were collected, concentrated and 30 µL were used for the immunoblots. Representative immunoblots of three independent experiment are shown. On the left graphical representation of MMP-13 normalized on 25 mM, using MMP-2 as loading control. Data represent mean of 3 independent experiments. Graph and statistical analyses were made using GraphPad Prism software. Data are presented as means ± S.D and analyzed using t-test student or one-way ANOVA test. Asterisks represents significant differences between cells growth at 2.5 mM (* $p < 0.05$, ** $p < 0.01$, *** $p < 0.001$).

2.4 Discussion

Accumulating evidence indicates that diabetes is an independent risk factor of OA and in the past years a lot of models have been proposed to explain their correlation (Bellou, Belbasis, Tzoulaki, & Evangelou, 2018; Dawson et al., 2018; Piva et al., 2015). T2DM has a pathogenic effect on OA through 2 major pathways. First, chronic hyperglycemia induces oxidative stress, overproduction of pro-inflammatory cytokines and AGEs in joint tissues and reduced the stem cells potential of differentiation. Second the insulin resistance could play a role locally but also through the systemic low-grade inflammation state (Courties & Sellam, 2016). However, the complicated pathophysiology of T2DM and OA interfere with the discovery of the molecular mechanism underlying the diabetes-associated OA phenotypes. The role of hyperglycemia as gained a lot of attention in the past years and it has been discovered that due to it's local toxicity and systemic toxicity, high glucose levels could induce a plenty of biochemical events like the formation of AGEs, low grade inflammation, neuromuscular impairment and oxidative stress. All of that biochemical events can lead to matrix stiffness, abnormal subchondral bone and chondrocytes activation which leads to joint degradation in OA (Mendes, Rosa, Rufino, Ribeiro, & Judas, 2015). In this study, we want to understand better the role of hyperglycemia on human chondrocytes cells, for this reason we used the human immortalized C28/I2 cell lines, which present a phenotype very similar to the primary chondrocytes cells (Finger et al., 2003). Firstly, we demonstrate that in medium with FBS which promotes C28/I2 cells growth, an higher number of cells was obtained using the 2.5 mM of glucose concentration which is in line with the findings that chondrocytes prefers and lives in an environment with a glucose concentration between 1 mM to 5 mM and that 5 mM is a threshold regulating oxygen consumption from chondrocytes (Heywood, Bader, & Lee, 2006; Otte, 1991; Windhaber, Wilkins, & Meredith, 2003). Normal media used to maintain

chondrocytes in monolayer culture used media with high glucose from 10 to 25 mM, which can promote the dedifferentiation process in primary chondrocytes (Heywood, Nalesso, Lee, & Dell'Accio, 2014a). Furthermore it has been shown that primary chondrocytes cultivated in 1 mM of glucose media maintain their phenotype producing COL2A and other proteoglycans (Heywood et al., 2014a). However, we used a different cellular type that was produced with retroviral-mediated transfection of primary rib chondrocytes with the large T antigen of Simian virus 40 (SV40) to increase the proliferative rate of chondrocytes and for this reason we didn't show a decrease in cell growth as Heywood et. al showed in primary chondrocytes growth at 1 mM of glucose media. Another relevant fact is that we changed the media every 24 h to maintain constant the glucose concentration. For the other experiments we used 2.5 mM of glucose concentration as normal glucose and 25 mM as high glucose concentration media and we maintained chondrocytes in that glucose concentrations for 72 h, because the significantly growth retardation at 25 mM was detectable after 96 h of cell growth and we wanted to see the signaling and the molecular events which leads to this lower cell growth. We found that high glucose concentration in the media increase ROS levels in chondrocytes (Figure 2 A-B). Oxidative stress is known to be a key factor in the degeneration of cartilage by disrupting cartilage homeostasis and affecting chondrocytes viability (Bolduc et al., 2019; Collins et al., 2016). Our results are in accordance with the fact that high glucose conditions directly increase ROS and NO• generation in articular chondrocytes (Laiguillon et al., 2015). These high glucose-induced-oxidative stress could leads to pro-inflammatory cytokine production from chondrocytes (Bolduc et al., 2019; Laiguillon et al., 2015; Lepetsos et al., 2019). Excessive ROS production contributes to matrix degradation by destroying ECM, inhibiting matrix production, activating MMPs and inducing apoptosis (Del Carlo & Loeser, 2008; Hosseinzadeh et al., 2016). This is in accordance with our result showing that

chondrocytes growth in high glucose environment exhibit an increase cell death in comparison to C28/I2 chondrocytes growth under normal glucose condition (figure 2 C). However, we don't find an increase in the apoptotic process but in the overall cell death process; this could be explained by the differences in the experiment condition, for example Hosseinzadeh et. al uses a very high glucose condition, 75 mM, in comparison to glucose oncentration used in this study. Chondrocytes loss by cell death could be an important process in the pathogenesis of OA, and ROS could promote this cell death process (DelCarlo & Loeser, 2006; Ishizaki, Burne, & Raff, 1994). Also we demonstrate that high glucose concentration tends to increase NF-κB levels (Figure 4 D, figure 7 B), which could leads to an higher NF-κB response if its activated. NF-κB is a transcription factor which induce the expression of inflammatory cytokines in human chondrocytes (Hosseinzadeh et al., 2019; Lepetsos et al., 2019; M. Lin et al., 2012; R.F. Loeser, Erickson, & Long, 2011). We also found that High glucose concentrations in the media could promotes the expression of iNOS (figure 5 and 7C) which is responsible to NO• production which seems to be implicated in the pathomechanisms of OA (Cuzzocrea, 2006). In the experiments with ITS media in figure 7C is clear how important is the glucose concentration for iNOS expression in chondrocytes. However high glucose was not able to induce the same increase in chondrocytes stimulated with IL-1β this could be explained with the fact that glucose and IL-1β pathways could interact each other leading to a reduction in iNOS expression in comparison to cells maintained under high glucose concentration without IL-1β (Figure 7 C). Furthermore, previously it has been shown that glucose can reduce the IL-1β-induced MMP-1 expression, and this reduction occurred through FAK, MEK, ERK and AP-1 pathways. We show that high glucose itself decrease ERK phosphorylation in chondrocytes after 72 h of stimulation. We found also that the presence of glucose and IL-1β maintain low ERK phosphorylation. This is in accordance with the hypothesis that glucose

can reduce the effect of IL-1β in chondrocytes (T. J. Wu, Lin, Tsai, Huang, & Tang, 2018). NF-κB expression is also increase in cells stimulated by IL-1β which is a pro-inflammatory cytokine that as a key role in the pathogenesis of OA. So, all results in our studies are in agreement with the idea that high glucose concentrations is able to increase ROS levels and also to stimulate an inflammatory process in chondrocytes cells. We also found that chondrocytes cells growth in high glucose concentration in FBS supplemented media exhibit lower autophagy. Indeed, autophagy plays an important role in articular cartilage, regulating the removal of dysfunctional organelles and macromolecules (Lotz & Caramés, 2011). Basal levels of autophagy activity are indispensable for the homeostasis of many tissues, including cartilage. In opposite, defects in basal levels of autophagy have been associated with various degenerative and metabolic diseases (Sridhar, Botbol, MacIan, & Cuervo, 2012). Previous studies reported a dysfunction of autophagy, either in OA and T2DM (Caramés, Taniguchi, Otsuki, Blanco, & Lotz, 2010). In fact we found that C28/I2 chondrocytes maintained at normal glucose concentration exhibit a basal level of LC3II which is required for the formation of autophagosome and is used as autophagy marker. Both high glucose and IL-1β decrease the basal level of LC3II, indicating a lower autophagic process (Figure 4 C). However, the power of glucose seems to be higher as autophagy inhibitor, indeed in chondrocytes maintained with 25 mM of glucose the autophagy process is completely abrogated. On the other hand, LC3II signal was totally absent in chondrocytes maintained in ITS supplemented media, this could be explained because insulin was found to be a potent autophagy inhibitor in chondrocytes. Insulin and also high glucose was found to impact the autophagy process through Akt/mTOR pathways in human immortalized chondrocytes and in human primary chondrocytes (Ribeiro et al., 2016). Chondrocytes cytoskeleton play a fundamental role in the maintenance of chondrocytes phenotypes and in sensing

extracellular stimuli acting as a physical interface between chondrocytes and extracellular matrix (Blain, 2009). In this study high glucose concentration can also promote a disorganization of actin and tubulin cytoskeleton in human chondrocytes (Figure 3 A). More in detail chondrocyte growth in normal glucose concentration exhibit a very intricated tubulin and actin network with filaments well defined from the nucleus to the cell periphery. However, in chondrocyte growth in high glucose concentration actin and tubulin appear very disorganized and no defined actin or tubulin filaments or fibers were visible. Furthermore, cell morphology appears to be different with cells that have more rounded shape. In previous studies it was observed a connection between a disorganized/disassembled chondrocyte cytoskeleton and cartilage pathology (Capín-Gutiérrez, Talamás-Rohana, González-Robles, Lavalle-Montalvo, & Kourí, 2004; Fioravanti et al., 2003; Holloway et al., 2004; Lambrecht, Verbruggen, Verdonk, Elewaut, & Deforce, 2008). It has been suggested that the actin cytoskeleton is important in maintaining cell–extracellular matrix interactions; disruption of the actin filaments with cytochalasin D reduced both the amount of pericellular matrix synthesized and retention of the proteoglycans in the matrix surrounding the chondrocyte, by reducing the cell's anchorage of CD44 (localized to the cell membrane) to its extracellular ligand (Delve, Parreno, Wu, & Co, 2016; Nofal & Knudson, 2002). On the other hand it is well know the role of actin filament in maintenance the chondrocytes phenotypes and disorganization of actin filament by cytochalasin B/D result in re-expression of type II collagen and sulphated glycosaminoglycans (Brown & Benya, 1988; Loty et al., 1995). In chondrocytes, the integrity of the tubulin network is also crucial for the synthesis and secretion of both collagens and proteoglycans. It has been reported that tubulin is present in the primary cilia of chondrocytes, and ultrastructural studies have identified a direct connection between the extracellular collagen fibers and the proteins which decorate the ciliary

microtubules, suggesting a matrix-cilium-Golgi continuum in chondrocytes (Poole, Zhang, and Ross 2001). Disruption of the chondrocyte microtubular network with colchicine inhibited the synthesis and secretion of proteoglycans and collagens (Takigawa et al., 1984). It was suggested that the cytoskeletal structures might not be normally assembled in OA cartilage (Fioravanti et al., 2003) which could compromise the metabolic activities of the chondrocytes and hence the biomechanical integrity of the tissue leading to cartilage pathology. However, our data demonstrate that high glucose could change the organization of cytoskeletal elements in C28/I2 chondrocyte cell line; this could be another mechanism which links hyperglycemia to OA disease. Although C28/I2 cells were largely used as a model of chondrocyte functions, it is proliferative rate may not reflect exactly the physiological conditions of primary chondrocytes, so it could be important to replicate these studies using human primary chondrocytes (Mary B. Goldring, 2004; Kokenyesi et al., 2000). Furthermore, we found that high glucose environment leads to reduction in RalA activation levels (Figure 4 B and 6 C), this could explain the cytoskeletal disruption induced by high glucose concentration. RalA is a small G protein which is involved in the regulation of both tubulin and actin cytoskeleton organization towards Cdc42 and Rac1. Decrease in RalA activation could leads to decrease activation of RalBP1 which normally inhibits Rac1 and Cdc42. So, high glucose decrease RalA activation in chondrocytes which could leads to an increase activation of Cdc42 and Rac1 these could promote a disorganization of tubulin network (Moghadam et al., 2017). More experiments are needed to confirm this model.

Experiments on primary human chondrocytes were made in Richard Loeser's lab at the university of North Carolina at Chapel Hill. We decided to observe the effect of high glucose concentration after 24 h in chondrocytes cells. To observe an effect after this early time of treatment we decided to increase the glucose concentration used (25 mM normal glucose, 50 mM and 75 mM high glucose).

Result show an increase in p-ERK1/2, p-p38 and p-p65 levels and a reduction of p-Akt levels (Figure 8 A-B). Levels of p-ERK1/2, p-65 seems to increase in a manner directly proportional to the glucose concentration in the media as well as the decrease in p-Akt levels (Figure 8 A-B). Only p38 seems to increase and reach a plateau at 50 mM of glucose concentration (Figure 8 A-B). ERK1/2, p38 and NF-κB subunits p65 are key pathways in chondrocytes; their activation can leads to MMPs production, apoptosis and cytokine released by chondrocytes (Bolduc et al., 2019; Richard F. Loeser, 2017; Marcu et al., 2010). Akt phosphorylation is promoted by IGF-1 stimulation in chondrocytes which is a pro-survival signaling (Collins et al., 2019). Our results demonstrate that high glucose stimulate a decrease in Akt phosphorylation levels. All these pathways could leads to cells death and promote the release of MMPs. We saw that high glucose concentration can leads to an increase secretion of MMP13 into the media; this could promote degradation of extracellular matrix which is an hallmark of OA (B. Ji, Ma, Wang, Fang, & Shi, 2019; Johanne Martel-Pelletier et al., 2016). All data are in accordance with some other studies on the role of high glucose levels on chondrocytes cells (Heywood, Nalesso, Lee, & Dell'Accio, 2014b; Hosseinzadeh et al., 2019; Juybari, Hosseinzadeh, & Sharifi, 2019; Liang et al., 2019).

In conclusion, all these data demonstrate that high glucose concentration could deregulate chondrocytes homeostasis activating inflammatory pathways like NF-κB, promoting the release of MMP-13, altering the cytoskeletal organization via RalA pathway and increasing ROS and cell death in chondrocytes. However, in the future, it could be interesting to evaluate better the exact role of RalA pathways in chondrocytes to understand better if this deregulation occur even in primary chondrocytes cells. RalA role in chondrocytes cells was studied only regarding it's ability to regulate SOX9 expression influencing the differentiation state of chondrocytes (Karlsen, Jakobsen, Mikkelsen, & Brinchmann, 2014;

Zhang, Huang, & Yuan, 2017). In these studies RalA regulates SOX9 at protein levels and is a target protein for the miR-140-3p, which is involved in the chondrogenic differentiation of mesenchymal stem cells.

Chapter 3 - PRX6 expression and function in primary chondrocyte cells

3.1 Aim of the work

In this chapter the role of PRX6 in primary chondrocytes cells was analyzed. Prxs are a family of cysteine-dependent peroxidases which react with H_2O_2 present inside in the cell compartment. They are considered the major antioxidant enzyme that contribute to the maintenance of cellular redox state in cells. Prx6 is the only 1-Cys PRX, and the oxidation to PRX6-SOH is resolved by the binding with a molecule of glutathione (GSH) mediated by glutathione S-transferase. PRX6 has another enzymatic activity and can function as a calcium-independent phospholipase (PLA_2) promoting the hydrolysis of acyl group of phospholipids. PRX6 was found to be implicated especially in the pathogenesis of diabetes. Increased levels of hyperoxidized PRXs are present in human cartilage from older adults with a further increase in OA cartilage (Collins et al., 2016). Chondrocytes from older patients are more susceptible to PRXs hyperoxidation when exposed to ROS and this with inhibition of IGF-1-mediated phosphoinositide 3 (PI-3) kinase-Akt signaling and promotion of p38 activation that results in chondrocytes cell death promoting OA development (Collins et al., 2016). In this work Collins et al. evaluated the role and the function of PRX1, PRX2 and PRX3 in chondrocytes after stimuli which promote the production of H_2O_2 in chondrocytes cells. Here the aim of this work is to observe if PRX6 is responsible for the ROS detoxification in chondrocytes treated with different molecule which stimulate the generation of H_2O_2 and if this enzyme is able to regulate signaling pathways which are normally activated by this stimuli and especially by FN-f treatment. We focus our attention on PRX6 because its function in chondrocytes cells is not well known. PRX6 has been found to promote lung cancer invasion (Walsh et al., 2009). In particular its role as a PLA_2 is a key regulator of cell invasion and metastasis, especially by its ability to

regulate NOXs needed for cell proliferation (Ho et al., 2010). Furthermore PRX6 can regulate and interact with MAPK, JNK, JAK/STA and AP-1 signaling pathways promoting lung tumor development (Yun et al., 2014). PRX6 was linked to the inflammation state regulating NOX and NF-κB (Chhunchha et al., 2013). PRX6 is involved in brain injury and neurodegeneration process, like Alzheimer's and Parkinsons's disease, in male infertility and in ocular oxidative damage (Arevalo & Vázquez-Medina, 2018). Indeed PRX6 is linked to the development of type 2 diabetes (Pacifici et al., 2014). Human PRX6 has 2-cys residues in its aminoacidic sequence, however, cys-41 is the catalytic cys and the other is a non-conservative sequence which is inside of the protein core (Suzuki et al., 2019). Similar to the other PRXs, the catalytic cysteine of PRX6 is oxidized by H_2O_2 but then to resolve the oxidized cys PRX6 need the binding with GSH, which form a mixed disulfide bond with PRX6. This binding is promoted by the GSH S-transferase. Final step require another molecule of GSH, which reacts with glutathionylated PRX6 forming an oxidized GSH (GSSG) which is reduced by NADPH-dependent enzymes (Aron B. Fisher, 2017).

In chondrocytes the exact role of PRX6 was not known so here we focused our attention to find a technique which permits us to observe the oxidized form of PRX6 through a western blot experiments like one used from Collins et al. (Collins et al., 2019, 2016). After we decided to see if PRX6 could impact the MAPK signaling pathways activated by ROS.

3.2 Materials and Methods

3.2.1 Reagent and antibodies

Antibodies purchased from Cell Signaling Technology were to phospho-Akt (Ser473), total-Akt, phospho-p38 (Thr180/Tyr182), total-p38, phospho-ERK (Thr202/Tyr204), total-ERK, phospho-JNK (Thr183/Tyr185), total JNK, phospho c-Jun (Ser73), total c-Jun, and GAPDH. Antibodies purchased from Abcam were to PRX6, LDH, TBP, 4-HNE, MMP-13 and MMP-2. Purified endotoxin-free recombinant human FN-f of 42 kd, consisting of domains 7–10 of native fibronectin, which includes the cell-binding RGD domain (27), were produced using a plasmid expression construct obtained from Dr. Harold Erickson (Duke University, Durham, NC). Endotoxin was removed using high-capacity endotoxin-removal columns (Pierce). Menadione, DMNQ, H_2O_2, N-ethylmaleimide (NEM) and catalase were purchased from Sigma Aldrich. The p38 inhibitor SB203580 was purchased from Sigma (St. Louis, MO). Lambda phosphatase protein kit was purchased from New England Biolabs. RIPA buffer was purchased form Cell Signaling Technology.

3.2.2 Human primary chondrocyte isolation and culture

Normal articular cartilage was obtained from the talus of human tissue donors provided by the Gift of Hope Organ and Tissue Donor Network (Itasca, IL) through collaboration with Rush University Medical Center (Chicago, IL). Prior to dissection, cartilage was macroscopically inspected for gross evidence of damage and only normal appearing cartilage was used. Chondrocytes were isolated and cultured in monolayer culture. Cartilage was dissected from the joint, with care taken to avoid underlying bone or tissue from osteophytes. Cartilage slices were digested in DMEM/F-12 medium (1:1) containing 0.2% Pronase (Calbiochem, San Diego, CA) in an incubator with continuous agitation for 1 hour, and then overnight with 0.025% collagenase P (Roche, Indianapolis, IN) in

DMEM/F-12 supplemented with 5% fetal bovine serum. After isolation, the cells were counted. The initial viability prior to culture was assessed using trypan blue dye exclusion and was determined to be 90% (Richard F. Loeser et al., 2003). Cells were plated and maintained in monolayer culture with 10% FBS in DMEM/F-12 for at least 24 h. Prior to each experiment cells were incubated overnight with serum-free DMEM/F-12.

3.2.3 Analysis of PRX6 Oxidation

Cells were cultured overnight in serum-free conditions and then treated with 25 μM menadione, 25 μM DMNQ, 100 μM H_2O_2 or 1 μM of Fn-f. Reduced, oxidized forms of PRX6 were analysed adjusting a technique previously described (Collins et al., 2019). Briefly, cultured cells were treated with menadione, DMNQ, H_2O_2 or Fn-f, for the indicated times, washed in 1X PBS. Cells were lysed at 4 °C under gentle agitation for 30 min in a RIPA lysis buffer containing 200 units/mL catalase, PMSF and phosphatase inhibitor cocktail 2 (pH 7.4). To remove the insoluble protein fraction, cell lysates were centrifuged at 13,000 rpm for 10 min. Soluble protein concentrations were quantified using the Pierce Micro BCA kit (Thermo Scientific). Protein lysates were boiled and immunoblotted under reducing or nonreducing conditions (in the presence or absence of 10% β-mercaptoethanol) as described (Collins et al., 2019; Del Carlo & Loeser, 2002). For identification of PRX6 oxidation forms, cell lysates were immunoblotted under reducing conditions and probed with an antibody that reacts with PRX6. GAPDH were used as loading control. Protocol used by Collins et al. was used but no oxidation band was observed. For p38 inhibition studies, cells were pretreated for 30 min with 10 μM SB203580 prior to treatment with 25 μM menadione, 25 μM DMNQ, 100 μM H_2O_2 or 1 μM of Fn-f for 30 min. Immunoblots in non-reducing condition were made as described above.

3.2.4 4-HNE protein adducts

4-HNE protein adduct were made to detect the lipid peroxidation in chondrocyte. Chondrocytes cultures were incubated overnight in serum-free media prior to experimental treatments and washed with 1X PBS. Cells were lysed at 4 °C under gentle agitation for 30 min in RIPA lysis buffer containing PMSF and phosphatase inhibitor cocktail 2 (pH 7.4). To remove the insoluble protein fraction, cell lysates were centrifuged at 13,000 rpm for 10 min. Soluble protein concentrations were quantified using the Pierce Micro BCA kit (Thermo Scientific). Protein lysates were boiled and immunoblotted under reducing conditions and probed with Pierce Reversible Protein Stain Kit for Nitrocellulose Membranes for a total protein staining and with 4-HNE antibody. Total protein staining was used as loading control.

3.2.5 Adenoviral transduction

Human chondrocytes were transduced with adenoviral construct encoding PRX6 (Adv-Prx6) (Vector Biolabs). For test the correct viral particle number to obtain an higher overexpression of PRX6, chondrocyte monolayers at 60% confluency, were incubated for 2 h at 37 °C in serum-free media containing different dilution (4x, 2x, 1x, ½, ¼, ⅛) of 4×10^8 viral particles/mL of adenoviral construct and $CaCl_2$ (25 µL/mL media, 1 M). Adenoviral containing media was removed, monolayers were rinsed three times with 10% serum containing media and monolayers were cultured in 10% serum containing media for 48 h. Cell lysates were made and PRX6 were visualized by immunoblots. For the next experiment 4 times 4×10^8 viral particles/mL of adenoviral construct was used following the same infection time. Chondrocytes cultures were incubated overnight in serum-free media prior to experimental treatments. Non-specific effects of viral transduction were tested by transducing chondrocytes with a null empty vector control adenovirus (ad-Null) (Cell Biolabs).

3.2.6 PRX6 immunoprecipitation

Chondrocytes were plated in 10 cm dishes and after an overnight incubation in serum-free media, cells were treated with 25 µM menadione, 25 µM DMNQ, 100 µM H_2O_2 or 1 µM of Fn-f for 30 min. At the end, cells were mechanically lysed in RIPA buffer containing PMSF and phosphatase inhibitor cocktail 2 (pH 7.4). To remove the insoluble protein fraction, cell lysates were centrifuged at 13,000 rpm for 10 min. Soluble protein concentrations were quantified using the Pierce Micro BCA kit (Thermo Scientific). Equal amounts (500 µg) of total protein extracts for each sample were incubated with 1.5 µl of Normal Rabbit IgG (Thermo Scientific) and incubated at 4°C on a wheel for 2 h to remove the proteins who binds the IgG protein in a non-specific manner. Non-specific immunocomplex are then recovered with Pierce Protein A/G Agarose Beads (Thermo Scientific). Supernatants were incubated with 4 µl of anti-PRX6 antibodies on a wheel at 4°C overnight. Immunocomplex were then recovered with Pierce Protein A/G Agarose Beads (Thermo Scientific). Flow through were also recovered. Both immunocomplexes and Flow through were analyzed by immunoblots in non-reducing condition with anti-PRX6 antibodies and revealed with anti-rabbit HRP secondary antibody (Sigma Aldrich) and ECL system (Azura Biosystem). Also an equal amount of total protein extract were analyzed with non-reducing immunoblots and anti-PRX6 antibody. Experiments were repeated three times.

3.2.7 Phosphatase lambda

For phosphatase lambda (New England Biolabs) experiments a commercial protocol was followed. Briefly, equal amount of total protein extracts were incubated for 30 min at 30°C with 1 uL phosphatase lambda, NEBuffer for Protein MetalloPhosphatases (PMP), and 1mM $MnCl_2$. Then samples were analyzed using a non-reducing immunoblots with anti-PRX6 antibody.

3.2.8 Analyses of cell signaling

For cell signaling analysis, after treatment with menadione and IGF-1, chondrocytes were incubated in serum-free conditions overnight prior to treatment with 25 μM menadione or 50 ng/ml IGF-1 for 30 min. For menadione pretreatment experiments, cells were treated with 25 μM menadione for 30 min prior to treatment with 50 ng/ml IGF-1 for 30 min. All cell signaling immunoblots were performed under reducing conditions using phospho-specific antibodies, with antibodies to total protein serving as loading controls, with the exception of phospho c-Jun, which was normalized to β-actin (Collins et al., 2019).

For analysis of cell signaling after treatment with Fn-f, chondrocytes were incubated in serum-free conditions overnight prior to treatment with 1 μM Fn-f for 30 min or 60 min. All cell signaling immunoblots were performed under reducing conditions using phospho-specific antibodies, with antibodies to total protein serving as loading controls, with the exception of phospho c-Jun, which was normalized to β-actin.

For MMP-13, primary chondrocytes were incubated in serum-free conditions for at least 12 h prior to treatment with 1 μM Fn-f overnight. Conditioned media were taken and concentrated (10:1) and 30 μl was analyzed by immunoblotting using non-reducing condition using antibody against MMP-13. Densitometric analysis of MMP-13 bands was performed using ImageJ software. MMP-2 was used as loading control and data were normalized on untreated cells (Forsyth et al., 2002; S. T. Wood et al., 2016).

3.2.9 Analyses of PRX6 expressions

For these experiments, younger donors were < 50 years old, and older donors were ≥ 50 years old. The age cut-off for young and old donors was chosen based

on a previous study from our group that demonstrated a decline in the response to IGF-1 and altered signaling under conditions of oxidative stress in chondrocytes from donors older than 50 years (Richard F. Loeser et al., 2014). OA chondrocyte were obtained from cartilage tissue classified as grade IV (severe changes) obtained from patients submitted to a total knee-joint replacement surgery. Chondrocytes were isolated as described above and after overnight incubation in serum free media total protein extract were obtained using RIPA buffer and 30 µg of total protein extract were loaded on polyacrylamide gels. Western blots were made according to standard procedures using nitrocellulose membranes (Protran). Immunoblots were probed with anti-PRX6 antibody and GAPDH was used as loading control. Densitometry analyses were made using ImageJ software. Graph and statistical analyses were made using GraphPad Prism 6 software.

3.2.10 Analyses of nuclear and cytosolic fractions

Nuclear and cytoplasmic fractions were obtained using NE-PER Nuclear and Cytoplasmic Extraction Kit (Thermo Scientific). Briefly chondrocytes were incubated in serum-free conditions overnight prior to treatment with 25 µM menadione, 25 µM DMNQ, 100 µM H_2O_2 or 1 µM of Fn-f for 30 min. Cells were lysed and cytoplasmic/nuclear fraction were obtained according to the manufacturer's instruction. Briefly, the treated cells were washed twice with cold PBS and centrifuged at 500 g for 3 min. The cell pellet was suspended in 200 µl of cytoplasmic extraction reagent I by vortexing. The suspension was incubated on ice for 10 min followed by the addition of 11 µl of a second cytoplasmic extraction reagent II, vortexed for 5 s, incubated on ice for 1 min and centrifuged for 5 min at 16 000 g. The supernatant fraction (cytoplasmic extract) was transferred to a pre-chilled tube. The insoluble pellet fraction, which contains crude nuclei, was resuspended in 100 µl of nuclear extraction reagent by

vortexing 15 s and incubated on ice for 10 min, then centrifuged for 10 min at 16 000 g. The resulting supernatant, constituting the nuclear extract, was used for the subsequent experiments. Immunoblots were made as described above under reducing conditions. LDH was used as cytoplasmic loading control and TBP was used as nuclear loading control.

3.2.11 MS analyses

Cells were cultured overnight in serum-free conditions and then treated with 100 μM H_2O_2 or 1 μM of Fn-f for 30 min. After the protein extraction with RIPA buffer non oxidized cys were blocked with 10 mM of the blocker agents 4-(5-methanesulfonyl-[1,2,3,4]tetrazol-1-yl)-phenol (MSTP) for 1 h at 24 °C which react specifically with the reduced cys (SH) and is more specific then N-ethylmaleimide (NEM) (X. Chen et al., 2017). Furthermore, protein was precipitated by the addition of acetone and resuspended in 0.1% (v/v) SDS. Oxidized cys were reduced with 10 mM DTT treatment and then the thiol affinity enrichment was performed using commercially available thiol-affinity resin (Thiopropyl Sepharose 6B) to directly capture free thiol-containing proteins through a disulfide exchange reaction followed by on-resin protein digestion and multiplexed isobaric labeling using TMT10plex™ Isobaric Mass Tag Labeling Kit (Thermo Scientific). Peptides were eluted from beads and then analyzed with LC–MS/MS using a Q Exactive HF hybrid quadrupole-Orbitrap mass spectrometer (Thermo Scientific) coupled to a Dionex Ultimate-3000 nano-UPLC system (Thermo Scientific) using a Nanospray Flex Ion Source (Thermo Scientific) (Nelson et al., 2018). MS analyses was made by Dr. Crtistina Furdui from Wake Forest School of Medicine.

3.2.12 Statistical analyses

Data were analyzed by Student's *t* test (for two-sample comparisons) or a one-way or two-way ANOVA (for comparison of more than two samples) with a Dunnett's or Tukey honestly significant difference post hoc correction, as appropriate, using GraphPad Prism version 6 (GraphPad Software, Inc.). Results are presented as mean values ±S.D. from a minimum of three independent biological replicates. A level of $p < 0.05$ was considered to be significant.

3.2.13 Study approval

Use of human tissue was in accordance with the Institutional Review Board at the Rush University Medical Center and the University of North Carolina at Chapel Hill.

3.3 Results

3.3.1 *Preliminary MS data revealed that PRX3 and PRX6 are oxidized in primary chondrocytes after treatment with H_2O_2 and Fn-f*

Preliminary data obtained with the Mass spectrometry analyses have shown that the treatment with H_2O_2 and Fn-f increase cys oxidation on PRX3 and PRX6 which are the most abundant protein after the MS analyses of sample treated with the protocol developed by PhD Megan Arrington. This protocol permits to enrich and analyzed the abundance of the protein with cys oxidation occurring after the treatment with H_2O_2 and Fn-f for 30 min in normal primary chondrocytes. The same approach used by Guo et. al was adapted to obtain an enrichment for proteins with a reversible oxidized cys obtained after treatment with both H_2O_2 and Fn-f for 30 min, increasing the ROS levels (J. Guo et al., 2014). After the protein extraction non oxidized cys were blocked with the blocker agents 4-(5-methanesulfonyl-[1,2,3,4]tetrazol-1-yl)-phenol (MSTP) which react specifically with the reduced cys (SH) and is more specific then N-ethylmaleimide (NEM) (X. Chen et al., 2017). Furthermore, oxidized cys were reduced with DTT treatment and then the thiol affinity enrichment was performed using commercially available thiol-affinity resin (Thiopropyl Sepharose 6B) to directly capture free thiol-containing proteins through a disulfide exchange reaction followed by on-resin protein digestion and multiplexed isobaric labeling to facilitate LC–MS/MS based quantitative site-specific analysis of cysteine-reversible oxidation (Supplementary Figure 1). As shown in Table 1 the most abundant protein in cell treated with H_2O_2 and Fn-f respect to the Control cells is PRX3, however its role in primary chondrocytes cells is well known and previously studied by Collins et. al (Collins et al., 2019, 2016). PRX6 was found to be the second most abundant protein in chondrocytes treated with H_2O_2 and Fn-f in comparison to the Control, indicated that both treatment could oxidized

PRX6. So this PRX6 could be essential for ROS detoxification which occur in chondrocytes cells.

Protein	Average			Ratio		P-value	
	Control	H2O2	FN-f	H2O2/Control	FN-f/control	H2O2/Control	FN-f/Control
Thioredoxin-dependent peroxide reductase GN=PRDX3 PE=1 SV=3	65.5	117.8	100.6	1.80	1.54	0.000257	0.028692
Peroxiredoxin-6 OS=Homo sapiens GN=PRDX6 PE=1 SV=3	75.3	113.3	106.8	1.51	1.42	0.000213	0.006047

Table 1 **Mass-Spectrometric analysis of cysteine-reversible oxidation proteins in primary chondrocytes cells treated with H_2O_2 and Fn-f for 30 min**. PRX3 and PRX6 were found to be the most abundant protein in sample treated with H_2O_2 and Fn-f for 30 min, indicating that this two peroxiredoxin could be essential in the detoxification process in chondrocytes cells.

3.3.2 *PRX6 oxidation is visible on western blot in primary chondrocytes after Menadione and H_2O_2 stimulation*

PRXs oxidation state can be detected using the western blot technique, using non-reducing and reducing gels. Non-reducing gels doesn't contain reducing agents (like DTT and BME) so disulfide bonds remain intact during the running. This technique was used by Collins et. al to visualized the oxidation state of PRX1, PRX2 and PRX3 which are three typical 2-cys peroxiredoxin and during their catalytic cycle can homodimerize to resolve the oxidation which occurs on their cys (Collins et al., 2019). This technique developed by Cox et. al used the NEM treatment to blocks the reduced cys and to avoid the cys oxidation by the H_2O_2 released after the cell extraction catalase enzymes is added to the cell lysates (Cox et al., 2010). Unlikely the normal PRXs, PRX6 has only one catalytic cys at 47 position in the aminoacidic sequence, and require the binding with GSH to resolve the cys oxidation. However, PRX6 has another non catalytic cys in the internal core of the protein. For this reasons, PRX6 oxidation is not possible to detect using the normal protocol with NEM. Cox et. al protocol has been adapted to observe PRX6 oxidation; cells were lysates without NEM treatment and

subjected to the same catalase enzyme treatment to avoid the oxidation after the cell extraction. So, normal primary chondrocytes were treated with 2,3-Dimethoxy-1,4-naphthoquinone (DMNQ), Menadione, H_2O_2 and Fn-f which are known to increase the ROS levels in chondrocytes (Collins et al., 2019, 2016; Richard F. Loeser, 2002; D. L. Long, Willey, & Loeser, 2013). Time course experiment were performed treating cells with DMNQ (25 µM), Menadione (25 µM) and H_2O_2 (100 µM) from 0 to 60 mins (0, 5, 10, 15, 30, 60 mins), and with Fn-f (1 µM) from 0 to 360 mins (0, 10, 30, 60, 180, 360 mins) because the increse of H_2O_2 generated by Fn-f is slower in comparison to others treatments. Cellular extracts were collected and loaded in non-reducing an reducing gels. As shown in Figure 13, PRX6 oxidation were detected by western blot in normal primary chondrocytes after 5 min of treatment with Menadione (25 µM) and H_2O_2 (100 µM). PRX6 non-oxidized band has been found at 25 KDa molecular weight and the oxidation seems to promote a band shift to 26 KDa molecular weight in non-reducing gels. In non-treated conditions two PRX6 bands were always present in non-reducing gels. In reducing gels the total reduced PRX6 migrate as 25 KDa band indicating that this band is relative to the reduced PRX6. PRX6 oxidation doesn't increase after the treatment with DMNQ and Fn-f as shown by the figure 13 in which the two bands were present even after 60 mins of DMNQ treatment and 360 mins of Fn-f treatment.

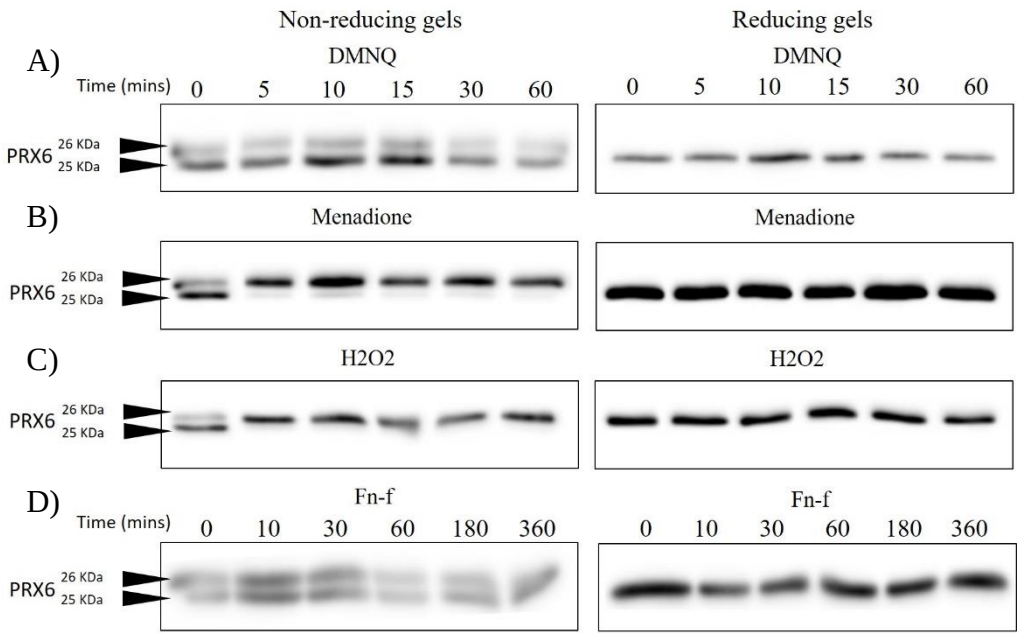

Figure 13 **Effect of DMNQ, Menadione, H_2O_2 and Fn-f on PRX6 oxidation in normal human primary chondrocytes**. Normal human chondrocytes cells were cultured into 12 well plates and after confluency medium was changed with serum-free medium the night before the experiments. After 12 h in serum free medium cells were treated with A) DMNQ 25 µM, B) Menadione 25 µM and C) H_2O_2 100 µM for 0, 5, 10, 15, 30, 60 minutes, and with D) Fn-f 1 µM for 0, 10, 30, 60, 180, 360 minutes. After treatments protein extracts were made using RIPA buffer (Cell Signaling) adding catalase enzyme. 10 µg of each cell lysates were loaded and run into both reducing and non-reducing gels. Immunoblots were made using PRX6 antibody. A) PRX6 immunoblots of reducing and non reducing gels of chondrocytes lysates treated with DMNQ. B) PRX6 immunoblots of reducing and non reducing gels of chondrocytes lysates treated with Menadione. C) PRX6 immunoblots of reducing and non reducing gels of chondrocytes lysates treated with H_2O_2. D) PRX6 immunoblots of reducing and non reducing gels of chondrocytes lysates treated with Fn-f. Representative immunoblots from 3 independent experiments (n = 3) are showing. All the experiments for each treatment were performed three-times using cells from three-different donors, represented immunoblots are showed.

3.3.3 *Lipid peroxidation is not induced by H_2O_2 and Menadione after 60 min of treatments.*

PRX6 is the only peroxiredoxins with the capacity to resolve phospholipid hydroperoxides in addition to reducing H_2O_2 produced into the cells. Lipid peroxidation produce two major toxic product malondialdehyde (MDA) and 4-hydroxynonenal (4-HNE) which are used to detect the phenomenon (Arevalo & Vázquez-Medina, 2018). PRX6 oxidation were found in chondrocytes treated with H_2O_2 and Menadione from 0 to 60 mins, so we want to analyze if these two

compounds were able to induce lipid peroxidation in normal human primary chondrocytes. For this reason, 4-HNE protein adduct were evaluated in chondrocytes treated with the two compounds from 0 to 60 mins (0, 5, 10, 15, 30, 60 mins). Results in Figure 14 demonstrate that overall lipid peroxidation doesn't increase after treatment with H_2O_2 and Menadione. However, we can't say that it doesn't occur because it could be that detoxification system (such as PRX6) in the cells is able to resolve the lipid peroxidation maintaining it at basal levels.

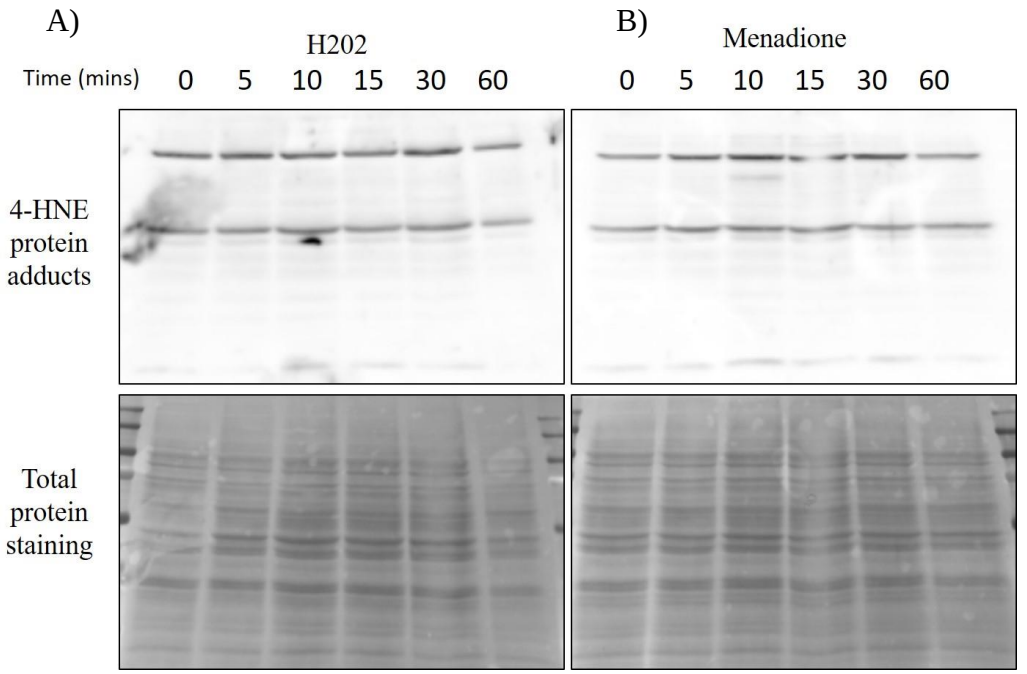

Figure 14 **Lipid peroxidation in human chondrocytes cells treated with H_2O_2 and Menadione**. A) Immunoblots of 4-HNE protein adducts present in cell extract from human chondrocytes cells treated with H_2O_2 100 µM from 0 to 60 mins (upper blot). Total protein staining used as loading control for H_2O_2 time courses (lower panel). B) Immunoblots of 4-HNE protein adducts present in cell extract from human chondrocytes cells treated with Menadione 25 µM from 0 to 60 mins (upper blot). Total protein staining used as loading control for Menadione time courses (lower panel). Representative immunoblots from 3 independent experiments (n = 3) are showing. All the experiments for each treatment were performed three-times using cells from three-different donors, represented immunoblots are showed.

3.3.4 *H_2O_2 increased GSH-PRX6 complex in chondrocytes.*

Unlike the other PRXs, PRX6 needs the binding with GSH to resolve cys oxidation. So to further understand the oxidation state of PRX6 in chondrocytes, immunoprecipitation of PRX6 were performed to see if PRX6 was bonded with GSH after 30 mins of treatment with Fn-f, H_2O_2 and Menadione. Total extracts (figure 15 A) confirm that PRX6 band shift was induced by H_2O_2 and Menadione treatment. Indeed, two bands of PRX6 were visible in the control (untreated chondrocytes) lane and chondrocytes treated for 30 mins with Fn-f. Lowest PRX6 band at 25 KDa disappear when chondrocytes were treated with H_2O_2 for 30 mins and it is less detected when cells are treated with Menadione for 30 mins. Figure 15 B - C demonstrate that the immunoprecipitation protocol worked well as in the flow through the intensity of PRX6 bands was very low. Immunoblots of total cell extracts and immunoprecipitation sample showed the same pattern of PRX6 bands (Figure 15 A – C). GSH strong band was present only in the sample treated with H_2O_2 and this strong band merged with PRX6 band at 26 kDa. So GSH-PRX6 complex is present in sample treated with H_2O_2 (Figure 15 D-E). However other bands with very low intensity were present in the others lane indicating that GSH co-immunoprecipitate with PRX6 (Figure 15 D-E). These low intensity band are present in each lane and two of that merged with the two bands of PRX6 both in chondrocytes untreated (control), treated with Fn-f and Menadione (Figure 15 D-E). Other two GSH bands with higher molecular weight than 26 kDa were found in chondrocytes cells treated with H_2O_2 and could indicate that other Glutathionylated proteins co-immunoprecipitate with PRX6.

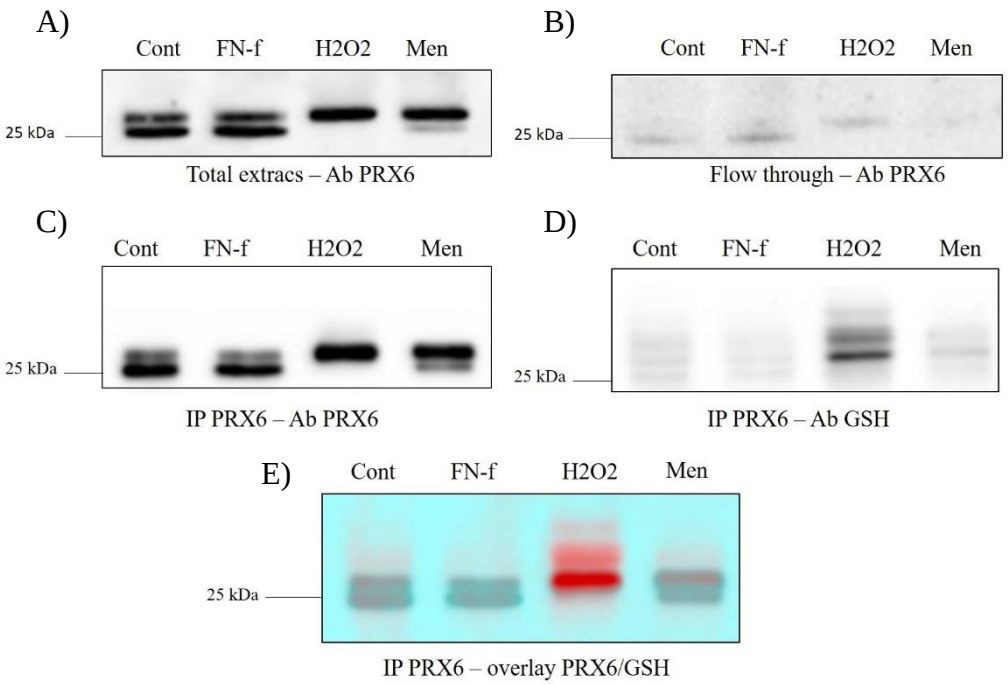

Figure 15 **PRX6 immunoprecipiation: strong GSH-PRX6 complex is formed in chondrocytes treated with H_2O_2.** All immunoblots are relative to a non-reducing gels conditions. A) PRX6 Immunoblot of total protein extracts obtained from chondrocytes treated with no compound (Control), Fn-f 1 µM, H_2O_2 100 µM, menadione 25 µM for 30 mins in serum-free media. B) PRX6 Immunoblots of flow through obtained after immunoprecipitation of PRX6 of protein extract from chondrocytes treated with no compound (Control), Fn-f 1 µM, H_2O_2 100 µM, menadione 25 µM for 30 mins in serum-free media. C) PRX6 Immunoblot of chondrocytes cell lysates immunoprecipitated using PRX6 antibody obtained in chondrocytes after treatment with no compound (Control), Fn-f 1 µM, H_2O_2 100 µM, menadione 25 µM for 30 mins in serum-free media. D) GSH Immunoblot of chondrocytes cell lysates immunoprecipitated using PRX6 antibody obtained in chondrocytes after treatment with no compound (Control), Fn-f 1 µM, H_2O_2 100 µM, menadione 25 µM for 30 mins in serum-free media. E) Merge of GSH and PRX6 immunoblots of chondrocytes cell lysates immunoprecipitated using PRX6 antibody obtained in chondrocytes after treatment with no compound (Control), Fn-f 1 µM, H_2O_2 100 µM, menadione 25 µM for 30 mins in serum-free media. Merge were made using GIMP software and inverting the color of GSH immunoblots. GSH bands in red, on blue background. PRX6 signal in black. Representative immunoblots from 3 independent experiments (n = 3) are showing. All the experiments for each conditions were performed three-times using cells from three-different donors, represented immunoblots are showed.

3.3.5 *PRX6 band shift is not associate with phosphorylation.*

PRX6 can be phosphorylated by p38, for this reason we wanted to understand if the phosphorylation of PRX6 could promote the band shift at 26 kDa. So, chondrocytes cell were treated with H_2O_2 for 30 mins and cell lysates were

collected, then cell lysates were treated with phosphatase λ following the commercial suggested protocol. In Figure 16 A – B in all sample the upper band disappear indicting that the upper band was the p-PRX6. However further analysis permits to understand that this was a false result of the experiment, because phosphatase λ reaction mix contain the reducing agent DTT which reduce oxidized cys of PRX6 (Figure 16 C-D). So PRX6 upper band disappear for the reducing agent present into the reaction mix.

Phosphorylation PRX6 band-shift hypothesis was tested using p38 inhibitor (SB203580). Chondrocytes cell were pretreated for 1 h with the inhibitor prior to the treatment with Fn-f, H_2O_2 and Menadione for 30 mins. Cell lysates were collected and run into non reducing gels. PRX6 bands pattern doesn't change after the treatment with p38 inhibitor. So, phosphorylation of PRX6 in not the cause of the upper band detected in chondrocytes cells (Figure 16 E).

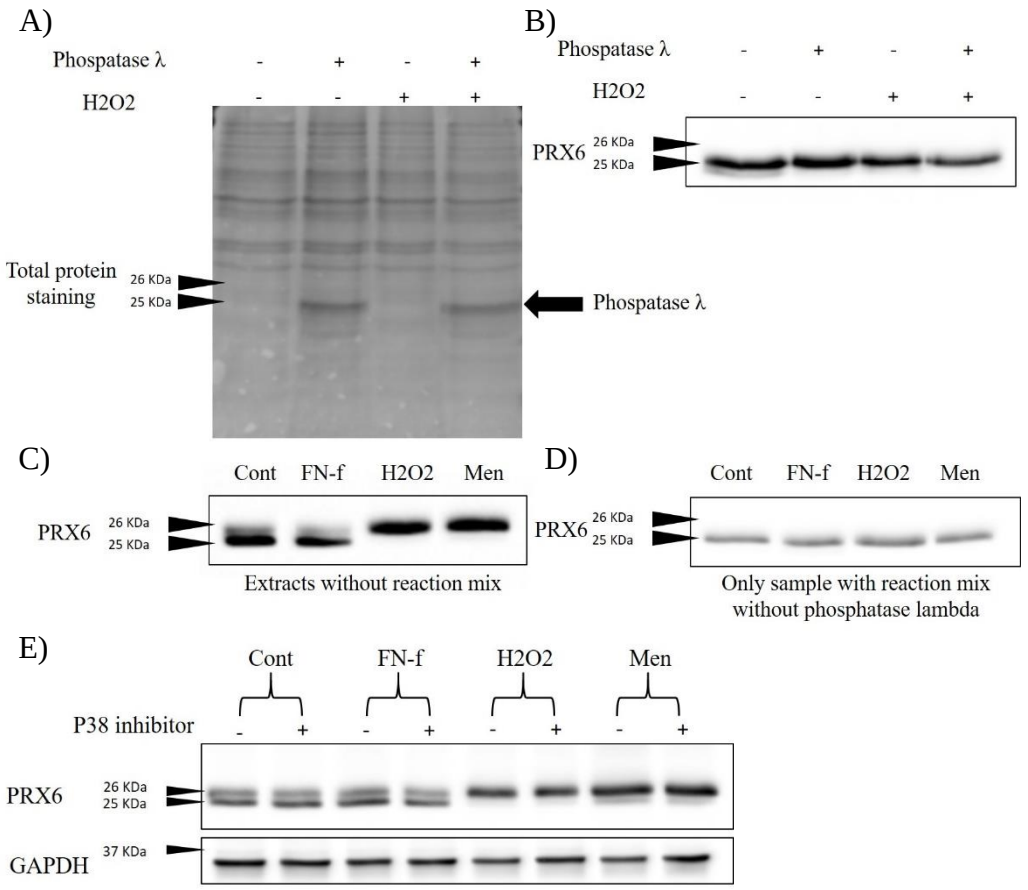

Figure 16 **Phosphatase λ and p38 inhibitor don't produce any change in PRX6 bands pattern.** A-B) Phosphatase λ was added to cell lysates of chondrocytes non treated and treated with H_2O_2 100 µM for 30 mins. Reaction mix and enzyme were added and maintained at 37 °C for 30 mins before loading into 12% gels. A) Total protein staining evaluation. B) PRX6 immunoblot. C-D) Phosphatase λ was added to cell lysates of chondrocytes non treated and treated with FN-f 1 µM, H_2O_2 100 µM and Menadione 25 µM for 30 mins. C) Enzyme were added to cell lysates and maintained at 37 °C for 30 mins before loading into 12% gels D) Reaction mix without enzyme were added and maintained at 37 °C for 30 mins before loading into 12% gels. Immunoblots show PRX6 signal on non-reducing gels. E) Chondrocytes were plated into 8 wells / 12 well plates. At confluency, medium was changed with serum-free media and maintained overnight. 4 well were pretreated 1 h with p38 inhibitor prior to 30 mins treatment with FN-f 1 µM, H_2O_2 100 µM and Menadione 25 µM. Cell lysates were collected and 10 µg of proteins were loaded and run in 12% non-reducing gels (for PRX6) and reducing gel (for GAPDH). All the experiments for each condition were performed three-times using cells from three-different donors, represented immunoblots are showed.

3.3.6 *PRX6 protein levels don't change in chondrocytes from young, old or OA donors.*

PRX6 protein levels were evaluated in young, old and OA chondrocytes of 8 different donors for each group, to understand if PRX6 could be a key protein in chondrocytes ageing or in the degeneration process occurring during OA disease. As shown in Figure 17 levels of PRX6 are the same for each group, so PRX6 expression is not influenced by the age of the donor and doesn't change in chondrocytes derived from OA patients.

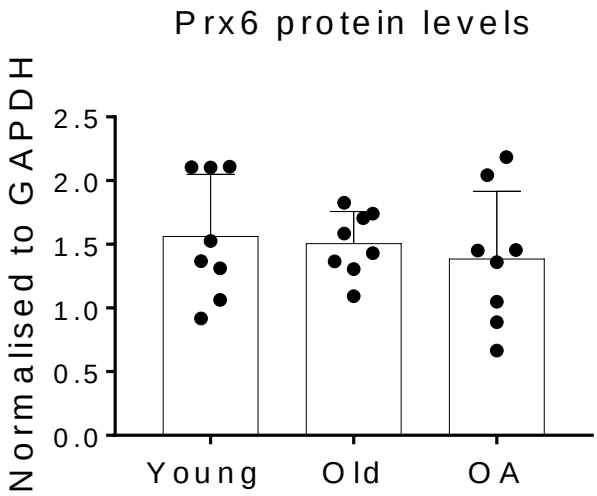

Figure 17 **PRX6 protein levels are not influenced by age or by OA disease in chondrocytes.** Chondrocytes from 24 different donors were collected, 8 donors for each group: young < 50 years old, old > than 50 years old and OA from cartilage tissue classified as grade IV (severe changes) obtained form patients submitted to a total joint replacement surgery. Chondrocytes were cultivated till confluency. Medium was changed with serum-free media and leaved overnight. Then cell lysates were collected and run in a reducing gels. Western blots are performed and expression of PRX6 was normalized on GAPDH used as loading control. Densitometry was performed using imageJ software and graphs are generated using GraphPad Prism 6. Data are presented as means ± S.D and were analyzed by one-way ANOVA. Asterisks represents significant differences (* $p < 0.05$, ** $p < 0.01$, *** $p < 0.001$).

3.3.7 *PRX6 overexpression regulate the phosphorylation of Akt and p38 after combined treatment with IGF-1 and Menadione*

In order to determine if the PRX6 could alter MAPK signaling activated in chondrocytes by the treatment with Menadione, IGF-1 and the combination of both stimuli, human chondrocytes cells were transduced with adenoviral vectors encoding PRX6 or Null empty vector control and phosphorylation levels of MAPK signaling pertinent to Menadione and IGF-1 were analyzed. Before the correct viral particle number to use for transduction was analyzed. Briefly different dilution of the viral particle number 4 x 10^8 particle/mL were made. Then cell were infected with the viruses and after 48h cell extracts were collected and analyzed by western blot. The best dilution which promotes the higher overexpression of PRX6 was 4 times of the viral particle number 4 x 10^8 particle/mL (figure 18 A). So this dilution was adopted for the further experiment adapting even the viral particle number of adenovirus for the Null empty vector control. It is well known, that IGF-1 signaling pathway is pro-anabolic in chondrocytes, stimulating the phosphorylation of Akt, but doesn't induce the phosphorylation of p38, JNK, c-Jun and ERK. Treatment with menadione increases the ROS levels and induce the activation of p38 and ERK pathways, and doesn't activate Akt, c-Jun and JNK (Collins et al., 2019). Overexpression of PRX6 led to enhanced basal levels of p-Akt if compared to cells transduced with the Null empty vector control (Figure 18 B-C). However, the phosphorylation levels of Akt, when chondrocytes are treated with IGF-1 are similar to the levels of chondrocytes transduced with the Null empty vector control (Figure 18 B-C). Treatment with menadione doesn't induce the phosphorylation of Akt, but chondrocyte pretreated with menadione for 30 min and then treated with IGF-1 for 30 min were able to restore completely the phosphorylation of Akt. IGF-1-induced restoration of Akt phosphorylation were inhibited in chondrocytes overexpressing PRX6 (Figure 18 B-C). Treatment with

menadione induce the phosphorylation of p38 MAPK which is a pro-death signal in chondrocytes. Treatment with IGF-1 is not able to reduce the phosphorylation of p38 induced by the pretreatment with menadione in cells transduced with Null empty vector control. However, overexpression of PRX6 leads to a significant reduction in the levels of p-p38 in cells pretreated with menadione and then treated with IGF-1 in respect of chondrocytes transduced with the Null empty vector control. So overexpression of PRX6 increases at least in part the ability of IGF-1 to reduce p-p38 levels in human chondrocytes (Figure 18 B-G).

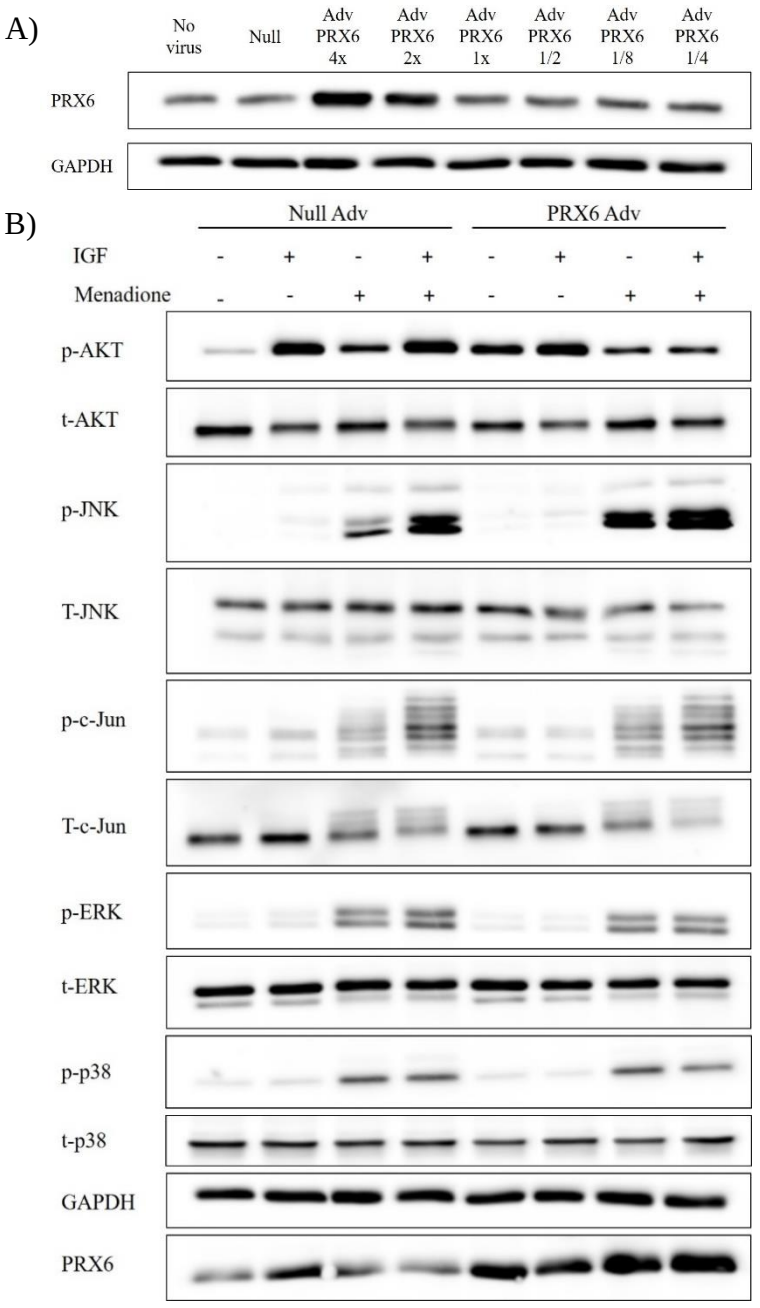
A)
No virus
Null
Adv PRX6 4x
Adv PRX6 2x
Adv PRX6 1x
Adv PRX6 1/2
Adv PRX6 1/8
Adv PRX6 1/4
PRX6
GAPDH
B)
Null Adv
PRX6 Adv
IGF
Menadione
p-AKT
t-AKT
p-JNK
T-JNK
p-c-Jun
T-c-Jun
p-ERK
t-ERK
p-p38
t-p38
GAPDH
PRX6

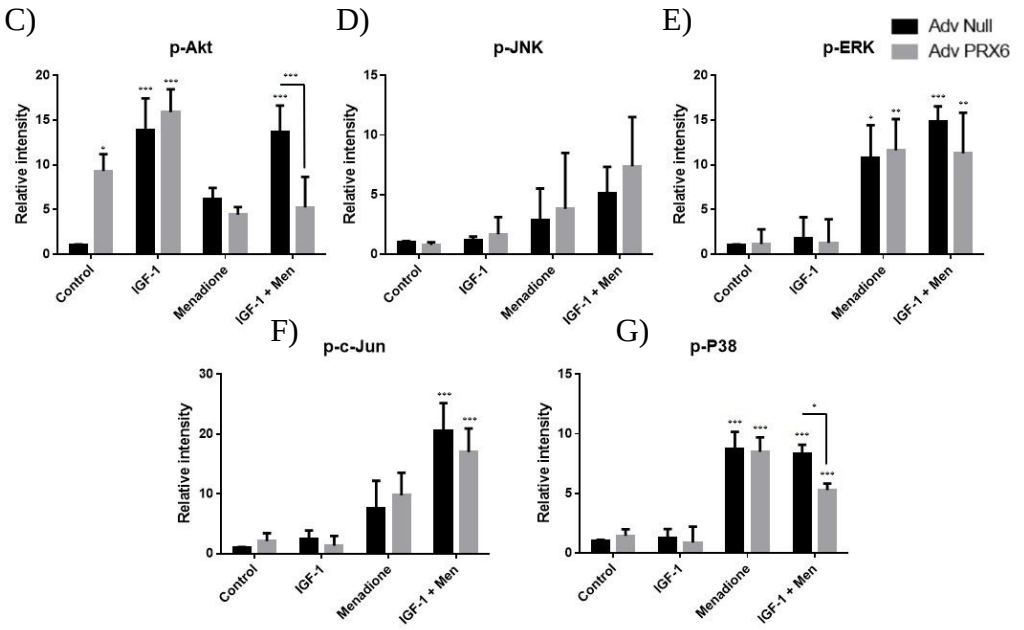

Figure 18 **Effect of adenoviral overexpression of PRX6 on IGF-1 and MAPK signaling with and without menadione**. A) Chondrocytes were transduced using different viral particles number of adenoviral vector encoding for PRX6 or with normal viral particle number of adenoviral vector encoding for Null empty vector. Proteins extracts were immunoblotted with antibodies against GAPDH and PRX6. 4 x of normal viral particle number for the adenoviral vector encoding PRX6 was used for further experiments. B-G) Chondrocytes were transduced with an adenoviral vector encoding PRX6 or a Null empty vector control and were treated with IGF-1 alone (50 ng/mL), menadione (25 µM), or pre-treated with menadione (25 µM) for 30 min prior to IGF-1 treatment for 30 min. Cell lysates were immunoblotted with antibodies to proteins pertinent to IGF-1 and MAP kinase signaling cascades (Akt, ERK, p38, JNK, c-Jun). B) Representative immunoblots from 3 independent experiments (n = 3) showing the effect of PRX6 overexpression on phosphorylation of Akt, JNK, c-Jun, ERK and p38. C-G) Results of densitometric analysis showing the effect of PRX6 overexpression on phosphorylation of Akt, JNK, c-Jun, ERK and p38. Phospho-proteins are normalized to respective total protein. For c-Jun, GAPDH was used as a loading control. Data are mean ± SD expressed as relative intensity compared to Adv-Null control. Asterisks represent significant differences compared to control (* $p < 0.05$, ** $p < 0.01$, *** $p < 0.001$) or to the highlighted condition (showed by the lines). Data were analyzed by two-way ANOVA.

3.3.8 *PRX6 overexpression attenuates Fn-f-induced phosphorylation of p38 and c-Jun in human chondrocytes.*

In order to determine if the PRX6 could alter MAPK signaling activated in chondrocytes by the treatment with Fn-f for 30 and 60 min human chondrocytes cells were transduced with adenoviral vectors encoding PRX6 or Null empty vector control and phosphorylation levels of MAPK signaling pertinent to Fn-f

were analyzed (S. T. Wood et al., 2016). Fn-f treatment leads to increase the phosphorylation levels of p38 and ERK after 30 min of stimulation in human chondrocytes cells (figure 19 A-B-C). Furthermore, increase phosphorylation levels of JNK and c-Jun were detectable after 60 min of Fn-f treatment in human chondrocytes (Figure 19 A-D-E). Fn-f was previously found to increase ROS levels in human chondrocytes cells, so we evaluate if the overexpression of PRX6 which is a ROS detoxification enzyme, could impact the signaling pathways activated by Fn-f in chondrocyte cells (S. T. Wood et al., 2016). Overexpression of PRX6 attenuates but don't abolish the phosphorylation of p38 after 30 mins and 60 mins of Fn-f treatments (Figure 19 A and B). As show in Figure 19 B levels of p-p38 decrease in human chondrocytes transduced with adenovirus vector encoding for PRX6 in comparison to human chondrocytes transduced with adenovirus vector encoding for Null empty vector control after 30 and 60 mins of Fn-f stimulation. However, PRX6 overexpression doesn't produce the same phosphorylation decrease for ERK and JNK after Fn-f treatment both at 30 and 60 mins. As shown in figure 19 C-D no differences were found between chondrocytes cells overexpressing PRX6 and chondrocytes transduced with adenovirus vector encoding for Null empty vector control. Nevertheless overexpression of PRX6 led to a significant decrease in the phosphorylation levels of p-c-Jun in human chondrocytes treated with Fn-f for 60 mins (figure 19 E). As show in figure 19 E, p-c-Jun level decrease in human chondrocytes transduced with adenovirus vector encoding for PRX6 in comparison to human chondrocytes transduced with adenovirus vector encoding for Null empty vector control after 60 mins of Fn-f stimulation.

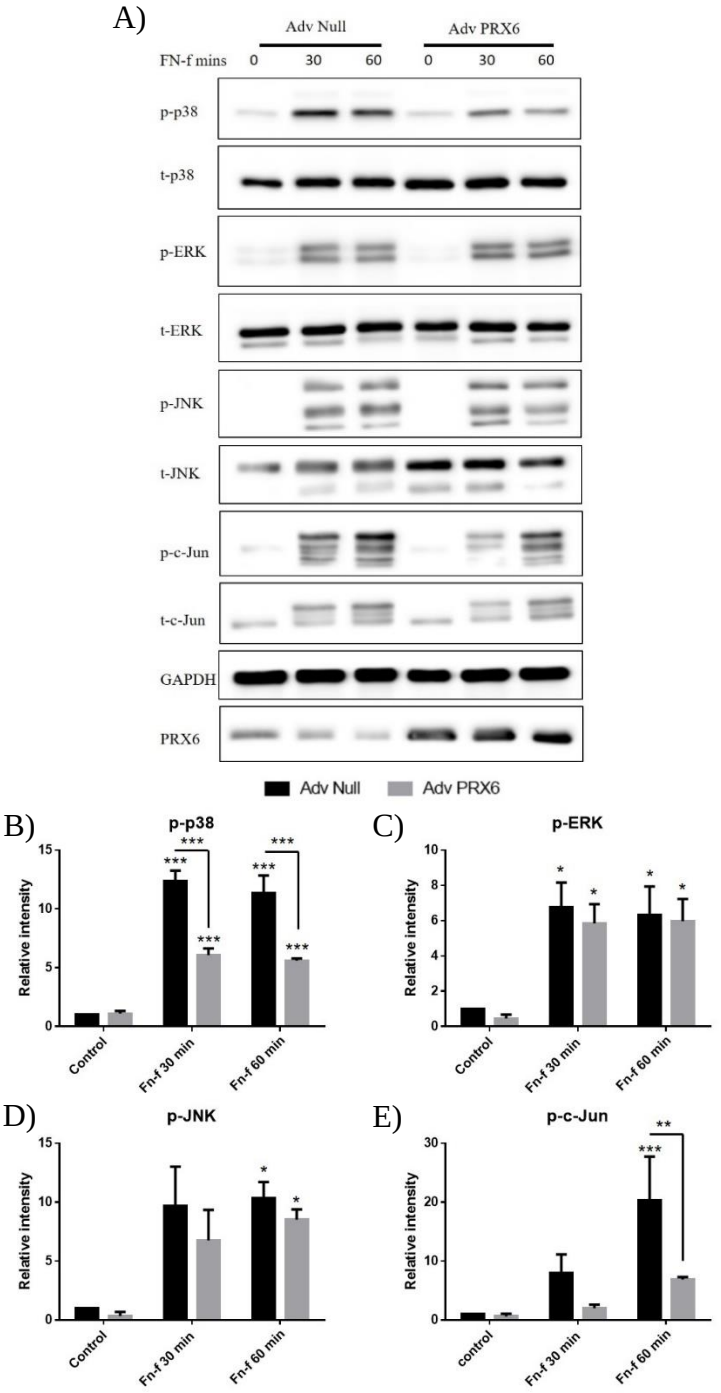

Figure 19 **Effect of adenoviral overexpression of PRX6 on Fn-f-induced MAPK signaling.** Chondrocytes were transduced with an adenoviral vector encoding PRX6 or a Null empty vector control and were treated

with Fn-f (1 μM) for 30 or 60 mins. Cell lysates were immunoblotted with antibodies to proteins pertinent to Fn-f-induced MAPK signaling (ERK, p38, JNK, c-Jun) and GAPDH, PRX6 antibodies. A) Representative immunoblots from 3 independent experiments (n = 3) showing the effect of PRX6 overexpression on phosphorylation of p38, ERK, JNK and c-Jun. B-E) Results of densitometric analysis showing the effect of PRX6 overexpression on phosphorylation of p38, ERK, JNK and c-Jun. Phospho-proteins were normalized to respective total protein. For c-Jun, GAPDH was used as a loading control. Data are mean ± SD expressed as relative intensity compared to Adv-Null control. Asterisks represent significant differences compared to control (* $p < 0.05$, ** $p < 0.01$, *** $p < 0.001$) or to the highlighted condition (showed by the lines). Data were analyzed using two-way ANOVA test.

3.3.9 *PRX6 overexpression increase Fn-f-induced MMP-13 secretion in human chondrocytes.*

Since PRX6 overexpression was able to reduce significatively the phosphorylation of two proteins (p38 and c-Jun) which are known to be very important for the catabolic signaling activated by Fn-f, MMP-13 levels in conditioned media were assessed after overnight Fn-f treatment which induce an higher MMP-13 production. Human chondrocyte cells were transduced with adenoviral vectors encoding PRX6 or Null empty vector control and MMP-13, MMP-2 levels were analyzed collecting conditioned media after Fn-f overnight treatment. As expected, MMP-13 levels increase significantly after Fn-f overnight stimulation (Figure 20 A-B). Surprisingly, MMP-13 levels in the media are higher in human chondrocytes cell overexpressing PRX6 in respect of human chondrocytes transduced with adenovirus vector encoding for Null empty vector control (Figure 20 A-B).

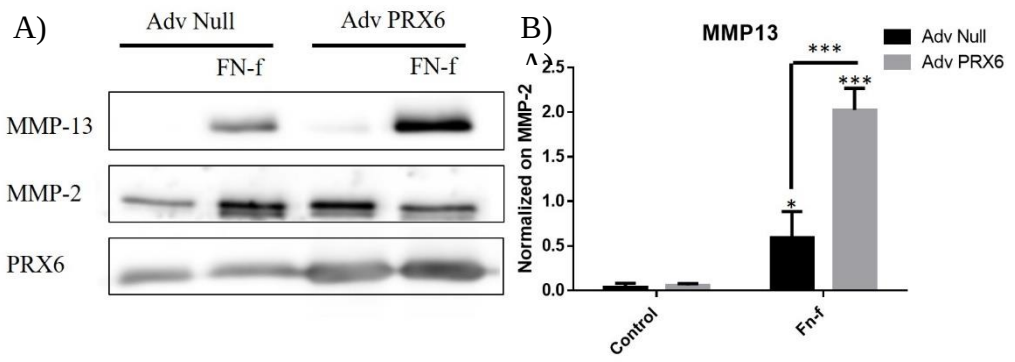

Figure 20 **Effect of adenoviral overexpression of PRX6 on Fn-f-induced MMP-13 released in human chondrocytes.** Chondrocytes were transduced with an adenoviral vector encoding PRX6 or a Null empty vector control and were treated overnight with Fn-f (1 μM). Conditioned media were taken and immunoblots were made to asses MMP-13 and MMP-2 (used as control). Protein extracts were collecter and immunoblots are made to asses PRX6 expression. A) Representative immunoblots from 3 independent experiments (n = 3) showing the effect of PRX6 overexpression on MMP-13. B) Results of densitometric analysis showing the effect of PRX6 overexpression on MMP-13 secretion after Fn-f stimulation. MMP-13 was normalized to MMP-2 used as loading control. Data are mean ± SD and were analyzed using two-way ANOVA. Asterisks represent significant differences (* $p < 0.05$, ** $p < 0.01$, *** $p < 0.001$).

3.3.10 *PRX6 localize into the nucleus of human chondrocytes*

PRX6 functions are connected to their subcellular localization, and previous studies said that PRX6 is predominantly a cytosolic protein and that some post-translational modifications can change its localization regulating its enzymatic activities. However, Li et. al found that PRX6 were present into the nucleus interacting directly with Sirt6. In order to asses the subcellular localization of PRX6 in chondrocytes cells and if Fn-f, H_2O_2, Menadione and DMNQ treatment could change PRX6 localization, protein cells fractions were performed producing nuclear protein fraction and cytosolic protein fraction. PRX6 localize into the nucleus in human chondrocytes cells, so PRX6 is not only a cytosolic protein, but in chondrocytes cells, PRX6 is present into the nuclear compartment even in the untreated chondrocytes (Figure 21). So nuclear PRX6 may interact and regulate other transcription factors.

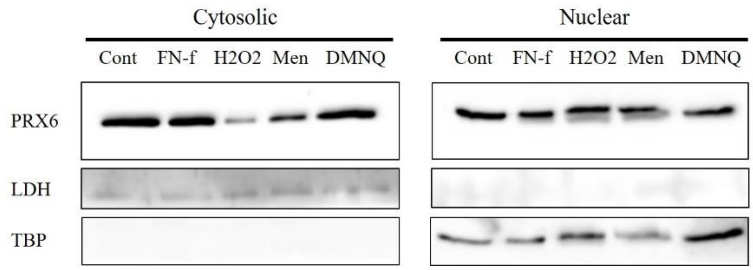

Figure 21 **PRX6 localize into the nucleus of human chondrocytes.** Human primary chondrocytes cells were plated into 5 well/6 well plate. After 48 h media was changed with serum-free media and maintained overnight. Then Fn-f (1 μM), H_2O_2 (100 μM), Menadione (25 μM) and DMNQ (25 μM) were added for 30 mins. At the end of the treatment, cells lysate were collected and commercial kit were used to fractionate protein extract into cytosolic fraction and nuclear fraction. For both fraction PRX6, LDH and TBP levels were assessed by immunoblots using specific antibodies. LDH was used as loading control for cytosolic fraction and TBP was used as loading control for nuclear fraction. Representative immunoblots from 3 independent experiments (n = 3) are shown.

3.4 Discussion

Recent advances in redox biology implicate PRXs oxidation as a key mechanism for regulating intracellular H_2O_2 levels and subsequent downstream cell signaling events. So, this study chooses to explore the effects and the role of PRX6 oxidation, on selected downstream cell signaling events using human articular chondrocytes as a cell model system. In previous studies at Richard Loeser's laboratory, DMNQ and menadione was used as H_2O_2-producing tools in chondrocytes to study the effect of PRX1-PRX3 hyperoxidation on specific cell pathways fundamental for chondrocytes cells (Collins et al., 2019, 2016). Collins et. al previously found that menadione generated higher levels of mitochondrial H_2O_2 than DMNQ, leading to PRX3 hyperoxidation. DMNQ generate H_2O_2 more disperse into the cytoplasmic compartment and is not so specific like menadione. Also Collins et. al characterize the role of PRX1, PRX2 and PRX3 in chondrocytes cell signaling after menadione, DMNQ and IGF-1 stimulation. So, after the MS results we decide to focus our studies understanding the role of PRX6 in chondrocytes which is a new area that had not been previously investigated. Data from MS reveal that PRX6 was the second most abundant protein found to be oxidized at cysteine levels by H_2O_2 and Fn-f treatments. So we started to analyzed the oxidation state of PRX6 in human primary chondrocytes adjusting the technique used from Collins et. al to detect the oxidation state of PRX1, PRX2 and PRX3 (Collins et al., 2019). Unlike normal 2-cys PRXs (PRX1-4) which after oxidation to a sulfenic acid react with another cysteine residue (resolving) on another monomer, forming a dimer subsequently reduced by an appropriate electron donor to complete a catalytic cycle (Aron B. Fisher, 2017; Patel & Chatterjee, 2019), PRX6 is called 1-cys PRX because the catalytic mechanism is based on a single conserved cys residue. Oxidation to PRX6-SOH is resolved by the binding with a molecule of glutathione (GSH) mediated by glutathione S-transferase (Aron B. Fisher, 2017). However, PRX6

can form dimers through hydrogen bonding involving its hydrophobic surface. Furthermore human PRX6 proteins has 2 cys and in a recent study authors show how PRX6 could be detected in dimeric and trimeric forms and that forms are downregulated by H_2O_2 treatemnts (Suzuki et al., 2019). In our study we used lower concentration of H_2O_2 in comparison to Suzuki et. al study and we didn't detect any changing in the 75 kDa or 50 kDa bands that following the antibody datasheets are believed to be a non-specific signal. However, in non-reducing gels, that preserve the disulfide bond, we detected PRX6 as two bands one at 26 kDa and one at 25 kDa in untreated chondrocytes. Treatment with H_2O_2 (100 µM) or menadione (25 µM) promote the band shift to 26 kDa and 25 kDa band was totally or partially absent, this shift was observed after 5 min of treatment with both H_2O_2 (100 µM) or menadione (25 µM). Moreover, chondrocytes treated with Fn-f and DMNQ for different time points didn't exhibit the same band shift, in fact the bands were the same as the untreated cells. We can say that the treatment with H_2O_2 (100 µM) or menadione (25 µM) change the oxidation state of PRX6 and that the shift is associated to a cys state, maybe it could be due to PRX6 binding with GSH or glutathione S-transferase which can change the molecular weight of PRX6; however binding to GSH is a more reliable reason because molecular weight difference between the two bands is about 1kDa. To confirm this hypothesis we performed an immunoprecipitation experiment to detect if the upper band at 26 kDa of PRX6 contain even GSH. The results show that only in chondrocyte treated with H_2O_2 there is an higher signal of GSH but that signal was not the same for lysates obtained from chondrocytes treated with menadione which promote PRX6 band shift. An explanation could be that H_2O_2 produce by menadione is lower that H_2O_2 generated after direct addition of H_2O_2 which leads to oxidize firstly PRX6. Another hypothesis is that probably the upper band at 26 kDa is not only due to PRX6 binding to GSH but it could be that the oxidation on PRX6 cys change it structure leading to a different gel

mobility. However more experiments could help to understand which is the cause of this PRX6 band shift that is for sure associated to the cys oxidation, because when the same lysates were run in reducing gels PRX6 band was detected only at 25 kDa. Moreover PRX6 Prdx6 also expresses acidic calcium-independent phospholipase A_2 ($aiPLA_2$) and lysophosphatidyl-choline acyl transferase (LPCAT) activities in separate catalytic sites (Aron B. Fisher, 2017; Aron B. Fisher et al., 2016; Huang et al., 2011). PRX6 is a unique enzyme as it has both phospholipase activity and peroxidase activity, making it an intriguing enzyme for both lipid-mediated inflammation and antioxidant defense (Aron B. Fisher, Dodia, Feinstein, & Ho, 2005). Moreover previous studies demonstrate that menadione as well as H_2O_2 can increase ROS leading to lipid peroxidation and membrane destabilization in cells (Chiou, Chu, & Tzeng, 2003; Siddique, Ara, & Afzal, 2012; Tiku, Shah, & Allison, 2000; Tzeng, Lee, & Chiou, 1995). Thus, we decided to detect if the treatment with menadione or H_2O_2 which induce a PRX6 shift at 26 kDa band could be due to an induction of lipid peroxidation by the treatment. However in our conditions the treatment for 60 min with menadione or H_2O_2 doesn't induce an increase in the amount of 4-HNE protein adducts which is a common marker of lipid peroxidation (Mihalas, De Iuliis, Redgrove, McLaughlin, & Nixon, 2017; Milkovic, Gasparovic, & Zarkovic, 2015). Several post-translational modifications can regulate the enzymatic activity of PRX6 promoting changes in the intracellular localization of the protein; an example is the phosphorylation of PRX6 at threonine 177 by p38 MAPK which is known to be activated by ROS in chondrocytes cells (Chatterjee et al., 2011; Collins et al., 2019; Y. Wu et al., 2009). So, phospholipase lambda and p38 inhibitor was used to understand if PRX6 was phosphorylated after Fn-f, menadione, DMNQ and H_2O_2 treatment in human chondrocytes, and if this phosphorylation could be implicated in PRX6 band shift. However, no differences in PRX6 bands pattern was observed, indicating that the

phosphorylation is not implicated in the band shift. We can't exclude that Fn-f, menadione, DMNQ and H_2O_2 treatments leads to PRX6 phosphorylation because for that we need an antibody specific for phosphorylated PRX6. Further experiments using this antibody could give more information on the role of PRX6 phosphorylation in chondrocyte, this could be interesting especially because the phosphorylation of PRX1 was observed to be important for PRX1 activity (Collins et al., 2019). Aging is a primary risk factor for OA, which is the most common cause of chronic disability in older adults and correlates with age-related redox imbalance and mitochondrial dysfunction (Richard F. Loeser, 2017; Richard F. Loeser, Carlson, Del Carlo, & Cole, 2002). Furthermore, PRX6 was recently found by Ikeda et. al to be a possible OA biomarker (Ikeda, Ageta, Tsuchida, & Yamada, 2013). In this study Ikeda et. al showed that cartilage from patients with OA has lower PRX6 levels in comparison to cartilage from control patients which has femoral neck fracture (Ikeda et al., 2013). We found no changing in PRX6 expression levels in chondrocytes isolated from cartilage of younger donors (age < 50 years old), older donors (age > 50 years old) and OA donors. So, PRX6 levels are not influenced by age or by OA disease contrary to what observed in Ikeda study which used cartilage from 6 patients instead of 8 patients used in our study. However our result are in agreement with the previous result indicating no changing in PRX2 and PRX3 levels in chondrocytes isolated from young and older mice (Collins et al., 2016). Instead of protein levels seems that older chondrocytes exhibit an increase basal levels of PRX hyperoxidation compared to younger chondrocytes (Collins et al., 2016). Future experiments can give us more information about the PRX6 hyperoxidation state maybe using a specific antibody against PRX6-$SO_{2/3}$ to understand if the treatments with Fn-f, menadione, DMNQ and H_2O_2 could increase the hyperoxidation of PRX6 and if levels could change by aging process. PRXs have recently been shown to participate in signal transduction pathways that regulate resistance to oxidative

stress and lifespan extension through regulation of JNK/FOXO signaling in *Drosophila melanogaster* (K. S. Lee et al., 2009). Furthermore PRX6 overexpression in mice exacerbates the development of collagen antibody–induced arthritis (CAIA) and antigen-induced arthritis (AIA) in mice through increasing proinflammatory pathways like p-38, JNK, ERK and NF-κB (D. H. Kim et al., 2015). However we found that PRX6 overexpression in human chondrocytes cells leads to an increase of basal levels of phospho(p)-Akt and no effect on p-JNK, p-p38, p-c-Jun and p-ERK1/2 basal levels. Menadione alone induce the phosphorylation of p38 and ERK1/2 in human primary chondrocytes, without any effect on JNK, c-Jun and Akt phosphorylation levels as previously observed (Collins et al., 2019). IGF-1 chondrocytes stimulation increases the levels of p-Akt and as no effect on the other MAPK signaling studied. Overexpression of PRX6 doesn't impact the cell signaling activated by menadione but alter the levels of p-Akt and p-p38 when chondrocytes were pretreated with menadione for 30 min and after treated with IGF-1. Previously it was observed that ROS levels can regulate the IGF-1 signaling pathways and that presence of higher ROS levels generated by menadione leads to an inhibition of IGF-1-mediated Akt phosphorylation (Collins et al., 2019, 2016). Our results showed that with 30 min of IGF-1 stimulation after the pretreatment with menadione for 30 min, it is possible to recover the Akt phosphorylation. However, this recover is inhibited in chondrocytes overexpressing PRX6. Notably the overexpression of PRX6 doesn't change the levels of p-p38 generated after menadione treatment, but overexpression of PRX6 is able to reduce the phosphorylation of p38 after the pretreatment with menadione and the subsequent treatment with IGF-1. Destruction of the articular cartilage is a key feature of OA and stems from an imbalance in chondrocyte anabolic and catabolic activities (Richard F. Loeser et al., 2012). This results in excessive production of proteolytic enzymes that break down the extracellular matrix,

generating matrix fragments that can further propagate catabolic activity through a positive feedback loop (L. Ding, Guo, & Homandberg, 2009; Richard F. Loeser et al., 2012). Fibronectin (Fn) is a protein present in cartilage ECM which during cartilage degradation undergoes to proteolytic cleavage forming fibronectin fragments (Fn-f). Furthermore, Fn-f have been found in OA cartilage and synovial fluid and have been shown to stimulate cartilage matrix destruction (L. Ding et al., 2009; Homandberg, Meyers, & Xie, 1992). Fn-f is known to bind to the α5β1 integrin receptor and to activate MAP kinase signaling, resulting in the up-regulation of a number of cytokines, chemokine, and MMP genes (Forsyth et al., 2002; Homandberg, Costa, & Wen, 2002). However endogenous activation of chondrocyte catabolic signaling by FN-f requires generation of endogenous reactive oxygen species (ROS) as second messengers (Del Carlo et al., 2007). In agreement with previous findings, treatment of human primary chondrocytes with Fn-f for 30 and 60 min leads to the phosphorylation of JNK, p38, c-Jun and ERK1/2 which pathways are involved in the MMP-13 production. Overexpression of PRX6 strongly decrease the Fn-f-induced phosphorylation of p38, this result together with the inhibition of p-38 phosphorylation after co-treatment with menadione and IGF-1 leads us to think that PRX6 regulate in a specific manner p38 and that p38 and PRX6 may probably interact each other's both in direct or indirect manner. Other study confirms that PRXs can regulate p38 activity and in particular it was found that depletion of PRX1 and PRX2 leads to lower p38 phosphorylation after H_2O_2 treatments, however low was known about PRX6 ability (Barata & Dick, 2019). Moreover, PRX6 can be phosphorylated by p38, inducing a conformational change in the protein which promotes its translocation to the plasma membrane, and increases its aiPLA_2 activity (Chatterjee et al., 2011; Y. Wu et al., 2009). PRX6 overexpression was also able to reduce the phosphorylation of c-Jun, which is a transcription factors activated by JNK and associated with dedifferentiation of primary chondrocytes

and with OA progression and development (Ge, Zou, Li, Liu, & Tu, 2017; S. G. Hwang, Yu, Poo, & Chun, 2005). However, overexpression of PRX6 has no effect on Fn-f-induced JNK and ERK1/2 phosphorylation. Fn-f treatment in human primary chondrocytes cells leads to MMP-13 production. However even if overexpression of PRX6 can reduce the phosphorylation of p38 and c-Jun after Fn-f treatments the MMP-13 released by chondrocytes overexpression PRX6 was higher in comparison to chondrocytes transduced with Null empty vectors. This could be due to a difference in MMP-13 endocytoses between normal cells and PRX6 overexpressing cells or by an increase MMP-13 production rates (Yamamoto et al., 2016). To understand better the mechanism involved it could be useful to detect the RNA expression levels of MMP-13. However overproduction of MMP13 is a catabolic marker of chondrocytes cells which leads to cartilage matrix degradation and to OA development (Mary B. Goldring & Marcu, 2009; Yamamoto et al., 2016). PRX6 localization is crucial for the regulation of its enzymatic activities. PRX6 exhibits maximal aiPLA$_2$ activity at an acidic pH and acts as peroxidase at neutral pH (Aron B. Fisher, 2011). So when PRX6 is localized in lysosomal-type organelles its functions as aiPLA$_2$ (A. B. Fisher, Dodia, Chander, & Jain, 1992; Aron B. Fisher, Dodia, Yu, Manevich, & Feinstein, 2006). Differently, cytosolic PRX6 functions mainly as peroxidase (Kang, Baines, & Rhee, 1998). However, we detected that PRX6 in chondrocytes cells is present even in the nuclear compartment and that PRX6 remain into the nucleus also in chondrocytes treated with Fn-f, menadione, DMNQ and H_2O_2. This are in agreement with some studies in which authors detected PRX6 into the nucleus and that PRX6 is able to regulate Sirt6 activity (Y. He et al., 2018; W. Li et al., 2018). Further experiments are needed to understand better the role of nuclear PRX6 in chondrocytes. In this study we demonstrate that PRX6 is into the nucleus in chondrocytes but the exact role of nuclear PRX6 remain to be clarified. In conclusion we can say that PRX6 change its gel mobility in lysates

from chondrocytes treated with menadione and H_2O_2 and that this band shift is associated for sure to a cys oxidation state because using the reducing gels PRX6 migrates at 25 kDa. Furthermore PRX6 seems to influence specifically the activation of p38 MAPK. However, even if the overexpression of PRX6 is able to reduce p38 phosphorylation levels in chondrocytes this is not enough to block the catabolic response activated by menadione and Fn-f, but seems to increase some catabolic effects of these treatments like reducing phosphorylation levels of Akt in combined treatments of menadione and IGF-1 and increase MMP-13 secreted in the media by chondrocytes treated with Fn-f.

Supplementary images

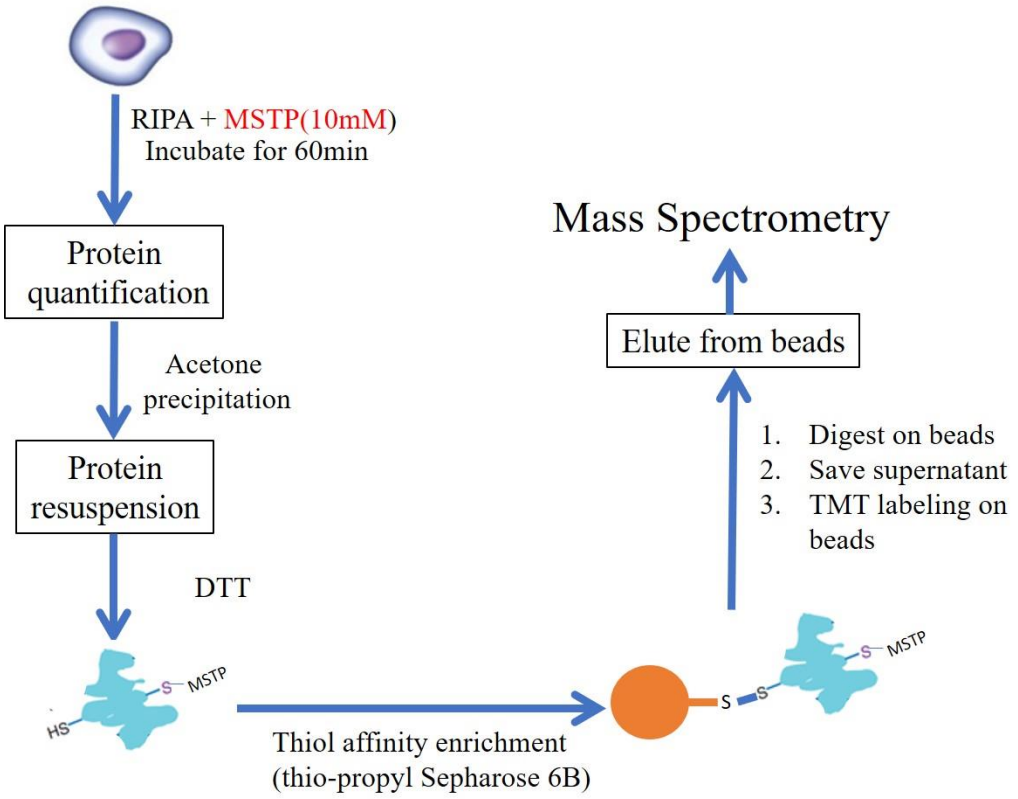

Supplementary Figure 1**: Schematic representation of protocol used for Mass Spectrometry analyses**. Human primary chondrocytes were treated for 30 min with FN-f and H_2O_2. After the protein extraction non oxidized cys were blocked with the blocker agents 4-(5-methanesulfonyl-[1,2,3,4]tetrazol-1-yl)-phenol (MSTP) which react specifically with the reduced cys (SH) and is more specific then N-ethylmaleimide (NEM) (X. Chen et al., 2017). Furthermore, oxidized cys were reduced with DTT treatment and then the thiol affinity enrichment was performed using commercially available thiol-affinity resin (Thiopropyl Sepharose 6B) to directly capture free thiol-containing proteins through a disulfide exchange reaction followed by on-resin protein digestion and multiplexed isobaric labeling to facilitate LC–MS/MS based quantitative site-specific analysis of cysteine-reversible oxidation

Chapter 4 - Novel squarate cross-linked gelatin hydrogels for 3D cell culture and drug delivery platforms

4.1 Aim of the work

Three-dimensional cell culture platforms offer *in vitro* better chances to mimic the native microenvironment extra-cellular matrix, ECM) and cell behavior over 2D cell culture techniques, despite the last ones still have their relevance, allowing the deconvolution of the influence of the chemistry of the material, of biocues on cell responses from the effect of the bulk material, cross-linking, and dimensional properties, providing great insight into key biochemical processes, such as adhesion, proliferation, differentiation, and cell−cell cross-talk, both in physiological and pathological states (Davidenko et al., 2016; Edmondson et al., 2014; D. Lv, Hu, Lu, Lu, & Xu, 2017). In order to recapitulate the native features of cellular microenvironment, several 3D-scaffolds have been proposed; among them, hydrogels, both natural or synthetic or as blend, have become popular as 3D cell culture techniques, since they are able to incorporate a great amount of water and provide robust platforms for investigating cell physiology, pathology (Caliari & Burdick, 2016; Tam et al., 2017; Tibbitt & Anseth, 2009), tissue regeneration (El-Sherbiny & Yacoub, 2013; Jung Hwan Lee & Kim, 2018) , and drug delivery (J. Li & Mooney, 2016).

Depending on the chemistry of the polymeric constituents, and cross-linking strategy, hydrogels show different physico-chemical and biological features, accompanied by peculiar advantages and limitations. In this framework, the search for new hydrogels and cross-linking strategies is still ongoing, in order to ameliorate their performances as ECM mimics and reliable cell culture scaffolds for tissue engineering, drug delivery, and wound dressing (El-Sherbiny & Yacoub, 2013). Among natural polymers, gelatin (obtained from collagen hydrolysis) is an attractive candidate for hydrogel preparation, since it is

biocompatible, possess cell-adhesive properties, has limited costs and it is easily accessible. However, gelatin is water-soluble at 37 °C and is featured by poor mechanical properties (Jaipan et al., 2017).

Given the presence of amino acid functional groups, the mechanical and chemical properties of gelatin can be modified with different crosslinking agents (i.e. glutaraldehyde, genipin, dextran dialdehyde, thiol-ene chemistry, Michael addition chemistry, carbodiimide chemistry, epoxy chemistry etc.) (Guizzardi et al., 2019; Occhetta et al., 2015; Russo et al., 2016).

However, researchers are still looking for new, more secure cross-linking agents. In this work we investigate the properties of gelatin-based hydrogels obtained by the use of 3,4-diethoxy-3-cyclobutene-1,2-dione or diethyl squarate (DES) as homobifunctional cross-linker. To the best of our knowledge, DES has not been used before as a cross-linking agent for gelatin hydrogel preparation.

4.2 Materials and Methods

4.2.1 Materials

All chemicals were purchased from Sigma-Aldrich and used without any further purification. Gelatin from porcine skin is provided by Sigma-Aldrich, catalog no. G2500, CAS Number 9000-70-8. Freeze-drying was performed by a Christ alpha 1–2 freeze dryer (Christ, Osterode am Harz, Germany). All samples were immersed in liquid nitrogen for about one hour before the drying procedure. *Clostridium histolyticum* collagenase (type I, ≥125 CDU/mg) was purchased from Sigma-Aldrich. Human cartilage cells C28/I2 were a kind gift from Prof. Francesco Dell'Accio (Queen Mary University of London, London, UK).

4.2.2 10 % hydrogel preparation (10 % Gel-DES)

Gelatin (200 mg) was dissolved in Na_2CO_3/$NaHCO_3$ buffer solution (pH 8.5, 2 mL) at 40 °C. After complete dissolution, 3,4-diethoxy-3-cyclobutene-1,2-dione (DES, 5 μL) was added. Gelatin was reacted for 90 minutes at 40 °C, then cooled to room temperature until complete gelation. Hydrogels were freeze-dried for 72 h.

4.2.3 5 % hydrogel preparation (5 % Gel-DES)

Gelatin (100 mg) was dissolved in Na_2CO_3/$NaHCO_3$ buffer solution (pH 8.5, 2 mL) at 40 °C. After complete dissolution, 3,4-diethoxy-3-cyclobutene-1,2-dione (DES, 5 μL) was added. Gelatin was reacted for 90 minutes at 40 °C, and then cooled to room temperature until complete gelation. Hydrogels were freeze-dried for 72 h.

4.2.4 *Fourier Transform Infrared (FTIR) analysis*

FTIR spectra were collected in attenuated total reflection (ATR) as previously described (Ami et al., 2019). In particular, samples were forced into close contact with the diamond ATR crystal using the clamp arm assembly of the device (Quest, Specac) and the spectra were recorded by the Varian 670-IR spectrometer (Varian Australia Pty Ltd.). The following conditions were employed: 2 cm^{-1}

spectral resolution, scan speed of 25 kHz, 512 scan coadditions, triangular apodization, and a nitrogen-cooled mercury cadmium telluride detector. Gelatin absorption spectra were normalized at the same Amide I band area. FTIR measurements and spectral analyses were performed with the Resolutions-Pro software (Varian Australia Pty Ltd.). Made by Antonino Natanello.

4.2.5 SEM analysis

Morphological analysis was performed by means of Scanning Electron Microscopy. For such kind of measurements Hydrogel samples were previously freeze-dried, fractured, attached with conductive carbon tape to standard SEM stubs and finally sputter-coated with 10 nm gold film order to preserve the samples under electron beam illumination. Imaging was performed by means of Field-Emission Scanning Electron Microscope (FE-SEM) ZEISS GeminiSEM 500, operating at 2kV accelerating voltage, using In-lens SE-detector configuration.

4.2.6 Swelling studies

Dynamic swelling measurements were made by gravimetric measurements. Three replicas of freeze-dried 5 % and 10 % Gel-DES specimens (ca. 1 g in weight) were soaked in distilled water at 25 °C. The swollen gels were periodically removed from water, blotted with filter paper, and weighed on an analytical balance (Analytical Balance 220 g x 0.1 mg, Radwag AS 220/C/2) and returned to the swelling medium till the equilibrium is reached.

Swelling Degree (SD; $g*g^{-1}$) was calculated from the following equation and reported as a function of time:

$$SD = \frac{(W_t - W_0)}{W_0} \quad (1)$$

where W_t is the weight of swelling hydrogel at different times and W_0 is the dry weight of the gel. At long times, an equilibrium swelling degree (ESD) is reached.

It is possible to fit the swelling kinetics by the integration of the the Berens-Hopfenberg differential equation (Berens & Hopfenberg, 1978):

$$\frac{Mt}{M\infty} = (1 - ae - t/\tau) \quad (2)$$

that gives the characteristic swelling time of the hydrogel. When only the first part of the swelling curve is considered (SDt/ESD $\leq$ 0.6), it is possible to determine the mechanism of water diffusion inside the hydrogel from the value of the exponent of the following law (Peppas & Sahlin, 1989):

$$\frac{Mt}{M\infty} = \frac{SDt}{ESD} = at^n \quad (3)$$

where n=0.5 account for Fickian (normal) water diffusion, when the diffusion rate of the penetrant is much lower that polymer relaxation, while n = 1 shows a transport (i.e., polymer relaxation controls the water diffusion into the network). Values of n in-between 0.5 and 1 indicates non-Fickian or anomalous transport, when both diffusion and polymer relaxation control water penetration into the network.

The equilibrium water content (EWC), was calculated from the following equation (Rohindra, Nand, & Khurma, 2004):

$$EWC\ (\%) = \frac{(w_e - w_0)}{w_e} \times 100 \quad (4)$$

where W_e is the swelling weight of the sample at equilibrium and W_0 is the dry weight of the gel (Ghobril & Grinstaff, 2015).

4.2.7 Collagenase assay

Hydrogel specimens (1 g in weight) were incubated with 1 mL of Tris-HCl buffer (0.1 M; pH 7.,4) and $CaCl_2$ (0.05 M) at 37 °C for 1 h and. 1 mL of *Clostridium histolyticum* collagenase solution (0.5 mg/mL in Tris-HCl 0.1 M, at pH 7.4 pH) was added to samples. All samples were kept at 37 °C and the degradation was determined by gravimetric analysis (Pieper, Oosterhof, Dijkstra, Veerkamp, & Van Kuppevelt, 1999).

4.2.8 Cell culture.

Human cartilage cells C28/I2 were cultured in Dulbecco's modified Eagle's medium/Ham's F-12 (DMEM/F-12, BioWest, USA) supplemented with 10% heat-inactivated fetal bovine serum (FBS, Euroclone S.p.A., Pero, Italy), 100U/mL penicillin, 100 mg/mL streptomycin, 4 mM L-glutamine, 17 mM D-glucose (BioWest, USA). C28/I2 cells were maintained at 37°C in a humidified atmosphere with 5% CO_2 in 100 mm Petri dishes. The medium was changed every three days. HEK293 cells, an embryonic renal immortalized cell line, were cultured in 100 mm Petri dishes using DMEM supplemented with 10% FBS, 100U/mL penicillin, 100mg/mL streptomycin and 4mM L-glutamine. HEK293 cells were maintained at 37°C in a humidified atmosphere with 5% CO_2. Medium was changed every three days. Cells were cultured in monolayers, grown sub-confluence (80%) and passaged at a ratio of 1:8.

4.2.9 Cell inoculation.

Cell inoculation into hydrogels cells was obtained after confluent monolayer cultures release by Trypsin-EDTA, cells were counted and re-suspended in growth medium at a density of 5×10^6 cells/mL.Before cell seeding, lyophilized hydrogels were sterilized in 75 % aq. ethanol for 20 min., followed by 30 min UV and several washing with 1 mL PBS. After sterilization, hydrogels were equilibrated in 1 mL culture medium (DMEM/F-12) for 12h. All sponges were aspirated dry prior to cell seeding and disposed in a 24-multiwell plate. 200 µL of C28/I2 or HEK293 suspension (5×10^6 cells/mL) per specimen were added to the wells and cells allowed to attach for 4 h at 37°C with 5 % CO_2 in a humidified atmosphere. Subsequently, 1 mL of culture medium was added in each well. The culture was conducted for 2 weeks, maintained at 37 °C in a humidified atmosphere with 5 % CO_2 and medium was changed twice a week. Cells were observed daily using an inverted microscope (CK40, Olympus, Tokyo, Japan).

4.2.10 Immunofluorescence analysis.

After two weeks of culture, gelatin hydrogels containing cells were fixed with PBS-4% paraformaldehyde for 2 h at 4 °C and washed twice with PBS. Afterwards, using vibratome (VT1000S, Leica, Wetzlar, Germany) gelatin hydrogels were cut into sections 300 µm-100 µm thick, depending on hydrogel composition. The gel sections were permeabilized with 1mL of 0.1% Triton X-100 in PBS for 15 min, blocked with 1 mL of 1 % BSA/PBS for 45 min., washed four times with 1 % BSA/PBS and stained with 1 µL of Phalloidin-TRITC (Sigma-Aldrich, Saint-Louis, Missouri, USA) in 1 ml of 1% BSA/PBS for 1h. After five washing with PBS, DNA was stained using DAPI (Sigma-Aldrich, Saint-Louis, Missouri, USA) and sections were washed four times with PBS. Finally, gel sections were mounted using Eukitt® quick-hardening mounting medium (Sigma-Aldrich, Saint-Louis, Missouri, USA). Fluorescence imaging of the sections was performed by a scanning microscope exploiting two photon excitation by a home assembled setup (Caccia et al., 2008). Briefly, a MaiTai Pro HP Titanium:Sapphire laser (Spectra Physics, Mountain View, Ca, USA) beam at 800 nm has been fed through a scanning head (FluoView 300, Olympus, Tokyo Jp) and focalized on the sample by an IR optimized objective (25x XLplan, NA=1.05, Olympus, Tokio, Jp). The fluorescence signal was collected in non-descanned mode and separated by dichroic and band pass filters in front of the detectors (for DAPI, 485/30 nm, for TRITC, 600/40 nm Chroma Techn. Brattelboro, VT).

4.2.11 Rhodamine loading study

Fresh jellified hydrogels (5 %, obtained from 100 mg of substrates) were placed in 3 mL of Rhodamine-6G solution (7 µM) in milliQ water. Every 20 minutes the absorbance of solution was measured by means of a spectrophotometer and the solution concentration was obtained according to the Lambert-Beer law $A= \varepsilon CL$, where $\varepsilon= 116000\ M^{-1}cm^{-1}$ is the Rhodamine extinction molar coefficient, L = 0.2

cm is the cuvette path length and C is the solution concentration in molar units. Made by Maddalena Collini Lab.

4.2.12 Rhodamine release study

The release kinetics is followed by soaking the hydrogel samples, containing Rhodamine solution, in 3 mL of milliQ water. We measured the absorbance at intervals of 15 minutes, changing the sample water every time at the same condition previously cited (molar extinction, path length). Also here, graph was reported as normalized data to equilibrium value. Made by Maddalena Collini Lab.

4.2.13 Diffusion studies.

Diffusion of small fluorescent probes (Rhodamine 6G and GFP, Sigma Chemical Co.) was characterized by Fluorescence Correlation Spectroscopy (FCS) technique. The home built FCS setup has been described elsewhere (Bosisio et al., 2008). Briefly, the output of a Titanium :Sapphire laser beam (Tsunami, Spectra Physics, Mountain View, Ca, USA) at 800 nm for Rhodamine or 890 nm for GFP excitation is focused by a water immersion objective (Plan Apochromat 60x water objective NA = 1.2, Nikon, Japan) mounted on inverted TE300 Nikon (Japan) microscope. The fluorescence in collected in epifluorescence geometry, separated from excitation by a set of dichroic mirrors and band pass filters (560/40 for Rhodamine and 535/50 for GFP), splitted in two by a 50% cube and focused on the active area of two APD detector set at 90° in a cross-correction geometry. This avoids artifacts due to detectors dead time or after pulsing. The digital signal from the APDs is fed into a two-channels autocorrelation board (ALV 7002/USB, ALV-Laser Vertriebsgesellschaft mbh, Langen, D) inserted in a personal computer and store for the analysis. The laser beam is tightly focused in a small volume (μm^3) and if the concentration of the fluorescent probe is sufficiently low (1-100 nanomolar range), fluorescence fluctuations arising from molecules moving in and out across the excitation volume can be easily detected.

The temporal behavior of the signal fluctuations can give information on the diffusion characteristics of the probe through the fluorescence autocorrelation function (FCS), defined as:

$$G(\tau) = \frac{<\delta F/t)\delta F(t+\tau)>}{<F(t)>2} \quad (5)$$

Where F(t)=F(t)-<F(t)> is the fluorescence fluctuation with respect to the average value and τ is the time lag. If only diffusing motions are taken into account as in the case treated here, the explicit expression for the autocorrelation function is given by (Krichevsky & Bonnet, 2002):

$$G(\tau) = G(0) \times \frac{1}{1+\frac{\tau}{\tau_D}} \times \frac{1}{\sqrt{1+\zeta^2\frac{\tau}{\tau_D}}} \quad (6)$$

Where $\tau_D=\omega_0^2/8D$ is the characteristic diffusion time through the beam waist (ω_0) for a species with diffusion coefficient D, ζ^2 is the axial ratio and G(0) the zero time-lag value of the autocorrelation. A fit of the ACF is performed using OriginLab 9 Software. For measuring longer diffusing species such as gold nanoparticles in the hydrogel, an EMCCD camera (Cascade II, Photometrics, Tucson, AZ) has been connected to the previous setup through a dedicated port. The EMCCD has a resolution of 512x512 pixels, a pixel size of 16 μm and a shortest acquisition time of 4 ms. Stacks of images has been acquired with a typical frame rate of 30 fps and a typical field of view of 15 x 15 μm^2. In some cases, a confocal scanning Leica SP5 microscope has been used employing the 488 nm excitation wavelength of an Argon laser. Made by Maddalena Collini Lab.

4.3 Results

4.3.1 Chemistry

Two different gelatin concentrations were tested, namely 5 % w/v and 10% w/v in buffer solution at pH 8.5. DES was added to gelatin (10 %) and (5 %) solutions at 40 °C, and reacted for 90 min; the reaction was then cooled to r.t. affording hydrogels (Figure 22). Cross-linked gelatin were freeze-dried, and then characterized for their physico-chemical and biological properties as 3D cell culture scaffolds, and studied for their drug release abilities.

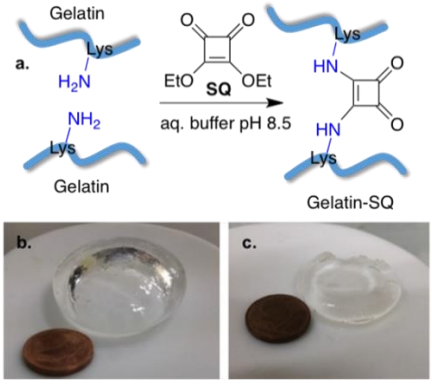

Figure 22 **Reaction for gelatin crosslinking with DES** a) Homo cross-linking of gelatin by 3,4-Diethoxy-3-cyclobutene-1,2-dione (SQ); b) gelatin cross-linked hydrogel; c) non cross-linked control at room temperature

4.3.2 Physico-chemical characterization: FTIR analyses

Gelatin crosslinking by DES was verified by FTIR spectroscopy. The absorption spectra of pristine gelatin, 5% gel-DES, and 10% gel-DES are dominated by the Amide I band due to the C=O stretching vibration of the protein peptide bond (Figure 23b), which is sensitive to the protein secondary structures (Barth, 2007). The three gelatin samples display superimposable Amide I band indicating comparable overall secondary structures (Figure 23b). The absorption spectra of 5% gelatin-DES and of 10% gelatin-DES show a weak band around 1804 cm^{-1}, absent in pristine gelatin. This component can be better evaluated in the second

derivative spectra (Figure 23c and 23d). The presence of this peak in the spectral region of squaramide absorption confirms the gelatin crosslinking by DES.

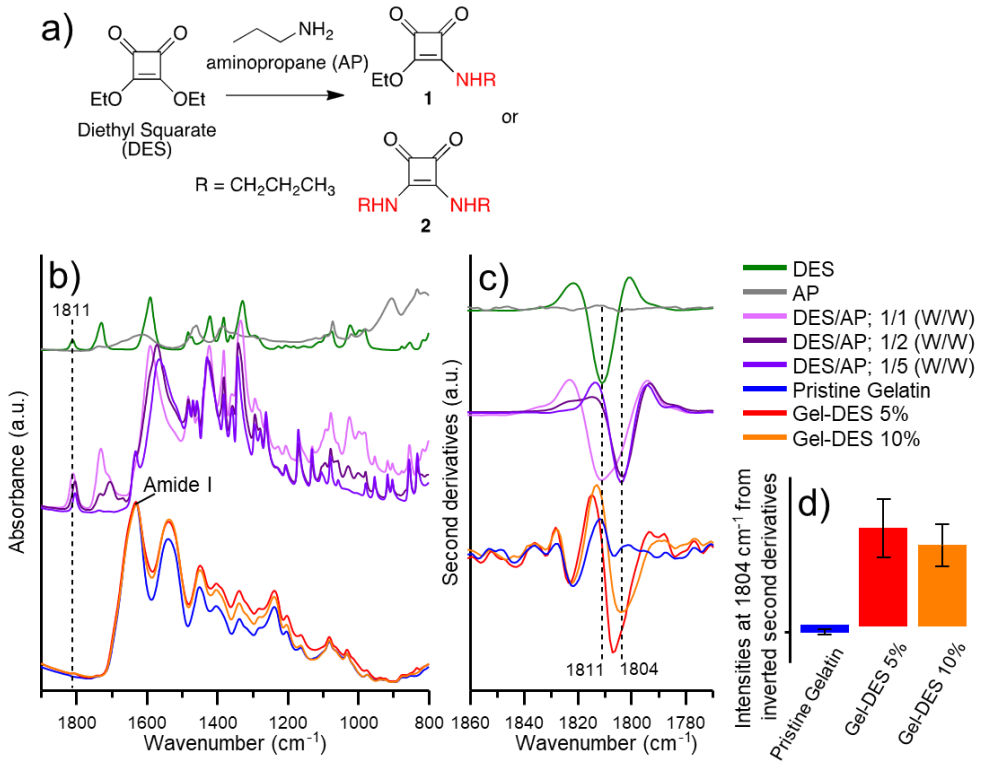

Figure 23 **FT-IR analyses** a) Reaction between DES and AP; b) Full FT-IR spectra; c) Second derivatives of spectra collected in "b". d) relative quantification of 1804 cm^{-1} absorption band

4.3.3 Physico-chemical characterization: SEM analysis

Gels were analyzed by SEM imaging to analyze the porosity and the mesh size of gels. Weighted gels (1 g) were cut in the middle using a blade, the upper and inner surface were analyzed by low-vacuum scanning electron microscopy, to measure pore sizes in different sections of the gel. 5% Gel-DES possess an average diameter of the pores of 31.77 ± 4.76 µm, roughly three times higher than 10% Gel-DES featured with 11.97 ± 2.41 µm pore sizes (Figure 24).

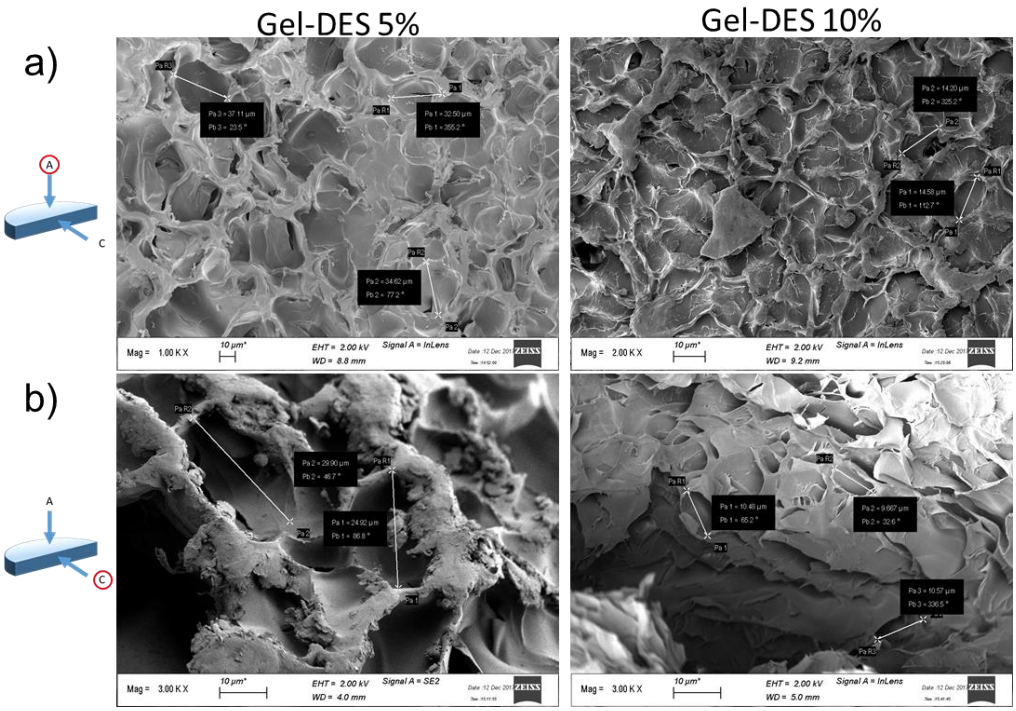

Figure 24 **SEM images of DES crosslinked hydrogels** a) Superficial portion SEM images of Gel-DES 5% (left) and Gel-DES 10% (right). b) Longitudinal cross section SEM images of Gel-DES 5% (left) and Gel-DES 10% (right).

4.3.4 Physico-chemical characterization: Swelling Properties

Freeze-dried cross-linked gelatins (1 g) were placed into 40 mL of deionized water, and weight increase was measured over time until equilibrium (Begam, Nagpal, & Singhal, 2003). 5 % Gel-DES shows a 9.94±0.96 g * g^{-1} SD value, while the 10 % Gel-DES reaches a 6.31±0.73 g * g^{-1} SD value (Figure 25a). Coherently, the percentage water content at the equilibrium (% EWC, Figure 25b) is 91.72±0.30 % for the 5 % Gel-DES and 87.99±0.32 for the 10 % Gel-DES, as determined using Eq.(4). For the 5% gel-DES sample, the swelling kinetic behavior has been also analyzed. As shown in Figure 25c, the equilibrium swelling content is reached at 84±9 % and the characteristic time is 50±3 minutes (best fit using Eq.(2) is shown in the panel as continuous line). By fitting the early

swelling time to Eq. (3), an exponent of n=0.64±0.05 has been obtained corresponding to anomalous (non-Fickian) diffusion.

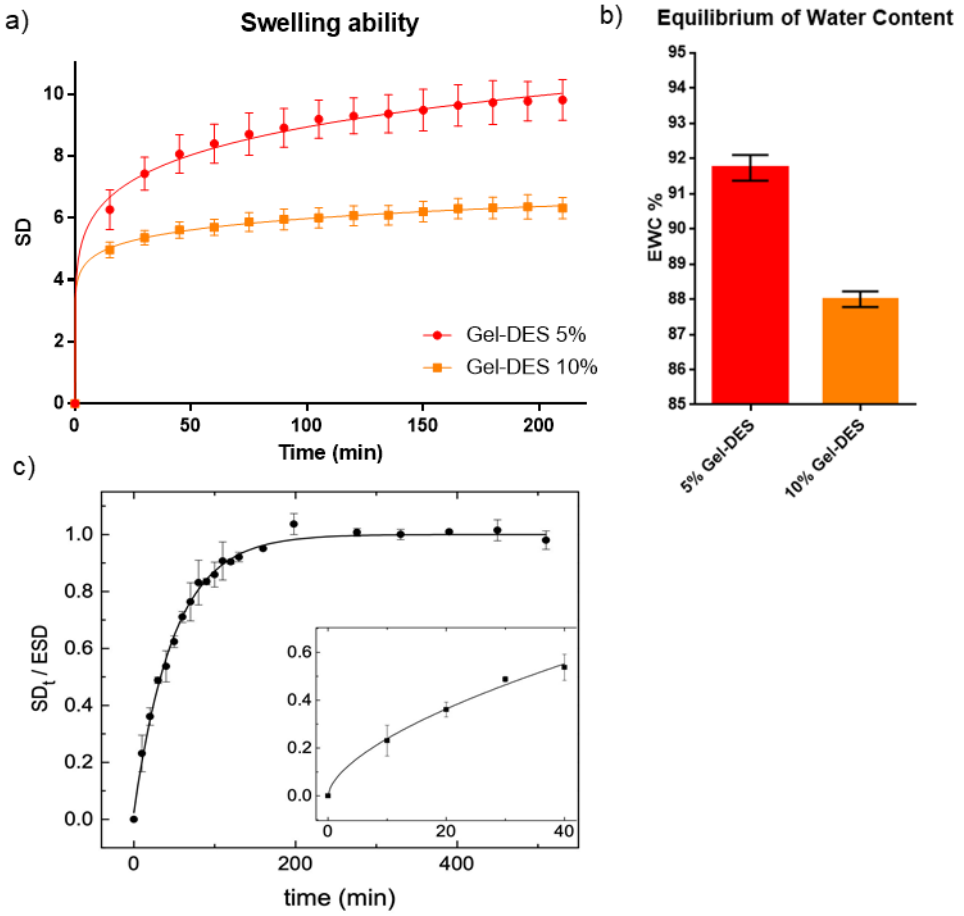

Figure 25 **Swelling analyses** a) Swelling abilities of 5% Gel-DES and 10% Gel-DES. SD values (calculated as shown in materials and methods). b) Percent of Equilibrium of water content (EWC) obtained as shown in materials and methods. c) 5% hydrogel swelling curves normalized to ESD value of sample in water at room temperature as function of time. Black line is the fit curve. Zoom on 60% of hydrogel swelling curves normalized to ESD value of sample in water at room temperature.

4.3.5 Biological characterization: Collagenase stability.

Freeze-dried 5% Gel-DES and 10% Gel-DES specimens (1 g) were treated with *Clostridium histolyticum type I collagenase*, and degradation was determined as weight loss as a function of time (Figure 26). 5% Gel-DES was fully digested by

collagenase in 50 min., while 10% Gel-DES required almost 150 min for complete degradation.

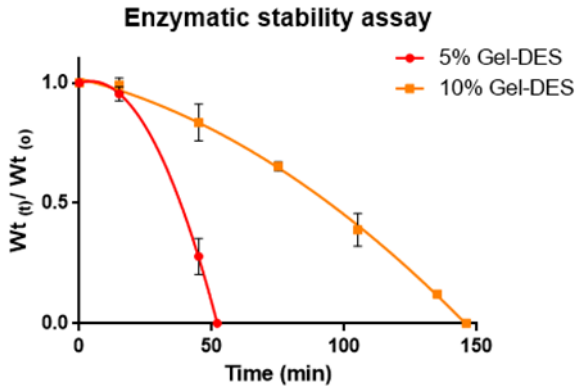

Figure 26 **Enzymatic stability assay** performed with collagenase type I from Clostridium histolyticum. 10% Gel-DES show higher time resistance to the enzymatic degradation in comparison to 5% Gel-DES

4.3.6 Biological characterization: Cell adhesion and spreading

In order to evaluate the biocompatibility of the novel gelatin-based hydrogels, immortalized C28/I2 chondrocytes were chosen as relevant cell line. In fact, hydrogels have become interesting platform in tissue engineering in general, and in cartilage engineering in particular (L. Li et al., 2019; Ponticiello, Schinagl, Kadiyala, & Barry, 2000; Yaylaoglu, Yildiz, Korkusuz, & Hasirci, 1999).

Freeze-dried hydrogels were placed in a 24-well plate, and C28/I2 suspension (5×10^6 cells/mL) were incubated for 4 h at 37 °C with 5% CO_2 and cultures lasted for 2 weeks. In order to evaluate cell morphology, adhesion and spreading, hydrogels were cut into sections and stained with TRITC-Phalloidin and DAPI for cytoskeleton and DNA respectively. C28/I2 cells showed good adhesion to pores of both the 5 % Gel-DES and 10 % Gel-DES (Figure 27). However, cell spreading through the hydrogel is more effective for the 5% Gel-DES than the 10% Gel-DES. The same procedure used for C28/I2 cell lines was adopted for HEK293 cells. While C28/I2 cells use the mesh of hydrogels as an attachment surface, HEK293 cells seems to attach to the material creating clustering of cells

inside mesh pores. Furthermore, the morphology of the two cell lines is different. C28/I2 cells appear polygonal and more elongated in respect of HEK293 cells which appear more rounded. Moreover, HEK293 cells seems to prefer cell-cell contact instead of cell-hydrogel contact, in fact a little fraction of cells attach to the hydrogel surface and on these other cells attach to each other forming cell aggregates which colonize the pore mesh.

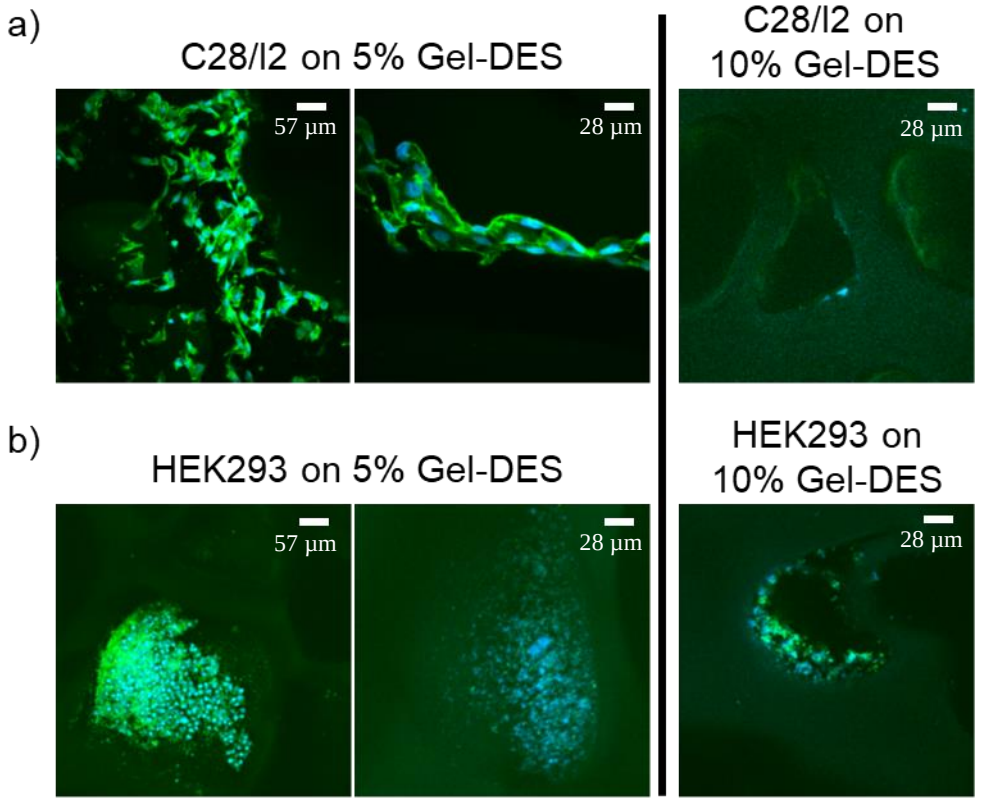

Figure 27 **C28/I2 chondrocytes and HEK293 cells plated on 5% or 10% Gel-DES.** C28/I2 and HEK293 cells were plated on 5% or 10% Gel-DES at high density and were growth for 2 weeks. Then hydrogels were cut into specimens and stained with Phalloidin-TRITC (Green) and DAPI (Blue). Images were taken by a scanning microscope exploiting two photon excitations. a) Representative images of C28/I2 cells into 5% Gel-DES and 10 % Gel-DES. b) Representative images of HEK293 cells into 5% Gel-DES and 10% Gel-DES.

4.3.7 Drug interaction studies: Rhodamine load and release

Since 5 % Gel-DES guarantees wider applicability to different cell lines, drug delivery and small molecule diffusion properties of the 5 % Gel-DES was investigated as well.

In order to study diffusivity and drug release properties, rhodamine 6G was chosen as a model compound. Rhodamine uptake kinetic was studied spectrophotometrically by soaking 5 % Gel-DES in Rhodamine-6G solution as explained in the Materials section.

Starting from an initial dye concentration of 7.0 ±0.15 mM, the hydrogels absorb about 64 ±2% of initial concentration when equilibrium is reached. The loading kinetics is shown in Figure 28 a e b by plotting the data normalized to the equilibrium value C¥= 4.5 ±0.1 mM. The time behavior can be also here analyzed according to the Berens-Hopfenberg model (Berens & Hopfenberg, 1978; Peppas & Sahlin, 1989). The characteristic release time is τ=55.6 ± 4 min, close to the characteristic swelling time of the hydrogel (Figure 28a).

The release kinetics is investigated by soaking the rhodamine loaded hydrogel in 3 mL of water and changing it every 15 minutes. The absorbance of the solution, checked spectrophotometrically, yield the concentration of rhodamine released at each time step. The time decrease of the hydrogel concentration as shown in Figure 28b, is quite slow and reaches an equilibrium at long times (>1000 min) at a 25 ± 2 % of dye released.

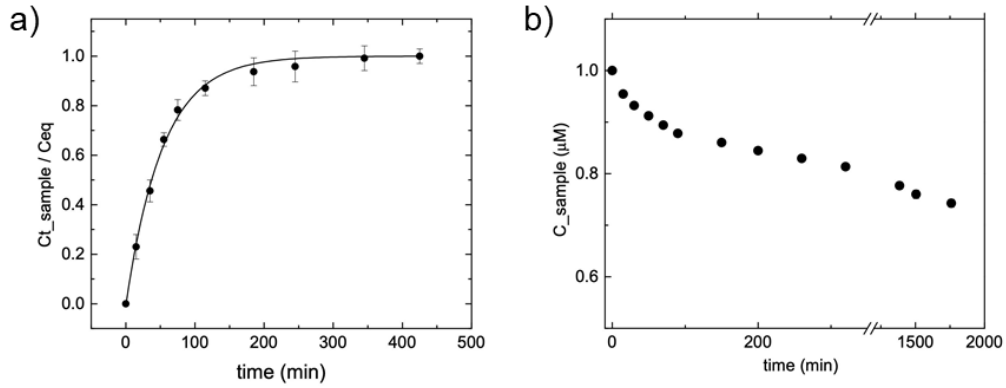

Figure 28 **Rhodamine uptake and release** a) Rhodamine uptake, ratio between concentration at time t and equilibrium concentration as function of time. Black line is the fit curves. b) Rhodamine released measured as rhodamine concentration curves normalized to equilibrium concentration as function of time, in hydrogel.

4.3.8 Drug interaction studies: Diffusion studies

The diffusion inside the hydrogel 5% of probes of different sizes has been characterized by the fluorescence correlation spectroscopy (FCS) technique.

By detecting the fluorescence fluctuation in the observation volume (few micron cubes) of a low concentration of a fluorescent probe (few tens of nanomolar, typically), it is possible to estimate how fast the molecules diffuse due to Brownian motion by building the fluorescence autocorrelation function as explained in the Material and Methods Section.

200 ml of 5% hydrogel was directly cast in a multi chambered cover slide and incubated with the diffusor containing solution at the proper concentration. After 4 hours of incubation, the FCS autocorrelation functions have been acquired and compared with the curves obtained for the same diffusor in solution.

The diffusion coefficient of 300 mm^2/s in solution for Rhodamine has also been used to determine the beam waist parameter w_0 that has been kept fixed in the ACF fitting in the other cases.

The autocorrelation function in hydrogel (continuous lines) and in aqueous solution (dashed lines) are shown in Figure 29. The ACFs obtained in the

hydrogel samples are shifted to longer lag times with respect to the curves obtained in water (or buffer) solutions, suggesting a longer diffusion time for the fluorescent probes. By fitting the ACFs diffusive part with Eq(6) (Figure 8, continuous lines), the diffusion coefficient of Rhodamine in hydrogel was found to be D_{hydr}=40 ±4 $\mu m^2/s$ to be compared with the value of 300 $\mu m^2/s$ in water. GFP diffusion coefficient in the hydrogel is D_{hydr}=13 ±2 $\mu m^2/s$ to be compared with the value of D_{sol}=90 $\mu m^2/s$ as reported in the literature (Bosisio et al., 2008). A different behavior is found when 20 nm fluorescent nanobeads were incubated with the hydrogel. Point FCS (as used for the previous measurements) does not allow to obtain reliable ACFs, as if the characteristic diffusion time were in the seconds range. Therefore, image stacks were acquired by means of a confocal scanning microscope. Small fields of view (~10 μm) has been acquired repeatedly up to several minutes. The superposition of the images show that the beads can be considered immobile in the time scale considered. Since their diffusion coefficient in aqueous solution is about D_{sol}= 0.4 $\mu m^2/s$, a seven time decrease in the diffusion coefficient would give characteristic times shorter than 200 ms, detectable with a minute's duration measurement.

Therefore, the diffusion in the 5% squarate hydrogel appears to be size dependent, even if the average size of the pores is much larger than the beads size.

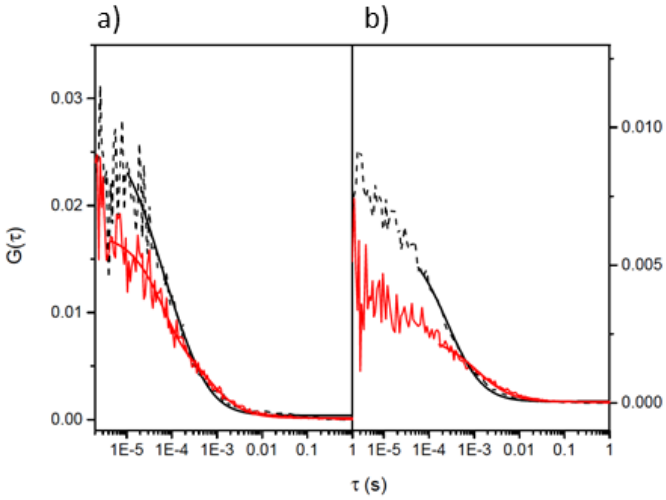

Figure 29 ***Diffusion of small fluorescent probes in Gel-DES 5%*** *a) ACF average curve versus time lag for Rhodamine 6G in water (dotted, black) and in Gel-DES 5% (solid, red). b) ACF average curve versus time lag for GFP in phosphate buffer (dotted, black) and in Gel-DES 5% (solid, red). The continuous lines represent the best fit with Eq. (6) in both panels.*

In the view of developing smart materials gold nanostars (GNS) has been incorporated in the hydrogel during preparation. These plasmonic anisotropic nanoparticles absorb light in the near infrared (NIR) region and convert the absorbed energy into heat, though a pronounced photothermal effect (Pallavicini et al., 2011). When a pulsed laser bear in the NIR is focused on a solution containing these nanoparticles, two photon excitation can occur and a strong luminescence is emitted from the GNS in the visible region of the electromagnetic spectrum to an inter-band conversion, thus allowing their detection.

A lot of applications are found of similar nanoparticles for tumor treatment and controlled drug delivery (Hamidi, Rostamizadeh, & Shahbazi, 2012).

It has been verified that GNS do not diffuse inside the hydrogel upon incubation once it has been formed. Also, when they are embedded in the hydrogel, their diffusion in hindered probably by their branching structure or by their slightly negative charge as proved by imaging the loaded hydrogel after 24 h of swelling

in water in reflection mode by means of a confocal scanning microscope. After repeated time stacks, no motion of the nanoparticles is detected.

However, the situation changes when the GNS photothermal effect is exploited: the diffusion has been measured by coupling to the same setup used for FCS measurement a EMCCD camera in order to obtain stack of images acquired for almost 10 seconds with typical frame rates about 30 fps, as shown in Figure 9. The strong luminescence of a gold nanoparticle or of a small group of nanoparticles is shown at three different times of a 1000 frames time stack using a laser power of 10 mW (Figure 30). Many frames are also dark, but the projection of the average intensity shown in the fourth panel suggests that the recruiting can interest a significant portion around the laser spot (the total field of view is 16.2 x 16.2 micron^2).

The GNS diffusion, that becomes more and more pronounced at increasing the laser power, is due to the photothermal effect primed by the nanoparticles. The local temperature increase can promote a thermophoretic force that recruits GNS from the surrounding of the excitation spot region, thus increasing the local concentration as shown in Figure 9. This effect might be exploited to drive a high concentration of nanoparticles in selected regions of the hydrogel where, for instance, a cell is present.

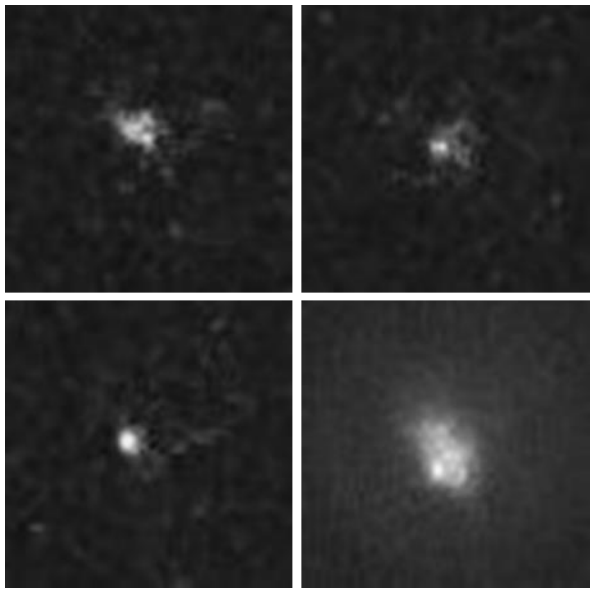

Figure 30 **Gold nanoparticles in 5% hydrogel after 24h of swelling**. The luminescence is detected by an EMCCD camera and promoted by two-photon excitation at 800 nm at 10 mW on the sample. 1000 frames are taken, and three images are shown at arbitrary times for exemplificatory purposes together with the average intensity plot over all frames shown in the fourth panel. Field of view, 16.2 x 16.2 μm^2.

4.4 Discussion

Squaric acid diesters, such as 3,4-diethoxy-3-cyclobutene-1,2-dione (DES), are useful reagents for amino-functional compounds coupling, and bioconjugation reactions [45]. Herein DES was used as a crosslinker agent between lysine side chain amino groups (Figure 22) of gelatin obtaining gelatin-based hydrogels (Figure 22b). Lysine occurs in porcine skin gelatin in 2.7 % in weight in respect to total amino acids residues (Hafidz, Yaakob, Amin, & Noorfaizan, 2011) and can be efficiently exploited for homo cross-linking reactions; in order to tune gelatin-based hydrogel properties as 3D scaffolds for cell culture, two different concentrations of gelatin, namely 5 % and 10 %, were used. In order to cross-link lysine side chains, reaction of DES should proceed to the bisamide product. In order to check the effectiveness of the cross-linking reaction, FTIR spectroscopy was selected. In order to validate the ability of this spectroscopic approach to discriminate between squarate esters and squaramides, a control experiment was set using model compounds (Figure 23a). In particular, the FTIR spectra of DES and those of the products of the reaction of DES with 1 to 5 equivalents of 1-aminopropane (AP, Figure 23a) were compared. It is well known that the treatment of squaric acid diesters with stoichiometric or even a slight excess of a primary or a secondary amine at room temperature produces the corresponding squaric acid esteramide (i.e. monoamide **1**, Figure 23a) without the formation of the bisamide (Tietze et al., 1991) (i.e. compound **2**, Figure 23a). The selective formation of the monoamide is explained by the much faster amidation of the diester compared to the resulting ester amide. This allows the selective and sequential amidation if additional amine is added (or a basic aqueous buffer solution) to the ester monoamide. As shown in Figure 23b and 23c, the DES absorption and second derivative spectra display a characteristic band around 1811 cm^{-1}, assigned to the C=O stretching vibration of carbonyl esters (Kolev et al., 2009). The formation of squaramides induces a shift of this peak down to

around 1804 cm^{-1} as can be better appreciated in the second derivative spectra, whose minima correspond to absorption maxima. AP has no peaks in this spectral region (Figure 23b and 23c). Based on the control experiments, FTIR analysis performed on pristine gelatin and cross-linked gelatin showed the effectiveness of the reaction. The different concentration of gelatin tested resulted in hydrogels with different physico-chemical and biological properties. In particular, the 5 % Gel-DES hydrogel resulted with larger pores (roughly 30 μm as determined by SEM), if compared to the 10% Gel-DES samples (10 μm pores), as a consequence of the higher cross-linking degree for the 10% Gel-DES than the 5 % gelatin-DES. Thus, the pore size is inversely proportional to gelatin concentration, as it may be expected. Freeze-dried gelatin specimens were characterized for their swelling abilities. Gel swelling properties are usually dependent upon several factors, including pore size of the network, interactions within the network (polymer chains and cross-linkers), solvent, and chain mobility during the swelling process (Branco da Cunha et al., 2014). As expected, the two hydrogel differs in their water-retaining abilities, characterized as equilibrium swelling degree and equilibrium water content. In particular, the higher the pore size (lower gelatin concentration), the higher are the equilibrium water content (and the equilibrium swelling degree). Based on the idea to use the synthesized hydrogels as 3D cell culture platforms, resistance to enzymatic degradation was tested with collagenase. As expected, the cross-linking degree influences the hydrogel stability against hydrolytic enzymes and the 5 % Gel-DES was degraded faster (50 min.) than the 10 % Gel-DES (150 min) (Figure 26). The two hydrogels were assayed as 3D scaffolds for cell culture (Figure 27). Two cell lines were selected, namely immortalized C28/I2 chondrocytes and HEK293. C28/I2 chondrocytes were chosen as relevant cell model, being hydrogels interesting platform in tissue engineering in general, and in cartilage engineering in particular (L. Li et al., 2019; Ponticiello et al., 2000; Yaylaoglu et

al., 1999). HEK293 cell line was selected due to its robustness, easy of growth and reliability in cell experiments, frequently applied as cellular model to test toxicity and biocompatibility of new biomaterials (Capella et al., 2019; Gong et al., 2009; Kouser, Vashist, Zafaryab, Rizvi, & Ahmad, 2018). Interestingly, the behavior of the two cell lines resulted different, both in terms of adhesion and cell morphology. In case of C28/I2 cell line, they showed good adhesion properties and elongated shape when grown in both the 5 % Gel-DES and 10 % Gel-DES, despite the 5 % Gel-DES was preferred. On the contrary, (Figure 27), HEK293 cells generate clusters within the pores and acquire a round shape. Thus, the 5 % Gel-DES resulted suitable as cell culture scaffold especially for C28/I2 cell line, confirming that 3D scaffolds should be tailored for the specific cell line and desired application. Given these observations, only the 5% Ge-DES was further characterized in terms of its swelling kinetics (Figure 25c), diffusion and as drug release platform. Rhodamine 6G was used as model drug, while, diffusion studies were performed with three model compounds, differing in size, such as rhodamine 6G (479 kDa), Green Fluorescent Protein (GFP, 27 kDa, 4nm x 2nm in size) and 20 nm diameter fluorescent polystyrene nanobeads. Rhodamine loading resulted good (over 60 % of drug is loaded into hydrogel), while the release is inefficient (only 25 % of drug release over 1000 min).

The diffusion behavior of the model compounds is resumed in Table 2.

Compound	**F.W. (kDa)**	**dimension (nm x nm)**	**diffusion solution (mm^2/s)**	**diffusion hydrogel (mm^2/s)**	**D_{sol}/D_{hydr}**
Rhodamine 6G	0.479	-	300	40	7.5
GFP	27	4 x 2	90	13	6.9
polystyrene nanobeads	n.a.	20 nm diameter	0.4	0	n.a.

Tabella 1 **Diffusion coefficient for the sample compounds used for the study in the 5 % Gel-DES hydrogel**.

With both Rhodamine and GFP the hydrogel affects the diffusion at the same extent within the experimental uncertainties, showing that Brownian diffusion is not hindered by the gel pores but slowed down almost seven-fold. Larger diffusers (as the fluorescent nanobeads) can slowly penetrate into the gel matrix but the sedimentation motion prevails on the hindered brownian motions, preventing further movements once the bottom of the chamber was reached. The ratio of the diffusion coefficients in the hydrogel and in solution is very close for the two diffusers, being 7.2 ± 0.6. This suggests that the same diffusion mechanism is involved for both probes, and that the hydrogel decreases the diffusion of the probes of the same amount but the brownian diffusive model still holds. Release and diffusion data suggest that the squarate hydrogel is efficient in favoring drug diffusion among its pores, it does not leak uptaken drug in solution and may be an interesting drug delivery system by in vivo controlled degradation. Interestingly, a temperature induced diffusion can be obtained when gold nanoparticles of asymmetric shapes that absorb NIR light are embedded in the hydrogel, and can be used to obtain an increase of nanoparticles concentration that acts as hot spots in the gel. This application can pave the way to selective apoptosis of cells grown in the hydrogel by exploiting the photothermal effect. In conclusion, diethyl-squarate (DES) resulted an effective cross-linking agent to produce novel gelatin-based hydrogels. The hydrogels obtained from 5 % gelatin solution are more suitable for chondrocyte adhesion and spreading, than the 10 % ones. In addition, the 5 % Gel-DES hydrogel resulted an interesting drug diffusion system and can be exploited for drug release *in vivo* upon degradation.

Bibliography

Abella, V., Scotece, M., Conde, J., López, V., Lazzaro, V., Pino, J., … Gualillo, O. (2014). Adipokines, metabolic syndrome and rheumatic diseases. *Journal of Immunology Research*. https://doi.org/10.1155/2014/343746

Abusarah, J., Bentz, M., Benabdoune, H., Rondon, P. E., Shi, Q., Fernandes, J. C., … Benderdour, M. (2017). An overview of the role of lipid peroxidation-derived 4-hydroxynonenal in osteoarthritis. *Inflammation Research*. https://doi.org/10.1007/s00011-017-1044-4

Aguiari, P., Leo, S., Zavan, B., Vindigni, V., Rimessi, A., Bianchi, K., … Rizzuto, R. (2008). High glucose induces adipogenic differentiation of muscle-derived stem cells. *Proceedings of the National Academy of Sciences*, *105*(4), 1226–1231. https://doi.org/10.1073/pnas.0711402105

Aibibula, Z., Ailixiding, M., Iwata, M., Piao, J., Hara, Y., Okawa, A., & Asou, Y. (2016). Xanthine oxidoreductase activation is implicated in the onset of metabolic arthritis. *Biochemical and Biophysical Research Communications*. https://doi.org/10.1016/j.bbrc.2016.02.039

Aigner, T., Hemmel, M., Neureiter, D., Gebhard, P. M., Zeiler, G., Kirchner, T., & McKenna, L. (2001). Apoptotic cell death is not a widespread phenomenon in normal aging and osteoarthritic human articular knee cartilage: A study of proliferation, programmed cell death (apoptosis), and viability of chondrocytes in normal and osteoarthritic human knee carti. *Arthritis and Rheumatism*. https://doi.org/10.1002/1529-0131(200106)44:6<1304::AID-ART222>3.0.CO;2-T

Aigner, Thomas, Fundel, K., Saas, J., Gebhard, P. M., Haag, J., Weiss, T., … Bartnik, E. (2006). Large-scale gene expression profiling reveals major pathogenetic pathways of cartilage degeneration in osteoarthritis. *Arthritis and Rheumatism*. https://doi.org/10.1002/art.22174

Aigner, Thomas, Zhu, Y., Chansky, H. H., Matsen, F. A., Maloney, W. J., &

Sandell, L. J. (1999). Reexpression of type IIA procollagen by adult articular chondrocytes in osteoarthritic cartilage. *Arthritis and Rheumatism*. https://doi.org/10.1002/1529-0131(199907)42:7<1443::AID-ANR18>3.0.CO;2-A

Akiyama, H., Chaboissier, M. C., Martin, J. F., Schedl, A., & De Crombrugghe, B. (2002). The transcription factor Sox9 has essential roles in successive steps of the chondrocyte differentiation pathway and is required for expression of Sox5 and Sox6. *Genes and Development*. https://doi.org/10.1101/gad.1017802

Akiyama, H., Kim, J. E., Nakashima, K., Balmes, G., Iwai, N., Deng, J. M., … De Crombrugghe, B. (2005). Osteo-chondroprogenitor cells are derived from Sox9 expressing precursors. *Proceedings of the National Academy of Sciences of the United States of America*. https://doi.org/10.1073/pnas.0504750102

Akizuki, S., Mow, V. C., Muller, F., Pita, J. C., & Howell, D. S. (1987). Tensile properties of human knee joint cartilage. II. Correlations between weight bearing and tissue pathology and the kinetics of swelling. *Journal of Orthopaedic Research*. https://doi.org/10.1002/jor.1100050204

Akkiraju, H., & Nohe, A. (2015). Role of chondrocytes in cartilage formation, progression of osteoarthritis and cartilage regeneration. *Journal of Developmental Biology*. https://doi.org/10.3390/jdb3040177

Allen, R. T., Robertson, C. M., Harwood, F. L., Sasho, T., Williams, S. K., Pomerleau, B. A., & Amiel, D. (2004). Characterization of mature vs aged rabbit articular cartilage: Analysis of cell density, apoptosis-related gene expression and mechanisms controlling chondrocyte apoptosis. *Osteoarthritis and Cartilage*. https://doi.org/10.1016/j.joca.2004.08.003

Altenhöfer, S., Kleikers, P. W. M., Radermacher, K. A., Scheurer, P., Hermans, J. J. R., Schiffers, P., … Schmidt, H. H. H. W. (2012). The NOX toolbox:

Validating the role of NADPH oxidases in physiology and disease. *Cellular and Molecular Life Sciences*. https://doi.org/10.1007/s00018-012-1010-9

Altindag, O., Erel, O., Aksoy, N., Selek, S., Celik, H., & Karaoglanoglu, M. (2007). Increased oxidative stress and its relation with collagen metabolism in knee osteoarthritis. *Rheumatology International*. https://doi.org/10.1007/s00296-006-0247-8

Ami, D., Mereghetti, P., Foli, A., Tasaki, M., Milani, P., Nuvolone, M., … Natalello, A. (2019). ATR-FTIR Spectroscopy Supported by Multivariate Analysis for the Characterization of Adipose Tissue Aspirates from Patients Affected by Systemic Amyloidosis. *Analytical Chemistry*. https://doi.org/10.1021/acs.analchem.8b05008

Andrades, J. A., Han, B., Becerra, J., Sorgente, N., Hall, F. L., & Nimni, M. E. (1999). A recombinant human TGF-β1 fusion protein with collagen-binding domain promotes migration, growth, and differentiation of bone marrow mesenchymal cells. *Experimental Cell Research*. https://doi.org/10.1006/excr.1999.4528

Andriacchi, T. P., & Favre, J. (2014). The Nature of In Vivo Mechanical Signals That Influence Cartilage Health and Progression to Knee Osteoarthritis. *Current Rheumatology Reports*. https://doi.org/10.1007/s11926-014-0463-2

Angele, P., Kujat, R., Nerlich, M., Yoo, J., Goldberg, V., & Johnstone, B. (1999). Engineering of osteochondral tissue with bone marrow mesenchymal progenitor cells in a derivatized hyaluronan-gelatin composite sponge. *Tissue Engineering*. https://doi.org/10.1089/ten.1999.5.545

Apostolakos, J., Durant, T. J. S., Dwyer, C. R., Russell, R. P., Weinreb, J. H., Alaee, F., … Mazzocca, A. D. (2014). The enthesis: A review of the tendon-to-bone insertion. *Muscles, Ligaments and Tendons Journal*. https://doi.org/10.11138/mltj/2014.4.3.333

Archer, C. W., & Francis-West, P. (2003). The chondrocyte. *International Journal of Biochemistry and Cell Biology*. https://doi.org/10.1016/S1357-2725(02)00301-1

Archer, C. W., Rooney, P., & Wolpert, L. (1982). Cell shape and cartilage differentiation of early chick limb bud cells in culture. *Cell Differentiation*. https://doi.org/10.1016/0045-6039(82)90072-0

Arevalo, J. A., & Vázquez-Medina, J. P. (2018). The role of peroxiredoxin 6 in cell signaling. *Antioxidants*, *7*(12). https://doi.org/10.3390/antiox7120172

Armiento, A. R., Alini, M., & Stoddart, M. J. (2019). Articular fibrocartilage - Why does hyaline cartilage fail to repair? *Advanced Drug Delivery Reviews*. https://doi.org/10.1016/j.addr.2018.12.015

Arokoski, J. P. A., Jurvelin, J. S., Väätäinen, U., & Helminen, H. J. (2000). Normal and pathological adaptations of articular cartilage to joint loading. *Scandinavian Journal of Medicine and Science in Sports*. https://doi.org/10.1034/j.1600-0838.2000.010004186.x

Arthur, A., Zannettino, A., & Gronthos, S. (2009). The therapeutic applications of multipotential mesenchymal/stromal stem cells in skeletal tissue repair. *Journal of Cellular Physiology*. https://doi.org/10.1002/jcp.21592

Asik, M., Ciftci, F., Sen, C., Erdil, M., & Atalar, A. (2008). The Microfracture Technique for the Treatment of Full-Thickness Articular Cartilage Lesions of the Knee: Midterm Results. *Arthroscopy - Journal of Arthroscopic and Related Surgery*. https://doi.org/10.1016/j.arthro.2008.06.015

Aszodi, A., Hunziker, E. B., Brakebusch, C., & Fässler, R. (2003). β1 integrins regulate chondrocyte rotation, G1 progression, and cytokinesis. *Genes and Development*. https://doi.org/10.1101/gad.277003

Athanasiou, K. A., Darling, E. M., DuRaine, G. D., Hu, J. C., & Hari Reddi, A. (2013). *Articular cartilage*. *Articular Cartilage*.

Atkinson, B. L., Fantle, K. S., Benedict, J. J., Huffer, W. E., & Gutierrez-

Hartmann, A. (1997). Combination of osteoinductive bone proteins differentiates mesenchymal C2H/10T1/2 cells specifically to the cartilage lineage. *Journal of Cellular Biochemistry*. https://doi.org/10.1002/(SICI)1097-4644(19970601)65:3<325::AID-JCB3>3.0.CO;2-U

Bae, S. E., Choi, D. H., Han, D. K., & Park, K. (2010). Effect of temporally controlled release of dexamethasone on in vivo chondrogenic differentiation of mesenchymal stromal cells. *Journal of Controlled Release*. https://doi.org/10.1016/j.jconrel.2009.12.024

Baker, M. S., Feigan, J., & Lowther, D. A. (1989). The mechanism of chondrocyte hydrogen peroxide damage. Depletion of intracellular ATP due to suppression of glycolysis caused by oxidation of glyceraldehyde-3-phosphate dehydrogenase. *Journal of Rheumatology*.

Barata, A. G., & Dick, T. P. (2019). A role for peroxiredoxins in H2O2- and MEKK-dependent activation of the p38 signaling pathway. *Redox Biology*, *28*(July 2019), 101340. https://doi.org/10.1016/j.redox.2019.101340

Barth, A. (2007). Infrared spectroscopy of proteins, *1767*, 1073–1101. https://doi.org/10.1016/j.bbabio.2007.06.004

Begam, T., Nagpal, A. K., & Singhal, R. (2003). A comparative study of swelling properties of hydrogels based on poly(acrylamide-co-methyl methacrylate) containing physical and chemical crosslinks. *Journal of Applied Polymer Science*. https://doi.org/10.1002/app.12270

Bellou, V., Belbasis, L., Tzoulaki, I., & Evangelou, E. (2018). Risk factors for type 2 diabetes mellitus: An exposure-wide umbrella review of meta-analyses. *PLoS ONE*. https://doi.org/10.1371/journal.pone.0194127

Bengtsson, T., Aszodi, A., Nicolae, C., Hunziker, E. B., Lundgren-Åkerlund, E., & Fässler, R. (2005). Loss of α10β1 integrin expression leads to moderate dysfunction of growth plate chondrocytes. *Journal of Cell Science*.

https://doi.org/10.1242/jcs.01678

Benjamin, M., Archer, C. W., & Ralphs, J. R. (1994). Cytoskeleton of cartilage cells. *Microscopy Research and Technique*. https://doi.org/10.1002/jemt.1070280503

Benjamin, M., & Ralphs, J. R. (1998). Fibrocartilage in tendons and ligaments - An adaptation to compressive load. *Journal of Anatomy*. https://doi.org/10.1017/S0021878298004300

Benjamin, M., & Ralphs, J. R. (2004). Biology of Fibrocartilage Cells. *International Review of Cytology*. https://doi.org/10.1016/S0074-7696(04)33001-9

Berenbaum, F. (2011). Diabetes-induced osteoarthritis: From a new paradigm to a new phenotype. *Annals of the Rheumatic Diseases*. https://doi.org/10.1136/ard.2010.146399

Berens, A. R., & Hopfenberg, H. B. (1978). Diffusion and relaxation in glassy polymer powders: 2. Separation of diffusion and relaxation parameters. *Polymer*. https://doi.org/10.1016/0032-3861(78)90269-0

Bernhard, J. C., & Vunjak-Novakovic, G. (2016). Should we use cells, biomaterials, or tissue engineering for cartilage regeneration? *Stem Cell Research and Therapy*, *7*(1), 3–11. https://doi.org/10.1186/s13287-016-0314-3

Bernhardt, A., Despang, F., Lode, A., Demmler, A., Hanke, T., & Gelinsky, M. (2009). Proliferation and osteogenic differentiation of human bone marrow stromal cells on alginate - gelatine - hydroxyapatite scaffolds with anisotropic pore structure. *Journal of Tissue Engineering and Regenerative Medicine*. https://doi.org/10.1002/term.134

Bert, J. M. (1993). Role of abrasion arthroplasty and debridement in the management of osteoarthritis of the knee. *Rheumatic Disease Clinics of North America*.

Bhardwaj, N., Devi, D., & Mandal, B. B. (2015). Tissue-engineered cartilage: The crossroads of biomaterials, cells and stimulating factors. *Macromolecular Bioscience*. https://doi.org/10.1002/mabi.201400335

Bhosale, A. M., & Richardson, J. B. (2008). Articular cartilage: Structure, injuries and review of management. *British Medical Bulletin*. https://doi.org/10.1093/bmb/ldn025

Blain, E. J. (2009). Involvement of the cytoskeletal elements in articular cartilage homeostasis and pathology. *International Journal of Experimental Pathology*. https://doi.org/10.1111/j.1365-2613.2008.00625.x

Bolduc, J. A., Collins, J. A., & Loeser, R. F. (2019). Reactive oxygen species, aging and articular cartilage homeostasis. *Free Radical Biology and Medicine*. https://doi.org/10.1016/j.freeradbiomed.2018.08.038

Bollet, A. J., & Nance, J. L. (1966). Biochemical Findings in Normal and Osteoarthritic Articular Cartilage. II. Chondroitin Sulfate Concentration and Chain Length, Water, and Ash Content*. *Journal of Clinical Investigation*. https://doi.org/10.1172/jci105423

Bosisio, C., Quercioli, V., Collini, M., D'Alfonso, L., Baldini, G., Bettati, S., … Chirico, G. (2008). Protonation and conformational dynamics of GFP mutants by two-photon excitation fluorescence correlation spectroscopy. *Journal of Physical Chemistry B*. https://doi.org/10.1021/jp801164n

Bradley, E. W., & Drissi, M. H. (2010). WNT5A regulates chondrocyte differentiation through differential use of the CaN/NFAT and IKK/NF-κB pathways. *Molecular Endocrinology*. https://doi.org/10.1210/me.2010-0037

Branco da Cunha, C., Klumpers, D. D., Li, W. A., Koshy, S. T., Weaver, J. C., Chaudhuri, O., … Mooney, D. J. (2014). Influence of the stiffness of three-dimensional alginate/collagen-I interpenetrating networks on fibroblast biology. *Biomaterials*, *35*(32), 8927–8936.

https://doi.org/10.1016/j.biomaterials.2014.06.047

Brent, B., Tanzer, R. C., Rueckert, F., & Brown, F. E. (1992). Auricular repair with autogenous rib cartilage grafts: Two decades of experience with 600 cases. *Plastic and Reconstructive Surgery*. https://doi.org/10.1097/00006534-199209000-00002

Brittberg, M., Lindahl, A., Nilsson, A., Ohlsson, C., Isaksson, O., & Peterson, L. (1994). Treatment of deep cartilage defects in the knee with autologous chondrocyte transplantation. *New England Journal of Medicine*. https://doi.org/10.1056/NEJM199410063311401

Brown, P. D., & Benya, P. D. (1988). Alterations in chondrocyte cytoskeletal architecture during phenotypic modulation by retinoic acid and dihydrocytochalasin B-induced reexpression. *Journal of Cell Biology*. https://doi.org/10.1083/jcb.106.1.171

Buckwalter, J. A., & Mankin, H. J. (1998). Articular cartilage: tissue design and chondrocyte-matrix interactions. *Instructional Course Lectures*.

Buckwalter, Joseph A., Mankin, H. J., & Grodzinsky, A. J. (2005). Articular cartilage and osteoarthritis. *Instructional Course Lectures*.

Burr, D. B., & Gallant, M. A. (2012). Bone remodelling in osteoarthritis. *Nature Reviews Rheumatology*. https://doi.org/10.1038/nrrheum.2012.130

Caccia, M., Sironi, L., Collini, M., Chirico, G., Zanoni, I., & Granucci, F. (2008). Image filtering for two-photon deep imaging of lymphonodes. *European Biophysics Journal*. https://doi.org/10.1007/s00249-008-0323-y

Caliari, S. R., & Burdick, J. A. (2016). A practical guide to hydrogels for cell culture. *Nature Methods*. https://doi.org/10.1038/nmeth.3839

Capella, V., Rivero, R. E., Liaudat, A. C., Ibarra, L. E., Roma, D. A., Alustiza, F., … Rodriguez, N. (2019). Cytotoxicity and bioadhesive properties of poly-N-isopropylacrylamide hydrogel. *Heliyon*. https://doi.org/10.1016/j.heliyon.2019.e01474

Capín-Gutiérrez, N., Talamás-Rohana, P., González-Robles, A., Lavalle-Montalvo, C., & Kourí, J. B. (2004). Cytoskeleton disruption in chondrocytes from a rat osteoarthrosic (OA) -induced model: Its potential role in OA pathogenesis. *Histology and Histopathology*.

Caramés, B., Taniguchi, N., Otsuki, S., Blanco, F. J., & Lotz, M. (2010). Autophagy is a protective mechanism in normal cartilage, and its aging-related loss is linked with cell death and osteoarthritis. *Arthritis and Rheumatism*. https://doi.org/10.1002/art.27305

Ceriani, M., Scandiuzzi, C., Amigoni, L., Tisi, R., Berruti, G., & Martegani, E. (2007). Functional analysis of RalGPS2, a murine guanine nucleotide exchange factor for RalA GTPase. *Experimental Cell Research*. https://doi.org/10.1016/j.yexcr.2007.03.016

Chang, S. C., Hoang, B., Thomas, J. T., Vukicevic, S., Luyten, F. P., Ryba, N. J. P., … Moos, M. (1994). Cartilage-derived morphogenetic proteins. New members of the transforming growth factor-β superfamily predominantly expressed in long bones during human embryonic development. *Journal of Biological Chemistry*.

Chansky, H., Robbins, J. R., Cha, S., Raskind, W. H., Conrad, E. U., & Sandell, L. J. (1998). Expression of cartilage extracellular matrix and potential regulatory genes in a new human chondrosarcoma cell line. *Journal of Orthopaedic Research*. https://doi.org/10.1002/jor.1100160502

Charalambous, C. P. (2014). Cell origin and differentiation in the repair of full-thickness defects of articular cartilage. In *Classic Papers in Orthopaedics*. https://doi.org/10.1007/978-1-4471-5451-8_95

Charlier, E., Deroyer, C., Ciregia, F., Malaise, O., Neuville, S., Plener, Z., … de Seny, D. (2019). Chondrocyte dedifferentiation and osteoarthritis (OA). *Biochemical Pharmacology*. https://doi.org/10.1016/j.bcp.2019.02.036

Chatterjee, S., Feinstein, S. I., Dodia, C., Sorokina, E., Lien, Y. C., Nguyen, S.,

… Fisher, A. B. (2011). Peroxiredoxin 6 phosphorylation and subsequent phospholipase A2 activity are required for agonist-mediated activation of NADPH oxidase in mouse pulmonary microvascular endothelium and alveolar macrophages. *Journal of Biological Chemistry*. https://doi.org/10.1074/jbc.M110.206623

Chen, H., Sun, J., Hoemann, C. D., Lascau-Coman, V., Ouyang, W., McKee, M. D., … Buschmann, M. D. (2009). Drilling and microfracture lead to different bone structure and necrosis during bone-marrow stimulation for cartilage repair. *Journal of Orthopaedic Research*. https://doi.org/10.1002/jor.20905

Chen, T. H., Chen, L., Hsieh, M. S., Chang, C. P., Chou, D. T., & Tsai, S. H. (2006). Evidence for a protective role for adiponectin in osteoarthritis. *Biochimica et Biophysica Acta - Molecular Basis of Disease*. https://doi.org/10.1016/j.bbadis.2006.06.008

Chen, X., Wu, H., Park, C. M., Poole, T. H., Keceli, G., Devarie-Baez, N. O., … Furdui, C. M. (2017). Discovery of Heteroaromatic Sulfones As a New Class of Biologically Compatible Thiol-Selective Reagents. *ACS Chemical Biology*. https://doi.org/10.1021/acschembio.7b00444

Chen, Y. J., Chan, D. C., Lan, K. C., Wang, C. C., Chen, C. M., Chao, S. C., … Liu, S. H. (2015). PPARγ is involved in the hyperglycemia-induced inflammatory responses and collagen degradation in human chondrocytes and diabetic mouse cartilages. *Journal of Orthopaedic Research*. https://doi.org/10.1002/jor.22770

Chen, Y. J., Sheu, M. L., Tsai, K. S., Yang, R. Sen, & Liu, S. H. (2013). Advanced Glycation End Products Induce Peroxisome Proliferator-Activated Receptor γ Down-Regulation-Related Inflammatory Signals in Human Chondrocytes via Toll-Like Receptor-4 and Receptor for Advanced Glycation End Products. *PLoS ONE*.

https://doi.org/10.1371/journal.pone.0066611

Chhunchha, B., Fatma, N., Kubo, E., Rai, P., Singh, S. P., & Singh, D. P. (2013). Curcumin abates hypoxia-induced oxidative stress based-ER stress-mediated cell death in mouse hippocampal cells (HT22) by controlling Prdx6 and NF-κB regulation. *American Journal of Physiology - Cell Physiology*. https://doi.org/10.1152/ajpcell.00345.2012

Chiou, T. J., Chu, S. T., & Tzeng, W. F. (2003). Protection of cells from menadione-induced apoptosis by inhibition of lipid peroxidation. *Toxicology*. https://doi.org/10.1016/S0300-483X(03)00189-6

Choi, Jo, Park, Kang, & Park. (2019). NF-B Signaling Pathways in Osteoarthritic Cartilage Destruction. *Cells*. https://doi.org/10.3390/cells8070734

Chua, K. H., Aminuddin, B. S., Fuzina, N. H., & Ruszymah, B. H. I. (2005). Insulin-Transferrin-Selenium prevent human chondrocyte dedifferentiation and promote the formation of high quality tissue engineered human hyaline cartilage. *European Cells and Materials*. https://doi.org/10.22203/eCM.v009a08

Clarke, S. P., Mellor, D., Clements, D. N., Gemmill, T., Farrell, M., Carmicheal, S., & Bennett, D. (2005). Prevalence of radiographic signs of degenerative joint disease in a hospital population of cats. *Veterinary Record*. https://doi.org/10.1136/vr.157.25.793

Clements, D. N., Fitzpatrick, N., Carter, S. D., & Day, P. J. R. (2009). Cartilage gene expression correlates with radiographic severity of canine elbow osteoarthritis. *Veterinary Journal*. https://doi.org/10.1016/j.tvjl.2007.08.027

Cohen, N. P., Foster, R. J., & Mow, V. C. (1998). Composition and dynamics of articular cartilage: Structure, function, and maintaining healthy state. *Journal of Orthopaedic and Sports Physical Therapy*. https://doi.org/10.2519/jospt.1998.28.4.203

Collins, J. A., Diekman, B. O., & Loeser, R. F. (2018). Targeting aging for disease modification in osteoarthritis. *Current Opinion in Rheumatology*. https://doi.org/10.1097/BOR.0000000000000456

Collins, J. A., Wood, S. T., Bolduc, J. A., Nurmalasari, N. P. D., Chubinskaya, S., Poole, L. B., … Loeser, R. F. (2019). Differential peroxiredoxin hyperoxidation regulates MAP kinase signaling in human articular chondrocytes. *Free Radical Biology and Medicine*. https://doi.org/10.1016/j.freeradbiomed.2019.01.005

Collins, J. A., Wood, S. T., Nelson, K. J., Rowe, M. A., Carlson, C. S., Chubinskaya, S., … Loeser, R. F. (2016). Oxidative stress promotes peroxiredoxin hyperoxidation and attenuates pro-survival signaling in aging chondrocytes. *Journal of Biological Chemistry*. https://doi.org/10.1074/jbc.M115.693523

Courties, A., & Sellam, J. (2016). Osteoarthritis and type 2 diabetes mellitus: What are the links? *Diabetes Research and Clinical Practice*. https://doi.org/10.1016/j.diabres.2016.10.021

Cox, A. G., Winterbourn, C. C., & Hampton, M. B. (2010). *Measuring the redox state of cellular peroxiredoxins by immunoblotting. Methods in enzymology* (1st ed., Vol. 474). Elsevier Inc. https://doi.org/10.1016/S0076-6879(10)74004-0

Craft, A. M., Ahmed, N., Rockel, J. S., Baht, G. S., Alma, B. A., Kandel, R. A., … Keller, G. M. (2013). Specification of chondrocytes and cartilage tissues from embryonic stem cells. *Development (Cambridge)*. https://doi.org/10.1242/dev.087890

Cramer, C., Freisinger, E., Jones, R. K., Slakey, D. P., Dupin, C. L., Newsome, E. R., … Izadpanah, R. (2010). Persistent High Glucose Concentrations Alter the Regenerative Potential of Mesenchymal Stem Cells. *Stem Cells and Development*, *19*(12), 1875–1884.

https://doi.org/10.1089/scd.2010.0009

Cross, J. V., & Templeton, D. J. (2006). Regulation of signal transduction through protein cysteine oxidation. *Antioxidants and Redox Signaling*. https://doi.org/10.1089/ars.2006.8.1819

Cucchiarini, M., Madry, H., Guilak, F., Saris, D. B., Stoddart, M. J., Koon Wong, M., & Roughley, P. J. (2014). A vision on the future of articular cartilage repair. *European Cells and Materials*. https://doi.org/10.22203/eCM.v027sa03

Cuzzocrea, S. (2006). Role of Nitric Oxide and Reactive Oxygen Species in Arthritis. *Current Pharmaceutical Design*. https://doi.org/10.2174/138161206778343082

D'Aloia, A., Berruti, G., Costa, B., Schiller, C., Ambrosini, R., Pastori, V., … Ceriani, M. (2018). RalGPS2 is involved in tunneling nanotubes formation in 5637 bladder cancer cells. *Experimental Cell Research*. https://doi.org/10.1016/j.yexcr.2017.11.036

Dahaghin, S., Bierma-Zeinstra, S. M. A., Koes, B. W., Hazes, J. M. W., & Pols, H. A. P. (2007). Do metabolic factors add to the effect of overweight on hand osteoarthritis? The Rotterdam Study. *Annals of the Rheumatic Diseases*. https://doi.org/10.1136/ard.2005.045724

Dai, S. M., Shan, Z. Z., Nakamura, H., Masuko-Hongo, K., Kato, T., Nishioka, K., & Yudoh, K. (2006). Catabolic stress induces features of chondrocyte senescence through overexpression of caveolin 1: Possible involvement of caveolin 1-induced down-regulation of articular chondrocytes in the pathogenesis of osteoarthritis. *Arthritis and Rheumatism*. https://doi.org/10.1002/art.21639

Dai, T., Natarajan, R., Nast, C. C., LaPage, J., Chuang, P., Sim, J., … Adler, S. G. (2006). Glucose and diabetes: Effects on podocyte and glomerular p38MAPK, heat shock protein 25, and actin cytoskeleton. *Kidney*

International. https://doi.org/10.1038/sj.ki.5000033

Davidenko, N., Schuster, C. F., Bax, D. V., Farndale, R. W., Hamaia, S., Best, S. M., & Cameron, R. E. (2016). Evaluation of cell binding to collagen and gelatin: a study of the effect of 2D and 3D architecture and surface chemistry. *Journal of Materials Science: Materials in Medicine*. https://doi.org/10.1007/s10856-016-5763-9

Dawson, L. P., Fairley, J. L., Papandony, M. C., Hussain, S. M., Cicuttini, F. M., & Wluka, A. E. (2018). Is abnormal glucose tolerance or diabetes a risk factor for knee, hip, or hand osteoarthritis? A systematic review. *Seminars in Arthritis and Rheumatism*. https://doi.org/10.1016/j.semarthrit.2018.02.008

De Bari, C., Dell'Accio, F., Tylzanowski, P., & Luyten, F. P. (2001). Multipotent mesenchymal stem cells from adult human synovial membrane. *Arthritis and Rheumatism*. https://doi.org/10.1002/1529-0131(200108)44:8<1928::AID-ART331>3.0.CO;2-P

De Rooij, J., & Bos, J. L. (1997). Minimal Ras-binding domain of Raf1 can be used as an activation-specific probe for Ras. *Oncogene*. https://doi.org/10.1038/sj.onc.1201005

Del Carlo, M., & Loeser, R. F. (2002). Nitric oxide-mediated chondrocyte cell death requires the generation of additional reactive oxygen species. *Arthritis and Rheumatism*. https://doi.org/10.1002/art.10056

Del Carlo, M., & Loeser, R. F. (2003). Increased Oxidative Stress with Aging Reduces Chondrocyte Survival: Correlation with Intracellular Glutathione Levels. *Arthritis and Rheumatism*. https://doi.org/10.1002/art.11338

Del Carlo, M., & Loeser, R. F. (2008). Cell death in osteoarthritis. *Current Rheumatology Reports*. https://doi.org/10.1007/s11926-008-0007-8

Del Carlo, M., Schwartz, D., Erickson, E. A., & Loeser, R. F. (2007). Endogenous production of reactive oxygen species is required for

stimulation of human articular chondrocyte matrix metalloproteinase production by fibronectin fragments. *Free Radical Biology and Medicine*. https://doi.org/10.1016/j.freeradbiomed.2007.01.035

DelCarlo, M., & Loeser, R. F. (2006). Chondrocyte cell death mediated by reactive oxygen species-dependent activation of PKC-βI. *American Journal of Physiology - Cell Physiology*. https://doi.org/10.1152/ajpcell.00214.2005

Delve, E., Parreno, J., Wu, P., & Co, V. (2016). CDC42 regulates the superficial zone chondrocyte shape and expression of proteoglycan. *Journal of Orthopaedic Research*. https://doi.org/http://dx.doi.org/10.1002/jor.23247

Dhollander, A. A. M., de Neve, F., Almqvist, K. F., Verdonk, R., Lambrecht, S., Elewaut, D., … Verdonk, P. C. M. (2011). Autologous matrix-induced chondrogenesis combined with platelet-rich plasma gel: Technical description and a five pilot patients report. *Knee Surgery, Sports Traumatology, Arthroscopy*. https://doi.org/10.1007/s00167-010-1337-4

Di Lullo, G. A., Sweeney, S. M., Körkkö, J., Ala-Kokko, L., & San Antonio, J. D. (2002). Mapping the ligand-binding sites and disease-associated mutations on the most abundant protein in the human, type I collagen. *Journal of Biological Chemistry*. https://doi.org/10.1074/jbc.M110709200

Dickinson, B. C., & Chang, C. J. (2011). Chemistry and biology of reactive oxygen species in signaling or stress responses. *Nature Chemical Biology*. https://doi.org/10.1038/nchembio.607

Diekman, B. O., Christoforou, N., Willard, V. P., Sun, H., Sanchez-Adams, J., Leong, K. W., & Guilak, F. (2012). Cartilage tissue engineering using differentiated and purified induced pluripotent stem cells. *Proceedings of the National Academy of Sciences of the United States of America*. https://doi.org/10.1073/pnas.1210422109

Ding, C., Stannus, O., Cicuttini, F., Antony, B., & Jones, G. (2013). Body fat is associated with increased and lean mass with decreased knee cartilage loss

in older adults: A prospective cohort study. *International Journal of Obesity*. https://doi.org/10.1038/ijo.2012.136

Ding, L., Guo, D., & Homandberg, G. A. (2009). Fibronectin fragments mediate matrix metalloproteinase upregulation and cartilage damage through proline rich tyrosine kinase 2, c-src, NF-κB and protein kinase Cδ. *Osteoarthritis and Cartilage*. https://doi.org/10.1016/j.joca.2009.03.024

Edmondson, R., Broglie, J. J., Adcock, A. F., & Yang, L. (2014). Three-dimensional cell culture systems and their applications in drug discovery and cell-based biosensors. *Assay and Drug Development Technologies*. https://doi.org/10.1089/adt.2014.573

El-Sherbiny, I. M., & Yacoub, M. H. (2013). Hydrogel scaffolds for tissue engineering: Progress and challenges. *Global Cardiology Science and Practice*. https://doi.org/10.5339/gcsp.2013.38

Elisseeff, J., Anseth, K., Sims, D., Mcintosh, W., Randolph, M., & Langer, R. (1999). Transdermal photopolymerization for minimally invasive implantation. *Proceedings of the National Academy of Sciences of the United States of America*. https://doi.org/10.1073/pnas.96.6.3104

Elisseeff, J., Puleo, C., Yang, F., & Sharma, B. (2005). Advances in skeletal tissue engineering with hydrogels. *Orthodontics and Craniofacial Research*. https://doi.org/10.1111/j.1601-6343.2005.00335.x

Erlacher, L., Ng, C. K., Ullrich, R., Krieger, S., & Luyten, F. P. (1998). Presence of cartilage-derived morphogenetic proteins in articular cartilage and enhancement of matrix replacement in vitro. *Arthritis and Rheumatism*. https://doi.org/10.1002/1529-0131(199802)41:2<263::AID-ART10>3.0.CO;2-5

Eyre, D. (2002). Collagen of articular cartilage. *Arthritis Research*. https://doi.org/10.1186/ar380

Eyre, D. R. (2004). Collagens and cartilage matrix homeostasis. In *Clinical*

Orthopaedics and Related Research. https://doi.org/10.1097/01.blo.0000144855.48640.b9

Eyre, D. R., Weis, M. A., & Wu, J. J. (2006). Articular cartilage collagen: An irreplaceable framework? *European Cells and Materials*. https://doi.org/10.22203/eCM.v012a07

Felson, D. T., & Chaisson, C. E. (1997). Understanding the relationship between body weight and osteoarthritis. *Bailliere's Clinical Rheumatology*. https://doi.org/10.1016/S0950-3579(97)80003-9

Felson, David T., Naimark, A., Anderson, J., Kazis, L., Castelli, W., & Meenan, R. F. (1987). The prevalence of knee osteoarthritis in the elderly. the framingham osteoarthritis study. *Arthritis & Rheumatism*. https://doi.org/10.1002/art.1780300811

Fernández-Lloris, R., Viñals, F., López-Rovira, T., Harley, V., Bartrons, R., Rosa, J. L., & Ventura, F. (2003). Induction of the Sry-related factor SOX6 contributes to bone morphogenetic protein-2-induced chondroblastic differentiation of C3H10T1/2 cells. *Molecular Endocrinology*. https://doi.org/10.1210/me.2002-0254

Figenschau, Y., Knutsen, G., Shahazeydi, S., Johansen, O., & Sveinbjörnsson, B. (2001). Human articular chondrocytes express functional leptin receptors. *Biochemical and Biophysical Research Communications*. https://doi.org/10.1006/bbrc.2001.5543

Finger, F., Schörle, C., Zien, A., Gebhard, P., Goldring, M. B., & Aigner, T. (2003). Molecular Phenotyping of Human Chondrocyte Cell Lines T/C-28a2, T/C-28a4, and C-28/I2. *Arthritis and Rheumatism*. https://doi.org/10.1002/art.11341

Fioravanti, A., Nerucci, F., Annefeld, M., Collodel, G., & Marcolongo, R. (2003). Morphological and cytoskeletal aspects of cultivated normal and osteoarthritic human articular chondrocytes after cyclical pressure: A pilot

study. *Clinical and Experimental Rheumatology*.

Firestein, G. S., Budd, R., Gabriel, S. E., McInnes, I. B., & O'Dell, J. R. (2017). *Kelley and Firestein's Textbook of Rheumatology*. *Kelley and Firestein's Textbook of Rheumatology*. https://doi.org/10.1016/c2013-1-19259-3

Fisher, A. B., Dodia, C., Chander, A., & Jain, M. (1992). A competitive inhibitor of phospholipase A2 decreases surfactant phosphatidylcholine degradation by the rat lung. *Biochemical Journal*. https://doi.org/10.1042/bj2880407

Fisher, Aron B. (2011). Peroxiredoxin 6: A bifunctional enzyme with glutathione peroxidase and phospholipase a2 activities. *Antioxidants and Redox Signaling*. https://doi.org/10.1089/ars.2010.3412

Fisher, Aron B. (2017). Peroxiredoxin 6 in the repair of peroxidized cell membranes and cell signaling. *Archives of Biochemistry and Biophysics*. https://doi.org/10.1016/j.abb.2016.12.003

Fisher, Aron B., Dodia, C., Feinstein, S. I., & Ho, Y. S. (2005). Altered lung phospholipid metabolism in mice with targeted deletion of lysosomal-type phospholipase A2. In *Journal of Lipid Research*. https://doi.org/10.1194/jlr.M400499-JLR200

Fisher, Aron B., Dodia, C., Sorokina, E. M., Li, H., Zhou, S., Raabe, T., & Feinstein, S. I. (2016). A novel lysophosphatidylcholine acyl transferase activity is expressed by peroxiredoxin 6. *Journal of Lipid Research*. https://doi.org/10.1194/jlr.M064758

Fisher, Aron B., Dodia, C., Yu, K., Manevich, Y., & Feinstein, S. I. (2006). Lung phospholipid metabolism in transgenic mice overexpressing peroxiredoxin 6. *Biochimica et Biophysica Acta - Molecular and Cell Biology of Lipids*. https://doi.org/10.1016/j.bbalip.2006.05.009

Forsyth, C. B., Cole, A., Murphy, G., Bienias, J. L., Im, H. J., & Loeser, R. F. (2005). Increased matrix metalloproteinase-13 production with aging by human articular chondrocytes in response to catabolic stimuli. *Journals of*

Gerontology - Series A Biological Sciences and Medical Sciences. https://doi.org/10.1093/gerona/60.9.1118

Forsyth, C. B., Pulai, J., & Loeser, R. F. (2002). Fibronectin fragments and blocking antibodies to α2β1 and α5β1 integrins stimulate mitogen-activated protein kinase signaling and increase collagenase 3 (matrix metalloproteinase 13) production by human articular chondrocytes. *Arthritis and Rheumatism*. https://doi.org/10.1002/art.10502

Foss, C., Merzari, E., Migliaresi, C., & Motta, A. (2013). Silk fibroin/hyaluronic acid 3D matrices for cartilage tissue engineering. *Biomacromolecules*. https://doi.org/10.1021/bm301174x

Francin, P. J., Abot, A., Guillaume, C., Moulin, D., Bianchi, A., Gegout-Pottie, P., … Presle, N. (2014). Association between adiponectin and cartilage degradation in human osteoarthritis. *Osteoarthritis and Cartilage*. https://doi.org/10.1016/j.joca.2014.01.002

Fu, D., Lu, J., & Yang, S. (2016). Oleic/palmitate induces apoptosis in human articular chondrocytes via upregulation of nox4 expression and ros production. *Annals of Clinical and Laboratory Science*.

Fu, Y., Kinter, M., Hudson, J., Humphries, K. M., Lane, R. S., White, J. R., … Griffin, T. M. (2016). Aging Promotes Sirtuin 3–Dependent Cartilage Superoxide Dismutase 2 Acetylation and Osteoarthritis. *Arthritis and Rheumatology*. https://doi.org/10.1002/art.39618

Gao, S. G., Zeng, C., Li, L. J., Luo, W., Zhang, F. J., Tian, J., … Lei, G. H. (2016). Correlation between senescence-associated beta-galactosidase expression in articular cartilage and disease severity of patients with knee osteoarthritis. *International Journal of Rheumatic Diseases*. https://doi.org/10.1111/1756-185X.12096

Gawlitta, D., Van Rijen, M. H. P., Schrijver, E. J. M., Alblas, J., & Dhert, W. J. A. (2012). Hypoxia impedes hypertrophic chondrogenesis of human

multipotent stromal cells. *Tissue Engineering - Part A*. https://doi.org/10.1089/ten.tea.2011.0657

Ge, H. X., Zou, F. M., Li, Y., Liu, A. M., & Tu, M. (2017). JNK pathway in osteoarthritis: pathological and therapeutic aspects. *Journal of Receptors and Signal Transduction*. https://doi.org/10.1080/10799893.2017.1360353

Ghobril, C., & Grinstaff, M. W. (2015). The chemistry and engineering of polymeric hydrogel adhesives for wound closure: A tutorial. *Chemical Society Reviews*. https://doi.org/10.1039/c4cs00332b

Gille, J., Schuseil, E., Wimmer, J., Gellissen, J., Schulz, A. P., & Behrens, P. (2010). Mid-term results of Autologous Matrix-Induced Chondrogenesis for treatment of focal cartilage defects in the knee. *Knee Surgery, Sports Traumatology, Arthroscopy*. https://doi.org/10.1007/s00167-010-1042-3

Glineur, C., Davioud-Charvet, E., & Vandenbunder, B. (2000). The conserved redox-sensitive cysteine residue of the DNA-binding region in the c-Rel protein is involved in the regulation of the phosphorylation of the protein. *Biochemical Journal*. https://doi.org/10.1042/0264-6021:3520583

Glowacki, J., Trepman, E., & Folkman, J. (1983). Cell Shape and Phenotypic Expression in Chondrocytes. *Proceedings of the Society for Experimental Biology and Medicine*. https://doi.org/10.3181/00379727-172-41533

Goldring, M. B., Otero, M., Tsuchimochi, K., Ijiri, K., & Li, Y. (2008). Defining the roles of inflammatory and anabolic cytokines in cartilage metabolism. In *Annals of the Rheumatic Diseases*. https://doi.org/10.1136/ard.2008.098764

Goldring, Mary B. (2004). Immortalization of human articular chondrocytes for generation of stable, differentiated cell lines. *Methods in Molecular Medicine*.

Goldring, Mary B. (2012). Chondrogenesis, chondrocyte differentiation, and articular cartilage metabolism in health and osteoarthritis. *Therapeutic*

Advances in Musculoskeletal Disease. https://doi.org/10.1177/1759720X12448454

Goldring, Mary B., & Marcu, K. B. (2009). Cartilage homeostasis in health and rheumatic diseases. *Arthritis Research & Therapy*, *11*(3), 224. https://doi.org/10.1186/ar2592

Goldring, Mary B., Otero, M., Plumb, D. A., Dragomir, C., Favero, M., El Hachem, K., … Marcu, K. B. (2011). Roles of inflammatory and anabolic cytokines in cartilage metabolism: Signals and multiple effectors converge upon MMP-13 regulation in osteoarthritis. *European Cells and Materials*. https://doi.org/10.22203/eCM.v021a16

Goldring, Mary B, & Marcu, K. B. (2009). Cartilage homeostasis in health and rheumatic diseases. *Arthritis Research & Therapy*, *11*(3), 224. https://doi.org/10.1186/ar2592

Goldring, S. R., & Goldring, M. B. (2016). Changes in the osteochondral unit during osteoarthritis: Structure, function and cartilage bone crosstalk. *Nature Reviews Rheumatology*. https://doi.org/10.1038/nrrheum.2016.148

Gong, C. Y., Shi, S., Dong, P. W., Kan, B., Gou, M. L., Wang, X. H., … Qian, Z. Y. (2009). Synthesis and characterization of PEG-PCL-PEG thermosensitive hydrogel. *International Journal of Pharmaceutics*. https://doi.org/10.1016/j.ijpharm.2008.08.027

Gosset, M., Berenbaum, F., Salvat, C., Sautet, A., Pigenet, A., Tahiri, K., & Jacques, C. (2008). Crucial role of visfatin/pre-B cell colony-enhancing factor in matrix degradation and prostaglandin E2 synthesis in chondrocytes: Possible influence on osteoarthritis. *Arthritis and Rheumatism*. https://doi.org/10.1002/art.23431

Grande, D. A., Pitman, M. I., Peterson, L., Menche, D., & Klein, M. (1989). The repair of experimentally produced defects in rabbit articular cartilage by autologous chondrocyte transplantation. *Journal of Orthopaedic Research*.

https://doi.org/10.1002/jor.1100070208

Grayson, M. (2010). Nutrigenomics. *Nature*, *468*(7327), S1–S1. https://doi.org/10.1038/468S1a

Greco, K. V., Iqbal, A. J., Rattazzi, L., Nalesso, G., Moradi-Bidhendi, N., Moore, A. R., … Perretti, M. (2011). High density micromass cultures of a human chondrocyte cell line: A reliable assay system to reveal the modulatory functions of pharmacological agents. *Biochemical Pharmacology*. https://doi.org/10.1016/j.bcp.2011.09.009

Gregor, M. F., & Hotamisligil, G. S. (2011). Inflammatory Mechanisms in Obesity. *Annual Review of Immunology*. https://doi.org/10.1146/annurev-immunol-031210-101322

Grogan, S. P., Miyaki, S., Asahara, H., D'Lima, D. D., & Lotz, M. K. (2009). Mesenchymal progenitor cell markers in human articular cartilage: Normal distribution and changes in osteoarthritis. *Arthritis Research and Therapy*. https://doi.org/10.1186/ar2719

Guilak, F., Nims, R. J., Dicks, A., Wu, C. L., & Meulenbelt, I. (2018). Osteoarthritis as a disease of the cartilage pericellular matrix. *Matrix Biology*. https://doi.org/10.1016/j.matbio.2018.05.008

Guizzardi, R., Vaghi, L., Marelli, M., Natalello, A., Andreosso, I., Papagni, A., & Cipolla, L. (2019). Gelatin-based hydrogels through homobifunctional triazolinediones targeting tyrosine residues. *Molecules*. https://doi.org/10.3390/molecules24030589

Guo, H., Maher, S. A., & Torzilli, P. A. (2015). A biphasic finite element study on the role of the articular cartilage superficial zone in confined compression. *Journal of Biomechanics*. https://doi.org/10.1016/j.jbiomech.2014.11.007

Guo, J., Gaffrey, M. J., Su, D., Liu, T., Camp, D. G., Smith, R. D., & Qian, W. J. (2014). Resin-Assisted enrichment of thiols as a general strategy for

proteomic profiling of cysteine-based reversible modifications. *Nature Protocols*. https://doi.org/10.1038/nprot.2013.161

Hafidz, R. N. R. M., Yaakob, C. M., Amin, I., & Noorfaizan, A. (2011). Chemical and functional properties of bovine and porcine skin gelatin. *International Food Research Journal*.

Hall, K. C., Hill, D., Otero, M., Plumb, D. A., Froemel, D., Dragomir, C. L., … Blobel, C. P. (2013). ADAM17 Controls Endochondral Ossification by Regulating Terminal Differentiation of Chondrocytes. *Molecular and Cellular Biology*. https://doi.org/10.1128/mcb.00291-13

Hamidi, M., Rostamizadeh, K., & Shahbazi, M. A. (2012). Hydrogel Nanoparticles in Drug Delivery. *Intelligent Nanomaterials: Processes, Properties, and Applications*, *60*, 583–624. https://doi.org/10.1002/9781118311974.ch15

Hangody, L., Kish, G., Módis, L., Szerb, I., Gáspár, L., Diószegi, Z., & Kendik, Z. (2001). Mosaicplasty for the treatment of osteochondritis dissecans of the talus: Two to seven year results in 36 patients. *Foot and Ankle International*. https://doi.org/10.1177/107110070102200704

Hao, D., Li, M., Wu, Z., Duan, Y., Li, D., & Qiu, G. (2011). Synovial fluid level of adiponectin correlated with levels of aggrecan degradation markers in osteoarthritis. *Rheumatology International*. https://doi.org/10.1007/s00296-010-1516-0

Harrison, P. E., Ashton, I. K., Johnson, W. E. B., Turner, S. L., Richardson, J. B., & Ashton, B. A. (2000). The in vitro growth of human chondrocytes. *Cell and Tissue Banking*.

He, S., & Sharpless, N. E. (2017). Senescence in Health and Disease. *Cell*. https://doi.org/10.1016/j.cell.2017.05.015

He, Y., Xu, W., Xiao, Y., Pan, L., Chen, G., Tang, Y., … Cao, J. (2018). Overexpression of Peroxiredoxin 6 (PRDX6) promotes the aggressive

phenotypes of esophageal squamous cell carcinoma. *Journal of Cancer*. https://doi.org/10.7150/jca.26041

Herndon, J. H., Davidson, S. M., & Apazidis, A. (2001). Recent socioeconomic trends in orthopaedic practice. *Journal of Bone and Joint Surgery - Series A*. https://doi.org/10.2106/00004623-200107000-00018

Heywood, H. K., Bader, D. L., & Lee, D. A. (2006). Rate of oxygen consumption by isolated articular chondrocytes is sensitive to medium glucose concentration. *Journal of Cellular Physiology*. https://doi.org/10.1002/jcp.20491

Heywood, H. K., Nalesso, G., Lee, D. A., & Dell'Accio, F. (2014a). Culture Expansion in Low-Glucose Conditions Preserves Chondrocyte Differentiation and Enhances Their Subsequent Capacity to Form Cartilage Tissue in Three-Dimensional Culture. *BioResearch Open Access*, *3*(1), 9–18. https://doi.org/10.1089/biores.2013.0051

Heywood, H. K., Nalesso, G., Lee, D. A., & Dell'Accio, F. (2014b). Culture Expansion in Low-Glucose Conditions Preserves Chondrocyte Differentiation and Enhances Their Subsequent Capacity to Form Cartilage Tissue in Three-Dimensional Culture. *BioResearch Open Access*. https://doi.org/10.1089/biores.2013.0051

Hien, T. T., Turczyńska, K. M., Dahan, D., Ekman, M., Grossi, M., Sjögren, J., … Albinsson, S. (2016). Elevated glucose levels promote contractile and cytoskeletal gene expression in vascular smooth muscle via rho/protein kinase C and actin polymerization. *Journal of Biological Chemistry*. https://doi.org/10.1074/jbc.M115.654384

Hiran, T. S., Moulton, P. J., & Hancock, J. T. (1997). Detection of superoxide and NAPDH oxidase in porcine articular chondrocytes. *Free Radical Biology and Medicine*. https://doi.org/10.1016/S0891-5849(97)00054-3

Ho, J. N., Lee, S. B., Lee, S. S., Yoon, S. H., Kang, G. Y., Hwang, S. G., & Um,

H. D. (2010). Phospholipase A 2 activity of peroxiredoxin 6 promotes invasion and metastasis of lung cancer cells. *Molecular Cancer Therapeutics*. https://doi.org/10.1158/1535-7163.MCT-09-0904

Holloway, I., Kayser, M., Lee, D. A., Bader, D. L., Bentley, G., & Knight, M. M. (2004). Increased presence of cells with multiple elongated processes in osteoarthritic femoral head cartilage. *Osteoarthritis and Cartilage*. https://doi.org/10.1016/j.joca.2003.09.001

Homandberg, G. A., Costa, V., & Wen, C. (2002). Fibronectin fragments active in chondrocytic chondrolysis can be chemically cross-linked to the alpha5 integrin receptor subunit. *Osteoarthritis and Cartilage*. https://doi.org/10.1053/joca.2002.0854

Homandberg, G. A., Meyers, R., & Xie, D. L. (1992). Fibronectin fragments cause chondrolysis of bovine articular cartilage slices in culture. *Journal of Biological Chemistry*.

Horiuchi, K., Kimura, T., Miyamoto, T., Miyamoto, K., Akiyama, H., Takaishi, H., … Toyama, Y. (2009). Conditional Inactivation of TACE by a Sox9 Promoter Leads to Osteoporosis and Increased Granulopoiesis via Dysregulation of IL-17 and G-CSF . *The Journal of Immunology*. https://doi.org/10.4049/jimmunol.0802491

Horner, A., Kemp, P., Summers, C., Bord, S., Bishop, N. J., Kelsall, A. W., … Compston, J. E. (1998). Expression and distribution of transforming growth factor-β isoforms and their signaling receptors in growing human bone. *Bone*. https://doi.org/10.1016/S8756-3282(98)00080-5

Hosseinzadeh, A., Bahrampour Juybari, K., Kamarul, T., & Sharifi, A. M. (2019). Protective effects of atorvastatin on high glucose-induced oxidative stress and mitochondrial apoptotic signaling pathways in cultured chondrocytes. *Journal of Physiology and Biochemistry*. https://doi.org/10.1007/s13105-019-00666-8

Hosseinzadeh, A., Kamrava, S. K., Joghataei, M. T., Darabi, R., Shakeri-Zadeh, A., Shahriari, M., … Mehrzadi, S. (2016). Apoptosis signaling pathways in osteoarthritis and possible protective role of melatonin. *Journal of Pineal Research*. https://doi.org/10.1111/jpi.12362

Hötten, G. C., Matsumoto, T., Kimura, M., Bechtold, R. F., Kron, R., Ohara, T., … Kudo, A. (1996). Recombinant human growth/differentiation factor 5 stimulates mesenchyme aggregation and chondrogenesis responsible for the skeletal development of limbs. *Growth Factors*. https://doi.org/10.3109/08977199609034567

Hou, Q., De Bank, P. A., & Shakesheff, K. M. (2004). Injectable scaffolds for tissue regeneration. *Journal of Materials Chemistry*. https://doi.org/10.1039/b401791a

Huang, C. F., Sun, Z. J., Zhao, Y. F., Chen, X. M., Jia, J., & Zhang, W. F. (2011). Increased expression of peroxiredoxin 6 and cyclophilin A in squamous cell carcinoma of the tongue. *Oral Diseases*. https://doi.org/10.1111/j.1601-0825.2010.01730.x

Huey, D. J., Hu, J. C., & Athanasiou, K. A. (2012). Unlike bone, cartilage regeneration remains elusive. *Science*. https://doi.org/10.1126/science.1222454

Hunter, D. J., & Bierma-Zeinstra, S. (2019). Osteoarthritis. *The Lancet*. https://doi.org/10.1016/S0140-6736(19)30417-9

Hunziker, E. B., Lippuner, K., Keel, M. J. B., & Shintani, N. (2015). An educational review of cartilage repair: Precepts & practice - myths & misconceptions - progress & prospects. *Osteoarthritis and Cartilage*. https://doi.org/10.1016/j.joca.2014.12.011

Hunziker, Ernst B., Michel, M., & Studer, D. (1997). Ultrastructure of adult human articular cartilage matrix after cryotechnical processing. *Microscopy Research and Technique*. https://doi.org/10.1002/(SICI)1097-

0029(19970515)37:4<271::AID-JEMT3>3.0.CO;2-O

Hwang, H. S., & Kim, H. A. (2015). Chondrocyte apoptosis in the pathogenesis of osteoarthritis. *International Journal of Molecular Sciences*. https://doi.org/10.3390/ijms161125943

Hwang, S. G., Yu, S. S., Poo, H., & Chun, J. S. (2005). c-Jun/activator protein-1 mediates interleukin-1β-induced dedifferentiation but not cyclooxygenase-2 expression in articular chondrocytes. *Journal of Biological Chemistry*. https://doi.org/10.1074/jbc.M411793200

Ikeda, D., Ageta, H., Tsuchida, K., & Yamada, H. (2013). ITRAQ-based proteomics reveals novel biomarkers of osteoarthritis. *Biomarkers*. https://doi.org/10.3109/1354750X.2013.810667

Inerot, S., Heinegard, D., Audell, L., & Olsson, S. E. (1978). Articular-cartilage proteoglycans in aging and osteoarthritis. *Biochemical Journal*. https://doi.org/10.1042/bj1690143

Inoue, H., Kato, Y., Iwamoto, M., Hiraki, Y., Sakuda, M., & Suzuki, F. (1989). Stimulation of cartilage-matrix proteoglycan synthesis by morphologically transformed chondrocytes grown in the presence of fibroblast growth factor and transforming growth factor-beta. *Journal of Cellular Physiology*. https://doi.org/10.1002/jcp.1041380216

Insall, J. (1974). The Pridie debridement operation for osteoarthritis of the knee. *CLIN.ORTHOP.*

Ireland, J. L., Wylie, C. E., Collins, S. N., Verheyen, K. L. P., & Newton, J. R. (2013). Preventive health care and owner-reported disease prevalence of horses and ponies in Great Britain. *Research in Veterinary Science*. https://doi.org/10.1016/j.rvsc.2013.05.007

Ishizaki, Y., Burne, J. F., & Raff, M. C. (1994). Autocrine signals enable chondrocytes to survive in culture. *Journal of Cell Biology*. https://doi.org/10.1083/jcb.126.4.1069

Iwamoto, M., Tamamura, Y., Koyama, E., Komori, T., Takeshita, N., Williams, J. A., … Pacifici, M. (2007). Transcription factor ERG and joint and articular cartilage formation during mouse limb and spine skeletogenesis. *Developmental Biology*. https://doi.org/10.1016/j.ydbio.2007.01.037

Jackson, D. W., Lalor, P. A., Aberman, H. M., & Simon, T. M. (2001). Spontaneous repair of full-thickness defects of articular cartilage in a goat model: A preliminary study. *Journal of Bone and Joint Surgery - Series A*. https://doi.org/10.2106/00004623-200101000-00008

Jaipan, P., Nguyen, A., & Narayan, R. J. (2017). Gelatin-based hydrogels for biomedical applications. *MRS Communications*. https://doi.org/10.1557/mrc.2017.92

Janssen-Heininger, Y. M. W., Poynter, M. E., & Baeuerle, P. A. (2000). Recent advances towards understanding redox mechanisms in the activation of nuclear factor κB. *Free Radical Biology and Medicine*. https://doi.org/10.1016/S0891-5849(00)00218-5

Jeon, O. H., Kim, C., Laberge, R. M., Demaria, M., Rathod, S., Vasserot, A. P., … Elisseeff, J. H. (2017). Local clearance of senescent cells attenuates the development of post-traumatic osteoarthritis and creates a pro-regenerative environment. *Nature Medicine*. https://doi.org/10.1038/nm.4324

Ji, B., Ma, Y., Wang, H., Fang, X., & Shi, P. (2019). Activation of the P38/CREB/MMP13 axis is associated with osteoarthritis . *Drug Design, Development and Therapy*. https://doi.org/10.2147/dddt.s209626

Ji, C., Kozak, K. R., & Marnett, L. J. (2001). IκB Kinase, a Molecular Target for Inhibition by 4-Hydroxy-2-nonenal. *Journal of Biological Chemistry*. https://doi.org/10.1074/jbc.M101266200

Johnson, K. A., & Terkeltaub, R. A. (2005). External GTP-bound transglutaminase 2 is a molecular switch for chondrocyte hypertrophic differentiation and calcification. *Journal of Biological Chemistry*.

https://doi.org/10.1074/jbc.M500962200

Johnstone, B., Hering, T. M., Caplan, A. I., Goldberg, V. M., & Yoo, J. U. (1998). In vitro chondrogenesis of bone marrow-derived mesenchymal progenitor cells. *Experimental Cell Research*. https://doi.org/10.1006/excr.1997.3858

Jones, C. W., Willers, C., Keogh, A., Smolinski, D., Fick, D., Yates, P. J., … Zheng, M. H. (2008). Matrix-induced autologous chondrocyte implantation in sheep: Objective assessments including confocal arthroscopy. *Journal of Orthopaedic Research*. https://doi.org/10.1002/jor.20502

Jung, Y. K., Jeong, J. H., Ryoo, H. M., Kim, H. N., Kim, Y. J., Park, E. K., … Choi, J. Y. (2004). Gene expression profile of human chondrocyte HCS-2/8 cell line by EST sequencing analysis. *Gene*. https://doi.org/10.1016/j.gene.2004.01.007

Juybari, K. B., Hosseinzadeh, A., & Sharifi, A. M. (2019). Protective effects of atorvastatin against high glucose-induced nuclear factor-κB activation in cultured C28I2 chondrocytes. *Journal of Receptors and Signal Transduction*, *39*(1), 1–8. https://doi.org/10.1080/10799893.2018.1557206

Kabeya, Y. (2000). LC3, a mammalian homologue of yeast Apg8p, is localized in autophagosome membranes after processing. *The EMBO Journal*. https://doi.org/10.1093/emboj/19.21.5720

Kang, S. W., Baines, I. C., & Rhee, S. G. (1998). Characterization of a mammalian peroxiredoxin that contains one conserved cysteine. *Journal of Biological Chemistry*. https://doi.org/10.1074/jbc.273.11.6303

Kapoor, M., Martel-Pelletier, J., Lajeunesse, D., Pelletier, J. P., & Fahmi, H. (2011). Role of proinflammatory cytokines in the pathophysiology of osteoarthritis. *Nature Reviews Rheumatology*. https://doi.org/10.1038/nrrheum.2010.196

Karlsen, T. A., Jakobsen, R. B., Mikkelsen, T. S., & Brinchmann, J. E. (2014). MicroRNA-140 targets RALA and regulates chondrogenic differentiation

of human mesenchymal stem cells by translational enhancement of SOX9 and ACAN. *Stem Cells and Development*. https://doi.org/10.1089/scd.2013.0209

Karp, S. J., Schipani, E., St-Jacques, B., Hunzelman, J., Kronenberg, H., & McMahon, A. P. (2000). Indian Hedgehog coordinates endochondral bone growth and morphogenesis via Parathyroid Hormone related-Protein-dependent and -independent pathways. *Development*.

Kato, Y., & Gospodarowicz, D. (1985). Sulfated proteoglycan synthesis by confluent cultures of rabbit costal chondrocytes grown in the presence of fibroblast growth factor. *Journal of Cell Biology*. https://doi.org/10.1083/jcb.100.2.477

KATO, Y., HIRAKI, Y., INOUE, H., KINOSHITA, M., YUTANI, Y., & SUZUKI, F. (1983). Differential and Synergistic Actions of Somatomedin-Like Growth Factors, Fibroblast Growth Factor and Epidermal Growth Factor in Rabbit Costal Chondrocytes. *European Journal of Biochemistry*. https://doi.org/10.1111/j.1432-1033.1983.tb07103.x

Kegel, K. B., Kim, M., Sapp, E., McIntyre, C., Castano, J. G., Aronin, N., & DiFiglia, M. (2000). Huntingtin expression stimulates endosomal-lysosomal activity, endosome tubulation, and autophagy. *Journal of Neuroscience*.

Khan, I. M., Gilbert, S. J., Singhrao, S. K., Duance, V. C., & Archer, C. W. (2008). Cartilage integration: Evaluation of the reasons for failure of integration during cartilage repair. A review. *European Cells and Materials*.

Khan, N. M., Ahmad, I., & Haqqi, T. M. (2018). Nrf2/ARE pathway attenuates oxidative and apoptotic response in human osteoarthritis chondrocytes by activating ERK1/2/ELK1-P70S6K-P90RSK signaling axis. *Free Radical Biology and Medicine*. https://doi.org/10.1016/j.freeradbiomed.2018.01.013

Kim, D. H., Lee, D. H., Jo, M. R., Son, D. J., Park, M. H., Hwang, C. J., … Hong, J. T. (2015). Exacerbation of collagen antibody-induced arthritis in transgenic mice overexpressing peroxiredoxin 6. *Arthritis and Rheumatology*. https://doi.org/10.1002/art.39284

Kim, H. A., Lee, Y. J., Seong, S. C., Choe, K. W., & Song, Y. W. (2000). Apoptotic chondrocyte death in human osteoarthritis. *Journal of Rheumatology*.

Kim, J., Xu, M., Xo, R., Mates, A., Wilson, G. L., Pearsall IV, A. W., & Grishko, V. (2010). Mitochondrial DNA damage is involved in apoptosis caused by pro-inflammatory cytokines in human OA chondrocytes. *Osteoarthritis and Cartilage*. https://doi.org/10.1016/j.joca.2009.09.008

Kirsch, T., Swoboda, B., & von der Mark, K. (1992). Ascorbate independent differentiation of human chondrocytes in vitro: simultaneous expression of types I and × collagen and matrix mineralization. *Differentiation*. https://doi.org/10.1111/j.1432-0436.1992.tb00503.x

Klein, T. J., Malda, J., Sah, R. L., & Hutmacher, D. W. (2009). Tissue engineering of articular cartilage with biomimetic zones. *Tissue Engineering - Part B: Reviews*. https://doi.org/10.1089/ten.teb.2008.0563

Knoops, B., Goemaere, J., Van Der Eecken, V., & Declercq, J. P. (2011). Peroxiredoxin 5: Structure, mechanism, and function of the mammalian atypical 2-cys peroxiredoxin. *Antioxidants and Redox Signaling*. https://doi.org/10.1089/ars.2010.3584

Knutsen, G., Drogset, J. O., Engebretsen, L., Grøntvedt, T., Isaksen, V., Ludvigsen, T. C., … Johansen, O. (2007). A randomized trial comparing autologous chondrocyte implantation with microfracture: Findings at five years. *Journal of Bone and Joint Surgery - Series A*. https://doi.org/10.2106/JBJS.G.00003

Ko, J. Y., Kim, K. Il, Park, S., & Im, G. Il. (2014). In vitro chondrogenesis and

in vivo repair of osteochondral defect with human induced pluripotent stem cells. *Biomaterials*. https://doi.org/10.1016/j.biomaterials.2014.01.009

Kokenyesi, R., Tan, L., Robbins, J. R., & Goldring, M. B. (2000). Proteoglycan production by immortalized human chondrocyte cell lines cultured under conditions that promote expression of the differentiated phenotype. *Archives of Biochemistry and Biophysics*. https://doi.org/10.1006/abbi.2000.2044

Kolev, T., Seidel, R. W., Mayer-Figge, H., Spiteller, M., Sheldrick, W. S., & Koleva, B. B. (2009). Crystal structures and spectroscopic properties of ester amide and diamide of squaric acid with prolinamide. *Spectrochimica Acta - Part A: Molecular and Biomolecular Spectroscopy*. https://doi.org/10.1016/j.saa.2008.10.060

Kouser, R., Vashist, A., Zafaryab, M., Rizvi, M. A., & Ahmad, S. (2018). Biocompatible and mechanically robust nanocomposite hydrogels for potential applications in tissue engineering. *Materials Science and Engineering C*. https://doi.org/10.1016/j.msec.2017.11.018

Kozhemyakina, E., Cohen, T., Yao, T.-P., & Lassar, A. B. (2009). Parathyroid Hormone-Related Peptide Represses Chondrocyte Hypertrophy through a Protein Phosphatase 2A/Histone Deacetylase 4/MEF2 Pathway. *Molecular and Cellular Biology*. https://doi.org/10.1128/mcb.00415-09

Kozhemyakina, Elena, Lassar, A. B., & Zelzer, E. (2015). A pathway to bone: Signaling molecules and transcription factors involved in chondrocyte development and maturation. *Development (Cambridge)*. https://doi.org/10.1242/dev.105536

Kreuz, P. C., Erggelet, C., Steinwachs, M. R., Krause, S. J., Lahm, A., Niemeyer, P., … Südkamp, N. (2006). Is Microfracture of Chondral Defects in the Knee Associated With Different Results in Patients Aged 40 Years or Younger? *Arthroscopy - Journal of Arthroscopic and Related Surgery*.

https://doi.org/10.1016/j.arthro.2006.06.020

Krichevsky, O., & Bonnet, G. (2002). Fluorescence correlation spectroscopy: The technique and its applications. *Reports on Progress in Physics*. https://doi.org/10.1088/0034-4885/65/2/203

Krishnan, Y., & Grodzinsky, A. J. (2018). Cartilage diseases. *Matrix Biology*, *71–72*, 51–69. https://doi.org/10.1016/j.matbio.2018.05.005

Kuroda, R., Ishida, K., Matsumoto, T., Akisue, T., Fujioka, H., Mizuno, K., … Kurosaka, M. (2007). Treatment of a full-thickness articular cartilage defect in the femoral condyle of an athlete with autologous bone-marrow stromal cells. *Osteoarthritis and Cartilage*. https://doi.org/10.1016/j.joca.2006.08.008

Labrador, J. P., Azcoitia, V., Tuckermann, J., Lin, C., Olaso, E., Mães, S., … Klein, R. (2001). The collagen receptor DDR2 regulates proliferation and its elimination leads to dwarfism. *EMBO Reports*. https://doi.org/10.1093/embo-reports/kve094

Lago, R., Gomez, R., Otero, M., Lago, F., Gallego, R., Dieguez, C., … Gualillo, O. (2008). A new player in cartilage homeostasis: adiponectin induces nitric oxide synthase type II and pro-inflammatory cytokines in chondrocytes. *Osteoarthritis and Cartilage*. https://doi.org/10.1016/j.joca.2007.12.008

Laiguillon, M. C., Courties, A., Houard, X., Auclair, M., Sautet, A., Capeau, J., … Sellam, J. (2015). Characterization of diabetic osteoarthritic cartilage and role of high glucose environment on chondrocyte activation: Toward pathophysiological delineation of diabetes mellitus-related osteoarthritis. *Osteoarthritis and Cartilage*. https://doi.org/10.1016/j.joca.2015.04.026

Lambrecht, S., Verbruggen, G., Verdonk, P. C. M., Elewaut, D., & Deforce, D. (2008). Differential proteome analysis of normal and osteoarthritic chondrocytes reveals distortion of vimentin network in osteoarthritis. *Osteoarthritis and Cartilage*. https://doi.org/10.1016/j.joca.2007.06.005

Le Clanche, S., Bonnefont-Rousselot, D., Sari-Ali, E., Rannou, F., & Borderie, D. (2016a). Inter-relations between osteoarthritis and metabolic syndrome: A common link? *Biochimie*. https://doi.org/10.1016/j.biochi.2015.12.008

Le Clanche, S., Bonnefont-Rousselot, D., Sari-Ali, E., Rannou, F., & Borderie, D. (2016b). Inter-relations between osteoarthritis and metabolic syndrome: A common link? *Biochimie*, *121*, 238–252. https://doi.org/10.1016/j.biochi.2015.12.008

Le Clanche, S., Bonnefont-Rousselot, D., Sari-Ali, E., Rannou, F., & Borderie, D. (2016c). Inter-relations between osteoarthritis and metabolic syndrome: A common link? *Biochimie*. https://doi.org/10.1016/j.biochi.2015.12.008

Lee, C. R., Grodzinsky, A. J., & Spector, M. (2001). The effects of cross-linking of collagen-glycosaminoglycan scaffolds on compressive stiffness, chondrocyte-mediated contraction, proliferation and biosynthesis. *Biomaterials*. https://doi.org/10.1016/S0142-9612(01)00067-9

Lee, J. H., Ort, T., Ma, K., Picha, K., Carton, J., Marsters, P. A., … Blake, S. (2009). Resistin is elevated following traumatic joint injury and causes matrix degradation and release of inflammatory cytokines from articular cartilage in vitro. *Osteoarthritis and Cartilage*. https://doi.org/10.1016/j.joca.2008.08.007

Lee, Jung Hwan, & Kim, H. W. (2018). Emerging properties of hydrogels in tissue engineering. *Journal of Tissue Engineering*. https://doi.org/10.1177/2041731418768285

Lee, K. S., Iijima-Ando, K., Iijima, K., Lee, W. J., Lee, J. H., Yu, K., & Lee, D. S. (2009). JNK/FOXO-mediated neuronal expression of fly homologue of peroxiredoxin II reduces oxidative stress and extends life span. *Journal of Biological Chemistry*. https://doi.org/10.1074/jbc.M109.028027

Lefebvre, V., & Dvir-Ginzberg, M. (2017). SOX9 and the many facets of its regulation in the chondrocyte lineage. *Connective Tissue Research*.

https://doi.org/10.1080/03008207.2016.1183667

Leitinger, B., & Kwan, A. P. L. (2006). The discoidin domain receptor DDR2 is a receptor for type X collagen. *Matrix Biology*. https://doi.org/10.1016/j.matbio.2006.05.006

Lepetsos, P., & Papavassiliou, A. G. (2016). ROS/oxidative stress signaling in osteoarthritis. *Biochimica et Biophysica Acta - Molecular Basis of Disease*. https://doi.org/10.1016/j.bbadis.2016.01.003

Lepetsos, P., Papavassiliou, K. A., & Papavassiliou, A. G. (2019). Redox and NF-κB signaling in osteoarthritis. *Free Radical Biology and Medicine*, *132*(September 2018), 90–100. https://doi.org/10.1016/j.freeradbiomed.2018.09.025

Li, C. H., Chik, T. K., Ngan, A. H. W., Chan, S. C. H., Shum, D. K. Y., & Chan, B. P. (2011). Correlation between compositional and mechanical properties of human mesenchymal stem cell-collagen microspheres during chondrogenic differentiation. *Tissue Engineering - Part A*. https://doi.org/10.1089/ten.tea.2010.0078

Li, J., & Mooney, D. J. (2016). Designing hydrogels for controlled drug delivery. *Nature Reviews Materials*. https://doi.org/10.1038/natrevmats.2016.71

Li, L., Yu, F., Zheng, L., Wang, R., Yan, W., Wang, Z., … Jiang, Q. (2019). Natural hydrogels for cartilage regeneration: Modification, preparation and application. *Journal of Orthopaedic Translation*. https://doi.org/10.1016/j.jot.2018.09.003

Li, W., Zhu, Y., Liu, X., Hou, J., Fang, J., Shen, J., & Ma, X. (2018). Phencynonate mediates antidepressant response by activating sirtuin 6-SOD2/Prdx6 pathway. *Biochemical and Biophysical Research Communications*. https://doi.org/10.1016/j.bbrc.2018.10.017

Li, Y., Jiang, W., Wang, H., Deng, Z., Zeng, C., Tu, M., … Lei, G. (2016). Osteopontin promotes expression of matrix metalloproteinase 13 through

NF- B signaling in osteoarthritis. *BioMed Research International*. https://doi.org/10.1155/2016/6345656

Liang, H., Wang, H., Luo, L., Fan, S., Zhou, L., Liu, Z., … Zha, Z. (2019). Toll-like receptor 4 promotes high glucose-induced catabolic and inflammatory responses in chondrocytes in an NF-κB-dependent manner. *Life Sciences*, *228*(March), 258–265. https://doi.org/10.1016/j.lfs.2019.04.011

Lin, M., Yiu, W. H., Wu, H. J., Chan, L. Y. Y., Leung, J. C. K., Au, W. S., … Tang, S. C. W. (2012). Toll-like receptor 4 promotes tubular inflammation in diabetic nephropathy. *Journal of the American Society of Nephrology*. https://doi.org/10.1681/ASN.2010111210

Lin, Z., Willers, C., Xu, J., & Zheng, M. H. (2006). The chondrocyte: Biology and clinical application. *Tissue Engineering*. https://doi.org/10.1089/ten.2006.12.1971

Liu-Bryan, R., & Terkeltaub, R. (2015). Emerging regulators of the inflammatory process in osteoarthritis. *Nature Reviews Rheumatology*. https://doi.org/10.1038/nrrheum.2014.162

Liu, S., Zhang, E., Yang, M., & Lu, L. (2014). Overexpression of Wnt11 promotes chondrogenic differentiation of bone marrow-derived mesenchymal stem cells in synergism with TGF-β. *Molecular and Cellular Biochemistry*. https://doi.org/10.1007/s11010-014-1963-0

Liu, Y. X., Wang, G. D., Wang, X., Zhang, Y. Le, & Zhang, T. L. (2017). Effects of TLR-2/NF-κB signaling pathway on the occurrence of degenerative knee osteoarthritis: An in vivo and in vitro study. *Oncotarget*. https://doi.org/10.18632/oncotarget.16199

Lo, Y. Y. C., Conquer, J. A., Grinstein, S., & Cruz, T. F. (1998). Interleukin-1β induction of c-fos and collagenase expression in articular chondrocytes: Involvement of reactive oxygen species. *Journal of Cellular Biochemistry*. https://doi.org/10.1002/(SICI)1097-4644(19980401)69:1<19::AID-

JCB3>3.0.CO;2-Y

Loeser, R. F. (2009). Aging and osteoarthritis: the role of chondrocyte senescence and aging changes in the cartilage matrix. *Osteoarthritis and Cartilage*. https://doi.org/10.1016/j.joca.2009.03.002

Loeser, R.F., Erickson, E. A., & Long, D. A. (2011). Rac1 and nadph oxidase regulate NFB activity and mmp-13 expression in chondrocytes in response to integrin activation. *Arthritis and Rheumatism*.

Loeser, Richard F. (2000). Chondrocyte integrin expression and function. In *Biorheology*.

Loeser, Richard F. (2002). Integrins and cell signaling in chondrocytes. In *Biorheology*.

Loeser, Richard F. (2013). Aging processes and the development of osteoarthritis. *Current Opinion in Rheumatology*. https://doi.org/10.1097/BOR.0b013e32835a9428

Loeser, Richard F. (2017). The Role of Aging in the Development of Osteoarthritis. *Transactions of the American Clinical and Climatological Association*.

Loeser, Richard F., Carlson, C. S., Del Carlo, M., & Cole, A. (2002). Detection of nitrotyrosine in aging and osteoarthritic cartilage: Correlation of oxidative damage with the presence of interleukin-1β and with chondrocyte resistance to insulin-like growth factor 1. *Arthritis and Rheumatism*. https://doi.org/10.1002/art.10496

Loeser, Richard F., Collins, J. A., & Diekman, B. O. (2016). Ageing and the pathogenesis of osteoarthritis. *Nature Reviews Rheumatology*. https://doi.org/10.1038/nrrheum.2016.65

Loeser, Richard F., Gandhi, U., Long, D. L., Yin, W., & Chubinskaya, S. (2014). Aging and oxidative stress reduce the response of human articular chondrocytes to insulin-like growth factor 1 and osteogenic protein 1.

Arthritis and Rheumatology. https://doi.org/10.1002/art.38641

Loeser, Richard F., Goldring, S. R., Scanzello, C. R., & Goldring, M. B. (2012). Osteoarthritis: A disease of the joint as an organ. *Arthritis and Rheumatism*. https://doi.org/10.1002/art.34453

Loeser, Richard F., Pacione, C. A., & Chubinskaya, S. (2003). The combination of insulin-like growth factor 1 and osteogenic protein 1 promotes increased survival of and matrix synthesis by normal and osteoarthritic human articular chondrocytes. *Arthritis and Rheumatism*. https://doi.org/10.1002/art.11209

Long, D. L., Willey, J. S., & Loeser, R. F. (2013). Rac1 is required for matrix metalloproteinase 13 production by chondrocytes in response to fibronectin fragments. *Arthritis and Rheumatism*. https://doi.org/10.1002/art.37922

Long, H., Ma, K., Xiao, Z., Ren, X., & Yang, G. (2017). Preparation and characteristics of gelatin sponges crosslinked by microbial transglutaminase. *PeerJ*. https://doi.org/10.7717/peerj.3665

López-Armada, M. J., Caramés, B., Martín, M. A., Cillero-Pastor, B., Lires-Dean, M., Fuentes-Boquete, I., … Blanco, F. J. (2006). Mitochondrial activity is modulated by TNFα and IL-1β in normal human chondrocyte cells. *Osteoarthritis and Cartilage*. https://doi.org/10.1016/j.joca.2006.03.008

López-Otín, C., Blasco, M. A., Partridge, L., Serrano, M., & Kroemer, G. (2013). The hallmarks of aging. *Cell*. https://doi.org/10.1016/j.cell.2013.05.039

Lorenzo, P., Bayliss, M. T., & Heinegård, D. (2004). Altered patterns and synthesis of extracellular matrix macromolecules in early osteoarthritis. *Matrix Biology*. https://doi.org/10.1016/j.matbio.2004.07.007

Loty, S., Forest, N., Boulekbache, H., & Sautier, J. M. (1995). Cytochalasin D induces changes in cell shape and promotes in vitro chondrogenesis: A morphological study. *Biology of the Cell*. https://doi.org/10.1016/0248-

4900(96)81303-7

Lotz, M. K., & Caramés, B. (2011). Autophagy and cartilage homeostasis mechanisms in joint health, aging and OA. *Nature Reviews Rheumatology*. https://doi.org/10.1038/nrrheum.2011.109

Louati, K., Vidal, C., Berenbaum, F., & Sellam, J. (2015). Association between diabetes mellitus and osteoarthritis: Systematic literature review and meta-analysis. *RMD Open*. https://doi.org/10.1136/rmdopen-2015-000077

Lowther, W. T., & Haynes, A. C. (2011). Reduction of cysteine sulfinic acid in eukaryotic, typical 2-Cys peroxiredoxins by sulfiredoxin. *Antioxidants and Redox Signaling*. https://doi.org/10.1089/ars.2010.3564

Luo, P., Gao, F., Niu, D., Sun, X., Song, Q., Guo, C., … Sun, W. (2019). The Role of Autophagy in Chondrocyte Metabolism and Osteoarthritis: A Comprehensive Research Review. *BioMed Research International*. https://doi.org/10.1155/2019/5171602

Lv, D., Hu, Z., Lu, L., Lu, H., & Xu, X. (2017). Three-dimensional cell culture: A powerful tool in tumor research and drug discovery. *Oncology Letters*. https://doi.org/10.3892/ol.2017.7134

Lv, Z., Hu, M., Ren, X., Fan, M., Zhen, J., Chen, L., … Wang, R. (2016). Fyn Mediates High Glucose-Induced Actin Cytoskeleton Reorganization of Podocytes via Promoting ROCK Activation in Vitro. *Journal of Diabetes Research*. https://doi.org/10.1155/2016/5671803

Mackay, A. M., Beck, S. C., Murphy, J. M., Barry, F. P., Chichester, C. O., & Pittenger, M. F. (1998). Chondrogenic differentiation of cultured human mesenchymal stem cells from marrow. *Tissue Engineering*. https://doi.org/10.1089/ten.1998.4.415

Madry, H., Grün, U. W., & Knutsen, G. (2011). Cartilage repair and joint preservation: Medical and surgical treatment options. *Deutsches Arzteblatt*. https://doi.org/10.3238/arztebl.2011.0669

Madry, H., Luyten, F. P., & Facchini, A. (2012). Biological aspects of early osteoarthritis. *Knee Surgery, Sports Traumatology, Arthroscopy*. https://doi.org/10.1007/s00167-011-1705-8

Magnusson, K., Hagen, K. B., Østera˚s, N., Nordsletten, L., Natvig, B., & Haugen, I. K. (2015). Diabetes is associated with increased hand pain in erosive hand osteoarthritis: Data from a population-based study. *Arthritis Care and Research*. https://doi.org/10.1002/acr.22460

Marchand, C., Chen, G., Tran-Khanh, N., Sun, J., Chen, H., Buschmann, M. D., & Hoemann, C. D. (2012). Microdrilled cartilage defects treated with thrombin-solidified chitosan/blood implant regenerate a more hyaline, stable, and structurally integrated osteochondral unit compared to drilled controls. *Tissue Engineering - Part A*. https://doi.org/10.1089/ten.tea.2011.0178

Marcu, K. B., Otero, M., Olivotto, E., Borzi, R. M., & Goldring, M. B. (2010). NF-kappaB signaling: multiple angles to target OA. *Current Drug Targets*.

Martel-Pelletier, J., Di Battista, J. A., Lajeunesse, D., & Pelletier, J. P. (1998). IGF/IGFBP axis in cartilage and bone in osteoarthritis pathogenesis. *Inflammation Research*. https://doi.org/10.1007/s000110050288

Martel-Pelletier, Johanne, Barr, A. J., Cicuttini, F. M., Conaghan, P. G., Cooper, C., Goldring, M. B., … Pelletier, J.-P. (2016). Osteoarhritis. *Nature Reviews Disease Primer*.

Martin, I., Suetterlin, R., Baschong, W., Heberer, M., Vunjak-Novakovic, G., & Freed, L. E. (2001). Enhanced cartilage tissue engineering by sequential exposure of chondrocytes to FGF-2 during 2D expansion and BMP-2 during 3D cultivation. *Journal of Cellular Biochemistry*. https://doi.org/10.1002/jcb.1203

Martin, J. A., & Buckwalter, J. A. (2002). Aging, articular cartilage chondrocyte senescence and osteoarthritis. *Biogerontology*.

https://doi.org/10.1023/A:1020185404126

McAlinden, A., Shim, K. H., Wirthlin, L., Ravindran, S., & Hering, T. M. (2012). Quantification of type II procollagen splice forms using alternative transcript-qPCR (AT-qPCR). *Matrix Biology*. https://doi.org/10.1016/j.matbio.2012.08.002

McNulty, A. L., Miller, M. R., O'Connor, S. K., & Guilak, F. (2011). The effects of adipokines on cartilage and meniscus catabolism. *Connective Tissue Research*. https://doi.org/10.3109/03008207.2011.597902

Mead, T. J., & Yutzey, K. E. (2009). Notch pathway regulation of chondrocyte differentiation and proliferation during appendicular and axial skeleton development. *Proceedings of the National Academy of Sciences of the United States of America*. https://doi.org/10.1073/pnas.0902306106

Mendes, A. F., Rosa, S. C., Rufino, A. T., Ribeiro, M., & Judas, F. (2015). Diabetes-induced osteoarthritis: role of hyperglycemia in joint destruction. *BMC Musculoskeletal Disorders*. https://doi.org/10.1186/1471-2474-16-s1-s1

Mendis, E., Kim, M. M., Rajapakse, N., & Kim, S. K. (2008). Sulfated glucosamine inhibits oxidation of biomolecules in cells via a mechanism involving intracellular free radical scavenging. *European Journal of Pharmacology*. https://doi.org/10.1016/j.ejphar.2007.10.027

Mihalas, B. P., De Iuliis, G. N., Redgrove, K. A., McLaughlin, E. A., & Nixon, B. (2017). The lipid peroxidation product 4-hydroxynonenal contributes to oxidative stress-mediated deterioration of the ageing oocyte. *Scientific Reports*. https://doi.org/10.1038/s41598-017-06372-z

Milkovic, L., Gasparovic, A. C., & Zarkovic, N. (2015). Overview on major lipid peroxidation bioactive factor 4-hydroxynonenal as pluripotent growth-regulating factor. *Free Radical Research*. https://doi.org/10.3109/10715762.2014.999056

Mobasheri, A., Neama, G., Bell, S., Richardson, S., & Carter, S. D. (2002). Human articular chondrocytes express three facilitative glucose transporter isoforms: GLUT1, GLUT3 and GLUT9. *Cell Biology International*. https://doi.org/10.1006/cbir.2001.0850

Mobasheri, Ali. (2012). Glucose: An energy currency and structural precursor in articular cartilage and bone with emerging roles as an extracellular signaling molecule and metabolic regulator. *Frontiers in Endocrinology*. https://doi.org/10.3389/fendo.2012.00153

Moghadam, A. R., Patrad, E., Tafsiri, E., Peng, W., Fangman, B., Pluard, T. J., … Farassati, F. (2017). Ral signaling pathway in health and cancer. *Cancer Medicine*. https://doi.org/10.1002/cam4.1105

Mow, V. C., & Guo, X. E. (2002). Mechano-Electrochemical Properties Of Articular Cartilage: Their Inhomogeneities and Anisotropies. *Annual Review of Biomedical Engineering*. https://doi.org/10.1146/annurev.bioeng.4.110701.120309

Mow, V. C., Ratcliffe, A., & Robin Poole, A. (1992). Cartilage and diarthrodial joints as paradigms for hierarchical materials and structures. *Biomaterials*. https://doi.org/10.1016/0142-9612(92)90001-5

Muir, H. (1995). The chondrocyte, architect of cartilage. Biomechanics, structure, function and molecular biology of cartilage matrix macromolecules. *BioEssays*. https://doi.org/10.1002/bies.950171208

Müller, B., & Kohn, D. (1999). [Indication for and performance of articular cartilage drilling using the Pridie method]. *Der Orthopade*.

Munarin, F., Petrini, P., Bozzini, S., & Tanzi, M. C. (2012). New perspectives in cell delivery systems for tissue regeneration: Natural-derived injectable hydrogels. *Journal of Applied Biomaterials and Functional Materials*. https://doi.org/10.5301/JABFM.2012.9418

Nelson, K. J., Bolduc, J. A., Wu, H., Collins, J. A., Burke, E. A., Reisz, J. A., …

Loeser, R. F. (2018). H2O2 oxidation of cysteine residues in c-Jun N-terminal kinase 2 (JNK2) contributes to redox regulation in human articular chondrocytes. *Journal of Biological Chemistry*. https://doi.org/10.1074/jbc.RA118.004613

Nicoll, S. B., Barak, O., Csóka, A. B., Bhatnagar, R. S., & Stern, R. (2002). Hyaluronidases and CD44 undergo differential modulation during chondrogenesis. *Biochemical and Biophysical Research Communications*. https://doi.org/10.1006/bbrc.2002.6697

Nofal, G. A., & Knudson, C. B. (2002). Latrunculin and cytochalasin decrease chondrocyte matrix retention. *Journal of Histochemistry and Cytochemistry*. https://doi.org/10.1177/002215540205001004

Occhetta, P., Visone, R., Russo, L., Cipolla, L., Moretti, M., & Rasponi, M. (2015). VA-086 methacrylate gelatine photopolymerizable hydrogels: A parametric study for highly biocompatible 3D cell embedding. *Journal of Biomedical Materials Research - Part A*. https://doi.org/10.1002/jbm.a.35346

Oh, C. Do, & Chun, J. S. (2003). Signaling mechanisms leading to the regulation of differentiation and apoptosis of articular chondrocytes by insulin-like growth factor-1. *Journal of Biological Chemistry*. https://doi.org/10.1074/jbc.M304857200

Ohba, S. (2016). Hedgehog signaling in endochondral ossification. *Journal of Developmental Biology*. https://doi.org/10.3390/jdb4020020

Olivotto, E., Otero, M., Marcu, K. B., & Goldring, M. B. (2015). Pathophysiology of osteoarthritis: Canonical NF-κB/IKKβ-dependent and kinase-independent effects of IKKα in cartilage degradation and chondrocyte differentiation. *RMD Open*. https://doi.org/10.1136/rmdopen-2015-000061

Olney, R. C., Wang, J., Sylvester, J. E., & Mougey, E. B. (2004). Growth factor

regulation of human growth plate chondrocyte proliferation in vitro. In *Biochemical and Biophysical Research Communications*. https://doi.org/10.1016/j.bbrc.2004.03.170

Onyekwelu, I., Goldring, M. B., & Hidaka, C. (2009). Chondrogenesis, joint formation, and articular cartilage regeneration. *Journal of Cellular Biochemistry*. https://doi.org/10.1002/jcb.22149

Ortega, N., Behonick, D. J., & Werb, Z. (2004). Matrix remodeling during endochondral ossification. *Trends in Cell Biology*. https://doi.org/10.1016/j.tcb.2003.12.003

Otte, P. (1991). Basic cell metabolism of articular cartilage. Manometric studies. *Zeitschrift Fur Rheumatologie*.

Pacifici, F., Arriga, R., Sorice, G. P., Capuani, B., Scioli, M. G., Pastore, D., … Lauro, D. (2014). Peroxiredoxin 6, a novel player in the pathogenesis of diabetes. *Diabetes*. https://doi.org/10.2337/db14-0144

Pallavicini, P., Chirico, G., Collini, M., Dacarro, G., Donà, A., D'Alfonso, L., … Taglietti, A. (2011). Synthesis of branched Au nanoparticles with tunable near-infrared LSPR using a zwitterionic surfactant. *Chemical Communications*. https://doi.org/10.1039/c0cc02682d

Panday, A., Sahoo, M. K., Osorio, D., & Batra, S. (2015). NADPH oxidases: An overview from structure to innate immunity-associated pathologies. *Cellular and Molecular Immunology*. https://doi.org/10.1038/cmi.2014.89

Park, H., Temenoff, J. S., Holland, T. A., Tabata, Y., & Mikos, A. G. (2005). Delivery of TGF-β1 and chondrocytes via injectable, biodegradable hydrogels for cartilage tissue engineering applications. *Biomaterials*. https://doi.org/10.1016/j.biomaterials.2005.05.083

Patel, P., & Chatterjee, S. (2019). Peroxiredoxin6 in endothelial signaling. *Antioxidants*. https://doi.org/10.3390/antiox8030063

Peppas, N. A., & Sahlin, J. J. (1989). A simple equation for the description of

solute release. III. Coupling of diffusion and relaxation. *International Journal of Pharmaceutics*. https://doi.org/10.1016/0378-5173(89)90306-2

Perkins, A., Nelson, K. J., Parsonage, D., Poole, L. B., & Karplus, P. A. (2015). Peroxiredoxins: Guardians against oxidative stress and modulators of peroxide signaling. *Trends in Biochemical Sciences*. https://doi.org/10.1016/j.tibs.2015.05.001

Pieper, J. S., Oosterhof, A., Dijkstra, P. J., Veerkamp, J. H., & Van Kuppevelt, T. H. (1999). Preparation and characterization of porous crosslinked collagenous matrices containing bioavailable chondroitin sulphate. *Biomaterials*. https://doi.org/10.1016/S0142-9612(98)00240-3

Pitsillides, A. A., & Beier, F. (2011). Cartilage biology in osteoarthritis - Lessons from developmental biology. *Nature Reviews Rheumatology*. https://doi.org/10.1038/nrrheum.2011.129

Piva, S. R., Susko, A. M., Khoja, S. S., Josbeno, D. A., Fitzgerald, G. K., & Toledo, F. G. S. (2015). Links between osteoarthritis and diabetes: Implications for management from a physical activity perspective. *Clinics in Geriatric Medicine*. https://doi.org/10.1016/j.cger.2014.08.019

Pizette, S., & Niswander, L. (2000). BMPs are required at two steps of limb chondrogenesis: Formation of prechondrogenic condensations and their differentiation into chondrocytes. *Developmental Biology*. https://doi.org/10.1006/dbio.2000.9610

Ponticiello, M. S., Schinagl, R. M., Kadiyala, S., & Barry, F. P. (2000). Gelatin-based resorbable sponge as a carrier matrix for human mesenchymal stem cells in cartilage regeneration therapy. *Journal of Biomedical Materials Research*. https://doi.org/10.1002/1097-4636(200011)52:2<246::AID-JBM2>3.0.CO;2-W

Poole, A. R., Kojima, T., Yasuda, T., Mwale, F., Kobayashi, M., & Laverty, S. (2001). Composition and structure of articular cartilage: A template for

tissue repair. In *Clinical Orthopaedics and Related Research*.

Poole, C. A., Ayad, S., & Gilbert, R. T. (1992). Chondrons from articular cartilage. V. Immunohistochemical evaluation of type VI collagen organisation in isolated chondrons by light, confocal and electron microscopy. *Journal of Cell Science*.

POOLE, C. A., ZHANG, Z.-J., & ROSS, J. M. (2001). The differential distribution of acetylated and detyrosinated alpha-tubulin in the microtubular cytoskeleton and primary cilia of hyaline cartilage chondrocytes. *Journal of Anatomy*. https://doi.org/10.1046/j.1469-7580.2001.19940393.x

Poole, L. B., & Nelson, K. J. (2016). Distribution and features of the six classes of peroxiredoxins. *Molecules and Cells*. https://doi.org/10.14348/molcells.2016.2330

Pörtner, R., Goepfert, C., Wiegandt, K., Janssen, R., Ilinich, E., Paetzold, H., … Morlock, M. (2009). Technical strategies to improve tissue engineering of cartilage-carrier- constructs. *Advances in Biochemical Engineering/Biotechnology*. https://doi.org/10.1007/978-3-540-69357-4_7

Quinn, T. M., Grodzinsky, A. J., Hunziker, E. B., & Sandy, J. D. (1998). Effects of injurious compression on matrix turnover around individual cells in calf articular cartilage explants. *Journal of Orthopaedic Research*. https://doi.org/10.1002/jor.1100160415

Rasheed, Z., Akhtar, N., & Haqqi, T. M. (2011). Advanced glycation end products induce the expression of interleukin-6 and interleukin-8 by receptor for advanced glycation end product-mediated activation of mitogen-activated protein kinases and nuclear factor-κB in human osteoarthritis chondrocytes. *Rheumatology*. https://doi.org/10.1093/rheumatology/keq380

Rasheed, Z., & Haqqi, T. M. (2012). Endoplasmic reticulum stress induces the

expression of COX-2 through activation of eIF2α, p38-MAPK and NF-κB in advanced glycation end products stimulated human chondrocytes. *Biochimica et Biophysica Acta - Molecular Cell Research*. https://doi.org/10.1016/j.bbamcr.2012.08.021

Rebhun, J. F., Chen, H., & Quilliam, L. A. (2000). Identification and characterization of a new family of guanine nucleotide exchange factors for the Ras-related GTPase Ral. *Journal of Biological Chemistry*. https://doi.org/10.1074/jbc.C000085200

Rhee, S. G., & Kil, I. S. (2017). Multiple Functions and Regulation of Mammalian Peroxiredoxins. *Annual Review of Biochemistry*. https://doi.org/10.1146/annurev-biochem-060815-014431

Ribeiro, M., López de Figueroa, P., Blanco, F. J., Mendes, A. F., & Caramés, B. (2016). Insulin decreases autophagy and leads to cartilage degradation. *Osteoarthritis and Cartilage*. https://doi.org/10.1016/j.joca.2015.10.017

Richardson, S., Neama, G., Philips, T., Bell, S., Carter, S. D., Moley, K. H., … Mobasheri, A. (2003). Molecular characterization and partial cDNA cloning of facilitative glucose transporters expressed in human articular chondrocytes; stimulation of 2-deoxyglucose uptake by IGF-I and elevated MMP-2 secretion by glucose deprivation. *Osteoarthritis and Cartilage*, *11*(2), 92–101. https://doi.org/10.1053/joca.2002.0858

Robbins, J. R., Thomas, B., Tan, L., Choy, B., Arbiser, J. L., Berenbaum, F., & Goldring, M. B. (2000). Immortalized human adult articular chondrocytes maintain cartilage-specific phenotype and responses to interleukin-1β. *Arthritis and Rheumatism*. https://doi.org/10.1002/1529-0131(200010)43:10<2189::AID-ANR6>3.0.CO;2-S

Robertson, C. M., Pennock, A. T., Harwood, F. L., Pomerleau, A. C., Allen, R. T., & Amiel, D. (2006). Characterization of pro-apoptotic and matrix-degradative gene expression following induction of osteoarthritis in mature

and aged rabbits. *Osteoarthritis and Cartilage*. https://doi.org/10.1016/j.joca.2005.11.010

Robinson, W. H., Lepus, C. M., Wang, Q., Raghu, H., Mao, R., Lindstrom, T. M., & Sokolove, J. (2016). Low-grade inflammation as a key mediator of the pathogenesis of osteoarthritis. *Nature Reviews Rheumatology*. https://doi.org/10.1038/nrrheum.2016.136

Rohindra, D. R., Nand, A. V, & Khurma, J. R. (2004). Swelling properties of chitosan hydrogels. *The South Pacific Journal of Natural and Applied Sciences*. https://doi.org/10.1071/sp04005

Roman-Blas, J. A., & Jimenez, S. A. (2006). NF-κB as a potential therapeutic target in osteoarthritis and rheumatoid arthritis. *Osteoarthritis and Cartilage*. https://doi.org/10.1016/j.joca.2006.04.008

Rosa, S. C., Rufino, A. T., Judas, F., Tenreiro, C., Lopes, M. C., & Mendes, A. F. (2011). Expression and function of the insulin receptor in normal and osteoarthritic human chondrocytes: Modulation of anabolic gene expression, glucose transport and GLUT-1 content by insulin. *Osteoarthritis and Cartilage*. https://doi.org/10.1016/j.joca.2011.02.004

Rosa, Susana C., Gonçalves, J., Judas, F., Mobasheri, A., Lopes, C., & Mendes, A. F. (2009). Impaired glucose transporter-1 degradation and increased glucose transport and oxidative stress in response to high glucose in chondrocytes from osteoarthritic versus normal human cartilage. *Arthritis Research and Therapy*. https://doi.org/10.1186/ar2713

Rosa, Susana C., Rufino, A. T., Judas, F. M., Tenreiro, C. M., Lopes, M. C., & Mendes, A. F. (2011). Role of glucose as a modulator of anabolic and catabolic gene expression in normal and osteoarthritic human chondrocytes. *Journal of Cellular Biochemistry*. https://doi.org/10.1002/jcb.23196

Rosselot, G., Vasilatos-Younken, R., & Leach, R. M. (1994). Effect of growth hormone, insulin-like growth factor I, basic fibroblast growth factor, and

transforming growth factor β on cell proliferation and proteoglycan synthesis by avian postembryonic growth plate chondrocytes. *Journal of Bone and Mineral Research*. https://doi.org/10.1002/jbmr.5650090320

Rousset, F., Hazane-Puch, F., Pinosa, C., Nguyen, M. V. C., Grange, L., Soldini, A., … Lardy, B. (2015). IL-1beta mediates MMP secretion and IL-1beta neosynthesis via upregulation of p22phox and NOX4 activity in human articular chondrocytes. *Osteoarthritis and Cartilage*. https://doi.org/10.1016/j.joca.2015.02.167

Ruiz-Romero, C., Carreira, V., Rego, I., Remeseiro, S., López-Armada, M. J., & Blanco, F. J. (2008). Proteomic analysis of human osteoarthritic chondrocytes reveals protein changes in stress and glycolysis. *Proteomics*. https://doi.org/10.1002/pmic.200700249

Russo, L., Sgambato, A., Visone, R., Occhetta, P., Moretti, M., Rasponi, M., … Cipolla, L. (2016). Gelatin hydrogels via thiol-ene chemistry. *Monatshefte Fur Chemie*. https://doi.org/10.1007/s00706-015-1614-5

Saito, T., Yano, F., Mori, D., Kawata, M., Hoshi, K., Takato, T., … Tanaka, S. (2015). Hyaline cartilage formation and tumorigenesis of implanted tissues derived from human induced pluripotent stem cells. *Biomedical Research (Japan)*. https://doi.org/10.2220/biomedres.36.179

Sandell, L. J., Nalin, A. M., & Reife, R. A. (1994). Alternative splice form of type II procollagen mRNA (IIA) is predominant in skeletal precursors and non-cartilaginous tissues during early mouse development. *Developmental Dynamics*. https://doi.org/10.1002/aja.1001990206

Sasagawa, S., Takemori, H., Uebi, T., Ikegami, D., Hiramatsu, K., Ikegawa, S., … Tsumaki, N. (2012). SIK3 is essential for chondrocyte hypertrophy during skeletal development in mice. *Development*. https://doi.org/10.1242/dev.072652

Schett, G., Kleyer, A., Perricone, C., Sahinbegovic, E., Iagnocco, A., Zwerina,

J., … Kiechl, S. (2013). Diabetes is an independent predictor for severe osteoarthritis: Results from a longitudinal cohort study. *Diabetes Care*. https://doi.org/10.2337/dc12-0924

Schmidt, N., Pautz, A., Art, J., Rauschkolb, P., Jung, M., Erkel, G., … Kleinert, H. (2010). Transcriptional and post-transcriptional regulation of iNOS expression in human chondrocytes. *Biochemical Pharmacology*. https://doi.org/10.1016/j.bcp.2009.10.012

Schulz, R. M., & Bader, A. (2007). Cartilage tissue engineering and bioreactor systems for the cultivation and stimulation of chondrocytes. *European Biophysics Journal*. https://doi.org/10.1007/s00249-007-0139-1

Scott, J. L., Gabrielides, C., Davidson, R. K., Swingler, T. E., Clark, I. M., Wallis, G. A., … Young, D. A. (2010). Superoxide dismutase downregulation in osteoarthritis progression and end-stage disease. *Annals of the Rheumatic Diseases*. https://doi.org/10.1136/ard.2009.119966

Sellam, J., & Berenbaum, F. (2013). Is osteoarthritis a metabolic disease? *Joint Bone Spine*. https://doi.org/10.1016/j.jbspin.2013.09.007

Shakibaei, M., John, T., Schulze-Tanzil, G., Lehmann, I., & Mobasheri, A. (2007). Suppression of NF-κB activation by curcumin leads to inhibition of expression of cyclo-oxygenase-2 and matrix metalloproteinase-9 in human articular chondrocytes: Implications for the treatment of osteoarthritis. *Biochemical Pharmacology*. https://doi.org/10.1016/j.bcp.2007.01.005

Shen, Y., Fu, Y., Wang, J., Li, G., Zhang, X., Xu, Y., & Lin, Y. (2014). Biomaterial and Mesenchymal Stem Cell for Articular Cartilage Reconstruction. *Current Stem Cell Research & Therapy*. https://doi.org/10.2174/1574888x09666140213202700

Shikhman, A. R., Brinson, D. C., Valbracht, J., & Lotz, M. K. (2001). Cytokine Regulation of Facilitated Glucose Transport in Human Articular Chondrocytes. *The Journal of Immunology*.

https://doi.org/10.4049/jimmunol.167.12.7001

Siddique, Y. H., Ara, G., & Afzal, M. (2012). Estimation of lipid peroxidation induced by hydrogen peroxide in cultured human lymphocytes. *Dose-Response*. https://doi.org/10.2203/dose-response.10-002.Siddique

Simkin, P. A. (2012). Consider the tidemark. *Journal of Rheumatology*. https://doi.org/10.3899/jrheum.110942

Simopoulou, T., Malizos, K. N., Iliopoulos, D., Stefanou, N., Papatheodorou, L., Ioannou, M., & Tsezou, A. (2007). Differential expression of leptin and leptin's receptor isoform (Ob-Rb) mRNA between advanced and minimally affected osteoarthritic cartilage; effect on cartilage metabolism. *Osteoarthritis and Cartilage*. https://doi.org/10.1016/j.joca.2007.01.018

Singh, P., Marcu, K. B., Goldring, M. B., & Otero, M. (2019). Phenotypic instability of chondrocytes in osteoarthritis: on a path to hypertrophy. *Annals of the New York Academy of Sciences*. https://doi.org/10.1111/nyas.13930

Singh, P., & Schwarzbauer, J. E. (2014). Fibronectin matrix assembly is essential for cell condensation during chondrogenesis. *Journal of Cell Science*. https://doi.org/10.1242/jcs.150276

Sledge, S. L. (2001). Microfracture techniques in the treatment of osteochondral injuries. *Clinics in Sports Medicine*.

Snedeker, J. G., & Gautieri, A. (2014). The role of collagen crosslinks in ageing and diabetes - The good, the bad, and the ugly. *Muscles, Ligaments and Tendons Journal*. https://doi.org/10.11138/mltj/2014.4.3.303

Sokolove, J., & Lepus, C. M. (2013). Role of inflammation in the pathogenesis of osteoarthritis: Latest findings and interpretations. *Therapeutic Advances in Musculoskeletal Disease*. https://doi.org/10.1177/1759720X12467868

Song, B., Estrada, K. D., & Lyons, K. M. (2009). Smad signaling in skeletal development and regeneration. *Cytokine and Growth Factor Reviews*.

https://doi.org/10.1016/j.cytogfr.2009.10.010

Sophia Fox, A. J., Bedi, A., & Rodeo, S. A. (2009). The basic science of articular cartilage: Structure, composition, and function. *Sports Health*. https://doi.org/10.1177/1941738109350438

Spiller, K. L., Maher, S. A., & Lowman, A. M. (2011). Hydrogels for the repair of articular cartilage defects. *Tissue Engineering - Part B: Reviews*. https://doi.org/10.1089/ten.teb.2011.0077

Sridhar, S., Botbol, Y., MacIan, F., & Cuervo, A. M. (2012). Autophagy and disease: Always two sides to a problem. *Journal of Pathology*. https://doi.org/10.1002/path.3025

St-Jacques, B., Hammerschmidt, M., & McMahon, A. P. (1999). Indian hedgehog signaling regulates proliferation and differentiation of chondrocytes and is essential for bone formation. *Genes and Development*. https://doi.org/10.1101/gad.13.16.2072

Stabler, T., Zura, R. D., Hsueh, M. F., & Kraus, V. B. (2015). Xanthine oxidase injurious response in acute joint injury. *Clinica Chimica Acta*. https://doi.org/10.1016/j.cca.2015.09.025

Stevenson, S. (1987). The immune response to osteochondral allografts in dogs. *Journal of Bone and Joint Surgery - Series A*. https://doi.org/10.2106/00004623-198769040-00015

Stickens, D., Behonick, D. J., Ortega, N., Heyer, B., Hartenstein, B., Yu, Y., … Werb, Z. (2004). Altered endochondral bone development in matrix metalloproteinase 13-deficient mice. *Development*. https://doi.org/10.1242/dev.01461

Stockwell, R. A. (1967). The cell density of human articular and costal cartilage. *Journal of Anatomy*.

Sun, M. M. G., & Beier, F. (2014). Chondrocyte hypertrophy in skeletal development, growth, and disease. *Birth Defects Research Part C - Embryo*

Today: Reviews. https://doi.org/10.1002/bdrc.21062

Suzuki, Y. J., Marcocci, L., Shimomura, T., Tatenaka, Y., Ohuchi, Y., & Brelidze, T. I. (2019). Protein Redox State Monitoring Studies of Thiol Reactivity. *Antioxidants*. https://doi.org/10.3390/antiox8050143

Takigawa, M., Tajima, K., Pan, H. O., Enomoto, M., Kinoshita, A., Suzuki, F., … Mori, Y. (1989). Establishment of a Clonal Human Chondrosarcoma Cell Line with Cartilage Phenotypes. *Cancer Research*.

Takigawa, M., Takano, T., Shirai, E., & Suzuki, F. (1984). Cytoskeleton and differentiation: effects of cytochalasin B and colchicine on expression of the differentiated phenotype of rabbit costal chondrocytes in culture. *Cell Differentiation*. https://doi.org/10.1016/0045-6039(84)90046-0

Tam, R. Y., Smith, L. J., & Shoichet, M. S. (2017). Engineering Cellular Microenvironments with Photo- and Enzymatically Responsive Hydrogels: Toward Biomimetic 3D Cell Culture Models. *Accounts of Chemical Research*. https://doi.org/10.1021/acs.accounts.6b00543

Thorogood, P. V., & Hinchliffe, J. R. (1975). An analysis of the condensation process during chondrogenesis in the embryonic chick hind limb. *Journal of Embryology and Experimental Morphology*.

Tibbitt, M. W., & Anseth, K. S. (2009). Hydrogels as extracellular matrix mimics for 3D cell culture. *Biotechnology and Bioengineering*. https://doi.org/10.1002/bit.22361

Tietze, L. F., Schröter, C., Gabius, S., Brinck, U., Goerlach-Graw, A., & Gabius, H. J. (1991). Conjugation of p-Aminophenyl Glycosides with Squaric Acid Diester to a Carrier Protein and the Use of Neoglycoprotein in the Histochemical Detection of Lectins. *Bioconjugate Chemistry*. https://doi.org/10.1021/bc00009a003

Tiku, M. L., Shah, R., & Allison, G. T. (2000). Evidence linking chondrocyte lipid peroxidation to cartilage matrix protein degradation: Possible role in

cartilage aging and the pathogenesis of osteoarthritis. *Journal of Biological Chemistry*. https://doi.org/10.1074/jbc.M907604199

Toegel, S., Wu, S. Q., Piana, C., Unger, F. M., Wirth, M., Goldring, M. B., … Viernstein, H. (2008). Comparison between chondroprotective effects of glucosamine, curcumin, and diacerein in IL-1β-stimulated C-28/I2 chondrocytes. *Osteoarthritis and Cartilage*. https://doi.org/10.1016/j.joca.2008.01.013

Tognana, E., Padera, R. F., Chen, F., Vunjak-Novakovic, G., & Freed, L. E. (2005). Development and remodeling of engineered cartilage-explant composites in vitro and in vivo. *Osteoarthritis and Cartilage*. https://doi.org/10.1016/j.joca.2005.05.003

Trickey, W. R., Vail, T. P., & Guilak, F. (2004). The role of the cytoskeleton in the viscoelastic properties of human articular chondrocytes. *Journal of Orthopaedic Research*. https://doi.org/10.1016/S0736-0266(03)0150-5

Tsai, T. L., Manner, P. A., & Li, W. J. (2013). Regulation of mesenchymal stem cell chondrogenesis by glucose through protein kinase C/transforming growth factor signaling. *Osteoarthritis and Cartilage*, *21*(2), 368–376. https://doi.org/10.1016/j.joca.2012.11.001

Tsuda, M., Takahashi, S., Takahashi, Y., & Asahara, H. (2003). Transcriptional co-activators CREB-binding protein and p300 regulate chondrocyte-specific gene expression via association with Sox9. *Journal of Biological Chemistry*. https://doi.org/10.1074/jbc.M303471200

Tuckermann, J. P., Pittois, K., Partridge, N. C., Merregaert, J., & Angel, P. (2000). Collagenase-3 (MMP-13) and integral membrane protein 2a (Itm2a) are marker genes of chondrogenic/osteoblastic cells in bone formation: Sequential temporal, and spatial expression of Itm2a, alkaline phosphatase, MMP-13, and osteocalcin in the mouse. *Journal of Bone and Mineral Research*. https://doi.org/10.1359/jbmr.2000.15.7.1257

Turrens, J. F. (2003). Mitochondrial formation of reactive oxygen species. *Journal of Physiology*. https://doi.org/10.1113/jphysiol.2003.049478

Tzeng, W. F., Lee, J. L., & Chiou, T. J. (1995). The role of lipid peroxidation in menadione-mediated toxicity in cardiomyocytes. *Journal of Molecular and Cellular Cardiology*. https://doi.org/10.1016/0022-2828(95)90021-7

Unsworth, A., Dowson, D., & Wright, V. (1975). The Frictional Behavior of Human Synovial Joints—Part I: Natural Joints. *Journal of Lubrication Technology*. https://doi.org/10.1115/1.3452605

Vaamonde-Garcia, C., Courties, A., Pigenet, A., Laiguillon, M. C., Sautet, A., Houard, X., … Sellam, J. (2017). The nuclear factor-erythroid 2-related factor/heme oxygenase-1 axis is critical for the inflammatory features of type 2 diabetes–associated osteoarthritis. *Journal of Biological Chemistry*, *292*(35), 14505–14515. https://doi.org/10.1074/jbc.M117.802157

Van den Bosch, M. H., Blom, A. B., van Lent, P. L., van Beuningen, H. M., Blaney Davidson, E. N., van der Kraan, P. M., & van den Berg, W. B. (2014). Canonical Wnt signaling skews TGF-β Signaling in chondrocytes towards signaling via ALK1 and smad 1/5/8. *Cellular Signalling*. https://doi.org/10.1016/j.cellsig.2014.01.021

Van Saase, J. L. C. M., Van Romunde, L. K. J., Cats, A., VanDenBroucke, J. P., & Valkenburg, H. A. (1989). Epidemiology of osteoarthritis: Zoetermeer survey. Comparison of radiological osteoarthritis in a Dutch population with that in 10 other populations. *Annals of the Rheumatic Diseases*. https://doi.org/10.1136/ard.48.4.271

Vandeweerd, J. M., Hontoir, F., Kirschvink, N., Clegg, P., Nisolle, J. F., Antoine, N., & Gustin, P. (2013). Prevalence of naturally occurring cartilage defects in the ovine knee. *Osteoarthritis and Cartilage*. https://doi.org/10.1016/j.joca.2013.05.006

Verzijl, N, DeGroot, J., Thorpe, S. R., Bank, R. A., Shaw, J. N., Lyons, T. J., …

TeKoppele, J. M. (2000). Effect of collagen turnover on the accumulation of advanced glycation end products. *The Journal of Biological Chemistry*, *275*(50), 39027–39031. https://doi.org/10.1074/jbc.M006700200

Verzijl, Nicole, Bank, R. A., TeKoppele, J. M., & DeGroot, J. (2003). Ageing and osteoarthritis: A different perspective. *Current Opinion in Rheumatology*. https://doi.org/10.1097/00002281-200309000-00016

Verzijl, Nicole, DeGroot, J., Zaken, C. Ben, Braun-Benjamin, O., Maroudas, A., Bank, R. A., … TeKoppele, J. M. (2002). Crosslinking by advanced glycation end products increases the stiffness of the collagen network in human articular cartilage: A possible mechanism through which age is a risk factor for osteoarthritis. *Arthritis and Rheumatism*. https://doi.org/10.1002/1529-0131(200201)46:1<114::AID-ART10025>3.0.CO;2-P

Vinatier, C., Mrugala, D., Jorgensen, C., Guicheux, J., & Noël, D. (2009). Cartilage engineering: a crucial combination of cells, biomaterials and biofactors. *Trends in Biotechnology*. https://doi.org/10.1016/j.tibtech.2009.02.005

Vincent, T. L. (2013). Targeting mechanotransduction pathways in osteoarthritis: A focus on the pericellular matrix. *Current Opinion in Pharmacology*. https://doi.org/10.1016/j.coph.2013.01.010

Višňa, P., Paša, L., Čižmář, I., Hart, R., & Hoch, J. (2004). Treatment of deep cartilage defects of the knee using autologous chondrograft transplantation and by abrasive techniques - A randomized controlled study. *Acta Chirurgica Belgica*. https://doi.org/10.1080/00015458.2004.11679648

Visser, A. W., De Mutsert, R., Le Cessie, S., Den Heijer, M., Rosendaal, F. R., Kloppenburg, M., … Penninx, B. W. (2015). The relative contribution of mechanical stress and systemic processes in different types of osteoarthritis: The NEO study. *Annals of the Rheumatic Diseases*.

https://doi.org/10.1136/annrheumdis-2013-205012

Vogel, W., Gish, G. D., Alves, F., & Pawson, T. (1997). The discoidin domain receptor tyrosine kinases are activated by collagen. *Molecular Cell*. https://doi.org/10.1016/S1097-2765(00)80003-9

Vortkamp, A., Lee, K., Lanske, B., Segre, G. V., Kronenberg, H. M., & Tabin, C. J. (1996). Regulation of rate of cartilage differentiation by Indian Hedgehog and PTH-related protein. *Science*. https://doi.org/10.1126/science.273.5275.613

Vos, T., Flaxman, A. D., Naghavi, M., Lozano, R., Michaud, C., Ezzati, M., … Moradi-Lakeh, M. (2012). Years lived with disability (YLDs) for 1160 sequelae of 289 diseases and injuries 1990-2010: A systematic analysis for the Global Burden of Disease Study 2010. *The Lancet*, *380*(9859), 2163–2196. https://doi.org/10.1016/S0140-6736(12)61729-2

Vuolteenaho, K., Moilanen, T., Al-Saffar, N., Knowles, R. G., & Moilanen, E. (2001). Regulation of the nitric oxide production resulting from the glucocorticoid-insensitive expression of iNOS in human osteoarthritic cartilage. *Osteoarthritis and Cartilage*. https://doi.org/10.1053/joca.2001.0431

Wachsmuth, L., Söder, S., Fan, Z., Finger, F., & Aigner, T. (2006). Immunolocalization of matrix proteins in different human cartilage subtypes. *Histology and Histopathology*.

Walsh, B., Pearl, A., Suchy, S., Tartaglio, J., Visco, K., & Phelan, S. A. (2009). Overexpression of Prdx6 and resistance to peroxide-induced death in Hepa1-6 cells: Prdx suppression increases apoptosis. *Redox Report*. https://doi.org/10.1179/135100009X12525712409652

Wang, J., Wang, G., & Sun, G. W. (2016). Role of PPARα in down-regulating AGE-induced TGF-β and MMP-9 expressions in chondrocytes. *Genetics and Molecular Research*. https://doi.org/10.4238/gmr.15027963

Wang, M., Sampson, E. R., Jin, H., Li, J., Ke, Q. H., Im, H. J., & Chen, D. (2013). MMP13 is a critical target gene during the progression of osteoarthritis. *Arthritis Research and Therapy*. https://doi.org/10.1186/ar4133

Wang, Q., Cai, J., Wang, J., Xiong, C., Yan, L., Zhang, Z., … Zhao, J. (2014). Down-Regulation of Adiponectin Receptors in Osteoarthritic Chondrocytes. *Cell Biochemistry and Biophysics*. https://doi.org/10.1007/s12013-014-9946-z

Weil, Y., Zeng, W., Wan, R., Wang, J., Zhou, Q., Qiu, S., & Singh, S. R. (2012). Chondrogenic differentiation of induced pluripotent stem cells from osteoarthritic chondrocytes in alginate matrix. *European Cells and Materials*.

Williams, M. F., London, D. A., Husni, E. M., Navaneethan, S., & Kashyap, S. R. (2016). Type 2 diabetes and osteoarthritis: A systematic review and meta-analysis. *Journal of Diabetes and Its Complications*, *30*(5), 944–950. https://doi.org/10.1016/j.jdiacomp.2016.02.016

Williams, S. K., Howarth, N. L., Devenny, J. J., & Bitensky, M. W. (1982). Structural and functional consequences of increased tubulin glycosylation in diabetes mellitus. *Proceedings of the National Academy of Sciences of the United States of America*. https://doi.org/10.1073/pnas.79.21.6546

Wilusz, R. E., Sanchez-Adams, J., & Guilak, F. (2014). The structure and function of the pericellular matrix of articular cartilage. *Matrix Biology*. https://doi.org/10.1016/j.matbio.2014.08.009

Windhaber, R. A. J., Wilkins, R. J., & Meredith, D. (2003). Functional characterisation of glucose transport in bovine articular chondrocytes. *Pflugers Archiv European Journal of Physiology*. https://doi.org/10.1007/s00424-003-1080-5

Wood, S. T., Long, D. L., Reisz, J. A., Yammani, R. R., Burke, E. A., Klomsiri, C., … Loeser, R. F. (2016). Cysteine-Mediated Redox Regulation of Cell

Signaling in Chondrocytes Stimulated with Fibronectin Fragments. *Arthritis and Rheumatology*. https://doi.org/10.1002/art.39326

Wood, Z. A., Poole, L. B., & Karplus, P. A. (2003). Peroxiredoxin evolution and the regulation of hydrogen peroxide signaling. *Science*. https://doi.org/10.1126/science.1080405

Woods, A., Wang, G., & Beier, F. (2007). Regulation of chondrocyte differentiation by the act in cytoskeleton and adhesive interactions. *Journal of Cellular Physiology*. https://doi.org/10.1002/jcp.21110

Wu, T. J., Lin, C. Y., Tsai, C. H., Huang, Y. L., & Tang, C. H. (2018). Glucose suppresses IL-1β-induced MMP-1 expression through the FAK, MEK, ERK, and AP-1 signaling pathways. *Environmental Toxicology*. https://doi.org/10.1002/tox.22618

Wu, W., Billinghurst, R. C., Pidoux, I., Antoniou, J., Zukor, D., Tanzer, M., & Poole, A. R. (2002). Sites of collagenase cleavage and denaturation of type II collagen in aging and osteoarthritic articular cartilage and their relationship to the distribution of matrix metalloproteinase 1 and matrix metalloproteinase 13. *Arthritis and Rheumatism*. https://doi.org/10.1002/art.10428

Wu, Y., Feinstein, S. I., Manevich, Y., Chowdhury, I., Pak, J. H., Kazi, A., … Fisher, A. B. (2009). Mitogen-activated protein kinase-mediated phosphorylation of peroxiredoxin 6 regulates its phospholipase A2 activity. *Biochemical Journal*. https://doi.org/10.1042/BJ20082061

Xu, L., Polur, I., Servais, J. M., Hsieh, S., Lee, P. L., Goldring, M. B., & Li, Y. (2011). Intact pericellular matrix of articular cartilage is required for unactivated discoidin domain receptor 2 in the mouse model. *American Journal of Pathology*. https://doi.org/10.1016/j.ajpath.2011.05.023

Xu, L., Servais, J., Polur, I., Kim, D., Lee, P. L., Chung, K., & Li, Y. (2010). Attenuation of osteoarthritis progression by reduction of discoidin domain

receptor 2 in mice. *Arthritis and Rheumatism*. https://doi.org/10.1002/art.27582

Xu, M., Bradley, E. W., Weivoda, M. M., Hwang, S. M., Pirtskhalava, T., Decklever, T., … Kirkland, J. L. (2017). Transplanted Senescent Cells Induce an Osteoarthritis-Like Condition in Mice. *The Journals of Gerontology. Series A, Biological Sciences and Medical Sciences*. https://doi.org/10.1093/gerona/glw154

Xue, E. X., Lin, J. P., Zhang, Y., Sheng, S. R., Liu, H. X., Zhou, Y. L., & Xu, H. (2017). Pterostilbene inhibits inflammation and ROS production in chondrocytes by activating Nrf2 pathway. *Oncotarget*. https://doi.org/10.18632/oncotarget.16716

Yamamoto, K., Okano, H., Miyagawa, W., Visse, R., Shitomi, Y., Santamaria, S., … Nagase, H. (2016). MMP-13 is constitutively produced in human chondrocytes and co-endocytosed with ADAMTS-5 and TIMP-3 by the endocytic receptor LRP1. *Matrix Biology*. https://doi.org/10.1016/j.matbio.2016.03.007

Yaylaoglu, M. B., Yildiz, C., Korkusuz, F., & Hasirci, V. (1999). A novel osteochondral implant. *Biomaterials*. https://doi.org/10.1016/S0142-9612(99)00062-9

Ye, W., Zhong, Z., Zhu, S., Zheng, S., Xiao, J., Song, S., … Chen, J. (2016). Advanced oxidation protein products induce catabolic effect through oxidant-dependent activation of NF-κ B pathway in human chondrocyte. *International Immunopharmacology*. https://doi.org/10.1016/j.intimp.2016.07.018

Yoo, J. U., Barthel, T. S., Nishimura, K., Solchaga, L., Caplan, A. I., Goldberg, V. M., & Johnstone, B. (1998). The chondrogenic potential of human bone-marrow-derived mesenchymal progenitor cells. *Journal of Bone and Joint Surgery - Series A*.

You, J., Wang, Z., Xu, S., Zhang, W., Fang, Q., Liu, H., … Lou, J. (2016). Advanced Glycation End Products Impair Glucose-Stimulated Insulin Secretion of a Pancreatic β-Cell Line INS-1-3 by Disturbance of Microtubule Cytoskeleton via p38/MAPK Activation. *Journal of Diabetes Research*. https://doi.org/10.1155/2016/9073037

Yu, S. M., & Kim, S. J. (2015). The thymoquinone-induced production of reactive oxygen species promotes dedifferentiation through the ERK pathway and inflammation through the p38 and PI3K pathways in rabbit articular chondrocytes. *International Journal of Molecular Medicine*. https://doi.org/10.3892/ijmm.2014.2014

Yun, H. M., Park, K. R., Lee, H. P., Lee, D. H., Jo, M., Shin, D. H., … Hong, J. T. (2014). PRDX6 promotes lung tumor progression via its GPx and iPLA2 activities. *Free Radical Biology and Medicine*. https://doi.org/10.1016/j.freeradbiomed.2014.02.001

Yusuf, E., Nelissen, R. G., Ioan-Facsinay, A., Stojanovic-Susulic, V., DeGroot, J., Van Osch, G., … Kloppenburg, M. (2010). Association between weight or body mass index and hand osteoarthritis: A systematic review. *Annals of the Rheumatic Diseases*. https://doi.org/10.1136/ard.2008.106930

Zehentner, B. K., Dony, C., & Burtscher, H. (1999). The transcription factor Sox9 is involved in BMP-2 signaling. *Journal of Bone and Mineral Research*. https://doi.org/10.1359/jbmr.1999.14.10.1734

Zhang, Y., Huang, X., & Yuan, Y. (2017). MicroRNA-410 promotes chondrogenic differentiation of human bone marrow mesenchymal stem cells through down-regulating Wnt3a. *American Journal of Translational Research*.

Zheng, H., Martin, J. A., Duwayri, Y., Falcon, G., & Buckwalter, J. A. (2007). Impact of aging on rat bone marrow-derived stem cell chondrogenesis. *Journals of Gerontology - Series A Biological Sciences and Medical*

Sciences. https://doi.org/10.1093/gerona/62.2.136

Zhu, Y., Tchkonia, T., Fuhrmann-Stroissnigg, H., Dai, H. M., Ling, Y. Y., Stout, M. B., … Kirkland, J. L. (2016). Identification of a novel senolytic agent, navitoclax, targeting the Bcl-2 family of anti-apoptotic factors. *Aging Cell*. https://doi.org/10.1111/acel.12445

Zhuo, Q., Yang, W., Chen, J., & Wang, Y. (2012). Metabolic syndrome meets osteoarthritis. *Nature Reviews Rheumatology*. https://doi.org/10.1038/nrrheum.2012.135

Zouzias, I. C., & Bugbee, W. D. (2016). Osteochondral allograft transplantation in the knee. *Sports Medicine and Arthroscopy Review*. https://doi.org/10.1097/JSA.0000000000000109

Zscharnack, M., Poesel, C., Galle, J., & Bader, A. (2009). Low oxygen expansion improves subsequent chondrogenesis of ovine bone-marrow-derived mesenchymal stem cells in collagen type I hydrogel. *Cells Tissues Organs*. https://doi.org/10.1159/000178024

Appendix I

Biochemical Pharmacology 147 (2018) 93–103

Contents lists available at ScienceDirect

Biochemical Pharmacology

journal homepage: www.elsevier.com/locate/biochempharm

FoxO-1 contributes to the efficacy of the combination of the XPO1 inhibitor selinexor and cisplatin in ovarian carcinoma preclinical models

Cristina Corno [a,1], Simone Stucchi [a,1], Michelandrea De Cesare [a], Nives Carenini [a], Serena Stamatakos [a], Emilio Ciusani [b], Lucia Minoli [c,d], Eugenio Scanziani [c,d], Christian Argueta [e], Yosef Landesman [e], Nadia Zaffaroni [a], Laura Gatti [a], Paola Perego [a,*]

[a] Molecular Pharmacology Unit, Fondazione IRCCS Istituto Nazionale dei Tumori, via Amadeo 42, 20133 Milan, Italy
[b] Laboratory of Clinical Pathology and Medical Genetics, Fondazione IRCCS Istituto Neurologico C. Besta, via Celoria 11, 20133 Milan, Italy
[c] Department of Veterinary Medicine, Università degli Studi di Milano, Via Celoria 10, 20133 Milan, Italy
[d] Mouse and Animal Pathology Laboratory, Fondazione Filarete, viale Ortles 22/4, 20139 Milan, Italy
[e] Karyopharm Therapeutics, 85 Wells Ave., Newton, MA 02459, USA

ARTICLE INFO

Article history:
Received 5 October 2017
Accepted 14 November 2017
Available online 16 November 2017

Chemical compounds:
Cisplatin (PubChem CID: 2767)
Selinexor (PubChem CID: 71481097)

Keywords:
XPO1/CRM1 inhibitors
Cisplatin
Ovarian carcinoma

ABSTRACT

The XPO1/CRM1 inhibitor selinexor (KPT-330), is currently being evaluated in multiple clinical trials as an anticancer agent. XPO1 participates in the nuclear export of FoxO-1, which we previously found to be decreased in platinum-resistant ovarian carcinoma. The aim of this study was to determine whether enriching FoxO-1 nuclear localization using selinexor would increase ovarian cancer cell sensitivity to cisplatin. Selinexor, as a single agent, displayed a striking antiproliferative effect in different ovarian carcinoma cell lines. A schedule-dependent synergistic effect of selinexor in combination with cisplatin was found in cisplatin-sensitive IGROV-1, the combination efficacy being more evident in sensitive than in the resistant cells. In IGROV-1 cells, the combination was more effective when selinexor followed cisplatin exposure. A modulation of proteins involved in apoptosis (p53, Bax) and in cell cycle progression ($p21^{WAF1}$) was found by Western blotting. Selinexor-treated cells exhibited enriched FoxO-1 nuclear staining. Knock-down experiments with RNA interference indicated that FOXO1-silenced cells displayed a reduced sensitivity to selinexor. FOXO1 silencing also tended to reduce the efficacy of the drug combination at selected cisplatin concentrations. Selinexor significantly inhibited tumor growth, induced FoxO-1 nuclear localization and improved the efficacy of cisplatin in IGROV-1 xenografts. Taken together, our results support FoxO-1 as one of the key factors promoting sensitivity towards selinexor and the synergistic interaction between cisplatin and selinexor in ovarian carcinoma cells with selected molecular backgrounds, highlighting the need for treatment regimens tailored to the molecular tumor features.

1. Introduction

Ovarian carcinoma is the most lethal gynecological disease and the seventh most common cancer in women [1]. As with most cancers, early detection increases the probability of a favorable prognosis. However, due to the lack of symptoms associated with ovarian cancer development and the absence of a reliable screening regimen, most patients are diagnosed at later times making the disease hard to treat. The current standard of care for ovarian cancer patients involves the surgical removal of tumor followed by platinum-based chemotherapy. Consistently, late diagnosis and resistance to platinum-based chemotherapy in advanced disease account for a poor survival rate [2]. Although there has been an improvement in the understanding of the molecular features of ovarian cancer owing to pathological and genomic findings [3], the acquired knowledge has not been fully translated into substantial changes to disease treatment. Thus, despite the availability of various effective second-line treatments, and of poly ADP ribose polymerase (PARP) inhibitors in a specific subset of patients harbouring BRCA1/2 mutations, there is a need for novel therapeutic approaches.

Mechanistic studies have clearly defined resistance as a multifactorial phenomenon, in part explained by evolutionary models

* Corresponding author at: Molecular Pharmacology Unit, Fondazione IRCCS Istituto Nazionale dei Tumori, via Amadeo 42, 20133 Milano, Italy.
E-mail address: paola.perego@istitutotumori.mi.it (P. Perego).
[1] Equal contribution.

https://doi.org/10.1016/j.bcp.2017.11.009
0006-2952/

of clonal selection [4]. It is unclear how clonal heterogeneity impacts resistance in ovarian carcinoma, but the major pathways accounting for reduced drug efficacy have been defined. In particular, cellular resistance to platinum compounds can involve activation of cell survival and inhibition of cell death pathways [5]. In this context, the export of nuclear proteins into the cytoplasm has been proposed to play a role in evading apoptosis and promoting tumor growth [6]. The karyopherin exportin-1 (XPO1)/Chromosome Region Maintenance-1 (CRM1), a major nuclear export receptor, participates in the nuclear export of more than 230 cargos, including tumor suppressor proteins and cell cycle regulating proteins, such as p53, $p21^{WAF1}$, and FoxO family proteins [7]. Consistently, XPO1 has been shown to regulate multiple cellular functions, including cell cycle progression, proliferation and apoptosis [8]. In cancer, XPO1 expression is frequently up-regulated in different solid tumors (e.g., gynecological cancers) [9,10] and hematological malignancies [8], suggesting that its broad range of cellular functions is critical for malignant progression. Thus, targeting XPO1 and restoring the cellular localization of XPO1 cargos, which are critical for their biological activities, have emerged as an attractive therapeutic approach [11]. Incidentally, activation of FoxO transcriptional properties has been implicated in resistance to treatment [12]. Specifically, FOXO1 has been shown to be down-regulated in cells resistant to cisplatin and target-specific agents [13,14].

Selinexor (KPT-330) is the first in class selective inhibitor of nuclear export (SINE) targeting XPO1. This orally available small molecule has demonstrated clinical activity in different tumor types as single agent or in combination with other treatments [15–17]. Selinexor has also been shown to restore platinum sensitivity in p53-dependent and independent manner in ovarian carcinoma preclinical models [18]. In addition to p53, other mechanisms have been proposed as the basis for the potent anti-cancer activity exhibited by selinexor, such as the deactivation of NF-kB or the transcriptional down-regulation of survivin [19,20]. Another pathway involves the transcriptional activity of FoxO-1 protein family, which has been implicated in the resistance to platinum-based treatment [12] and has been shown to be down-regulated in an ovarian carcinoma variant resistant to cisplatin and in lapatinib-resistant gastric cancer cells [13,14]. Because XPO1 participates in the nuclear export of FoxO-1, which we previously found to be decreased in ovarian carcinoma platinum-resistant cells, we hypothesized that FoxO-1 may contribute to the efficacy of the selinexor-cisplatin combination. Thus, the aim of this study was to examine the possibility to exploit the selinexor-induced enrichment of FoxO-1 nuclear localization to increase cisplatin sensitivity in ovarian carcinoma cells.

2. Materials and methods

2.1. Cell lines and drugs

The parental IGROV-1, cisplatin-resistant IGROV-1/Pt1, A2780 and OVCAR-5 ovarian carcinoma cell lines were obtained as previously described [13]. The TOV21G (# CRL-11730) and TOV112D (# CRL-11731) cell lines were from ATCC. All ovarian carcinoma cell lines were grown in RPMI-1640 medium (Lonza, Basel, Switzerland), supplemented with 10% FBS (Gibco, Life Technologies, Carlsbad, California). Cells were routinely checked for mycoplasma contamination (Lonza), used within 20 passages from thawing from a frozen stock, and authenticated using the Stem Elite ID System (Promega). For *in vitro* studies, cisplatin (Accord Healthcare Italia, Milan, Italy) was diluted in saline and selinexor (Karyopharm Therapeutics, Inc., Newton, MA, USA) dissolved in dimethylsulfoxide (DMSO, Sigma-Aldrich, St. Louis, Missouri). Final DMSO concentration in medium never exceeded 0.25%.

2.2. Cell growth inhibition and drug interaction analyses

Cells were seeded in 12-well plates and 24 h later exposed for 72 h to increasing concentrations of cisplatin, selinexor or to the combination. For combination studies, the cells were treated according to different schedules: a) 72 h concomitant exposure (simultaneous); b) selinexor 24 h treatment, followed by 48 h cisplatin exposure (pre-incubation with selinexor); c) pre-incubation with cisplatin for 24 h prior to addition of selinexor for 48 h (pre-incubation with cisplatin). At the end of treatment, cell growth inhibition was evaluated by counting cells (Z2 Particle Counter, Beckman Coulter, Milan, Italy). All experiments were performed at least three times. IC_{50} is defined as the concentration of a drug inhibiting 50% of cell growth. Drug interaction was evaluated according to the Chou–Talalay method, assigning a combination index (CI) value to each drug combination using the Calcusyn software (Biosoft, Cambridge, United Kingdom). CI values lower than 0.85–0.90 indicate synergistic drug interactions, whereas CI values higher than 1.20–1.45 or around 1 stand for antagonism or additive effect, respectively.

2.3. Western blot analyses

Western blot analysis was carried out as previously described [21]. Cells were lysed using 0.125 M Tris HCl pH 6.8 (Sigma-Aldrich), 5% sodium dodecyl sulfate (SDS, Lonza) and protease/phosphatase inhibitors (all purchased from Sigma-Aldrich) and a cell scraper was used to harvest cell lysate. When tumors from mice were processed, protein lysates were obtained from frozen tumor samples pulverized by a Mikro-Dismembrator II (B. Brown Biotech International, Melsungen, Germany) in lysis buffer as indicated above. Lysed samples were boiled for 5 min, sonicated for 25 s at 10% amplitude (Branson Digital Sonifier® S-250D, Emerson Electric Co, Ferguson, Missouri) and quantified using the bicinchoninic acid assay method (Pierce, Thermo Fisher Scientific, Waltham, Massachusetts, USA). Lysates were fractionated by SDS-polyacrylamide gel electrophoresis (SDS-PAGE) and proteins were transferred to nitrocellulose membranes using a wet transfer system (Trans-Blot® Turbo™ Transfert System, BIO-RAD, Milan, Italy). Binding of secondary antibodies to membranes was detected by chemiluminescence (ECL, GE Healthcare, Little Chalfont, United Kingdom). Western blot analyses were performed at least three times using independent biological cell line samples or tumors from different mice. Vinculin and actin were used as loading controls. FoxO-1 (C29H4; #2880) and Bax (# 2772) antibodies were purchased from Cell Signaling Technologies (Danvers, Massachusetts). Actin (# A2066) and vinculin (# V9131) antibodies were purchased from Sigma-Aldrich. XPO1 (ab3459), antibody was purchased from Abcam (Cambridge, United Kingdom). p53 (clone DO-7; # 544294) and $p21^{WAF1}$ (clone 70/Cip1/WAF1; # 610234) antibodies were purchased from BD Biosciences (New Jersey, USA). Secondary antibodies were obtained from GE Healthcare. Gel quantification was performed taking advantage of Image Studio Lite developed by LI-COR Biosciences (Bad Homburg vor der Höhe, Germany).

2.4. Analysis of apoptosis

Apoptosis was evaluated by Annexin V-binding assay (Immunostep, Salamanca, Spain) in IGROV-1 cells treated for 48 and 72 h with cisplatin (24 h pre-treatment) alone or in combination with selinexor and in tumors harvested from mice xenografted with IGROV-1 cells. Cells or tumor specimens, minced and mechanically dissociated on a 100 μm nylon cell strainer (BD Falcon, Milan, Italy), were washed with cold PBS. Cell suspensions were resuspended in binding buffer (10 mM HEPES-NaOH, pH

7.4, 2.5 mM $CaCl_2$, and 140 mM NaCl, Immunostep). A fraction of 10^5 cells were incubated in binding buffer at room temperature in the dark for 15 min with 5 μL of FITC-conjugated Annexin V and 10 μL of 2.5 μg/mL propidium iodide (Immunostep). Annexin V binding was detected by flow cytometry. At least 10^4 events/sample were acquired and analyzed using a specific software (CellQuestPro, Becton Dickinson).

2.5. Cell cycle analysis

Floating and adherent IGROV-1 cells were harvested and washed with saline following 48 or 72 h of treatment. Cells were pre-incubated with 0.3 μM cisplatin for 24 h prior to addition of 0.03 μM selinexor. Cells were fixed in 70% cold ethanol and incubated for 1 h at 4 °C with PBS containing 50 μg/ml propidium iodide (Sigma-Aldrich) and 1 mg/ml RNase A (Sigma-Aldrich). Cell cycle perturbations were measured using flow cytometry. At least 2×10^5 cells were collected and evaluated for DNA content. Cell cycle distribution was analyzed using FlowJo 10.

2.6. Immunofluorescence analysis

Cells were seeded in 12-well plates containing circular coverslips slides. Twenty-four hours later, cells were treated with cisplatin and, after 24 h, selinexor was added for further 24 h. Cells were fixed in 3.7% paraformaldehyde (MERCK, Darmstadt, Germany) in PBS for 15 min at room temperature. After washing in PBS, cells were incubated for 1 h in PBS containing 5% foetal bovine serum and 0.3% Triton X-100 (Fluka-Sigma-Aldrich). The coverslips slides were incubated overnight at 4 °C with the primary antibody against FoxO-1 (1:100, Cell Signaling). The slides were then washed in PBS and incubated for 1 h at room temperature with the secondary antibody conjugated with AlexaFluor 488 (1:500, Molecular Probes, Thermo Fisher). Samples were counterstained with Hoechst 33342 for 2 min and mounted with Prolong Gold AntiFade Reagent (Life Technologies). Images were collected using a fluorescence microscope (Leica Microsystems, Milan, Italy) with a Spot Insight digital camera (Delta Sistemi) equipped with a system of image analysis (IAS 2000, DeltaSistemi). Cells in three fields of the coverslips slides were counted to examine the number of FoxO-1 positive or negative nuclei.

2.7. FOXO1 loss of function studies

IGROV-1 cells were plated in 6-well plates (25,000 cells/cm^2), and 24 h later, cells were transfected using Opti-MEM transfection medium (Gibco by Life Technologies) and Lipofectamine RNAiMAX (Thermo Fisher Scientific) with 30 nM of small interfering RNA (siRNA) directed against FOXO1 (Silencer® Select s5259, Life Technologies, Thermo Fisher) or negative control siRNA (Silencer Select Negative Control #2 siRNA, Life Technologies). Cells were incubated with transfection mix for 5 h and then the transfection medium (Opti-MEM) was replaced with complete medium. Transfection efficiency was evaluated by qRT-PCR as indicated, 72 and 144 h after transfection start. Cells were harvested 72 h after transfection and were re-seeded in 12-well plates at a density of 10^4 cells/cm^2 for cell growth inhibition assays, performed after the treatment with cisplatin, selinexor or their combination (24 h pre-incubation with cisplatin followed by addition of selinexor for 48 h).

2.8. Quantitative real time PCR

RNA was isolated using the RNeasy Plus Mini Kit (Qiagen, Hilden, Germany). Reverse transcription was carried out using 1 μg RNA in the presence of RNAse inhibitors, using the High Capacity cDNA Reverse Transcription Kit according to manufacturer protocol (Applied Biosystems, Foster City, CA, USA). Gene expression was determined by quantitative Real-Time PCR (qRT-PCR) using TaqMan assays (FOXO1, Hs01054576_m1; GAPDH, Hs02758991_g1; Applied Biosystems). Technical triplicate reactions were carried out in 10 μl containing 2.5 μl cDNA, 5 μl master mix (TaqMan Universal Fast PCR Master Mix, Applied Biosystems), 0.5 μl of the specific assay. Reactions were performed using a 7900HT Fast Real-Time PCR System (Applied Biosystems) equipped with SDS (Sequence Detection Systems) 2.4 software (Applied Biosystems). Data analysis was performed with RQ manager software (Applied Biosystems). Relative levels of cDNA were determined as previously described [21], through the relative quantification (RQ) method. Untransfected cells were chosen as calibrator.

2.9. Antitumor activity studies

All experiments were carried out using 8–10 week-old female athymic CD-1 nude mice, (Charles River, Calco, Italy). Mice were maintained in laminar flow rooms at constant temperature and humidity with free access to food and water. Experiments were authorized by the Italian Ministry of Health according to the national law in compliance with international policies and guidelines. Selinexor was dissolved in Pluronic F-68 and PVP K-29/32 following manufacturer's instructions; cisplatin was diluted in saline. The compounds were delivered in a volume of 10 ml/kg of body weight.

IGROV-1 and IGROV-1/Pt1 human ovarian carcinoma xenografts were used in the study. Exponentially growing cells (10^7-/mouse) were subcutaneously injected into the right flank on day 0. Tumor diameter growth was observed biweekly using a Vernier caliper. Tumor volume (TV) was calculated according to the formula: TV (mm^3) = $d^2 \times D/2$, where d and D are the shortest and the longest diameters, respectively. Treatment started 5–6 days after cell inoculum, when tumors were established (around 90 mm^3 TV). As single treatment, 10 mg/kg selinexor was delivered orally every 3–4 days a week for 4 weeks and 4.5 mg/kg cisplatin i.v. every week for 3 weeks. In combination studies, selinexor at a dose of 5 mg/kg was delivered 24 h after cisplatin. Student's *t* test (two-tailed) was used for statistical comparison of TV in mice. Alternatively, IGROV-1 cells from cultures (10^7/mouse) were i.p. injected. For ethical reasons, the animals were inspected and weighed daily, and were sacrificed at the appearance of ascites. The days of disease onset were recorded and the median day (considered as median survival time, MST) was calculated. Treatment started 4 days after cell inoculum orally delivering 10 mg/kg selinexor every 3–4 days for 6 times. The ascitis take, i.e. the ratio between the number of mice developing ascitis over the number of cell-injected mice, was employed to assess treatment efficacy. T/C%, i.e. the ratio of MST in treated over control mice x 100 was calculated. A careful necropsy was performed to evaluate the ovarian tumor take and spread in the abdominal cavity. Solid masses were gently detached from organs and abdominal walls, removed and weighed to calculate the percentage of tumor weight inhibition (TWI%) in mice. For statistical analysis two-sided Student's *t* test was used to compare i.p. tumor weights in mice. Percent of disease-free mice over time was estimated by the Kaplan-Meier product method and compared by the Log-rank test.

2.10. Immunohistochemical evaluation of FoxO-1

IGROV-1 subcutaneous tumors were removed from mice 24 h after the last treatment (n = 8 for control group; n = 7 for selinexor group), fixed in 10% buffered formalin, and paraffin-embedded.

Sections (4 μm thick) were stained with haematoxylin-eosin for histopathological examination. Serial sections were stained immunohistochemically for FoxO-1. After heat-induced epitope retrieval, sections were incubated for one hour at room temperature with the primary antibody anti-FoxO-1 (1:100, rabbit monoclonal from Cell Signaling Technologies). Then incubated with a biotinylated secondary antibody (anti-rabbit IgG, Vinci Biochem) and labeled by the avidin-biotin-peroxidase (ABC) procedure with a commercial immunoperoxidase kit (Vectastain Standard Elite, Vector Laboratories, Burlingame, CA). The immunoreaction was revealed with 3,3′-diaminobenzidine substrate (Vector Laboratories, Burlingame, CA) for 5 min and sections were counterstained with Mayer's haematoxylin. Three microscopic fields were evaluated for each sample at 400×, to assess the number of cells in which the FoxO-1 protein was expressed in the nucleus. Histological and immunohistochemical analyses were performed in a blind fashion. Results were expressed as percent of cells with nuclear expression. Statistical analysis was performed by the Mann Whitney test.

2.11. Statistical analysis

Statistical analyses were performed using the GraphPad Prism™ software (GraphPad Software, San Diego, CA) as detailed in each paragraph. In addition, Student's *t* test (two tailed) was used for statistical analysis of western blots when comparing band intensities, after normalization with loading controls.

3. Results

3.1. Selinexor inhibits cell growth in ovarian carcinoma cell lines with variable FoxO-1 protein levels

Sensitivity to the XPO1 inhibitor selinexor was examined using growth-inhibition assays after 72 h drug exposure in the following ovarian carcinoma cell lines: A2780, OVCAR-5, TOV21G, TOV112D, IGROV-1 and the cisplatin-resistant variant IGROV-1/Pt1 (Table 1). In all tested cell lines, the IC_{50} values were in the submicromolar range. A striking antiproliferative effect was also observed in cell lines characterized by intrinsic (i.e., OVCAR-5) or acquired cisplatin resistance (IGROV-1/Pt1).

Western blot analyses indicated that the different cell lines all expressed the target of selinexor and variable levels of FoxO-1 were displayed by the cell lines (Fig. 1A), with decreased FoxO-1 in IGROV-1/Pt versus IGROV-1 cells ($P < 0.05$ by Student's *t* test, n = 3).

3.2. Selinexor displays a schedule-dependent interaction with cisplatin in FOXO1-expressing ovarian carcinoma cells

The transcription factor FoxO-1 has been reported to be a cargo of XPO1 [8]. We previously found that FOXO1 is down-regulated in the cisplatin-resistant variant IGROV-1/Pt1 [13]. IGROV-1 and IGROV-1/Pt1 cells were selected for drug combination studies, based on their differential expression of FoxO-1.

IGROV-1 cells were simultaneously exposed to increasing cisplatin and selinexor (0.01 and 0.03 μM) concentrations as single agents or in combination. The cells were exposed to selinexor concentrations of 0.01 and 0.03 μM, which represent subtoxic and near IC_{50} concentrations, respectively (Fig. 1B). According to the CI values calculated with the Chou and Talalay method, selinexor tended to synergize with cisplatin when 0.03 μM selinexor was combined with cisplatin concentrations ranging between 0.3 and 0.03 μM, which are at or below the IC_{50} value of cisplatin. CI values obtained with 0.01 μM selinexor ranged between 0.85 (with 0.03 μM cisplatin) and 2.39 (with 3 μM cisplatin).

Table 1
Sensitivity of ovarian carcinoma cell lines to cisplatin and to the XPO1 inhibitor selinexor.[1]

Cell line	Cisplatin	Selinexor
IC_{50} (μM)[2]		
A2780	0.4 ± 0.1	0.0173 ± 0.028
OVCAR-5	2.27 ± 0.7	0.2 ± 0.075
TOV21G	0.035 ± 0.01	0.058 ± 0.007
TOV112D	1.41 ± 0.1	0.068 ± 0.007
IGROV-1	0.33 ± 0.1	0.0178 ± 0.01
IGROV-1/Pt1	3.4 ± 1.3	0.0575 ± 0.02

[1] Sensitivity to cisplatin and to the inhibitor of XPO1 was assessed by cell growth inhibition assays. Cells were seeded and 24 h later exposed to the compounds for 72 h. Cells were counted using a cell counter.
[2] IC_{50} is defined as the concentration inhibiting cell growth by 50%. The reported values are the mean ± SD of at least three independent experiments.

The effect of the drug combination was not synergistic in the IGROV-1/Pt1 cells using the simultaneous schedule of treatment when employing 0.03 μM selinexor (Fig. 1C). Also CI values obtained with 0.01 μM selinexor, which ranged between 0.72 (with 0.03 μM cisplatin) and 4.26 (with 1 μM cisplatin), indicated a less favorable effect of the combination in the resistant variant.

Additional treatment schedules were tested in IGROV-1 cells to further optimize the effect of the drug combination. Specifically, we tested the effect of pre-incubation with selinexor prior to the addition of cisplatin, and *vice versa*.

In IGROV-1 cells pre-incubated with selinexor for 24 h prior to a 48 h co-incubation with cisplatin, the CI mean values ranged between 0.9 and 2.03, when the selinexor concentration was 0.03 μM (Fig. 2A). The CI values were always >1 in combination with 0.01 μM selinexor (data not shown). Conversely, a 24 h incubation with cisplatin prior to the co-incubation of the two drugs resulted in a synergistic effect evidenced at cisplatin concentrations below or near the IC_{50} values combined with 0.03 μM selinexor (Fig. 2B). This schedule appeared to be the most effective as CI values lower than 0.7 were obtained at 3 different cisplatin concentrations. When cisplatin was combined with 0.01 μM selinexor, the most favorable CI value was 0.91 ± 0.16, obtained in combination with 0.3 μM cisplatin.

The effect of the drug combination was also tested in an additional cell model, the TOV21G cell line, characterized by a remarkable FoxO-1 protein level. In cells pre-incubated with cisplatin before selinexor-cisplatin incubation, CI values below 0.7 were observed when 0.03 μM selinexor was combined with 0.03 and 0.1 μM cisplatin (Fig. 3).

3.3. Analysis of cell response to the drug combination in IGROV-1 cells

Cell response to the drug combination was examined with reference to proteins involved in cell cycle progression and apoptosis. We found that selinexor alone (0.03 μM) or in combination with cisplatin (0.3 μM) tended to induce an increase in $p21^{WAF1}$ (Student's *t* test – 48 h: $P = 0.05$ for selinexor versus control; $P < 0.05$ for combination versus control; 72 h: $P = 0.08$ for selinexor versus control; $P < 0.05$ for combination versus control; n = 3) and p53 (Student's *t* test – 48 h: $P = 0.06$ for selinexor versus control; $P = 0.06$ for combination versus control; 72 h: $P = 0.08$ for selinexor versus control; $P < 0.05$ for combination versus control, n = 3) in IGROV-1 cells (Fig. 4A). Bax up-modulation upon treatment was also observed ($P < 0.05$ for selinexor/combination versus control at 48 and 72 h by Student's *t* test, n = 3). In contrast, a negligible modulation of FoxO-1 levels was observed in treated as compared to control cells. The pattern of $p21^{WAF1}$ and Bax modulation was somehow similar when using a lower cisplatin concentration (0.1 μM) (data not shown). Selinexor (0.03 μM) alone and in

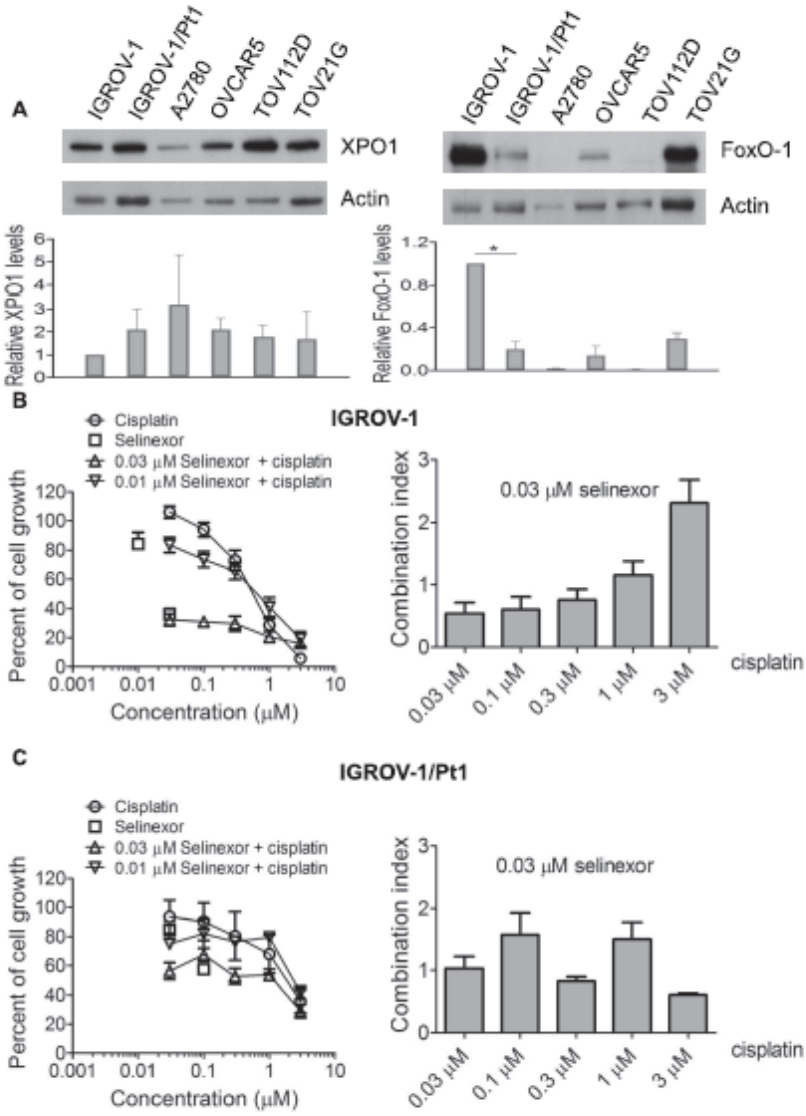

Fig. 1. Western blot analysis of XPO1 and FoxO-1 levels in ovarian carcinoma cell lines and effect of the simultaneous combination of cisplatin and selinexor. (A) Western blot analysis was carried out in ovarian carcinoma exponentially growing cells. Control loading is shown by actin. One experiment representative of 3 is reported. Band intensities were quantified (mean ± SE, n = 3) using ImageJ, normalized to actin and referred to IGROV-1 cells (set to 1). *, $P < 0.05$ by two tailed unpaired Student's t test. Cell sensitivity to drugs was assessed by cell growth inhibition assays in IGROV-1 (B) and IGROV-1/Pt1 (C) cells. Cells were seeded and 24 h later exposed to cisplatin and selinexor for 72 h. Cells were then counted using a cell counter. The combination index values obtained with the 0.03 μM selinexor concentration combined with different cisplatin concentrations are shown. The reported values are the mean ± SE of at least three independent experiments.

combination with cisplatin (0.3 μM) promoted FoxO-1 nuclear accumulation as shown by immunofluorescence analysis carried out 48 h after cisplatin exposure start (Fig. 4B). Analysis of cell cycle perturbations indicated that cells in G1 phase increased after 48 h selinexor treatment ($P < 0.05$ of selinexor-treated versus control cells by unpaired Student's t test, Fig. 4C). The drug combination induced the accumulation of cells in G2/M phase at 48 h and 72 h of exposure ($P < 0.05$ of cells treated with versus control cells/single agents treated cells by unpaired Student's t test). Moreover, the drug combination induced apoptosis in IGROV-1 cells pre-treated with cisplatin for 24 h and co-incubated with selinexor for additional 48 h, as shown by Annexin V-binding assay (Fig. 4D).

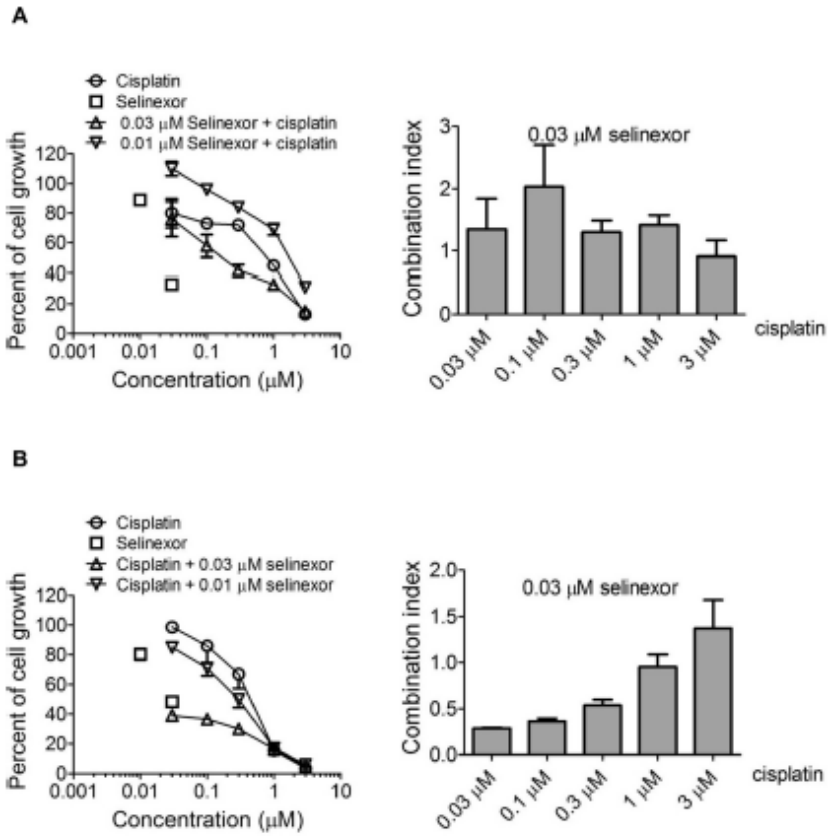

Fig. 2. Effect of the combination of cisplatin and selinexor in IGROV-1 cells according to different schedule treatments. Sensitivity to drugs was assessed by cell growth inhibition assays in IGROV-1 cells. (A) Cells were pretreated with selinexor for 24 h before coincubation with cisplatin for 48 h or (B) pre-incubated with cisplatin for 24 h before concomitant exposure to cisplatin-selinexor for 48 h. Cells were then counted using a cell counter. The combination index values obtained with the 0.03 μM selinexor concentration combined with different cisplatin concentrations are shown. The reported values are the mean ± SE of at least three independent experiments.

3.4. Effect of FOXO1 silencing on the cell response to the drug combination in IGROV-1 cells

We examined the effect of knocking down FOXO1 expression in IGROV-1 cells to clarify its contribution to the efficacy of the drug combination. Transient transfection of siRNA duplexes targeting FOXO1 mRNA markedly reduced the levels of FoxO-1 mRNA and protein (Fig. 5A and B, for western blot analysis at 72 h: $P < 0.05$ for comparison of negative control transfected cells versus siRNA transfected cells by Student's t test, n = 3). FOXO1 silencing resulted indecreased sensitivity to selinexor (IC_{50} > 0.3 μM in FOXO1 knock-down cells and 0.05 ± 0.001 μM in untransfected and negative control-transfected cells) and the cisplatin-selinexor combination tended to be slightly less effective as indicated by CI values at 0.3 and 1 μM obtained with 24 h pre-incubation with cisplatin followed by additional 48 h exposure to 0.03 μM selinexor (Fig. 5C).

3.5. Antitumor activity of selinexor in ovarian carcinoma in vivo models

The antitumor activity of oral selinexor was assayed in nude mice subcutaneously bearing the IGROV-1 and IGROV-1/Pt1 carcinomas. Selinexor significantly impaired tumor growth in both models producing TVI of 78 and 74% in IGROV-1 and IGROV-1/Pt1, respectively (Fig. 6A and Table 2). Immunohistochemical analysis of the intracellular localization of FoxO-1 in vehicle and selinexor-treated IGROV-1 tumors revealed that selinexor induced a nuclear enrichment of FoxO-1, as shown by the percent of cells with nuclear FoxO-1 expression whose median value was 0.45 (confidence interval 0.17–0.77, n = 8) in control and 8.30 (confidence interval 2.71–14.43, n = 7) in treated samples ($P < 0.001$, Mann Whitney's test, Fig. 6B).

The effects of oral selinexor were also evaluated on the IGROV-1 model system growing as i.p. carcinomatosis. Solvent-treated mice presented evidence of ascites by 17 days after cell injection and fluid and tumor masses in the peritoneal space at necropsy (Fig. 6C). In contrast, selinexor-treated mice did not exhibit ascites on the day of sacrifice (day 23, T/C > 164%, $P = 0.0002$), i.e., 6 days after the last disease appearance in the controls. Moreover, at necropsy, the animals receiving selinexor presented a reduced i. p. tumor load with respect to controls (TWI = 75%, $P = 0.0003$). Specifically, the tumor weights were 0.224 ± 0.146 and 0.914 ± 0. 303 g in treated and control groups, respectively. Therefore, the XPO1 inhibitor could impair the growth of the IGROV-1 carcinoma, even when this was xenografted in the abdominal cavity.

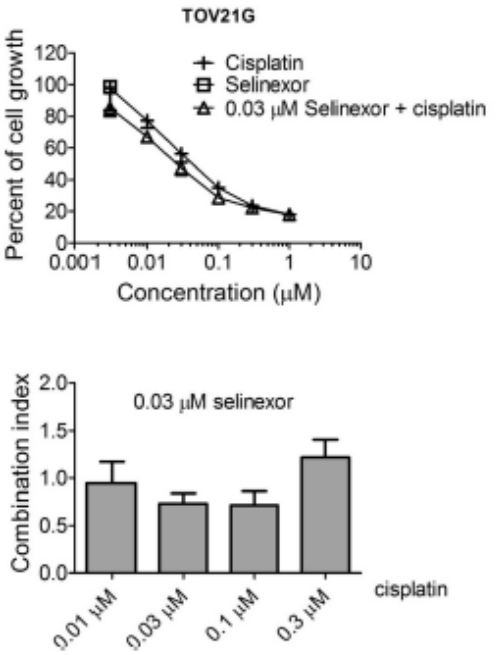

Fig. 3. Effect of the combination of cisplatin and selinexor in TOV21G cells. Cell sensitivity to drugs was evaluated by growth-inhibition assays. TOV21G cells were pre-incubated with cisplatin for 24 h before concomitant exposure to cisplatin-selinexor for 48 h. Cells were then counted using a cell counter. The combination index values obtained with the 0.03 μM selinexor concentration combined with different cisplatin concentrations are shown. The reported values are the mean ± SE of at least three independent experiments.

The effects of the combination of selinexor and cisplatin were also tested. Cisplatin and selinexor were sequentially delivered at suboptimal doses to mice bearing the subcutaneous IGROV-1 tumor (Fig. 6D). Despite negligible activity of single agents, the combination induced 65% TVI ($P < 0.001$ versus control mice and $P < 0.05$ versus cisplatin-treated mice), the effect being similar to that achieved by selinexor at its optimal dose and schedule, i.e. a TVI of 70% on day 16 (Table 2). All treatments were well tolerated. An analysis of apoptosis in tumors harvested 24 h after the last treatment indicated that the drug combination induced the highest level of apoptosis ($P < 0.01$, drug combination versus selinexor by Student's *t* test) (Fig. 6E). Treatment with the drug combination tended to increase $p21^{WAF1}$ protein levels as compared to the effect of selinexor alone (Student's *t* test: $P = 0.07$ for selinexor versus combination, Fig. 6F, n = 3). A slight up-modulation of p53 was observed under the same conditions, although it was not significant. FoxO-1 protein levels were not modulated.

4. Discussion

Cellular response to antitumor treatments involves multiple factors including components of apoptotic pathways. Tumor cell resistance to clinically available agents (e.g., cisplatin) is often associated with reduced susceptibility to drug-induced apoptosis, which can be related to reduced expression of the FoxO-1 transcription factor, a regulator of pro-apoptotic genes like PUMA and TRAIL [12,22,23]. XPO1, a nuclear export protein, contributes to the dynamic subcellular localization of FoxO-1, among other proteins promoting apoptosis induction [24,25]. Thus, the interference with XPO1 to improve FoxO-1 nuclear localization may be exploited to enhance cisplatin efficacy and represents a novel effective therapeutic strategy in this disease.

In this study, we used ovarian carcinoma cell lines representing different ovarian carcinoma histologies [26]. All cell lines displayed a marked sensitivity to selinexor which inhibited cell growth at submicromolar concentrations, and a variable sensitivity to cisplatin, not necessarily explained by FoxO-1 levels, but likely multifactorial, as A2780 cells similarly sensitive to cisplatin as IGROV-1 cells exhibited lower FoxO-1 levels than IGROV-1 cells. A marked sensitivity to the antiproliferative effect of selinexor was also observed in IGROV-1/Pt1 cells. The therapeutic potential of selinexor has been recently highlighted by the work of Chen *et al.*, [18] in which treatment efficacy was evaluated in an *in vivo* platinum-resistant ovarian carcinoma model as well as in *in vitro* models in which synergism was found in a cisplatin-resistant variant derived from A2780 cells, suggesting that the type of drug interaction may be dependent on the tumor molecular background. Previous studies have also pointed out the relevance of XPO1 inhibition in ovarian carcinoma, showing the growth inhibitory and pro-apoptotic effect of leptomycin B, the first discovered inhibitor of XPO1 mediated nuclear export, which proved inadequate for drug development due to *in vivo* toxicity [8]. Western blot analyses suggest that the sensitivity to the compound is not solely dependent on the XPO1 expression levels.

Given a genome-wide expression analysis [27] which identified FOXO1 as down-regulated in platinum-resistant ovarian carcinoma cells [12] and the known susceptibility to drug-induced apoptosis of IGROV-1 cells [12,28], this model was considered the most suitable for evaluation of the effect of the cisplatin-selinexor combination. The drug combination effect proved to be schedule dependent, as the best synergism was achieved in IGROV-1 cells when selinexor was added 24 h after cisplatin exposure. A favorable effect of the drug combination, although less marked than in IGROV-1 cells, was observed in the TOV21G cell line, likely due to the different features as reported based on an integrated analysis of immunohistochemical markers, copy number variations and mutations [29].

To define the mechanism underlying the drug interaction in IGROV-1 cells, we first examined the modulation of proteins involved in cell cycle arrest and apoptosis. The cell cycle protein $p21^{WAF1}$, undetectable in vehicle-treated cells, was markedly up-regulated in cells exposed to the selinexor-cisplatin combination. The combination-treated cells also exhibited higher levels of $p21^{WAF1}$ when compared to single agent-treated cells (similar to what was found in *in vivo* studies). A similar pattern was observed with p53, as expected based on the well-known transcriptional regulation of $p21^{WAF1}$ by p53. The effect on $p21^{WAF1}$ levels is likely p53-dependent in keeping with the presence of functional p53 in IGROV-1 cells [28]. Moreover, the pro-apoptotic protein Bax was up-regulated 48 and 72 h following every treatment, thereby indicating that the apoptotic pathway was triggered by all treatments. However, none of the treatments induced an up-regulation of FoxO-1 protein levels in total cell lysates. A quantitative analysis of drug-induced apoptosis by Annexin V-binding assay indicated the occurrence of apoptosis after exposure to each agent, although the effect was remarkable only upon exposure to the drug combination. Moreover, cell cycle perturbations were observed in treated cells with G1 accumulation after 48 h exposure to selinexor and time-dependent G2/M accumulation after exposure to the drug combination.

Fluorescence microscopy experiments in cells stained with an anti FoxO-1 antibody indicated that selinexor could promote nuclear localization of FoxO-1 in IGROV-1 cells, suggesting that under our experimental conditions XPO1-mediated nuclear export

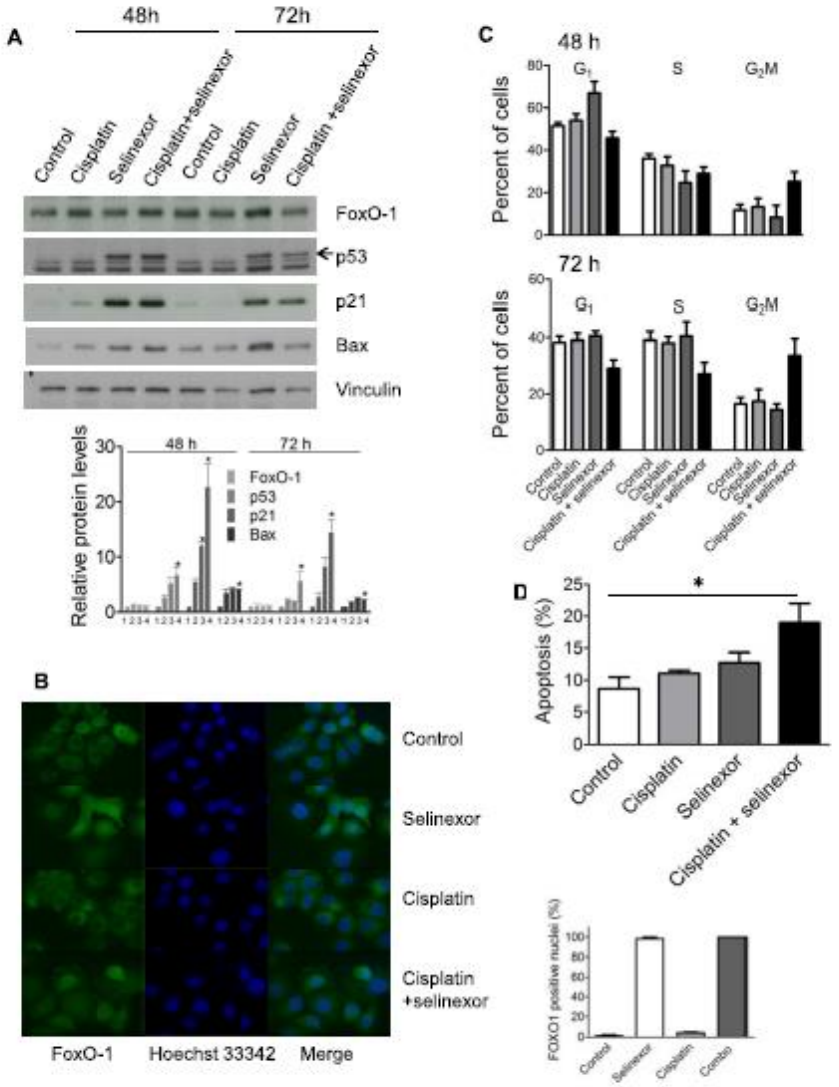

Fig. 4. Cell response to the combination of selinexor and cisplatin in IGROV-1 cells. (A) Western blot analysis was carried out in cells incubated with 0.3 μM cisplatin, 0.03 μM selinexor or their combination adding selinexor 24 h after cisplatin. Protein lysates were prepared from cells harvested 48 h or 72 h after cisplatin exposure start. Control loading is shown by vinculin. For each protein band intensity was quantified using ImageJ (mean ± SE, n = 3), normalized to loading control and referred to the levels of control cells (set to 1). 1, control; 2, cisplatin; 3, selinexor; 4, combination. *, $P < 0.05$ versus control by two tailed unpaired Student's *t* test (n = 3). (B) Immunofluorescence analysis of FoxO-1 (green) after cell treatment with 0.03 μM selinexor, 0.3 μM cisplatin or their combination adding selinexor 24 h after cisplatin. Cells were observed 24 h after selinexor exposure start. Nuclei were visualized by staining with Hoechst 33342. Cells were scored by fluorescence microscopy for FoxO-1 localization. Counts from three independent fields/group are shown. (C) Cell cycle analysis of cells incubated with cisplatin, selinexor or their combination as described in A. Cells were stained with propidium iodide and analyzed by flow cytometry. (D) Analysis of apoptosis in IGROV-1 cells exposed to cisplatin, selinexor and their combination adding selinexor 24 h after cisplatin. Apoptosis was assessed by Annexin V-binding assay 48 h after selinexor treatment start. *, $P < 0.005$ by two tailed unpaired Student's *t* test.

of FoxO-1 is inhibited; the effect was maintained in cells treated with the combination of cisplatin and selinexor.

The interest of selinexor for the treatment of ovarian carcinoma is supported by our antitumor efficacy studies, indicating a striking activity of the compound both in platinum-sensitive and resistant subcutaneous xenografts. Although cellular studies indicated that knockdown of FOXO1 results in reduced selinexor growth inhibitory activity, a significant tumor growth inhibition was found *in vivo* also in IGROV-1/Pt1, consistently with the capability of selinexor to regulate the localization of multiple proteins. It should

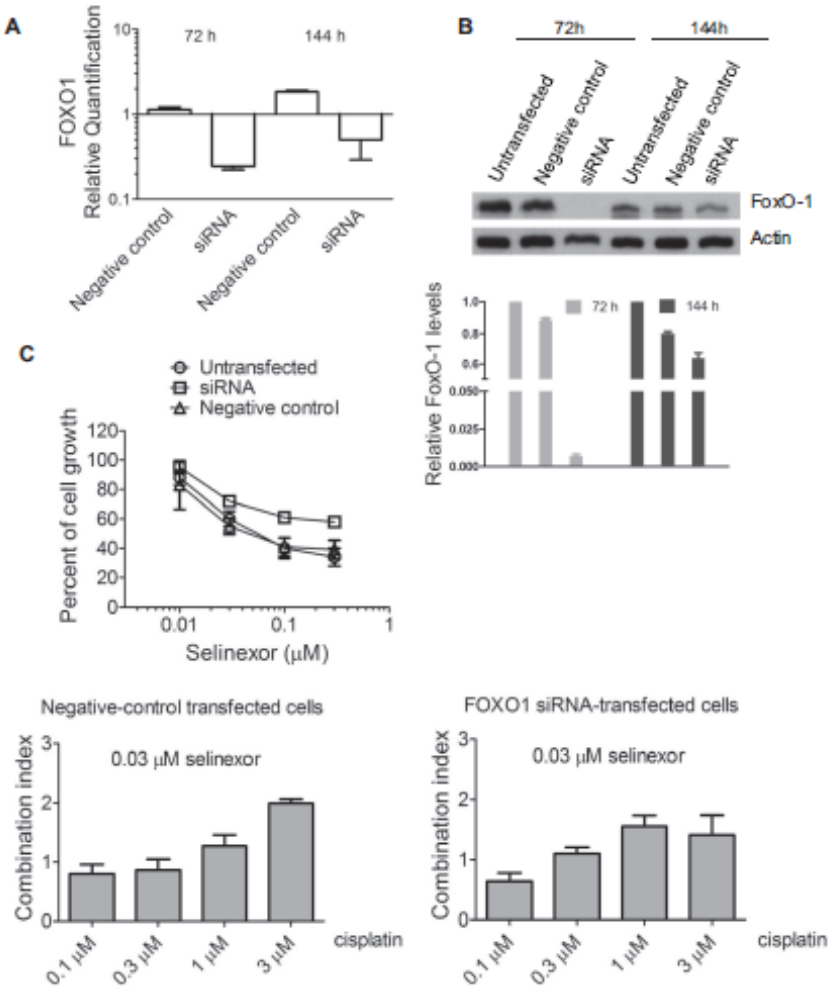

Fig. 5. Efficacy of cisplatin, selinexor and their combination upon FOXO1 knockdown. (A) qRT-PCR of FOXO1 levels in IGROV-1 cells at different times after siRNA transfection; untransfected cells were used as calibrator and GAPDH as housekeeping. RQ values (±SD) from triplicates are shown. (B) Western blot analysis of FoxO-1 levels in IGROV-1 cells at different times after siRNA transfection. The band intensity was quantified using ImageJ, normalized to loading control and referred to the levels of untransfected cells (set to 1). *, $P < 0.05$ FOXO1 siRNA- versus negative control siRNA transfected cells by two tailed unpaired Student's *t* test (n = 3). (C) Sensitivity of IGROV-1 cells to selinexor and effect of the selinexor-cisplatin combination. Cells were transfected with siRNA and 48 h later harvested and seeded for growth inhibition assays. Cells were incubated with cisplatin and 24 h later selinexor was added for 48 h. Cells were counted using a cell counter. The combination index values obtained with the 0.03 μM selinexor concentration combined with different cisplatin concentrations are shown. The reported values are the mean ± SE of at least three independent experiments.

be noted that orally administered selinexor exhibited a marked capability to reduce intraperitoneal tumor growth in cell-injected mice, in keeping with previous results obtained in orthotopic peritoneal mesothelioma model [30]. Moreover, selinexor-treated mice did not develop ascites, a clinically relevant observation. When selinexor and cisplatin were combined according to the best schedule identified in *in vitro* studies, a therapeutic advantage in terms of TVI was found as compared to single agents. These results are consistent with those by Chen et al., although we used a much lower selinexor dose [18]. In fact, drug combination experiments were carried out using a low dose of selinexor (5 mg/kg) given only once per week. Such a schedule has been shown to preserve normal immune functioning [31]. Thus, our findings may be useful in an attempt to optimize clinical dosing. Of note, a phase I clinical study has provided promising results in platinum-resistant ovarian cancer patients [18].

In conclusion, our findings show that FoxO-1 finely modulates the effect of selinexor and marginally of the combination with cisplatin providing preclinical evidence of potential clinical impact on ovarian carcinoma with selected molecular backgrounds. These results highlight the interest of combination therapies designed to increase cell death in tumor cells. However, given that XPO1 can

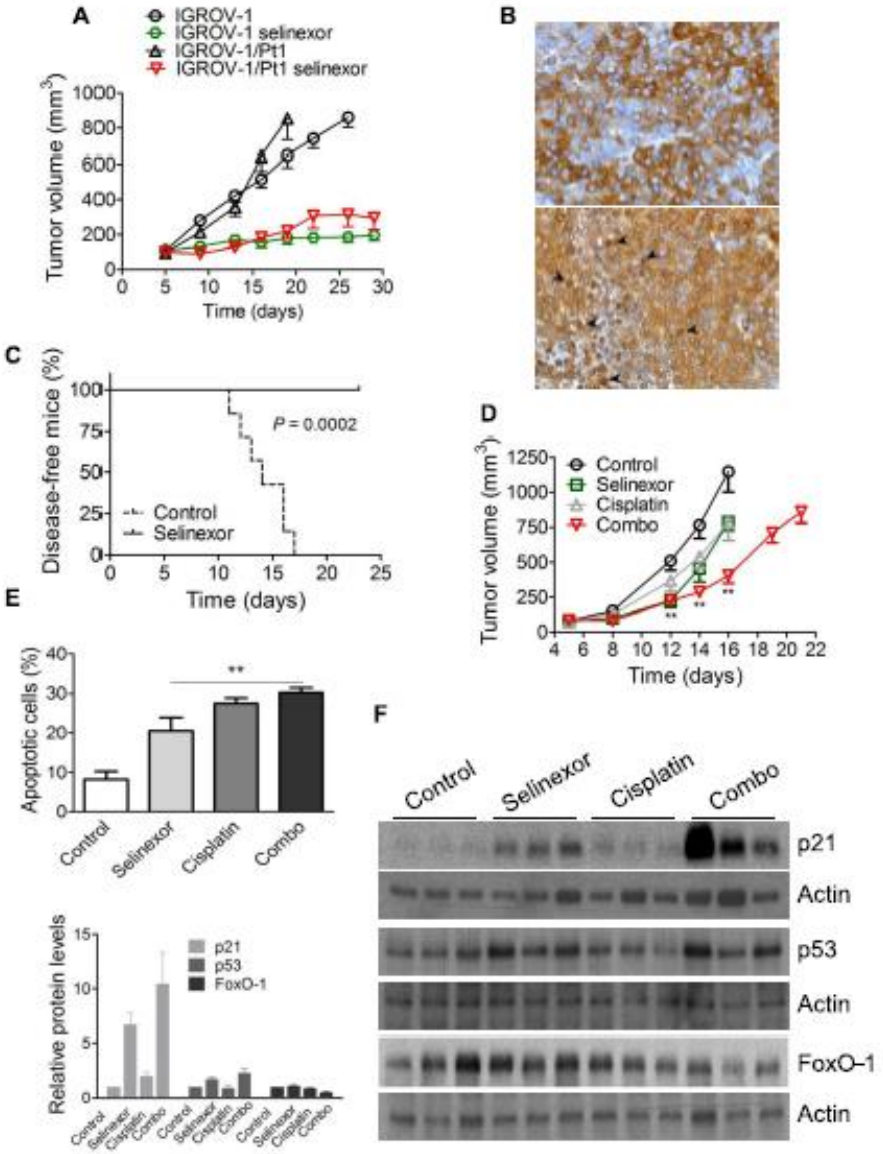

Fig. 6. Antitumor activity studies and analysis of apoptosis and protein modulation in tumors from mice treated with selinexor, cisplatin and their combination (combo). (A) Effects of oral selinexor, 10 mg/kg q3–4d/wx4w, on the growth of the IGROV-1 and IGROV-1/Pt1 carcinoma cells s.c. injected into the right flank of female nude mice (n = 8; 10^7 cells/mouse) on day 0. Treatment started on day 5–6. Mean values of tumor volumes (± SD) are shown. (B) IGROV-1 tumors from control and treated mice harvested 24 h after last treatment were processed for immunohistochemical analysis of FoxO–1. Cells with different pattern of expression of FoxO–1 with cytoplasmic positivity (top) and with both cytoplasmic and nuclear (arrowhead) positivity (bottom) are shown at 400x. (C) Effects of oral selinexor, 10 mg/kg q3–4d6, on the ascites onset in mice i.p. injected with the IGROV-1 carcinoma cells (n = 7; 10^7 cells/mouse) on day 0. Treatment started on day 4. Kaplan-Meier plot of the percentage of disease-free animals. P by log-rank test. (D) Effects of oral 5 mg/kg selinexor on the antitumor activity of 4.5 mg/kg i.v. cisplatin against the growth of the IGROV-1 carcinoma cells s.c. injected into the right flank of female nude mice (n = 7; 10^7 cells/mouse) on day 0. Cisplatin was given on day 5, 12 and 19, selinexor on day 6, 13 and 20. Mean values of tumor volumes (± SD) are shown. $^{**}P < 0.001$ by Student's t test versus control mice. (E) Samples from control and treated mice were processed for apoptosis analysis by Annexin V binding assay 24 h after the last selinexor treatment. The columns indicate late apoptotic (Annexin V-PI positive cells) cells. The values represent the mean ± SD. **, $P < 0.01$ by two-tailed unpaired Student's t test. (F) Tumors from control and treated mice were processed for western blot analyses to examine levels of the indicated proteins. Samples obtained from 3 mice/group 24 h after the last selinexor treatment were fractionated by SDS-PAGE. Control loading is shown by actin. Mean values with respect to control mean value arbitrarily set to 1 are shown in the histograms (n = 3).

Table 2
Antitumor activity of oral selinexor alone or in combination with cisplatin in nude mice s.c. bearing human ovarian carcinomas.[1]

Model	Drug	Days of treatment	Dose (mg/kg)	TVI% (day)[2]	BWL%[3]	Tox[4]
IGROV-1/Pt1	Selinexor	5, 8, 12, 16, 20, 23, 26, 29	10	69** (16) 74* (20)	5	0/8
IGROV-1		6, 9, 13, 16, 19, 22, 26, 29	1	70** (16) 78** (26)	2	0/8
		6, 13, 20	5	31 (16)	0	0/7
	Cisplatin	5, 12, 19	4.5	32 (16)	7	0/7
	Cisplatin →	5, 12, 19	4.5	65** (16)	7	0/7
	Selinexor	6, 13, 20	5			

[1] Tumor cells (10^7/mouse) were s.c. inoculated into the right flank on day 0. Treatment started when tumors were established.
[2] Tumor volume inhibition (TVI) percentage in treated over control mice, in parentheses the day on which it was assessed.
[3] Body weight loss (BWL) percentage induced by treatment; the highest value is reported.
[4] Dead/treated mice.
* $P < 0.001$ by Student's t test versus control mice.
** $P < 0.0001$ by Student's t test versus control mice.
° $P < 0.05$ by Student's t test versus cisplatin-treated mice.

control the localization of multiple cellular proteins it is likely that other cargos of XPO1 participate in the cellular response of ovarian cancer cells to cisplatin and its combination with selinexor.

Conflict of interest statement

Christian Argueta and Yosef Landesman are employees of Karyopharm Therapeutics. No other conflicts of interest to disclose.

Acknowledgements

The study was supported by Associazione Italiana per la Ricerca sul Cancro (AIRC-IG to PP rif. 15333).

References

[1] J. Ferlay, E. Steliarova-Foucher, J. Lortet-Tieulent, S. Rosso, J.W. Coebergh, H. Comber, et al., Cancer incidence and mortality patterns in Europe: estimates for 40 countries in 2012, Eur. J. Cancer 49 (2013) 1374–1403.
[2] D. Menzanzanica, Ovarian cancer: a molecularly insidious disease, Chin. J. Cancer. 34 (2015) 1–3.
[3] S. Vaughan, J.I. Coward, R.C. Bast Jr, A. Berchuck, J.S. Berek, J.D. Brenton, et al., Rethinking ovarian cancer: recommendations for improving outcomes, Nat. Rev. Cancer. 11 (2011) 719–725.
[4] R.A. Burrell, C. Swanton, Tumour heterogeneity and the evolution of polyclonal drug resistance, Mol. Oncol. 8 (2014) 1095–1111.
[5] G. Cossa, L. Gatti, F. Zunino, P. Perego, Strategies to improve the efficacy of platinum compounds, Curr. Med. Chem. 16 (2009) 2355–2365.
[6] M. El-Tanani, E. Dakir, B. Raynor, R. Morgan, Mechanisms of nuclear export in cancer and resistance to chemotherapy, Cancers (Basel) 8 (2016), https://doi.org/10.3390/cancers8030035.
[7] D. Xu, N.V. Grishin, Y.M. Chook, NESdb: a database of NES-containing CRM1 cargoes, Mol. Biol. Cell 23 (2012) 3673–3676.
[8] J. Ishizawa, K. Kojima, N. Hail Jr., Y. Tabe, M. Andreeff, Expression, function, and targeting of the nuclear exporter chromosome region maintenance 1 (CRM1) protein, Pharmacol. Ther. 153 (2015) 25–35.
[9] A. Noske, W. Weichert, S. Niesporek, A. Roske, A.C. Buckendahl, I. Koch, et al., Expression of the nuclear export protein chromosomal region maintenance/exportin 1/Xpo1 is a prognostic factor in human ovarian cancer, Cancer 112 (2008) 1733–1743.
[10] P.J. Van der Watt, C.P. Maske, D.T. Hendricks, M.I. Parker, L. Denny, D. Govender, et al., The Karyopherin proteins, Crm1 and Karyopherin beta1, are overexpressed in cervical cancer and are critical for cancer cell survival and proliferation, Int. J. Cancer 124 (2009) 1829–1840.
[11] D.R. Calnan, A. Brunet, The FoxO code, Oncogene 27 (2008) 2276–2288.
[12] A. Coomans de Brachene, J.B. Demoulin, FOXO transcription factors in cancer development and therapy, Cell Mol. Life Sci. 73 (2016) 1159–1172.
[13] G. Cossa, C. Lanzi, G. Cassinelli, N. Carenini, N. Arrighetti, L. Gatti, et al., Differential outcome of MEK1/2 inhibitor-platinum combinations in platinum-sensitive and -resistant ovarian carcinoma cells, Cancer Lett. 347 (2014) 212–224.
[14] J. Park, Y. Choi, Y.S. Ko, Y. Kim, J.S. Pyo, B.G. Jang, et al., FOXO1 suppression is a determinant of acquired lapatinib-resistance in HER2-positive gastric cancer cells through MET upregulation, Cancer Res. Treat. (2017), https://doi.org/10.4143/crt.2016.580 [Epub ahead of print].
[15] A.R. Abdul Razak, M. Mau-Soerensen, N.Y. Gabrail, J.F. Gerecitano, A.F. Shields, T.J. Unger, et al., First-in-class, first-in-human phase I study of selinexor, a selective inhibitor of nuclear export, in patients with advanced solid tumors, J. Clin. Oncol. 34 (2016) 4142–4150.
[16] M.R. Farren, R.C. Hennessey, R. Shakya, O. Elnaggar, G. Young, K. Kendra, et al., The Exportin-1 Inhibitor selinexor exerts superior antitumor activity when combined with T-cell checkpoint inhibitors, Mol. Cancer. Ther. 16 (2017) 417–427.
[17] J.G. Turner, T. Kashyap, J.L. Dawson, J. Gomez, A.A. Bauer, S. Grant, et al., XPO1 inhibitor combination therapy with bortezomib or carfilzomib induces nuclear localization of IkappaBalpha and overcomes acquired proteasome inhibitor resistance in human multiple myeloma, Oncotarget 7 (2016) 78896–78909.
[18] Y. Chen, S.C. Camacho, T.R. Silvers, A.R. Razak, N.Y. Gabrail, J.F. Gerecitano, et al., Inhibition of the nuclear export receptor XPO1 as a therapeutic target for platinum-resistant ovarian cancer, Clin. Cancer Res. 23 (2017) 1552–1563.
[19] T. Kashyap, C. Argueta, A. Aboukameel, T.J. Unger, B. Klebanov, R.M. Mohammad, et al., Selinexor, a selective inhibitor of nuclear export (SINE) compound, acts through NF-kappaB deactivation and combines with proteasome inhibitors to synergistically induce tumor cell death, Oncotarget 7 (2016) 78883–78895.
[20] J.S. Nair, E. Musi, G.K. Schwartz, Selinexor (KPT-330) induces tumor suppression through nuclear sequestration of IkappaB and down-regulation of survivin, Clin. Cancer Res. (2017), https://doi.org/10.1158/1078-0432.CCR-16-2632 [Epub ahead of print].
[21] C. Corno, L. Gatti, N. Arrighetti, N. Carenini, N. Zaffaroni, C. Lanzi, et al., Axl molecular targeting counteracts aggressiveness but not platinum-resistance of ovarian carcinoma cells, Biochem. Pharmacol. 15 (136) (2017 Jul) 40–50, https://doi.org/10.1016/j.bcp.2017.04.002.
[22] H.C. Chi, S.L. Chen, Y.H. Cheng, T.K. Lin, C.Y. Tsai, M.M. Tsai, et al., Chemotherapy resistance and metastasis-promoting effects of thyroid hormone in hepatocarcinoma cells are mediated by suppression of FoxO1 and Bim pathway, Cell. Death Dis. 7 (2016) e2324.
[23] Z. Fu, D.J. Tindall, FOXOs, cancer and regulation of apoptosis, Oncogene 27 (2008) 2312–2319.
[24] J. Zhao, S.B. Jin, L. Wieslander, CRM1 and Ran are present but a NES–CRM1-RanGTP complex is not required in Balbiani ring mRNP particles from the gene to the cytoplasm, J. Cell. Sci. 117 (2004) 1553–1566.
[25] T.Z. Tan, Q.H. Miow, R.Y. Huang, M.K. Wong, J. Ye, J.A. Lau, et al., Functional genomics identifies five distinct molecular subtypes with clinical relevance and pathways for growth control in epithelial ovarian cancer, EMBO Mol. Med. 5 (2013) 1051–1066.
[26] L. Du, X. Qian, C. Dai, L. Wang, D. Huang, S. Wang, et al., Screening the molecular targets of ovarian cancer based on bioinformatics analysis, Tumori 101 (2015) 384–389.
[27] N. Arrighetti, G. Cossa, L. De Cecco, S. Stucchi, N. Carenini, E. Corna, et al., PKC-alpha modulation by miR-483-3p in platinum-resistant ovarian carcinoma cells, Toxicol. Appl. Pharmacol. 310 (2016) 9–19.
[28] P. Perego, M. Giarola, S.C. Righetti, R. Supino, C. Caserini, D. Delia, et al., Association between cisplatin resistance and mutation of p53 gene and reduced bax expression in ovarian carcinoma cell systems, Cancer Res. 56 (1996) 556–562.
[29] M.S. Anglesio, K.C. Wiegand, N. Melnyk, C. Chow, C. Salamanca, L.M. Prentice, et al., Correction: type-specific cell line models for type-specific ovarian cancer research, PLoS One 8 (2013), https://doi.org/10.1371/annotation/ffcaf179,872f-470b-8bb6-f06d8ba6d03a. eCollection 2013.
[30] M. De Cesare, D. Cominetti, V. Doldi, A. Lopergolo, M. Deraco, P. Gandellini, S. Friedlander, et al., Anti-tumor activity of selective inhibitors of XPO1/CRM1-mediated nuclear export in diffuse malignant peritoneal mesothelioma: the role of survivin, Oncotarget 6 (2015) 13119–13132.
[31] P.M. Tyler, M.M. Servos, R.C. de Vries, B. Klebanov, T. Kashyap, S. Sacham, et al., Clinical dosing regimen of selinexor maintains normal immune homeostasis and T-cell effector function in mice: implications for combination with immunotherapy, Mol. Cancer. Ther. 16 (2017) 428–439.

Appendix II

frontiers

Differential exchange of multifunctional liposomes between glioblastoma cells and healthy astrocytes via tunnelling nanotubes

Beatrice Formicola[1], Alessia D'Aloia[2], Roberta Dal Magro[1], Simone Stucchi[2], Michela Ceriani[2], Francesca Re[1]*

[1]School of Medicine and Surgery, University of Milano Bicocca, Italy, [2]Department of Biotechnology and Biosciences, School of Science, University of Milano-Bicocca, Italy

Submitted to Journal:
Frontiers in Bioengineering and Biotechnology

Specialty Section:
Nanobiotechnology

Article type:
Original Research Article

Manuscript ID:
488013

Received on:
29 Jul 2019

Frontiers website link:
www.frontiersin.org

Conflict of interest statement

The authors declare that the research was conducted in the absence of any commercial or financial relationships that could be construed as a potential conflict of interest

Author contribution statement

B.F. performed the preparation and characterization of all liposomal formulations used. A.D. performed confocal microscopy experiments to detect TnTs. R.D. set up the cell culture conditions. S.S. performed statistical analysis of data. M.C. and F.R. contributed to the data interpretation and participated in the drafting of the manuscript. F.R. coordinated the study, designed the experiments, and analyzed the data. All authors contributed to the paper revision, read and approved the submitted version, and agree to be accountable for all the aspects of the work.

Keywords

Glioblastoma, Liposomes, tunneling nanotubes, Doxorubicin, Nanoparticles, Nanomedicine

Abstract

Word count: 340

Despite advances in cancer therapies, nanomedicine approaches included, the treatment of glioblastoma (GBM), the most common, aggressive brain tumour, remains inefficient. These failures are likely attributable to the complex, and not yet completely know, biology of this tumour, which is responsible for its strong invasiveness, high degree of metastasis, high proliferation potential and resistance to radiation and chemotherapy. The intimate connection through which the cells communicate between them plays an important role in these biological processes. In this scenario, tunneling nanotubes (TnTs) are recently gaining importance as a key features in tumor progression and in particular in the re-growth of GBM after surgery.

In this context, we firstly identified structural differences of TnTs formed by U87-MG cells, as model of GBM cells, in comparison to those formed by normal human astrocytes (NHA), used as a model of healthy cells. Successively, we have studied the possibility to exploit U87-MG TnTs as drug-delivery channels in cancer therapy, using liposomes composed of cholesterol/sphingomyelin and surface functionalized with mApoE and chlorotoxin peptides (Mf-LIP) as nanovehicle model. The results showed that U87-MG cells formed almost exclusively thick and long protrusions, while NHA formed more thin and short TnTs. Considering that only thick TnTs are really active in transport of vesicles and organelles, we showed that fluorescent-labelled Mf-LIP can be transported via TnTs between U87-MG cells, but not through the protrusions formed by NHA cells. Moreover, Mf-LIP boost the formation of thick TnTs in U87-MG cells, where they localized, but not in NHA cells, probably due to the interaction between ClTx and Annexin A2, which is involved in the formation of cell protrusions and in the high plasticity of GBM cells. Our results demonstrate that nanotubes are potentially useful as drug-delivery channels for cancer therapy, facilitating the intercellular redistribution of this drug in close and far away cells, thus reaching isolated tumour niches that are hardly targeted by simple drug diffusion in the brain parenchyma. Moreover, the differences identified in TnTs formed by GBM and NHA cells can be exploited to increase treatments precision and specificity.

Contribution to the field

Despite advances in cancer therapies, the treatment of glioblastoma remains inefficient due its complex pathogenesis. The intercellular communication within cancer cells via tunnelling nanotubes (TnTs) has been indicated in the re-growth of tumour after surgery and in conferring resistance to chemotherapy. Our goal was to investigate the possibility to exploit TnTs to increase the range of drug delivery between cancer cells. Our findings showed that normal human astrocytes formed thin and short TnTs, while U87-MG cells, used as GBM model, formed almost exclusively thick and long protrusions which were really active in the transport of liposomes functionalized with mApoE-chlorotoxin, as a model of GBM-targeting nanoparticles. These liposomes boosted the formation of thick TnTs in U87-MG cells, probably due to the interaction between ClTx and Annexin A2, which is involved in the formation of cell protrusions and in the high plasticity of GBM cells. Our results corroborate the idea of exploiting TnTs as drug-delivery channels for cancer therapy. This could facilitate the reaching of isolated tumour niches that are hardly targeted by simple drug diffusion in the brain parenchyma. Moreover, the differences identified in TnTs formed by GBM and NHA cells can be useful to increase treatments precision and specificity.

Funding statement

This work was partially supported by the Grant JPND-COFUND_FP-829-031 (2016-2019) to F.R.

Ethics statements

Studies involving animal subjects
Generated Statement: No animal studies are presented in this manuscript.

Studies involving human subjects
Generated Statement: No human studies are presented in this manuscript.

Inclusion of identifiable human data
Generated Statement: No potentially identifiable human images or data is presented in this study.

Data availability statement

Generated Statement: All datasets generated for this study are included in the manuscript/supplementary files.

frontiers

Differential exchange of multifunctional liposomes between glioblastoma cells and healthy astrocytes *via* tunnelling nanotubes

Running title: Liposomes trade-off between glioblastoma cells

Beatrice Formicola[1‡], Alessia D'Aloia[2‡], Roberta Dal Magro[1], Simone Stucchi[2], Michela Ceriani[2‡], Francesca Re[1‡*]

[1]School of Medicine and Surgery, University of Milano-Bicocca, Vedano al Lambro, Italy
[2]Department of Biotechnology and Biosciences, University of Milano-Bicocca, Milano, Italy

‡ These Authors contributed equally to this work.

***Correspondence:** Francesca Re; francesca.re1@unimib.it

Keywords: glioblastoma, liposomes, tunneling nanotubes, doxorubicin, nanoparticles, nanomedicine.

Abstract

Despite advances in cancer therapies, nanomedicine approaches included, the treatment of glioblastoma (GBM), the most common, aggressive brain tumour, remains inefficient. These failures are likely attributable to the complex, and not yet completely know, biology of this tumour, which is responsible for its strong invasiveness, high degree of metastasis, high proliferation potential and resistance to radiation and chemotherapy. The intimate connection through which the cells communicate between them plays an important role in these biological processes. In this scenario, tunneling nanotubes (TnTs) are recently gaining importance as a key features in tumor progression and in particular in the re-growth of GBM after surgery.

In this context, we firstly identified structural differences of TnTs formed by U87-MG cells, as model of GBM cells, in comparison to those formed by normal human astrocytes (NHA), used as a model of healthy cells. Successively, we have studied the possibility to exploit U87-MG TnTs as drug-delivery channels in cancer therapy, using liposomes composed of cholesterol/sphingomyelin and surface functionalized with mApoE and chlorotoxin peptides (Mf-LIP) as nanovehicle model. The results showed that U87-MG cells formed almost exclusively thick and long protrusions, while NHA formed more thin and short TnTs. Considering that only thick TnTs are really active in transport of vesicles and organelles, we showed that fluorescent-labelled Mf-LIP can be transported *via* TnTs between U87-MG cells, but not through the protrusions formed by NHA cells. Moreover, Mf-LIP boost the formation of thick TnTs in U87-MG cells, where they localized, but not in NHA cells, probably due to the interaction between ClTx and Annexin A2, which is involved in the formation of cell protrusions and in the high plasticity of GBM cells. Our results demonstrate that nanotubes are potentially useful as drug-delivery channels for cancer therapy, facilitating the intercellular redistribution of this drug in close and far away cells, thus reaching isolated tumour niches that are hardly targeted by simple drug diffusion in the brain parenchyma. Moreover, the differences identified in TnTs formed by GBM and NHA cells can be exploited to increase treatments precision and specificity.

1 Introduction

The limits of conventional therapies against tumours, in terms of effectiveness/damage ratio, lead to the development and application in clinics of different nanotechnological drugs in the last 25 years (Stupp et al., 2009). Many advancements have been achieved in this field, but different issues, such as the complexities and heterogeneity of tumour biology still remain unsolved. Gliomas, intrinsic brain tumours, are a dissimilar group of oncological diseases for which there is currently no cure, and only very limited progress has been made in the control of the disease course over the past three decades (Westphal et al., 2011). Among gliomas, glioblastoma multiforme (GBM, also called grade IV astrocytoma) is one of the most deadly brain tumors, with a short median patient survival and a very limited response to therapies (Louis et al., 2016). In this context, many efforts are underway towards the development of new therapeutic approaches and nanomedicine seems to be one of the most promising. Nevertheless, many obstacles have not been overcome yet. GBM has a very complex pathogenesis that involves alterations of several key cellular pathways, diffuse invasiveness and capacity to escape therapies. An important component of tumour growth is communication within cancer cells and with other cells in the microenvirons, which strengthen tumour progression and resistance to radio- and chemotherapy (Broekman et al., 2018).

Normal and tumour cells exploit different communication modalities and one of them is represented by the physical connection *via* tunnelling nanotubes (TnTs) and microtubes (TmTs), which form a cytoplasmic continuum between cells and allow the transport of non-secretable molecules and organelles. In particular, TnTs can mediate the transfer of cellular vesicles (Rustom et al., 2004; Onfelt et al., 2006), mitochondria (Ahmad et al., 2014), lysosomes (Abounit et al., 2016), miRNAs (Thayanithy et al., 2014), single proteins (Schiller et al., 2013) and viral particles (Sowinski et al., 2008) between cells, also very distant from each other (>100 μm of distance). TnTs are transient transcellular channels with a diameter of 50–200 nm, a length up to several cell diameters with variable lifetimes ranging from less than 60 min up to many hours. (Carone et al., 2015).

Lou et al. (2012a, 2012b) firstly described the presence of TnTs in human primary tumors and in many cancer cell lines, highlighting the key role of these membranous structures in cancer cell pathogenesis and invasion. The involvement of TnTs and TmTs has also been indicated in the re-growth of GBM after surgery and in conferring resistance to chemotherapy (Weil et al., 2017; Moschoi et al., 2016). Although TnTs are not apparent in some glioma cellular models (Van der Vos et al., 2016), they may represent a new tool for bidirectional intercellular transfer of drug-loaded nanoparticles.

In this context, there are some data supporting the direct cell-to-cell transfer of nanoparticles through TnTs and this strategy may be exploited to increase the range of drug delivery between cancer cells (Epperla et al., 2015; Sisakhtnezhad et al., 2015; Deng et al., 2018). One of the peculiarity of GBM is the presence of glioma stem cells both within the tumour bulk, which are able to reconstitute a whole tumour after surgical resection (Fan et al, 2010; Lin et al., 2010), and in other brain regions, where minor stem-cell niches represent a pool from which new tumour cells originate (Gould et al., 2007). Then, targeting primary GBM with nanotherapeutics may allow the possibility to reach *via* TnTs isolated, infiltrating tumor cells (stem cells included) that are hardly reached by drug diffusion in the brain parenchyma.

This study aims to evaluate *in vitro* the possible intercellular transport of multifunctional liposomes *via* TnTs between human primary glioblastoma cell line. We have recently designed liposomes carry doxorubicin, as an anti-cancer drug model, and dually-functionalized with apoE-derived peptide and with chlorotoxin (ClTx), as GBM targeting ligands (Maletínská et al., 2000; DeBin et al., 1993; Ojeda et al., 2016; Lyons et al., 2002). Liposomes trafficking *via* TnTs in GBM cells has not been reported yet. Moreover, we compared the heterogeneity of TnTs, in terms of structure, morphology, size and abundance between GBM cells and human healthy astrocytes, with the aim to increase the precision and specificity of treatments.

2 Materials and Methods

2.1 Materials

Cholesterol (Chol), Doxorubicin (DOX), Thiazolyl Blue Tetrazolium Bromide, 4-(2-Hydroxyethyl)piperazine-1-ethanesulfonic acid (HEPES), Triton X-100, Ultra-low Range Molecular Weight Marker (M.W. 1.060-26.600), EZBlue Gel Staining Reagent, 1,1′-Dioctadecyl-3,3,3′,3′-tetramethylindocarbocyanine perchlorate (DiI probe), TRITC-labelled phalloidin, mouse monoclonal anti-β-tubulin were purchased from Sigma-Aldrich (Milano, Italy). 1,2-Distearoyl-sn-glycero-3-phospho-ethanolamine-N[maleimide(polyethyleneglycol)-2000](mal-PEG-DSPE) and sphingomyelin from bovine brain (Sm) were purchased from Avanti Polar Lipids, Inc (Alabaster, AL, USA). 1,2-Distearoyl-sn-glycero-3-phospho-ethanolamine-N[(polyethyleneglycol)-2000] n-hydroxysuccinimide ester (NHS-PEG-DSPE) was purchased from Nanocs (Boston, USA).Ultrapure and deionized water were obtained from Direct-Q5 system (Millipore, Italy). Transwell permeable supports 0.4 µm polyester membrane 12 mm insert, 12 well plates were from Corning (NY, USA). mApoE peptide (CWG-LRKLRKRLLR, MW 1698.18 g/mol) and chlorotoxin (ClTx, MW 4004 g/mol) were synthetized by Karebay Biochem (Monmouth Junction, NJ, USA). Dialysis membranes (cut-off 12000-14000 Da) were purchased from Medicell International Ltd, (London, UK). Penicillin-streptomycin (P/S) solution 100X was purchased from Euroclone (Milan, Italy); PBS 1X, collagen, trypsin/EDTA solution and NuPAGE Bis-Tris (4-12%) were from Invitrogen. The lactate dehydrogenase (LDH) cytotoxicity detection kit was purchased from Roche Diagnostics GmbH (Germany). All other chemicals were of analytical grade and were obtained from either Sigma–Aldrich or Merck. Alexa Fluor 488 goat anti-mouse, Alexa Fluor 568 goat anti-mouse were from Life Technologies. 3,3'-Dioctadecyloxacarbocyanine Perchlorate (DiO) was from Sigma Aldrich (Milan, Italy).

2.2 Preparation of ClTx-PEG-DSPE

ClTx-lipid was prepared as described in (Xiang et al., 2011) with small modifications. Briefly, 0.1 µmol NHS-PEG-DSPE in $CHCl_3$/MeOH (2:1, vol/vol) was dried under N_2 to remove organic solvents. Then 5 eq (0.5 µmol) of ClTx dissolved in 10 mM Hepes, 150 mM NaCl pH 7.4, was added to the dried lipid. The reaction was conducted under gentle stirring for 90 min at room temperature. The resulting solution was dialyzed against MilliQ water for two days in a dialysis tube (MWCO=3500 Da) to remove unreacted ClTx and then lyophilized overnight.

2.3 Preparation multifunctional liposomes (Mf-LIP)

Liposomes (LIP) were composed of sphingomyelin, cholesterol (1:1, mol/mol) added with 2.5 mol % of mal-PEG-PE, for the covalent binding of mApoE peptide, and with 0.5 mol% of BODIPY-Sm as fluorescent probe (Re et al., 2010; Re et al., 2011). LIP were prepared in 10 mM Hepes, 150 mM NaCl pH 7.4 by extrusion procedure through polycarbonate membranes of 100 nm diameter pores, under N_2. mApoE peptide was covalently attached on LIP surface by thiol-maleimide coupling, as previously described (Re et al., 2010; Re et al., 2011). ClTx-lipid was added to mApoE-LIP by post-insertion technique, following the procedure previous described (Mare et al., 2018). These LIP were purified with a Sepharose G-25 fine column (25x1cm) to remove unbounded and unincorporated materials. This sample will be referred as Mf-LIP.

As controls, LIP composed of sphingomyelin, cholesterol (1:1, mol/mol) were prepared in ammonium sulphate (500 mM, pH 5.5) by extrusion procedure as described above. LIP were dialyzed against 10 mM Hepes, 150 mM NaCl pH 7.4, overnight, and then incubated with DOX (1.5 µmol DOX/ 10 µmol total lipids) for 1 h at 65°C to allow the incorporation of DOX in the LIP core. This sample will be

referred as DOX-LIP. Mf-LIP and DOX-LIP were purified with a Sepharose G-25 fine column (25x1cm) to remove unbounded and unincorporated materials.

2.4 Characterization of Mf-LIP

After purification, the amount recovered for each compound was determined by different techniques. Briefly, phospholipids content was quantified by Stewart Assay (Stewart, 1980); the amount of ClTx and mApoE on LIP surface was assessed by SDS-PAGE. DOX loading was quantified spectrofluorometrically (λex = 495 nm; λem =592 nm) after vesicle disruption with 0.1% Triton X-100. The DOX encapsulation yield in liposomes was calculated by comparing fluorescence intensities with a previously established calibration curve of free DOX in 10mM Hepes, 150 mM NaCl pH 7.4. Size and polydispersity index (PDI) were analyzed by dynamic light scattering (DLS) technique (Brookhaven Instruments Corporation, Holtsville, NY, USA). ζ-potential was determined by using an interferometric doppler velocimetry with the same instrument equipped with ZetaPALS device. LIP stability was measured in 10 mM Hepes, 150 mM NaCl pH 7.4 by following size and PDI by DLS for 1 week.

2.5 Cell cultures

U87-MG glioblastoma cells were purchased from da American Type Culture Collection (ATCC, VA, USA) and were grown in DMEM High Glucose, 10% FBS, 1% P/S, 1% glutamine (Tamborini et al., 2016). Normal Human Astrocytes (NHA), purchased from Lonza (Walkersville, Maryland, USA), were maintained in Astrocytes Basal Medium supplemented with AGM BulletKit™. All cell lines were cultured at 37 °C under a humidified atmosphere containing 5% CO_2.

2.6 TnTs analysis by confocal microscopy

NHA and U87-MG cells were seeded at a density of $2.37x10^4$ cell/ml or $7.5x10^4$ cell/ml respectively on porcine gelatin pretreated coverslips. The day after seeding, cells were treated for 1 h or 24 h with free DOX (15 or 25 µg/ml) or with DOX-LIP (15 µg/ml of DOX, 200 nmols of total lipids) or with fluorescent-labelled Mf-LIP (200 nmols of total lipids) at 37°C in 5% CO_2. Untreated cells were used as a control.

After treatment, cells were then leave for 2 h in each culture complete medium and then stained for 20 min with 1.9 µl/ml of DiI in PBS (membrane/endocytic vesicles), or with 5 µl/ml of DiO in PBS, to label cell membranes, TnTs included, according to the manufacturer's instructions. Cells were then fixed for 8 min with 3.7% paraformaldehyde in phosphate-buffered saline (PBS). Fluorescence images were examined with a 40x magnification on A1R Nikon (Nikon, Tokyo, Japan) laser scanning confocal microscope. Cells were carefully scored for the presence of TnTs. About #200 cells for each experiment were analyzed. TnTs were counted and their single length was measured using cell diameter as conventional unit. The measuring of TnTs diameter by light microscopy was not accurate due to the resolution limit. Experiments were performed in triplicate. Images were analyzed by Image J software.

2.7 Actin and tubulin staining

NHA and U87-MG cells were plated at a density of 2.37×10^4 cell/ml or 7.5×10^4 cell/ml, respectively, on porcine gelatin pretreated coverslips. The day after cells were fixed for 10 min with 3.7% paraformaldehyde in phosphate buffered saline (PBS), permeabilized for 4 min with 0.1% Triton X-100 in PBS and finally stained with different antibodies. In particular, cells were treated with TRITC-phalloidin (1:40 in 1% BSA in PBS) for actin staining, as described previously (Ceriani et al., 2007). For tubulin staining, cells were incubated with anti-mouse monoclonal anti-β-tubulin primary antibody (1:150 in 1% BSA in PBS) for 1h at 37°C. Then cells were washed and incubated with the secondary

antibody Alexa Fluor 488 goat anti-mouse IgG or Alexa Fluor 568 goat anti-mouse IgG (1:200 in 1% BSA in PBS) for 45 min at 37°C.

2.8 Statistical analysis

For TnTs quantification data were analyzed by Student *t* test. Data were expressed as a mean ± standard error (S.E.). All experiments were conducted at least in triplicate. All the analyses were performed with GraphPad Prism 8 software (license number: GP8-1519368-RFQS-B8CB4). Differences were considered significant at $p < 0.05$ (*).

3 Results

3.1 Characterization of LIP

The results showed that DOX-LIP displayed a diameter of 121 ± 6 nm with a PDI value of 0.098 ± 0.01; the ζ-potential was -19.32 ± 0.58 mV. Mf-LIP showed a diameter of 187 ± 5 nm with a PDI value of 0.087 ± 0.05; the ζ-potential was -14.5 ± 0.43 mV. These parameters remained constant for 1 week within the experimental error (<2.7 % of variation). For both preparations, the total lipid recovery after purification was 79.5 ± 8 %. For Mf-LIP the yield of functionalization with mApoE and ClTx was 88.5 ± 10 % (corresponding to 2.2 mol % of mApoE/total lipids) and 71.2 ± 3 % (corresponding to 1.42 mol% of ClTx/total lipids), respectively. For DOX-LIP, the incorporation yield of DOX was 70 ± 6 %, corresponding to 80 ± 5 µg of DOX/µmol of lipids. These results derived from at least five different batches.

3.2 U87-MG cells forms TnTs with different thickness, compared to NHA

To investigate if U87-MG cells (model of GBM tumor cells) are able to form *in vitro* intercellular connections with characteristics of TnTs, and if they are different from those formed by NHA cells (model of normal healthy astrocytes), we use confocal microscopy technique and 3D reconstruction. Both cell types form protrusions connecting distant cells with characteristics of TnTs (Fig. 1), which were not in contact with the substratum (Supplementary Fig. S1 and S2). To allow for a quantitative determination, the observed membrane protrusions of about 200 cells were scored for each cell line. The results showed that the number of cells forming TnTs is comparable between U87-MG and NHA (44 ± 6.6 % and 57 ± 3.5 % respectively) (Supplementary Fig.S3). Confocal images show the presence of TnTs of different thickness. More interestingly, we detected significant differences in both, thin and thick of TnTs: U87-MG cells formed almost exclusively thick protrusions, while NHA formed either thin and thick TnTs (Table 1). The measuring of TnTs diameter by light microscopy was not accurate due to the resolution limit. Confocal microscopy showed that some TnTs reach thicknesses of over 700 nm, which could be due to incorporation of additional components inside the TnTs, such as microtubules, as previously suggested (Onfelt et al., 2006).
To evaluate the presence of tubulin, typical marker for thick TnTs, and of actin, typical marker for thin TnTs, U87-GM and NHA cells were stained with anti-tubulin and anti-actin fluorescent antibodies.
The results showed that U87-MG were able to form thick TnTs, which contained both actin and tubulin (Fig. 2). NHA cells were able to form thick TnTs made of actin and tubulin, but they also established thin TnTs, which were positive only to actin staining (Fig. 3).

3.3 Doxorubicin treatment induced changes in the TnTs thickness of U87-MG cells

To evaluate the ability of U87-MG and NHA to exchange DOX via TnTs, cells were treated with two different doses of free DOX. Treatments with 25 µg/ml of DOX for 24 h induced a strong toxic effect on both cell types, hindering the images analysis (data not shown). Then, all the subsequent experiments were carried out by incubating cells with 15 µg/ml of DOX for 1 h. Analysis performed at confocal microscope showed that DOX localizes principally at the nucleus in both cell lines (Fig.

4), as expected (de Lange et al., 1992), but it was not detectable along TnTs structures. The quantitative determination of TnTs revealed that the % of cells forming TnTs was not affected by the treatment with free DOX (Fig. 5), for both the cell types used.
Comparing the thickness of TnTs, the DOX treatment on U87-MG cells induced the formation of about 80% of thin TnTs, with a strong reduction of thick TnTs (Table 2A). Prolonging the incubation time up to 24 h, TnTs disappeared and U87-GM cells died (Supplementary Fig. S4).
No significant changes in TnTs thickness were detected for NHA, which remained comparable to untreated NHA (Table 2B).

3.4 Mf-LIP boost the formation of thick TnTs in U87-MG cells, where they localized, but not in NHA cells.

The cellular uptake of Mf-LIP by U87-MG was evaluated by confocal microscopy and fluorescence measurements. The results showed that Mf-LIP displayed a 3- to 6-fold increase of cellular uptake, compared to DOX-LIP used as a control (Supplementary Fig. S5). Then, the ability of U87 cells to exchange LIP *via* TnTs was evaluated. The results showed that only few DOX-LIP were inside TnTs, and most of them were localized in thickest TnTs (Fig. 6). In agreement with the above results, the amount of Mf-LIP localized in TnTs was higher compared to DOX-LIP, and surprisingly, this treatment enhanced the formation of thick TnTs (Fig. 7). The treatment of U87-MG cells with DOX-LIP did not affects the % of cells forming TnTs (Supplementary Fig. S6A), but strongly increased thin TnTs, with a significant reduction of thick TnTs (Table 3A), similarly to the effect exerted by free DOX. Also the treatment with Mf-LIP did not affects the % of cells forming TnTs (Supplementary Fig. S6A); neither the ratio between thin and thick TnTs changed (Table 3B).
No differences were detected in TnTs formed by NHA cells after incubation with DOX-LIP or Mf-LIP (Supplementary Fig. S6B and Table S1). Images captured by confocal microscopy revealed that both, DOX-LIP and Mf-LIP, were localized in TnTs with a little extent and the few LIP inside in TnTs were localized in the thick ones (Fig. 8 and 9).

4 Discussion

In the context of searching more effective therapies against GBM, which remains an incurable brain tumour, we focus our attention on the cells communication. Intercellular communication plays an important role in tumour progression, invasiveness and resistance to conventional treatments (Broekman et al., 2018). Among the different ways that cells used to exchange non-secretable messages, tunnelling nanotubes (TnTs) and microtubes (TmTs) are involved in the re-growth of GBM after surgery and in conferring resistance to radio- and chemotherapy (Weil et al., 2017; Moschoi et al., 2016). Starting from our expertise in the design of nanoparticles, we synthesized and characterized LIP carry doxorubicin, as an anti-cancer drug model, and dually-functionalized with mApoE and with ClTx, as GBM targeting ligands (Maletínská et al., 2000; DeBin et al., 1993; Ojeda et al., 2016; Lyons et al., 2002). The ability of human primary glioblastoma cell line (U87-MG), in comparison to normal human astrocytes (NHA), to exchange Mf-LIP *via* TnTs has been investigated. Mf-LIP characterization shown that the different batches herein prepared were highly reproducible and stable over time, with the yield of the reactions comparable to previously reported ones (Re et al., 2010; Re et al., 2011).
Since it is reported in literature that TnTs are not apparent in some glioma cellular models (Van der Vos et al., 2016), we check if U87-MG cells and NHA cells herein used were able to form TnTs *in vitro*. The results showed that both types of cells were able to communicate between them by TnTs, as already reported (Reindl et al., 2019; Zhang et al., 2015; Rostami et al., 2017) and the percentage of cells forming TnTs was similar between U87-MG and NHA cells.
Since TnTs have been grouped into two main classes, very thin (≤ 0.7 µm, measuring a minimum of 100–200 nm) and thick (≥ 0.7 µm, up to 1 µm) (Gerdes et al., 2007), we analyzed the heterogeneity of TnTs formed by U87-MG and NHA.

Structural analysis and the comparison of the thickness of TnTs formed by these cells, shown that U87-MG cells formed almost exclusively thick protrusions, while NHA formed either thin and thick TnTs. Considering that only thick TnTs are really active in transport of molecules and organelles (Veranic et al., 2008), this difference could may be exploited to increase the range of drug delivery between cancer cells. Moreover, TnTs are also classified according to their different morphology/function in TnTs type I, short dynamic structures, containing actin filament and engaged in exploring the surrounding microenvironment, and TnTs type II, that are longer and more stable processes, containing actin and tubulin filaments and apparently involved in organelles shuttle (Veranic et al., 2008). Our immunofluorescence experiments staining actin and tubulin, showed that U87-MG mainly formed TnTs type II, compared to NHA, which formed mostly TnTs type I. Accordingly, U87-MG were able to exchange Mf-LIP, as shown by the detection of liposomes-associated fluorescence in thick TnTs. The surface functionalization of DOX-LIP with mApoE and ClTx strongly enhance the LIP uptake, compared to DOX-LIP, probably due to the overexpression of LDL-receptor by U87-MG cells (Maletínská et al., 2000; DeBin et al., 1993), which is the target ligand of mApoE peptide, and ClTx, which has been shown to selectively bind a specific chloride channel on glioma cell surface (Ojeda et al., 2016; Lyons et al., 2002).

Moreover, the encapsulation of DOX in Mf-LIP facilitates its passage through TnTs, respect to free DOX, that remains almost exclusively localized in the nuclear region. Considering that cells physiologically produced TnTs under stress conditions (e.g. hypoxia conditions, drugs, oxidative stress), we assessed the effect of DOX treatment on TnTs formed by U87-MG cells. The results showed that free DOX induced the formation of thin TnTs, with a strong reduction of thick TnTs and prolonging the incubation time, TnTs disappeared and U87-GM cells died as also showed for other cells types (Rustom, 2016). Contrarily, when DOX is incorporated in Mf-LIP, we observed an increase in the formation of thick TnTs by U87-MG. This could be ascribed to the already reported interaction between ClTx and Annexin A2 (Kesavan et al., 2010), which is involved in the remodeling of cells structures (cell protrusions included) and whose expression has been recently associated with cell dissemination and metastasis of GBM (Maule et al., 2016; Xing et al., 2013).

Comparing these results to those obtained in NHA cells, Mf-LIP were localized in TnTs with a little extent and the few LIP inside in NHA's TnTs were localized in the thick ones, suggesting that in this cell line LIP are scarcely exchanged by TnTs. This corroborate the fact that thick TnTs are mainly involved in the intercellular trafficking of drug-loaded liposomes. More appealing, the structural difference between TnTs formed by GBM cells and NHA could be useful to design precise and specific nanotherapeutics. The opportunity to exploit TnTs as drug-delivery channels can improve the cancer therapy, by reaching isolated, infiltrating tumor cells that are hardly targeted by drug diffusion in the brain parenchyma. Nowadays, few papers are available showing the involvement of TnTs-mediated intercellular transport of nanoparticles (Kristl et al., 2013; Epperla et al., 2015; Deng et al., 2018) and none of them is dedicated to the comparison between healthy and tumour cells in nanoparticles trafficking. In conclusion, the understanding of the possible intercellular delivery of nanotherapeutics cargo *via* TnTs can significantly influence the approaches to treat specific diseases.

5 Conflict of Interest

The authors declare that the research was conducted in the absence of any commercial or financial relationships that could be construed as a potential conflict of interest.

6 Author Contributions

B.F. performed the preparation and characterization of all liposomal formulations used. A.D. performed confocal microscopy experiments to detect TnTs. R.D. set up the cell culture conditions. S.S. performed statistical analysis of data. M.C. and F.R. contributed to the data interpretation and participated in the drafting of the manuscript. F.R. coordinated the study, designed the experiments,

and analyzed the data. All authors contributed to the paper revision, read and approved the submitted version, and agree to be accountable for all the aspects of the work.

7 Funding

This work was partially supported by the Grant JPND-COFUND_FP-829-031 (2016-2019) to F.R.

8 References

1. Abounit, S., Bousset, L., Loria, F., Zhu, S., de Chaumont, F., Pieri, L., et al. (2016). Tunneling nanotubes spread fibrillar α-synuclein by intercellular trafficking of lysosomes. *EMBO J.* 35:19. doi:10.15252/embj.201593411
2. Ahmad, T., Mukherjee, S., Pattnaik, B., Kumar, M., Singh, S., Kumar, M., et al. (2014). Miro1 regulates intercellular mitochondrial transport & enhances mesenchymal stem cell rescue efficacy. *EMBO J.* 33:9. doi:10.1002/embj.201386030
3. Broekman, M.L., Maas, S.L.N., Abels, E.R., Mempel, T.R., Krichevsky, A.M., Breakefield, X.O. (2018). Multidimensional communication in the microenvirons of glioblastoma. *Nat Rev Neurol.* 14:8. doi: 10.1038/s41582-018-0025-8
4. Carone, C., Genedani, S., Leo, G., Filaferro, M., Fuxe, K., Agnati, L. F. In vitro effects of cocaine on tunneling nanotube formation and extracellular vesicle release in glioblastoma cell cultures. (2015). *J Mol Neurosci.* 55:1. doi: 10.1007/s12031-014-0365-9
5. Ceriani, M., Scandiuzzi, C., Amigoni, L., Tisi, R., Berruti, G., Martegani, E. (2007) Functional analysis of RalGPS2, a murine guanine nucleotide exchange factor for RalA GTPase. *Exp Cell Res.* 313:11. doi: 10.1016/j.yexcr.2007.03.016
6. DeBin, J. A., Maggio, J. E., Strichartz, G. R. (1993). Purification and characterization of chlorotoxin, a chloride channel ligand from the venom of the scorpion. *Am. J. Physiol.* 264:2. doi:10.1152/ajpcell.1993.264.2.C361
7. de Lange. J,H,1, Schipper, N.W., Schuurhuis, G.J., ten Kate, T.K., van Heijningen, T.H., Pinedo, H.M., et al. (1992). Quantification by laser scan microscopy of intracellular doxorubicin distribution. *Cytometry.* 13:6. DOI: 10.1002/cyto.990130604
8. Deng, G., Wu, Z., Zhou, F., Dai, C., Zhao, J., Kang, Y., et al. (2018). Exchangeability of FITC-SiO_2 Nanoparticles Between Cancer Cells Increases the Range of Drug Delivery. *J Biomed Nanotechnol.* 14:1. doi: 10.1166/jbn.2018.2509
9. Epperla, C. P., Mohan, N., Chang, C. W., Chen, C. C., Chang, H. C. (2015). Nanodiamond-Mediated Intercellular Transport of Proteins through Membrane Tunneling Nanotubes. *Small.* 11:45. doi: 10.1002/smll.201502089
10. Fan, X., Khaki, L., Zhu, T. S., Soules, M. E., Talsma, C. E., Gul, N., et al. (2010). NOTCH pathway blockade depletes CD133-positive glioblastoma cells and inhibits growth of tumor neurospheres and xenografts. *Stem Cells.* 28:1. doi: 10.1002/stem.254
11. Gerdes, H.H., Bukoreshtliev, N.V., Barroso, J.F. (2007). Tunneling nanotubes: a new route for the exchange of components between animal cells. *FEBS Lett.* 581:11. doi: 10.1016/j.febslet.2007.03.071
12. Gould, E. (2017). How widespread is adult neurogenesis in mammals? *Nat Rev Neurosci.* 8:6. doi: 10.1038/nrn2147
13. Kesavan, K., Ratliff, J., Johnson, E.W., Dahlberg, W., Asara, J.M., Misra, P., et al. (2010). Annexin A2 is a molecular target for TM601, a peptide with tumor-targeting and anti-angiogenic effects. *J Biol Chem.* 285:7. doi: 10.1074/jbc.M109.066092

14. Kristl, J., Plajnšek, K.T., Kreft, M.E., Janković, B., Kocbek, P. (2013). Intracellular trafficking of solid lipid nanoparticles and their distribution between cells through tunneling nanotubes. *Eur J Pharm Sci.* 50:1. doi: 10.1016/j.ejps.2013.04.013
15. Lin, J., Zhang, X. M., Yang, J. C., Ye, Y. B., Luo, S. Q. (2010). γ-secretase inhibitor-I enhances radiosensitivity of glioblastoma cell lines by depleting CD133+ tumor cells. *Arch Med Res.* 41:7. doi: 10.1016/j.arcmed.2010.10.006
16. Lou, E., Fujisawa, S., Barlas, A., Romin, Y., Manova-Todorova, K., Moore, M.A., et al. (2012,a). Tunneling Nanotubes: A new paradigm for studying intercellular communication and therapeutics in cancer. *Commun Integr Biol.* 1;5(4). doi: 10.4161/cib.20569
17. Lou, E., Fujisawa, S., Morozov, A., Barlas, A., Romin, Y., Dogan, Y., et al. Tunneling nanotubes provide a unique conduit for intercellular transfer of cellular contents in human malignant pleural mesothelioma. (2012,b). *PLoS One.* 7(3):e33093. doi: 10.1371/journal.pone.0033093
18. Louis, D.N., Perry, A., Reifenberger, G., von Deimling, A., Figarella-Branger, D., Cavenee, W.K., et al. (2016) The 2016 World Health Organization Classification of Tumors of the Central Nervous System: a summary. *Acta Neuropathol.* 131:6. doi: 10.1007/s00401-016-1545-1
19. Lyons, S. A., O'Neal, J., Sontheimer, H. (2002). Chlorotoxin, a scorpion-derived peptide, specifically binds to gliomas and tumors of neuroectodermal origin. *Glia.* 39:2. doi:10.1002/glia.10083 162-173
20. Maletínská, L., Blakely, E. A., Bjornstad, K.A., Deen, D. F., Knoff, L. J., Forte, T. M. (2000). Human glioblastoma cell lines: levels of low-density lipoprotein receptor and low-density lipoprotein receptor-related protein. *Cancer Res.* 60:8
21. Mare, R., Paolino, D., Celia, C., Molinaro, R., Fresta, M., Cosco, D. (2018). Post-insertion parameters of PEG-derivatives in phosphocholine-liposomes. *Int J Pharm.* 552:1-2. doi: 10.1016/j.ijpharm.2018.10.028
22. Maule, F., Bresolin, S., Rampazzo, E., Boso, D., Della Puppa, A., Esposito, G., et al. (2016). Annexin 2A sustains glioblastoma cell dissemination and proliferation. *Oncotarget.* 7:34. doi: 10.18632/oncotarget.10565
23. Moschoi, R., Imbert, V., Nebout, M., Chiche, J., Mary, D., Prebet, T., et al. (2016). Protective mitochondrial transfer from bone marrow stromal cells to acute myeloid leukemic cells during chemotherapy. *Blood.* 128:2. doi: 10.1182/blood-2015-07-655860
24. Ojeda, P. G., Wang, C. K., Craik, D. J. (2016). Chlorotoxin: Structure, activity, and potential uses in cancer therapy. *Biopolymers.* 106:1. doi: 10.1002/bip.22748
25. Önfelt, B., Nedvetzki, S., Benninger, R. K. P., Purbhoo, M. A., Sowinski, S., Hume, A. N., et al. (2006). Structurally Distinct Membrane Nanotubes between Human Macrophages Support Long-Distance Vesicular Traffic or Surfing of Bacteria. *J Immunol.* 177:12. doi:10.4049/jimmunol.177.12.8476
26. Re, F., Cambianica, I., Sesana, S., Salvati, E., Cagnotto, A., Salmona, M., Couraud, P. O., et al. (2010). Functionalization with ApoE-derived peptides enhances the interaction with brain capillary endothelial cells of nanoliposomes binding amyloid-beta peptide. *J. Biotechnol.* 156:4. doi: 10.1016/j.jbiotec.2011.06.037
27. Re, F., Cambianica, I., Zona, C., Sesana, S., Gregori, M., Rigolio, R., et al. (2011). Functionalization of liposomes with ApoE-derived peptides at different density affects cellular

uptake and drug transport across a blood-brain barrier model. *Nanomedicine: NBM.* 7:5. doi: 10.1016/j.nano.2011.05.004

28. Reindl, J., Shevtsov, M., Dollinger, G., Stangl, S., Multhoff, G. (2019). Membrane Hsp70-supported cell-to-cell connections via tunneling nanotubes revealed by live-cell STED nanoscopy. *Cell Stress Chaperones*. 24:1. doi: 10.1007/s12192-018-00958-w
29. Rostami, J., Holmqvist, S., Lindström, V., Sigvardson, J., Westermark, G.T., Ingelsson, M. et al. (2017). Human Astrocytes Transfer Aggregated Alpha-Synuclein via Tunneling Nanotubes. *J Neurosci*. 37:49. doi: 10.1523/JNEUROSCI.0983-17.2017
30. Rustom, A. (2016). The missing link: does tunnelling nanotube-based supercellularity provide a new understanding of chronic and lifestyle diseases? *Open Biol.* 6:6. doi: 10.1098/rsob.160057
31. Rustom, A., Saffrich, R., Markovic, I., Walther, P., Gerdes, H. H. (2004). Nanotubular highways for intercellular organelle transport. *Science.* 303:5660. doi:10.1126/science.1093133
32. Schiller, C., Huber, J. E., Diakopoulos, K. N., Weiss, E.H. (2013). Tunneling nanotubes enable intercellular transfer of MHC class I molecules. *Hum. Immunol.* 74:4. doi:10.1016/j.humimm.2012.11.026
33. Sisakhtnezhad, S., Khosravi, L. (2015). Emerging physiological and pathological implications of tunneling nanotubes formation between cells. *Eur J Cell Biol.* 94:10. doi: 10.1016/j.ejcb.2015.06.010.
34. Sowinski, S., Jolly, C., Berninghausen, O., Purbhoo, M. A., Chauveau, A., Köhler, K., Oddos, S., et al. (2008). Membrane nanotubes physically connect T cells over long distances presenting a novel route for HIV-1 transmission. *Nat Cell Biol.* 10:2. doi:10.1038/ncb1682
35. Stewart, J. C. (1980). Colorimetric determination of phospholipids with ammonium ferrothiocyanate. *Anal Biochem*. 104:1. doi: 10.1016/0003-2697(80)90269-9
36. Stupp, R., Hegi, M.E., Mason, W.P., van den Bent, M.J., Taphoorn, M.J., Janzer, R.C., et al. (2009). Effects of radiotherapy with concomitant and adjuvant temozolomide versus radiotherapy alone on survival in glioblastoma in a randomised phase III study: 5-year analysis of the EORTC-NCIC trial. *Lancet Oncol*. 10:5. doi: 10.1016/S1470-2045(09)70025-7
37. Tamborini, M., Locatelli, E., Rasile, M., Monaco, I., Rodighiero, S., Corradini, I., et al. (2016). A Combined Approach Employing Chlorotoxin-Nanovectors and Low Dose Radiation To Reach Infiltrating Tumor Niches in Glioblastoma. *ACS Nano*. 10:2. doi: 10.1021/acsnano.5b07375
38. Thayanithy, V., Dickson, E. L., Steer, C., Subramanian, S., Lou, E. (2014). Tumor-stromal cross talk: direct cell-to-cell transfer of oncogenic microRNAs via tunneling nanotubes. *Transl Res*. 164:5. doi:10.1016/j.trsl.2014.05.011
39. Van der Vos, K. E., Abels, E. R., Zhang, X., Lai, C.,, Carrizosa, E., Oakley, D., et al. (2016). Directly visualized glioblastoma-derived extracellular vesicles transfer RNA to microglia/macrophages in the brain. *Neuro Oncol.* 18:1. doi: 10.1093/neuonc/nov244
40. Veranic, P., Lokar, M., Schütz, G.J., Weghuber, J., Wieser, S., Hägerstrand, H., et al. (2008). Different types of cell-to-cell connections mediated by nanotubular structures. *Biophys J*. 95:9. doi: 10.1529/biophysj.108.131375
41. Weil, S., Osswald, M., Solecki, G., Grosch, J., Jung, E., Lemke, D., et al. (2017). Tumor microtubes convey resistance to surgical lesions and chemotherapy in gliomas. *Neuro Oncol.* 19:10. doi: 10.1093/neuonc/nox070

42. Westphal, M., Lamszus, K. (2011). The neurobiology of gliomas: from cell biology to the development of therapeutic approaches. *Nature Rev*. 12:9. doi: 10.1038/nrn3060
43. Xiang, Y., Liang, L., Wang, X., Wang, J., Zhang, X., Zhang, Q. (2011). Chloride channel-mediated brain glioma targeting of chlorotoxin-modified doxorubicin-loaded liposomes. *J Control Release*. 152:3. doi: 10.1016/j.jconrel.2011.03.014
44. Xing, R., He, H., He, Y., Feng, Y., Zhang, C., Wu, H. et al. (2013). ANXA2 remodels the microstructures of caco2 cells. *Cell Mol Biol*. 59 Suppl:OL1848-54
45. Zhang, L., Zhang, Y. (2015). Tunneling nanotubes between rat primary astrocytes and C6 glioma cells alter proliferation potential of glioma cells. *Neurosci Bull*. 31:3. doi: 10.1007/s12264-014-1522-4

Figures Legends

Figure 1. U87-MG and NHA cells forms thin and thick TnTs. U87-MG cells (**A**) or NHA cells (**B**) were plated on gelatin pre-treated coverslips, fixed and stained with DiI (1.9 µl/ml) to detect TnTs. Fluorescence images were acquired by a 40x magnification on A1R Nikon laser scanning confocal microscope. White arrows indicate thin TnTs, while white triangles indicate thick TnTs. Scale bar: 10 µm. Optical images captured with an inverted Olympus CKX41 microscope were also shown. Black triangles indicate thick TnTs. Scale bar: 100 µm. Magnification of protrusion are shown.

Figure 2. Characterization of TnTs in U87-MG cells. U87-MG cells were plated on gelatine pre-treated coverslips. Cells were fixed, permeabilized and immunostained either with the anti-β-tubulin antibody (1:150) and TRITC-phalloidin (1:40) to detect microtubules and actin filaments. Fluorescence images were captured by confocal microscopy. White triangles indicate thick and thin TnTs. Magnification of protrusion are shown. Scale bar: 10µm.

Figure 3. Characterization of TnTs in NHA cells. NHA cells were plated on gelatine pre-treated coverslips. Cells were fixed, permeabilized and immunostained either with the anti-β-tubulin antibody (1:150) and TRITC-phalloidin (1:40) to detect microtubules and actin filaments. Fluorescence images were captured by confocal microscopy. White triangles indicate thin TnTs. Magnification of protrusion is shown. Scale bar: 10µm.

Figure 4. Doxorubicin localize into the nucleus of U87-MG and NHA cells. U87-MG cells (**A**) and NHA cells (**B**) were plated on gelatine pre-treated coverslips, incubated with 15 µg/ml of DOX for 1 h and then stained with DiO (5 µl/ml) to detect TnTs. Cells were fixed and fluorescence images were captured with a 40x magnification on A1R Nikon laser scanning confocal microscope. White triangles indicate thin TnTs. Magnification of protrusion are shown. Scale bar: 10µm. DOX = doxorubicin.

Figure 5. Percentage of cells forming TnTs after DOX treatment. Percentage of U87-MG cells (**A**) and NHA cells (**B**) forming TnTs on total cells is shown. At least 200 cells were analyzed per group in three independent experiments. Data are expressed as mean ± S.E from three independent experiments. Data were analyzed by Student *t* test; n.s.= not significant. DOX = doxorubicin; CTR = control untreated cells.

Figure 6. Localization of DOX-LIP in U87-MG TnTs. U87-MG cells were plated on gelatine pre-treated coverslips. Cells were leaved in culture complete medium for 48 h and then incubated with DOX-LIP (15 µg/ml of DOX, 200 nmols of total lipids) for 1 h. Cells were later stained for 20 min

with DiO (5 µl/ml), fixed and fluorescence images were captured with a 40x magnification on A1R Nikon laser scanning confocal microscope. Black triangles indicate the presence of DOX-LIP in thick TnTs. Magnification of protrusion and bright field images are shown. Scale bar: 10µm. DOX-LIP = liposomes embedding doxorubicin.

Figure 7. Localization of Mf-LIP in U87-MG TnTs. U87-MG cells were plated on gelatine pre-treated coverslips. Cells were leaved in culture complete medium for 48 h and then incubating cells with Mf-LIP (200 nmols of total lipids) for 1 h. Cells were later stained for 20 min with DiI (1.9 µl/ml). Cells were fixed and fluorescence images were captured with a 40x magnification on A1R Nikon laser scanning confocal microscope. Magnification of protrusion and bright field images are shown. Scale bar: 10µm. Mf-LIP = multi-functionalized liposomes.

Figure 8. Localization of DOX-LIP in NHA TnTs. NHA cells were seeded on gelatine pre-treated coverslips. Cells were leaved in culture complete medium for 48 h and then incubated with DOX-LIP (15 µg/ml of DOX, 200 nmols of total lipids) for 1 h. Cells were later stained for 20 min with DiO (5 µl/ml), fixed and fluorescence images were captured with a 40x magnification on A1R Nikon laser scanning confocal microscope. Black triangles indicate the presence of DOX-LIP in thick TnTs. Magnification of protrusion and bright field images are shown. Scale bar: 10µm. DOX-LIP = liposomes embedding doxorubicin.

Figure 9. Localization of Mf-LIP in NHA TnTs. NHA cells were plated on gelatine pre-treated coverslips. Cells were leaved in culture complete medium for 48 h and then incubating cells with Mf-LIP (200 nmols of total lipids) for 1 h. Cells were later stained for 20 min with DiI (1.9 µl/ml). Cells were fixed and fluorescence images were captured with a 40x magnification on A1R Nikon laser scanning confocal microscope. Black triangles indicate the presence of DOX-LIP in thick TnTs. Magnification of protrusion and bright field images are shown. Scale bar: 10µm. Mf-LIP = multi-functionalized liposomes.

Tables

Table 1. Percentage distribution of thin and thick TnTs in U87-MG and NHA cells.

Type of TnTs	NHA	U87	*p* value
Thin	63% ± 18.14%	4% ± 1.9%	0.0235
Thick	37% ± 18.14%	96% ± 2%	0.0239

Table 2. Percentage distribution of thin and thick TnTs in U87-MG (**A**) and NHA (**B**) cells after treatment with DOX.

A

Type of TnTs	U87 + DOX	*p* value
Thin	76% ± 2.08%	<0.0001
Thick	24% ± 2.08%	<0.0001

B

Type of TnTs	NHA + DOX	*p* value
Thin	59.67% ± 6.56 %	0.8713
Thick	40.33% ± 6.56 %	0.8713

Table 3. Percentage distribution of thin and thick TnTs in U87-MG cells after treatment with DOX-LIP (**A**) of Mf-LIP (**B**).

A

Type of TnTs	DOX-LIP	*p* value
Thin	75% ± 13%	<0.0001
Thick	25% ± 13%	<0.0001

B

Type of TnTs	Mf-LIP	*p* value
Thin	3.9% ± 1.95%	>0.999
Thick	96.1% ± 2%	>0.999

Figure 1.JPEG

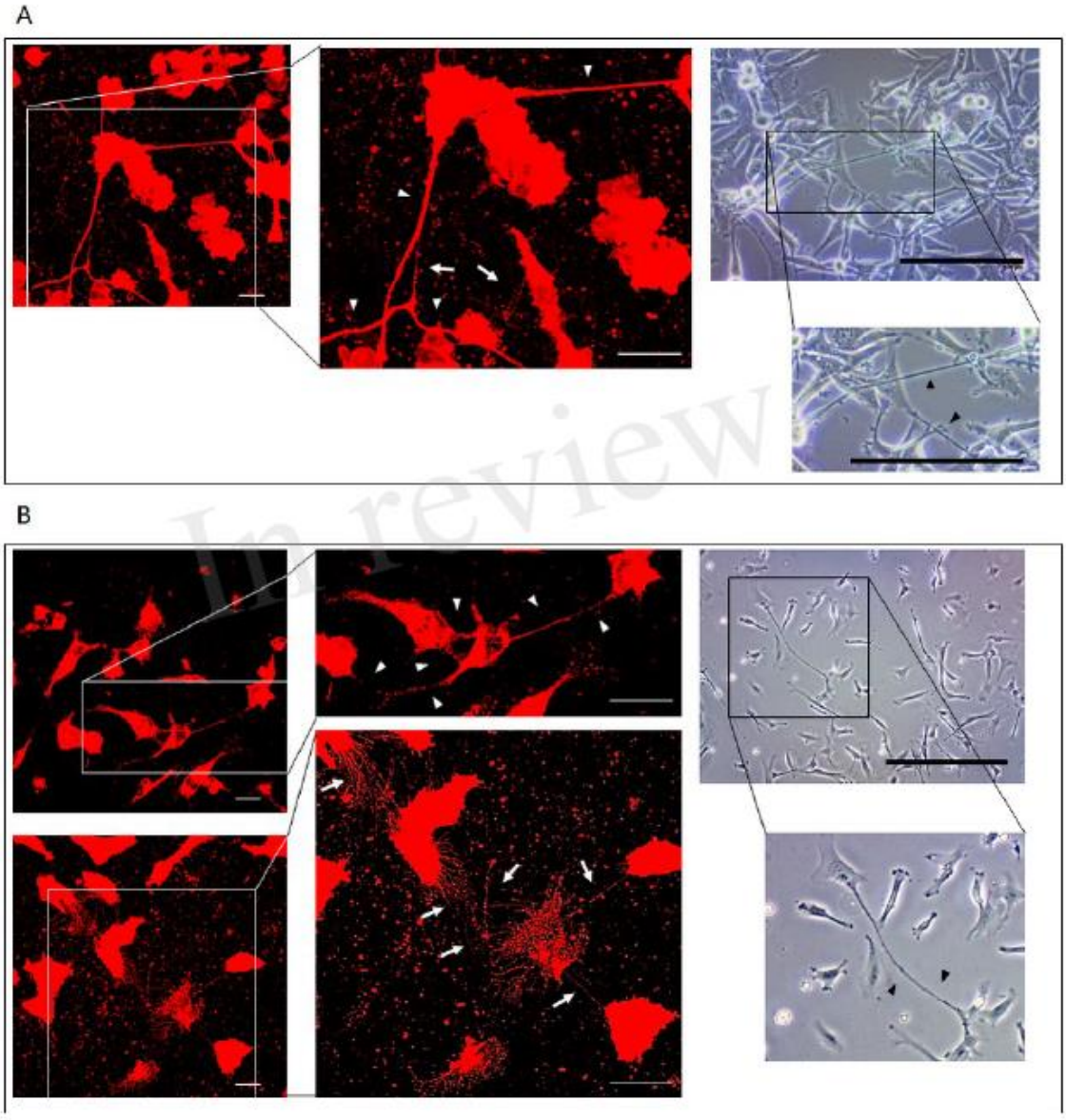

Figure 2.JPEG

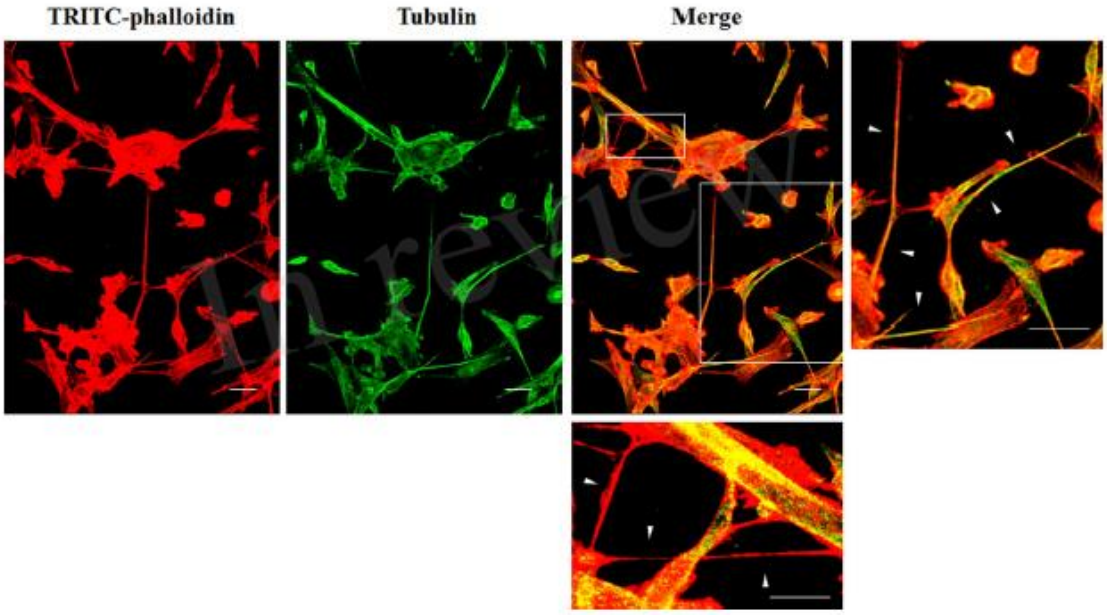

Figure 3.JPEG

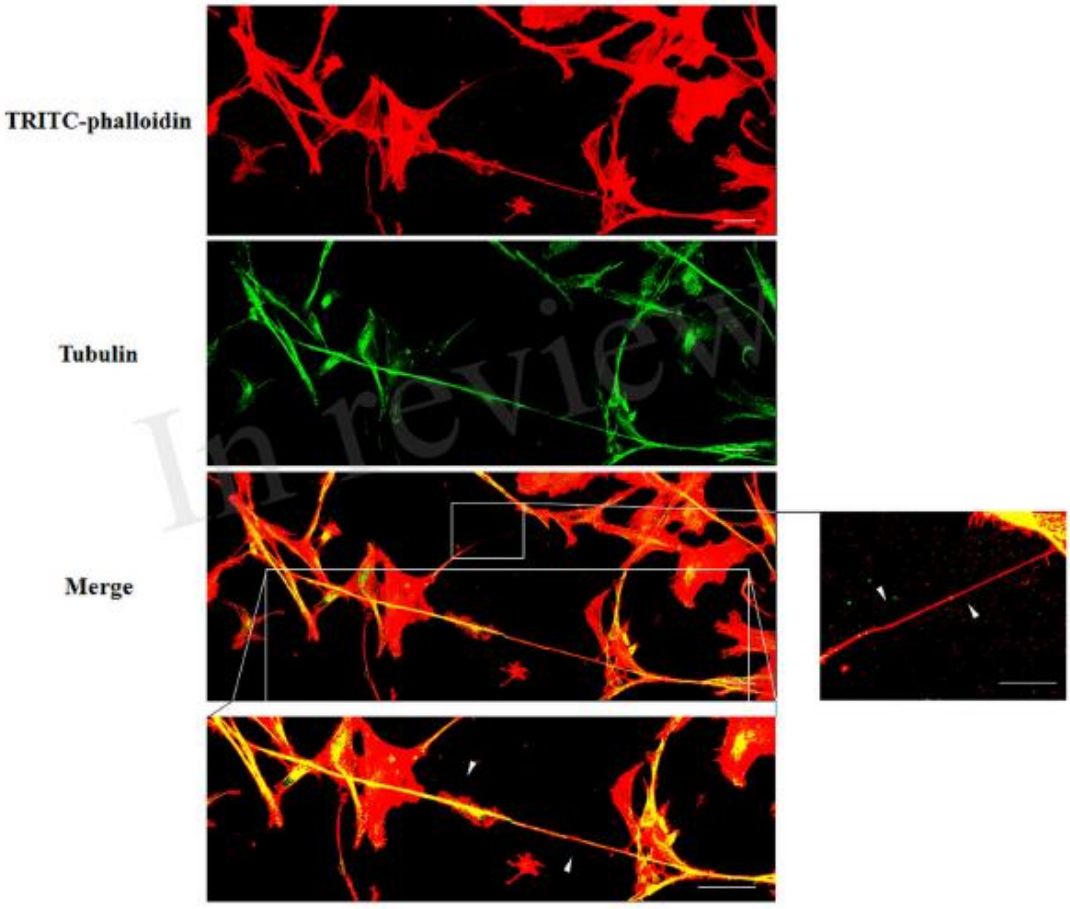

Figure 4.JPEG

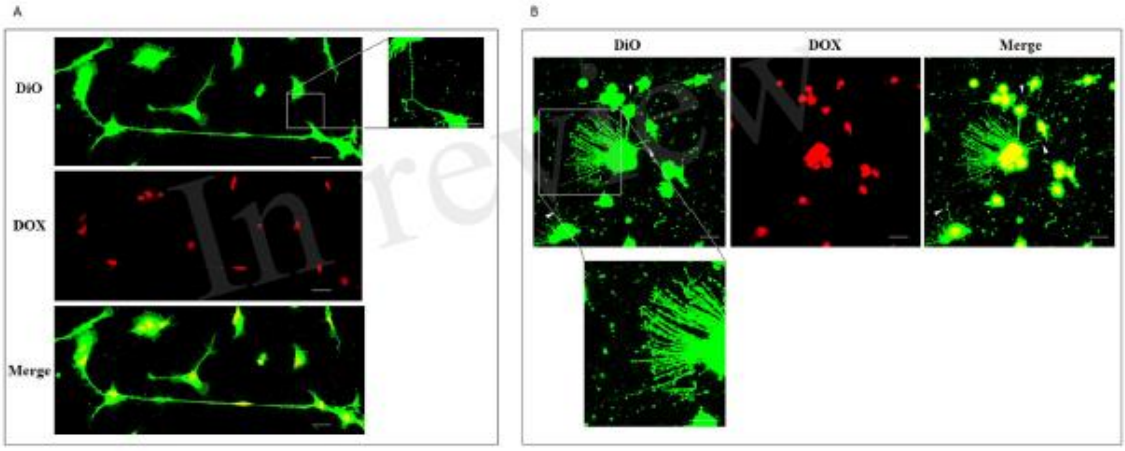

Figure 5.JPEG

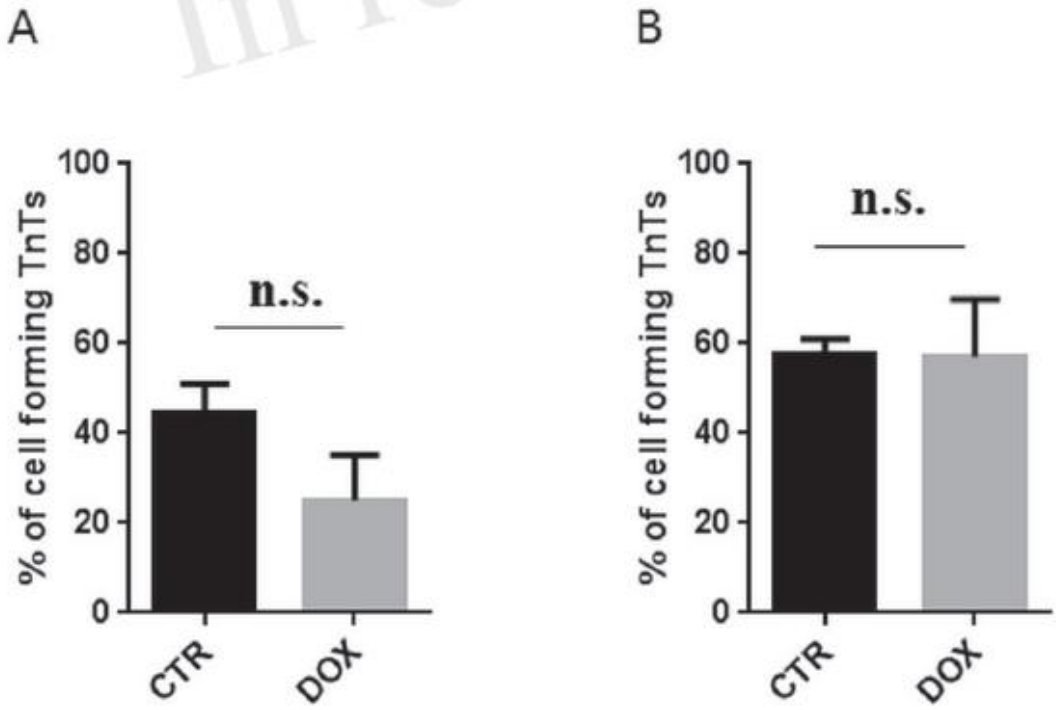

Figure 6.JPEG

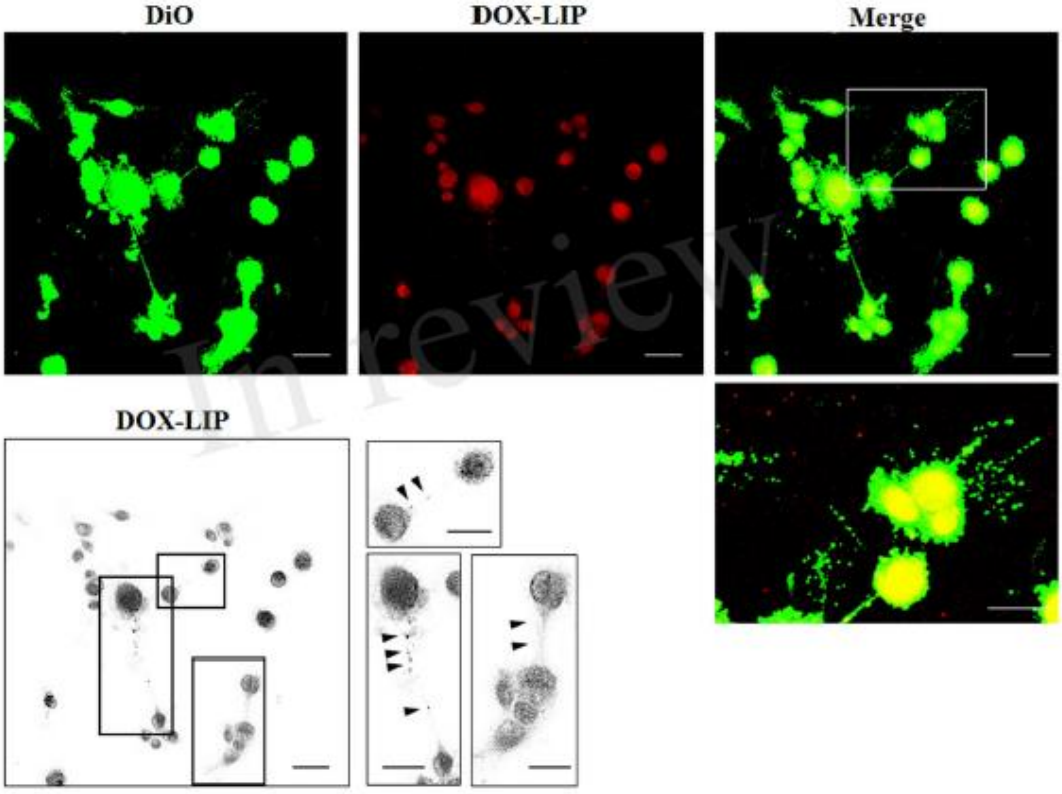

Figure 7.JPEG

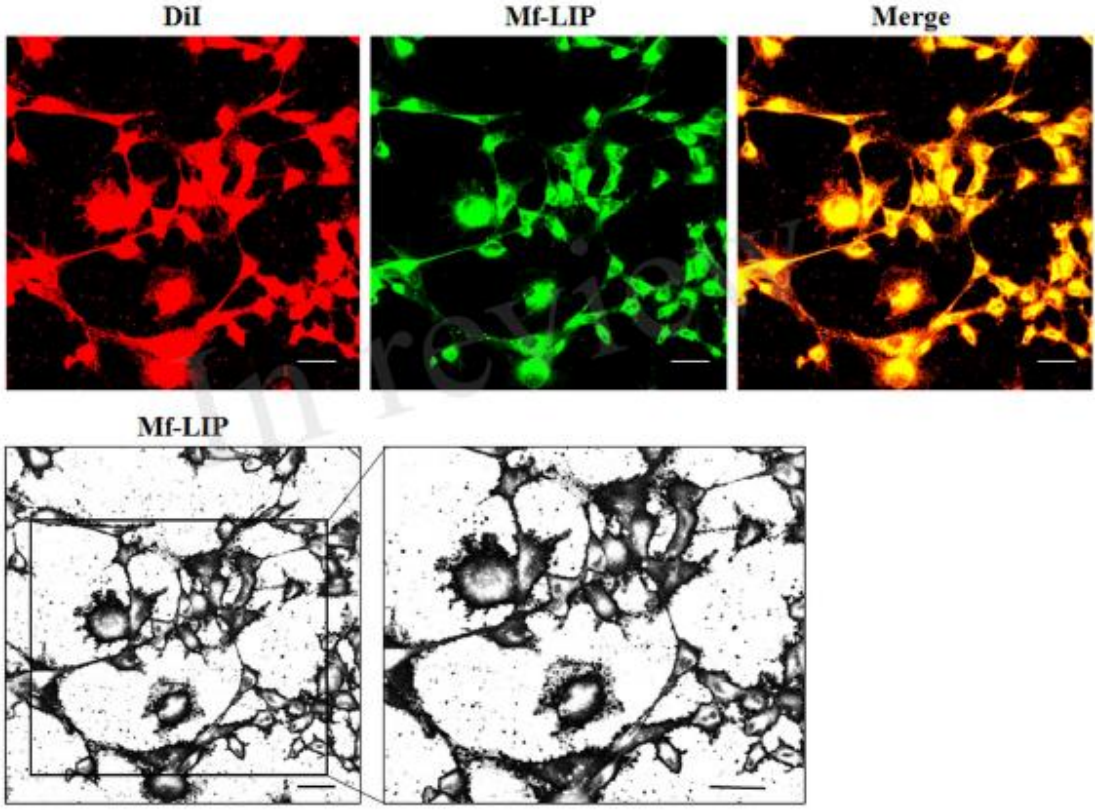

Figure 8.JPEG

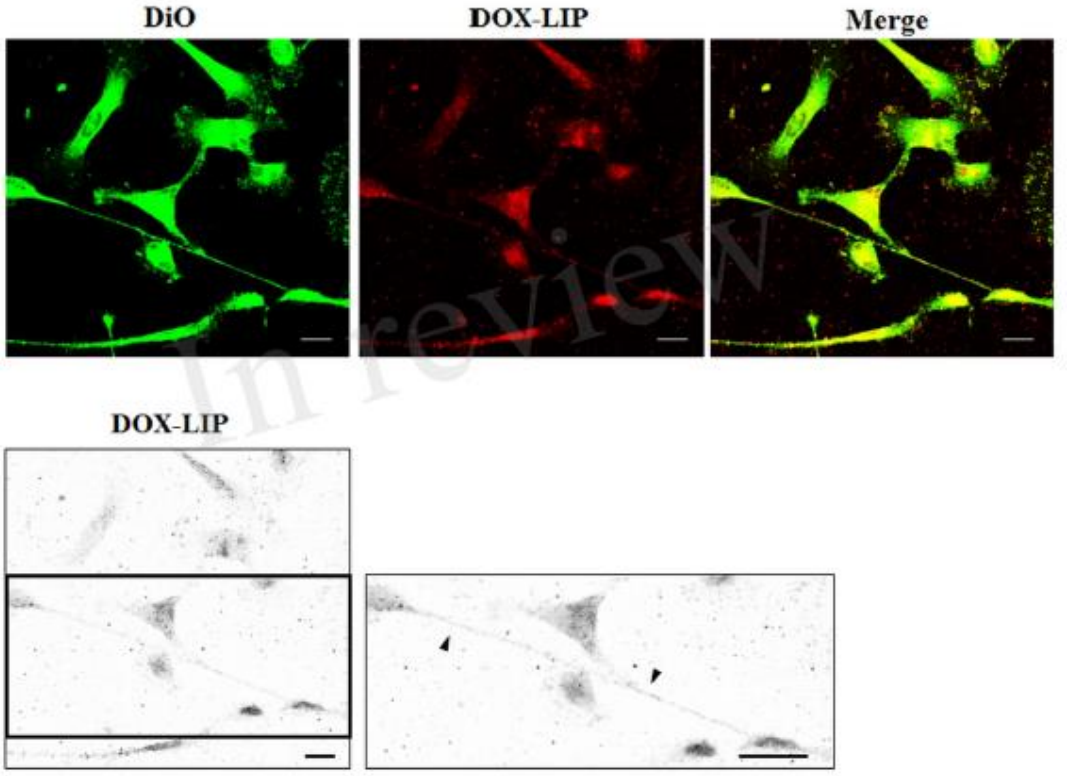

Figure 9.JPEG